

NATIONAL TRANSPORTATION SAFETY BOARD
Office of Research and Engineering
Washington, D.C. 20594

September 11, 1998

Aircraft Performance

**Addendum 1 to the
Group Chairman's Aircraft Performance Study**

A. ACCIDENT

Location: Near Monroe, Michigan
Date: January 9, 1997
Time: 1555 Eastern Standard Time (EST)
Aircraft: Embraer EMB-120; N265CA
NTSB #: DCA-97-MA-017

B. GROUP

Chairman: Daniel R. Bower, Ph.D.
National Transportation Safety Board

Member: Carla Worthy
Federal Aviation Administration

Member: Joseph Bracken
Air Line Pilots Association

Member: Len Magnor
Comair

Member: Decio Coelho Pullin
Embraer

Member: Steve Wade
Pratt and Whitney Canada

Member: Stephen W. Josephson
Hamilton Standard

C. SUMMARY

This document is a supplement to the original aircraft performance study dated May 4, 1998. During the completion of the original document, another incident involving an Embraer EMB-120 occurred¹. On March 5, 1998, about 2030 Pacific Standard Time (PST), an Embraer EMB-120, N284YV, registered and operated by Westair as a scheduled domestic passenger flight 233 (SDU233) from Sacramento, California experienced an in-flight upset while holding at 10,000 feet mean sea level (ft-msl) altitude enroute to San Francisco, California. The flight crew was holding with zero flaps when they reportedly experienced a buffet and felt the airplane pitch up. The flight crew added power and disconnected the autopilot, and the airplane experienced several roll oscillations. No emergency was declared and no altitude deviations were noted by Air Traffic Control (ATC). The airplane landed safely in San Francisco with no injuries to passengers and no damage noted.

This addendum report examines the motion of the Westair flight, and correlates when various events occurred. Flight Data Recorder (FDR) data, Federal Aviation Administration (FAA) radar data, and weather data, were used to develop the time history of the incident aircraft motion described in this report. Composite plots will graphically show the location and orientation of the airplane when key events occurred.

In the original document, several ongoing studies were discussed. This document discusses the results of computational work performed by the Icing Branch of NASA-Lewis Research Center and provides a further description of the ice accretion results obtained in NASA's Icing Research Tunnel (IRT).

D. DETAILS OF THE INVESTIGATION

Section I - Radar Data

Airport Surveillance Radar (ASR) data was obtained from Sacramento Terminal Radar Approach Control (TRACON) for Westair flight 233. ASR radar normally records data approximately every 4.6 seconds. The assigned beacon code for SDU233 was 4314.

The FAA provided the ASR range/azimuth transponder beacon radar data for

¹ This incident has been assigned NTSB Accident Number DCA98SA029.

the incident flight. The raw Sacramento ASR data is tabulated in attachment I-1 through I-5, which shows the radar clock time, range from the Sacramento ASR radar antenna, magnetic azimuth angle, and flight level for SDU233 from the takeoff from Sacramento to the level off at 10,000 ft-msl. The format supplied by the FAA contains time in hours, minutes, seconds, range from the radar site in nautical miles (n.m.), azimuth in ACP's (4096 ACP's = 360°), flight level in 100's of feet-msl, and beacon code. The range-azimuth-altitude format was converted to x-y-altitude format using a 15.9° easterly magnetic variation. In this converted x-y coordinate system, x represents true east and y is true north in nautical miles from the Sacramento ASR antenna. A plan view of the radar data ground track, labeled with the flight level for every eighth radar data point, is shown in attachment I-6.

Section II - Time Correlation

A time correlation was made between the ASR radar data and the FDR data. Times given in this report are in 24 hour format, in the form HHMM:SS Pacific Standard Time (PST). A comparison of the radar altitude versus time and FDR altitude versus local time was used to correlate FDR data elapsed time to the radar data local time. Attachment II-1 shows FDR derived mean sea level altitude and ASR radar altitude versus local time, using the time correlation given in this section.

Section III - Flight Path Description

Information from the flight data recorder (FDR) is shown in Attachments III-1 through III-4, for several time scales. Attachment III-1 shows several parameters in the 60 seconds before the autopilot disconnect, and Attachments III-2 and III-3 show the FDR data several minutes before the upset. There are portions of the FDR data that experienced a data dropout in the recording. These data points are represented as spikes in the FDR data plots, and are not representative of the airplane motion. The wheel position parameter experienced an acquisition error and did not record correct values.

FDR data show that during the flight, the airplane ascended from 9000 ft-msl to 10,000 ft-msl altitude with the autopilot engaged and wing flaps zero. The pilots had reported moderate rime ice at 9000 ft and requested to go to 10,000 feet to exit the icing environment. The pilots reported they had the deice boots operating in automatic "high" mode, which cycles the wing leading edge deice boots once per minute.

By 2031:20 SDU233 had leveled off at 10,000 feet. After leveling off, the airplane was flying on a heading of 180 degrees. SDU233 then entered a turn to heading 360. During this turn, the airplane reached 190 KIAS airspeed at 2032:20 and engine torque was reduced to approximately 50%. After this reduction in torque, the airspeed started to reduce. By 2035:20 the FDR airspeed had dropped below 160 KIAS. Both engines remained near 50% torque, while the autopilot maintained altitude at 10,000 feet. At 2036:45, airspeed had reduced to 155 KIAS and SDU233 started a left roll. The airplane reached the autopilot roll limit of 26° LWD by 2036:52. As the airplane turned to a heading of 180, the pitch angle remained close to 6° airplane nose up, and the airspeed continued to slowly decrease.

As the airplane heading passed through 220° in the turn, the autopilot began to command a rearward control column movement at 2037:30. Over the next five seconds, the autopilot began to apply an increasing nose up pitch trim, and the roll angle increased slightly to 29° LWD. By 2037:35, the airspeed had reduced to 148 KIAS, and altitude had dropped to 9950 feet. An increase in engine torque began at 2037:35, reaching 70% on both engines for one second. A second increase in torque to close to 100% occurred by 2037:37, as the airplane heading passed through 191°, and the roll angle began to decrease. By 2037:39, the roll angle reduced to 20° LWD. The autopilot continued to move the control column position and the pitch trim in the nose up position. The airspeed was 146 KIAS, and the altitude had reduced to 9895 feet. Slight oscillations in the vertical acceleration were also evident.

At 2037:40.5, the autopilot discrete changed to "disengaged", and the control column was moved forward. The torque on both engines was increased to close to 115%, and the aircraft rolled to 33° LWD. Starting at 2037:44, the aircraft then rolled sharply to the right at close to 40°/second until the roll reached 63° RWD in the next three seconds. During this roll, the pitch dropped from 10° airplane nose up (ANU) to just below zero, and the airspeed dropped further to 142 KIAS. Over the next three seconds, the airplane rolled back to the left to 45° LWD. During this roll back to the left, the torque was advanced to 133% on both engines and remained beyond the sensing range of the torque instrumentation for the next seventeen seconds. As the airplane went through the roll oscillation, the pitch attitude dropped to close to 7° AND then returned to close to zero as the roll oscillations diminished. After the 45° LWD excursion, the roll attitude was kept between 0 and 25° RWD for the next 40 seconds.

From 2037:50 to 2038:00, as the airplane experienced the roll oscillation, the airspeed had increased from 142 KIAS to 159 KIAS, and the altitude dropped from 9840 ft-msl to 9465 ft-msl. At 2038:00, the control column was being pulled in the ANU direction, the altitude began to increase, and the airspeed began to decrease from 159 KIAS. The airplane then climbed back to over 10,000 ft-msl altitude by 2038:15, and

airspeed decreased to 124 KIAS by 2038:20. During the climb back to 10,000 ft-msl, both engine's torque were reduced to approximately 120% at 2038:08. The roll angle continued to oscillate slightly between zero and 25° RWD during this climb. At 2038:30, the flaps began to be extended to 15°, and remained at 15° for the rest of the flight.

After the flaps were extended, the roll oscillations subsided, and the pitch of the airplane steadied. The airspeed was reduced to between 120 and 130 KIAS, and the airplane continued to climb to 13,000 ft-msl. The remainder of the flight was uneventful, and the airplane continued to its destination.

FDR data indicate that before the autopilot was disconnected, the airplane roll attitude began to slightly exceed the autopilot limit on roll angle. The autopilot applied an increasing pitch trim and nose up control column as the roll angle exceeded 25° LWD prior to the upset. In the 4 seconds before the autopilot disconnected, pitch attitude increased slightly and airspeed continued to decrease despite the flightcrew's application of close to 100% engine torque.

Section IV - Calculations

Angle of attack was not recorded on the FDR for the Westair airplane. FDR data was used as input for the computer program INT3DAOA, a FORTRAN computer program that calculates the angle of attack from the recorded pitch angle, and the flight path angle derived from the altitude time history. The angle of attack results are shown in Attachment IV-1 for the portion of the flight when the airplane was at 9000 feet and 10000 feet msl-altitude. Attachment IV-2 shows the angle of attack calculation for 200 seconds prior to autopilot disconnect. As shown in the graphs, the calculated angle of attack reaches close to 10 degrees as the airspeed dropped below 150 KIAS prior to the autopilot disconnect.

A 5-10 knot discrepancy has been reported by EMB-120 pilots in the indicated airspeed reading for the captain's and first officer's instruments. Hence, the accuracy of the recorded FDR airspeed was investigated, to assure the accuracy of the recorded airspeed. Radar data, aircraft data, weather data and the local magnetic variation were used as input for the computer program FLIGHT, a modified version of the National Aeronautics and Space Administration (NASA) FORTRAN program MANAT. This program calculates performance parameters such as groundspeed, indicated airspeed, roll angle, pitch angle, accelerations, and angle of attack. Parameters calculated by FLIGHT are mathematically smoothed to remove erratic data trends, and may not accurately reconstruct any short-duration flight path deviations. Smoothed values

calculated near the endpoints of data should be considered approximate. The airspeed parameter computed from the radar data for several minutes of flight before the autopilot disconnect are presented graphically in the attachments IV-3. A comparison of calculated indicated airspeed from the radar data, and FDR indicated airspeed versus time is shown, and shows good agreement.

Section V – FAA Wind Tunnel Data

As described in the original report, the Federal Aviation Administration sponsored a research program with the University of Illinois at Urbana-Champaign to investigate the airfoil aerodynamic affect of deice boot inter-cycle ice accretions. The FAA sponsored this research program to address aerodynamic issues arising from the delayed activation of deice boots. This data was not generated from performance group activities, but was provided to the Performance Group Chairman by the FAA In-flight Icing National Resource Specialist.

Shown in Attachment V-1 are some of the additional wind tunnel results from the University of Illinois study. This plot shows coefficient of lift versus of angle of attack for the airfoil with no contamination (clean) and the airfoil with a ridge type contamination. The 0.15-inch ($k/c = 0.00833$), $\frac{1}{4}$ round ridge was placed at different chordwise location on the top surface, and a small roughness strip was placed in front of the ridge to trip² the boundary layer. The clean and the ridge contaminated wing results for hinge moment and drag are shown in attachments V-2 and V-3. The ridge in this test was placed at three different chordwise locations, 0.06c, 0.10c, and 0.14c. The boundary layer trip was located at 0.05c for all three cases. The most notable feature in the data is the reduction in angle of attack at maximum lift coefficient (i.e. the stall angle of attack) with the ridge on the top surface, and the maximum lift coefficient change very little as the ridge is moved aft on the top surface.

Section VI – NASA Icing Study Results

As described in the original report, the first phase of the NASA study involved generating ice shapes on a section of an EMB-120 wing in the NASA–Lewis Icing Research Tunnel (IRT). The computer program LEWICE was also run for the

² In this context, “trip” refers to inducing the boundary layer to become turbulent. This is necessary to assure the boundary layer is turbulent, since the Reynolds number of the experiment is smaller than actual flight conditions.

environmental conditions used in the IRT. LEWICE cannot predict the surface roughness features that are generated, but will predict impingement limits and ice thickness for the conditions specified. The same icing exposure time, LWC, MVD, total temperature, and angle of attack were used in the LEWICE study for comparison with the ice impingement and ice shape results obtained in the IRT. The results from LEWICE the study are given in Attachments VI-1 through VI-38, and the conditions for each run are noted on each page. The overall impingement limits are given in Attachment VI-1.

The original report described the conditions for which the shapes were generated in the NASA IRT. Tracings of the shapes are shown in Attachments VI-40 through VI-120, with the appropriate conditions shown on each page. Attachments VI-103 through VI-120 show the comparison of separate runs with the same conditions to examine the repeatability of the shapes generated in these conditions.

As described in section X of the original report, the airfoil section used in the IRT spanned the entire wind tunnel section. Since the model spanned the entire test section, the airflow over the model was two-dimensional, and the drag on the airfoil was measured by measuring the dynamic pressure distribution across the test section. The 2-D drag coefficient for the airfoil was then calculated. This procedure was performed first for the clean airfoil to obtain the baseline drag coefficient. After the water spray was stopped for each ice accretion run, the tunnel continued to run to allow the wake dynamic pressure measurements to be performed. The airfoil drag coefficient with the accreted ice was then calculated for each ice condition. Due to the ice generating spray apparatus, freestream turbulence levels in the tunnel test section are greater than those in other wind tunnels and affect the calculated values. Also, due to the nature of the IRT environment, frost was noted to accrete, which would not have accreted in similar outside atmospheric conditions. These frost accretions tend to increase the drag measured via wake surveys. Drag coefficients determined should only be used qualitatively and are not representative of the drag that would occur in an actual flight.

The results for the clean airfoil and the baseline ice accretions are shown in attachments VI-122 through VI-127. For these cases, the drag was measured at several angles of attack with the airfoil clean, and with the ice shapes still on the airfoil. Shown for comparison with this data are the standard roughness results of Abbott and Von Doenhoff, denoted by A-V. The A-V data has not been adjusted to reflect the higher Reynold's number in the IRT tests. In Attachments VI-122, the data for the cases with repeat runs at several angles of attack are shown.

Attachments VI-128 through VI-135 show the drag data for several of the conditions tested. These plots show the data all at a single angle of attack as noted on

the plot, and compares the drag for the different ice accretions. Attachment VI-135 shows the drag data for the IRT tests with no boot activation, boots cycled after 2 minutes of accretion and then ice accreted for the next 3 minutes, and boots activated at 5 minutes, and boots activated at both 2 and 5 minutes. For the conditions tested, boot activation at both 2 and 5 minutes still showed an increase in drag as compared to the clean airfoil, yet less than the drag with a boot activation at 2 minutes only and less than no boot activation. This result shows the increased drag effects of residual ice, inter-cycle ice, and the combination thereof. It was observed in the tests that any residual ice left after the first boot activation at 2 minutes would accrete more ice (sometimes in a ridge), but was subsequently shed at the 5 minute boot activation.

Section VII – Simulator Studies in the Embraer Simulator

The original report described autopilot behavior introduced into the training simulator by Embraer. The simulator results are shown in Attachments VII-1 through VII-6. The simulation showed a similar entry and autopilot disconnect via excessive bank angle as shown on the COM3272 FDR. The simulation was also repeated with the maximum aileron torque of 120 in-lbs. (30 in-lbs. attributed to system friction) and the same autopilot disconnect due to excessive bank angle was obtained. The wheel position with this autopilot behavior matched the FDR wheel position, also. For aileron torque of 130 in-lbs. and above, the autopilot in the simulation was able to maintain the 27° roll angle throughout the turn. A slight stepping or ratcheting is noted in the wheel position results, and attributable to the lack of damping present in the simulator autopilot system, which exists in the airplane system due to friction and inertia effects.

Section VIII – NASA 2-D Computational Results

The second phase of the support provided by the researchers from the Icing Branch of the NASA-Lewis Research Center was to complete a two dimensional full Navier-Stokes flow solution for the airfoil with ice shapes accreted in the IRT to determine aerodynamic effects of the accreted ice. Included in this 2-D study was the airflow over the baseline airfoil, and the airfoil with a deflected rear surface (such as an aileron), and the relative aerodynamic effects of the accreted ice shapes was determined in terms of 2-D lift decrement and drag increase.

After digitizing the ice shapes obtained on the EMB-120 wing in the IRT, representative shapes were chosen for the computational study: 1.) shapes with prominent sand-paper type roughness; 2.) a shape with roughness and a ridge accretion on the top of the leading edge. The NASA researchers then used several

codes to accomplish this task. The first codes, TURBOGRD and GRIDGEN, generated the computational grid to be used in the full Navier-Stokes flow solution. The flow solution was generated by the fluid flow simulation code NPARC³.

The results of this computational study by NASA are given in attachments VIII-1 through VIII-56. Included in these results are the lift coefficient and drag coefficients for the computed ice shapes as a function of angle of attack. As noted in these results, two different turbulence models were used, and for the conditions computed the Baldwin-Barth turbulence model is considered to be the more accurate computation. The Baldwin-Barth results also compared favorably with the computations using a Spalart-Allmaras turbulence model as a check of the Baldwin-Barth results.

Results shown in Attachment VII-42 show the lift coefficient as a function of angle attack for the airfoil with a ridge type ice on the leading edge. Results are shown for two aileron deflections, and the computations were made at conditions⁴ corresponding to the time after the roll angle of the accident airplane exceeded the autopilot limit of 27 degrees. The results show a significant reduction of the stall angle of attack as compared to the results with no ice accretion, and a significant difference in the critical⁵ angle of attack for the upward and downward deflected aileron. The post-critical angle results show the iced airfoil with the downward deflecting aileron having less lift than the upward deflecting aileron. The computational results also show the airfoil separation proceeding from the rear (chordwise) of the airfoil and then proceeding forward as the angle of attack increases.

Additional computations were performed using the accident flight conditions and larger upward and downward deflected ailerons on the airfoil with the ice accretion. These results shown in Attachments VII-45 and VII-47 show a consistent behavior with the wind tunnel results from the FAA/UIUC study, in that a significant reduction in the lift differences between the downward and upward deflecting aileron occurs with the ice ridge present. This effect increases with increasing angle of attack.

As noted in the original report, only a qualitative comparison of these results to the three-dimensional flow situation is possible. The Reynolds number used for the

³ The NPARC flow simulator is a product of the NPARC Alliance, a partnership between the National Aeronautics and Space Administration's Lewis Research Center and the Air Force Material Command's Arnold Engineering Development Center. This Alliance seeks to enhance the military and commercial competitiveness of the United States through the establishment of the NPARC flow simulator as a national resource.



⁴ The conditions used in the computations were: 152 knots airspeed, Static temperature 25.5°, Reynold Number based on chord length 10.8 Million, 4000 feet altitude, left aileron 2.56° down, and right aileron 2.74° up.

⁵ Critical angle refers to the angle of attack at maximum lift, also referred to as the stall angle of attack.

computational results was approximately that experienced by the accident airplane, however the three-dimensional flow effects are not taken into consideration in this computation. The angle of attack distribution described in the original report must be considered when examining these two-dimensional results. Additional considerations in comparing these results to the accident airplane scenario not only include the three dimensional flow effects (i.e. the angle of attack distribution), but the dynamic effects of an increasing angle of attack in combination with increasing aileron deflections and increasing yaw angle.

Section IX – Correspondence Regarding NASA Results

During the investigation, a submission to the Safety Board by the Air Line Pilots Association (ALPA) contained some discussion of the NASA results. Attachments IX-1 contain some clarifications provided by NASA. A further response from ALPA is in Attachments IX-2 and IX-3. Also in response to the ALPA submission, BF Goodrich provided the letter contained in Attachments IX-4 and IX-5.

Daniel R. Bower, Ph.D.
Aerospace Engineer
Aircraft Performance Group Chairman

ATTACHMENTS Section I

Radar Data
Radar Plots

H,MM,Seconds	X range	Y Range	FL
4,12, 8.546,	-10.1388,	.7955,	1.0
4,12, 13.148,	-10.1397,	.9052,	2.0
4,12, 17.785,	-10.1477,	1.0316,	4.0
4,12, 22.387,	-10.1766,	1.2241,	5.0
4,12, 26.987,	-10.2046,	1.3229,	7.0
4,12, 31.621,	-10.2128,	1.4836,	10.0
4,12, 36.242,	-10.2259,	1.5978,	12.0
4,12, 40.823,	-10.2369,	1.7770,	13.0
4,12, 45.455,	-10.2468,	1.8922,	14.0
4,12, 50.087,	-10.2428,	2.0708,	14.0
4,12, 54.845,	-10.2196,	2.2298,	14.0
4,12, 59.451,	-10.2157,	2.4268,	15.0
4,13, 4.043,	-10.1984,	2.6219,	16.0
4,13, 8.636,	-10.1912,	2.8042,	17.0
4,13, 13.248,	-10.2004,	3.0268,	18.0
4,13, 17.901,	-10.2002,	3.2321,	19.0
4,13, 22.506,	-10.2148,	3.4449,	19.0
4,13, 27.097,	-10.2099,	3.6716,	19.0
4,13, 31.875,	-10.2281,	3.9101,	20.0
4,13, 36.361,	-10.2500,	4.1546,	20.0
4,13, 41.074,	-10.2411,	4.4094,	20.0
4,13, 45.669,	-10.2695,	4.6065,	20.0
4,13, 50.327,	-10.2751,	4.9379,	20.0
4,13, 54.922,	-10.2906,	5.2005,	20.0
4,13, 59.556,	-10.3001,	5.4861,	20.0
4,14, 4.141,	-10.3109,	5.7586,	20.0
4,14, 8.733,	-10.3235,	6.0388,	20.0
4,14, 13.388,	-10.3533,	6.3586,	20.0
4,14, 17.992,	-10.4234,	6.6239,	20.0
4,14, 22.600,	-10.5105,	6.9309,	21.0
4,14, 27.351,	-10.6151,	7.1884,	21.0
4,14, 31.928,	-10.7674,	7.4614,	22.0
4,14, 36.582,	-10.9542,	7.6657,	24.0
4,14, 41.171,	-11.1232,	7.9118,	25.0
4,14, 45.807,	-11.3514,	8.0741,	26.0
4,14, 50.403,	-11.5796,	8.2364,	28.0
4,14, 55.038,	-11.8125,	8.3747,	30.0
4,14, 59.634,	-12.0555,	8.4639,	31.0
4,15, 4.090,	-12.3291,	8.5436,	33.0
4,15, 8.684,	-12.5711,	8.5976,	35.0
4,15, 13.290,	-12.8325,	8.6041,	36.0
4,15, 18.053,	-13.0651,	8.6155,	38.0
4,15, 22.692,	-13.2997,	8.5668,	40.0
4,15, 27.160,	-13.5524,	8.4671,	42.0
4,15, 31.742,	-13.7450,	8.3836,	44.0
4,15, 36.379,	-13.9541,	8.2490,	46.0
4,15, 40.974,	-14.1150,	8.1120,	48.0
4,15, 45.627,	-14.2606,	7.9359,	50.0
4,15, 50.227,	-14.3745,	7.7698,	52.0
4,15, 54.831,	-14.4511,	7.5835,	54.0
4,15, 59.427,	-14.5163,	7.3920,	56.0
4,16, 4.070,	-14.5411,	7.2090,	57.0
4,16, 8.648,	-14.5473,	6.9911,	59.0
4,16, 13.288,	-14.5310,	6.7921,	60.0
4,16, 17.873,	-14.5211,	6.5985,	62.0
4,16, 22.501,	-14.4997,	6.4018,	63.0
4,16, 26.972,	-14.4848,	6.2102,	64.0
4,16, 31.724,	-14.4676,	6.0198,	65.0
4,16, 36.350,	-14.4565,	5.7823,	66.0
4,16, 40.827,	-14.4338,	5.5942,	68.0
4,16, 45.425,	-14.4171,	5.3852,	69.0
4,16, 50.059,	-14.3800,	5.1961,	70.0
4,16, 54.643,	-14.3653,	4.9677,	71.0
4,16, 59.280,	-14.3493,	4.7658,	73.0
4,17, 3.855,	-14.3374,	4.5431,	74.0
4,17, 8.500,	-14.3126,	4.3187,	75.0
4,17, 13.108,	-14.3069,	4.1261,	76.0
4,17, 17.737,	-14.2913,	3.8852,	78.0
4,17, 22.316,	-14.2661,	3.6676,	79.0

U12

I-1

4,17,	26.959,	-14.2571,	3.4562,	80.0
4,17,	31.566,	-14.2352,	3.2435,	82.0
4,17,	36.158,	-14.2245,	3.0123,	83.0
4,17,	40.633,	-14.2102,	2.7822,	84.0
4,17,	45.270,	-14.1921,	2.5533,	86.0
4,17,	49.905,	-14.1570,	2.3457,	87.0
4,17,	54.495,	-14.1320,	2.1194,	88.0
4,17,	59.114,	-14.1232,	1.8970,	88.0
4,18,	3.694,	-14.0984,	1.6959,	89.0
4,18,	8.306,	-14.0752,	1.4526,	89.0
4,18,	12.959,	-14.0498,	1.1891,	89.0
4,18,	17.572,	-14.0408,	.9068,	89.0
4,18,	22.203,	-14.0251,	.6468,	90.0
4,18,	26.787,	-14.0246,	.3882,	90.0
4,18,	31.378,	-14.0096,	.1084,	90.0
4,18,	35.866,	-13.9990,	-.1709,	90.0
4,18,	40.518,	-13.9934,	-.4285,	90.0
4,18,	45.118,	-13.9832,	-.6860,	90.0
4,18,	49.696,	-13.9752,	-.9869,	90.0
4,18,	54.338,	-13.9508,	-1.2867,	90.0
4,18,	58.916,	-13.9398,	-1.5883,	90.0
4,19,	3.571,	-13.9351,	-1.8699,	90.0
4,19,	8.147,	-13.9247,	-2.1520,	90.0
4,19,	12.763,	-13.9086,	-2.4344,	90.0
4,19,	17.250,	-13.8979,	-2.7635,	90.0
4,19,	21.838,	-13.8838,	-3.0274,	90.0
4,19,	26.487,	-13.8785,	-3.3625,	90.0
4,19,	31.058,	-13.8667,	-3.6539,	90.0
4,19,	35.687,	-13.8488,	-3.9461,	90.0
4,19,	40.321,	-13.8438,	-4.2449,	90.0
4,19,	44.916,	-13.8394,	-4.5239,	90.0
4,19,	49.560,	-13.8240,	-4.8498,	90.0
4,19,	54.133,	-13.8261,	-5.1383,	90.0
4,19,	58.765,	-13.8046,	-5.4460,	90.0
4,20,	3.345,	-13.8036,	-5.7414,	90.0
4,20,	7.991,	-13.7870,	-6.0598,	90.0
4,20,	12.457,	-13.7730,	-6.3586,	90.0
4,20,	17.041,	-13.7719,	-6.6422,	90.0
4,20,	21.651,	-13.7633,	-6.9532,	90.0
4,20,	26.296,	-13.7391,	-7.2615,	90.0
4,20,	30.929,	-13.7373,	-7.5598,	90.0
4,20,	35.521,	-13.7172,	-7.8811,	90.0
4,20,	40.162,	-13.7024,	-8.1832,	90.0
4,20,	44.734,	-13.6984,	-8.4976,	90.0
4,20,	49.376,	-13.6876,	-8.8141,	90.0
4,20,	53.960,	-13.6756,	-9.1062,	90.0
4,20,	58.418,	-13.6517,	-9.4265,	90.0
4,21,	3.077,	-13.6439,	-9.7336,	90.0
4,21,	7.678,	-13.6064,	-10.0575,	90.0
4,21,	12.271,	-13.5618,	-10.3500,	90.0
4,21,	16.909,	-13.4957,	-10.6310,	90.0
4,21,	21.548,	-13.3661,	-10.9678,	90.0
4,21,	26.139,	-13.2401,	-11.2435,	90.0
4,21,	30.740,	-13.0909,	-11.5382,	90.0
4,21,	35.385,	-12.9716,	-11.7915,	90.0
4,21,	39.958,	-12.7847,	-12.0959,	90.0
4,21,	44.478,	-12.6692,	-12.3604,	90.0
4,21,	49.056,	-12.5028,	-12.6556,	90.0
4,21,	53.702,	-12.3566,	-12.9370,	90.0
4,21,	58.292,	-12.2112,	-13.2245,	90.0
4,22,	2.935,	-12.0736,	-13.4848,	90.0
4,22,	7.526,	-11.9163,	-13.7697,	90.0
4,22,	12.156,	-11.7872,	-14.0505,	90.0
4,22,	16.738,	-11.6178,	-14.3328,	90.0
4,22,	21.375,	-11.5054,	-14.6018,	90.0
4,22,	25.948,	-11.3301,	-14.8894,	90.0
4,22,	30.582,	-11.2067,	-15.1569,	90.0
4,22,	35.211,	-11.0485,	-15.4328,	90.0
4,22,	39.842,	-10.9016,	-15.7319,	90.0
4,22,	44.423,	-10.7616,	-15.9971,	90.0

4,22,	49.061,	-10.6466,	-16.2534,	90.0
4,22,	53.514,	-10.4563,	-16.5661,	90.0
4,22,	58.101,	-10.3359,	-16.8295,	90.0
4,23,	2.743,	-10.1531,	-17.1150,	90.0
4,23,	7.319,	-10.0272,	-17.3856,	90.0
4,23,	11.967,	-9.9012,	-17.6644,	90.0
4,23,	16.551,	-9.7374,	-17.9488,	90.0
4,23,	21.185,	-9.5956,	-18.2173,	90.0
4,23,	25.778,	-9.4487,	-18.4851,	90.0
4,23,	30.409,	-9.3056,	-18.7699,	90.0
4,23,	35.003,	-9.1568,	-19.0539,	90.0
4,23,	39.632,	-9.0279,	-19.3142,	90.0
4,23,	44.217,	-8.8385,	-19.6102,	90.0
4,23,	48.851,	-8.7036,	-19.8780,	90.0
4,23,	53.314,	-8.5989,	-20.1412,	90.0
4,23,	58.066,	-8.4273,	-20.4301,	90.0
4,24,	2.699,	-8.3172,	-20.7017,	90.0
4,24,	7.168,	-8.1348,	-20.9887,	90.0
4,24,	11.742,	-8.0119,	-21.2498,	90.0
4,24,	16.377,	-7.8882,	-21.5198,	90.0
4,24,	21.017,	-7.7670,	-21.8082,	90.0
4,24,	25.596,	-7.7560,	-22.0985,	90.0
4,24,	30.205,	-7.6361,	-22.4150,	90.0
4,24,	34.801,	-7.6568,	-22.7037,	90.0
4,24,	39.434,	-7.7142,	-22.9903,	90.0
4,24,	44.030,	-7.7319,	-23.2796,	90.0
4,24,	48.622,	-7.7478,	-23.5692,	90.0
4,24,	53.254,	-7.7987,	-23.8472,	90.0
4,24,	57.833,	-7.8487,	-24.1254,	90.0
4,25,	2.469,	-7.8666,	-24.4349,	90.0
4,25,	7.076,	-7.9145,	-24.7136,	90.0
4,25,	11.694,	-7.9233,	-25.0047,	90.0
4,25,	16.331,	-7.9691,	-25.2839,	90.0
4,25,	20.938,	-7.9748,	-25.5755,	90.0
4,25,	25.521,	-7.9788,	-25.8674,	90.0
4,25,	30.165,	-8.0213,	-26.1473,	90.0
4,25,	34.756,	-8.0194,	-26.4302,	90.0
4,25,	39.336,	-8.0187,	-26.7228,	90.0
4,25,	43.986,	-8.0963,	-26.9814,	90.0
4,25,	48.575,	-8.0457,	-27.2678,	90.0
4,25,	53.226,	-8.1164,	-27.5076,	90.0
4,25,	57.799,	-8.0594,	-27.7847,	90.0
4,26,	2.441,	-8.0430,	-28.0496,	90.0
4,26,	7.031,	-8.0251,	-28.3147,	90.0
4,26,	11.619,	-8.0495,	-28.5676,	90.0
4,26,	16.249,	-8.0262,	-28.8234,	90.0
4,26,	20.848,	-8.0486,	-29.0766,	90.0
4,26,	25.495,	-7.9803,	-29.3546,	90.0
4,26,	30.077,	-7.9953,	-29.5888,	90.0
4,26,	34.715,	-7.9664,	-29.8451,	90.0
4,26,	39.303,	-7.9795,	-30.0796,	90.0
4,26,	43.937,	-7.9506,	-30.3458,	90.0
4,26,	48.513,	-7.9620,	-30.5805,	90.0
4,26,	53.156,	-7.9279,	-30.8372,	90.0
4,26,	57.742,	-7.9375,	-31.0722,	90.0
4,27,	2.390,	-7.9008,	-31.3291,	90.0
4,27,	6.968,	-7.9086,	-31.5643,	90.0
4,27,	11.615,	-7.8158,	-31.8140,	90.0
4,27,	16.174,	-7.8683,	-32.0277,	90.0
4,27,	20.815,	-7.8242,	-32.2752,	90.0
4,27,	25.403,	-7.8261,	-32.5010,	90.0
4,27,	30.044,	-7.7772,	-32.7389,	90.0
4,27,	34.676,	-7.7775,	-32.9649,	90.0
4,27,	39.259,	-7.7771,	-33.1910,	90.0
4,27,	43.893,	-7.7248,	-33.4291,	90.0
4,27,	48.484,	-7.7227,	-33.6553,	90.0
4,27,	53.142,	-7.7719,	-33.8697,	90.0
4,27,	57.714,	-7.6620,	-34.1100,	90.0
4,28,	2.343,	-7.6576,	-34.3365,	90.0
4,28,	6.935,	-7.6524,	-34.5630,	90.0

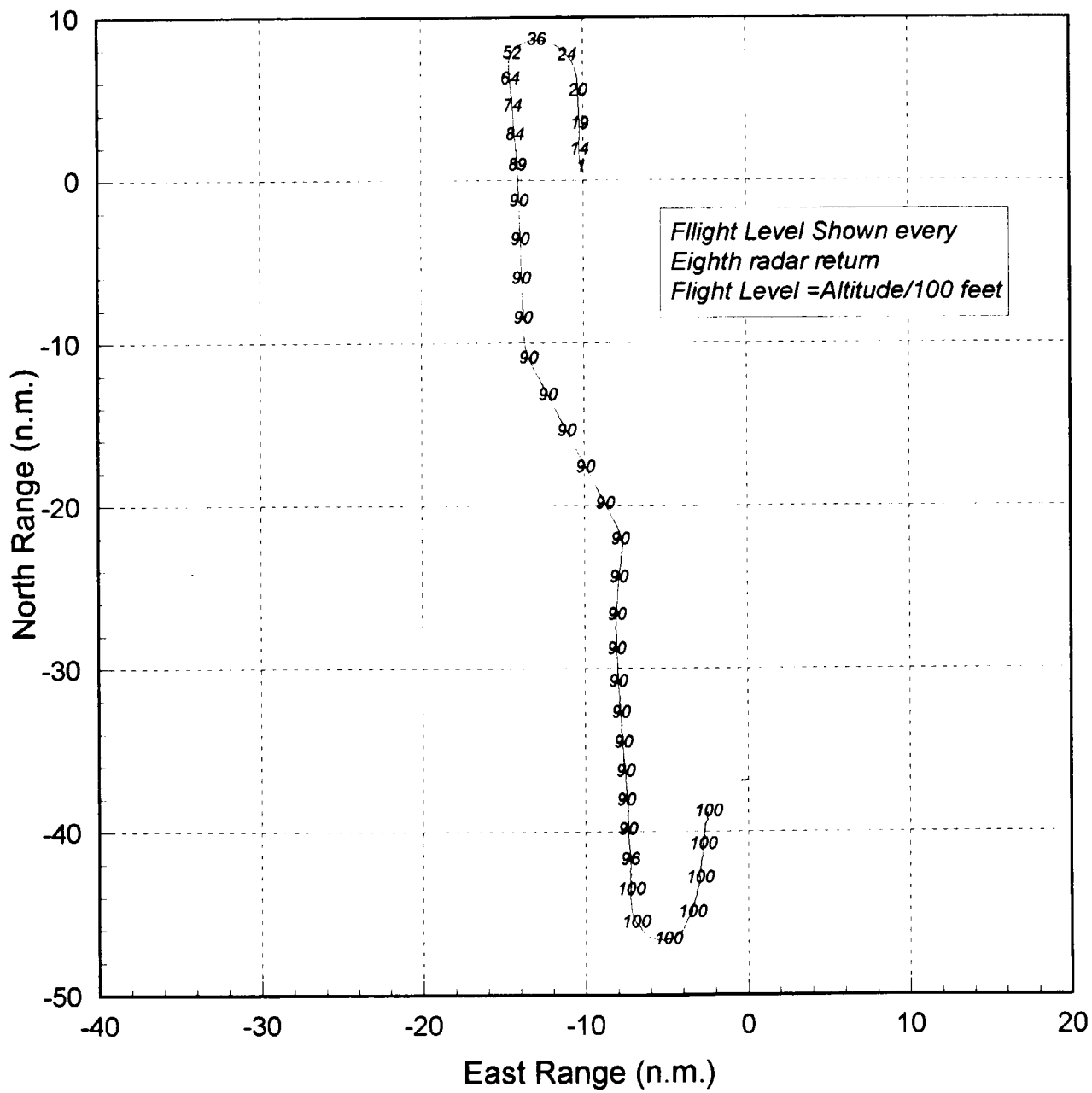
4, 28, 11.583,	-7.7000,	-34.7778,	90.0
4, 28, 16.155,	-7.6359,	-34.9966,	90.0
4, 28, 20.792,	-7.6288,	-35.2233,	90.0
4, 28, 25.387,	-7.6210,	-35.4501,	90.0
4, 28, 30.021,	-7.6125,	-35.6769,	90.0
4, 28, 34.606,	-7.5441,	-35.8958,	90.0
4, 28, 39.252,	-7.5340,	-36.1227,	90.0
4, 28, 43.834,	-7.5191,	-36.3301,	90.0
4, 28, 48.438,	-7.5076,	-36.5571,	90.0
4, 28, 53.087,	-7.4955,	-36.7841,	90.0
4, 28, 57.673,	-7.4806,	-37.0014,	90.0
4, 29, 2.322,	-7.4652,	-37.2187,	90.0
4, 29, 6.911,	-7.4510,	-37.4459,	90.0
4, 29, 11.564,	-7.4342,	-37.6633,	90.0
4, 29, 16.134,	-7.4168,	-37.8808,	90.0
4, 29, 20.593,	-7.4591,	-38.0967,	90.0
4, 29, 25.404,	-7.3819,	-38.3256,	90.0
4, 29, 29.994,	-7.3643,	-38.5529,	90.0
4, 29, 34.451,	-7.3443,	-38.7705,	90.0
4, 29, 39.084,	-7.3852,	-38.9867,	90.0
4, 29, 43.839,	-7.3660,	-39.2142,	90.0
4, 29, 48.302,	-7.3461,	-39.4417,	90.0
4, 29, 53.029,	-7.3256,	-39.6693,	90.0
4, 29, 57.541,	-7.3655,	-39.8856,	90.0
4, 30, 2.306,	-7.3458,	-40.1231,	90.0
4, 30, 6.775,	-7.3235,	-40.3508,	91.0
4, 30, 11.485,	-7.3005,	-40.5785,	91.0
4, 30, 16.001,	-7.2787,	-40.8161,	92.0
4, 30, 20.599,	-7.2543,	-41.0438,	93.0
4, 30, 25.237,	-7.2328,	-41.2913,	94.0
4, 30, 29.841,	-7.2071,	-41.5191,	95.0
4, 30, 34.421,	-7.2430,	-41.7260,	96.0
4, 30, 39.051,	-7.2162,	-41.9539,	96.0
4, 30, 43.694,	-7.1888,	-42.1818,	97.0
4, 30, 48.266,	-7.2292,	-42.4184,	98.0
4, 30, 52.909,	-7.2007,	-42.6464,	98.0
4, 30, 57.480,	-7.2357,	-42.8534,	99.0
4, 31, 2.113,	-7.2062,	-43.0815,	99.0
4, 31, 6.751,	-7.1794,	-43.3292,	100.0
4, 31, 11.331,	-7.2170,	-43.5561,	100.0
4, 31, 15.970,	-7.1890,	-43.8040,	100.0
4, 31, 20.549,	-7.2263,	-44.0310,	100.0
4, 31, 25.201,	-7.1988,	-44.2888,	100.0
4, 31, 29.787,	-7.1706,	-44.5466,	100.0
4, 31, 34.432,	-7.1416,	-44.8044,	100.0
4, 31, 39.016,	-7.1087,	-45.0425,	100.0
4, 31, 43.653,	-7.0072,	-45.3013,	100.0
4, 31, 48.225,	-6.9026,	-45.5500,	100.0
4, 31, 52.861,	-6.6532,	-45.7993,	100.0
4, 31, 57.505,	-6.5408,	-46.0175,	100.0
4, 32, 2.093,	-6.3548,	-46.2353,	100.0
4, 32, 6.743,	-6.2289,	-46.3735,	100.0
4, 32, 11.325,	-5.8143,	-46.5281,	100.0
4, 32, 15.924,	-5.6049,	-46.5941,	100.0
4, 32, 20.563,	-5.2462,	-46.6258,	100.0
4, 32, 25.198,	-4.9526,	-46.5875,	100.0
4, 32, 29.775,	-4.6567,	-46.5175,	100.0
4, 32, 34.411,	-4.4274,	-46.3792,	100.0
4, 32, 39.004,	-4.1958,	-46.1999,	100.0
4, 32, 43.585,	-3.9626,	-45.9796,	100.0
4, 32, 48.224,	-3.8709,	-45.7365,	100.0
4, 32, 52.856,	-3.7792,	-45.4833,	100.0
4, 32, 57.442,	-3.6182,	-45.2255,	100.0
4, 33, 2.073,	-3.4579,	-44.9572,	100.0
4, 33, 6.669,	-3.4372,	-44.6880,	100.0
4, 33, 11.312,	-3.3491,	-44.4340,	100.0
4, 33, 15.910,	-3.2611,	-44.1698,	100.0
4, 33, 20.553,	-3.1731,	-43.8955,	100.0
4, 33, 25.187,	-3.1544,	-43.6361,	100.0
4, 33, 29.766,	-3.0684,	-43.3716,	100.0

U25

I-4

4,33,	34.373,	-2.9832,	-43.1069,	100.0
4,33,	39.002,	-2.9653,	-42.8475,	100.0
4,33,	43.631,	-3.0119,	-42.5736,	100.0
4,33,	48.204,	-2.9294,	-42.3288,	100.0
4,33,	52.834,	-2.9114,	-42.0694,	100.0
4,33,	57.444,	-2.8928,	-41.8000,	100.0
4,34,	2.082,	-2.8111,	-41.5450,	100.0
4,34,	6.656,	-2.7942,	-41.2956,	100.0
4,34,	11.297,	-2.8403,	-41.0418,	100.0
4,34,	15.892,	-2.7591,	-40.7768,	100.0
4,34,	20.528,	-2.7422,	-40.5273,	100.0
4,34,	25.109,	-2.6636,	-40.2820,	100.0
4,34,	29.748,	-2.7085,	-40.0285,	100.0
4,34,	34.332,	-2.6293,	-39.7632,	100.0
4,34,	38.966,	-2.6128,	-39.5137,	100.0
4,34,	43.595,	-2.4758,	-39.2720,	100.0
4,34,	48.225,	-2.5199,	-39.0187,	100.0
4,34,	52.797,	-2.4443,	-38.7730,	100.0
4,34,	57.441,	-2.4286,	-38.5235,	100.0

WESTAIR 233 Ground Track March 06 1998



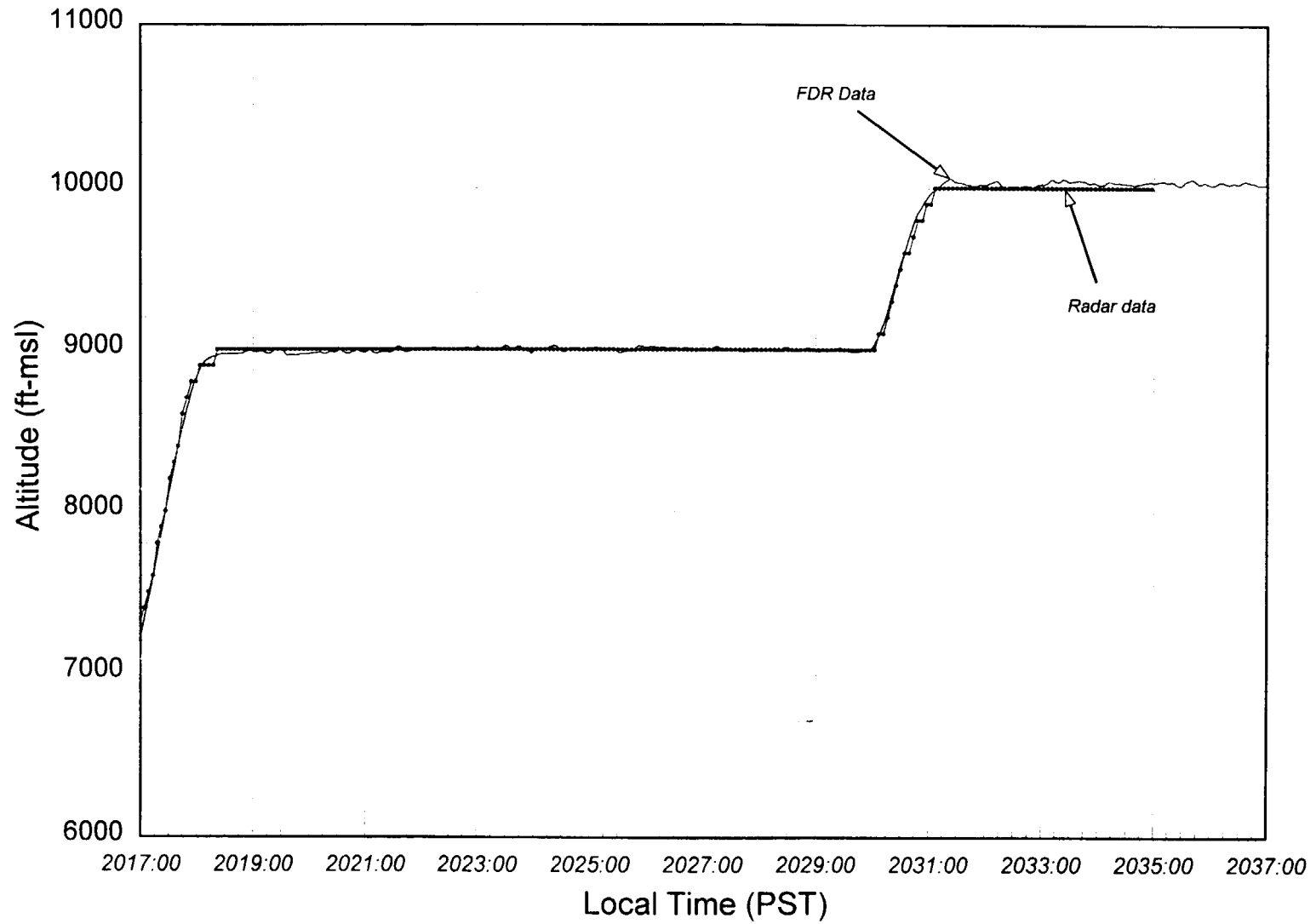
179

9-F

ATTACHMENTS Section II

FDR/Radar Data Altitude Comparison

**FDR and Radar Altitude Comparison
Westair Flight 233
March 5, 1998**



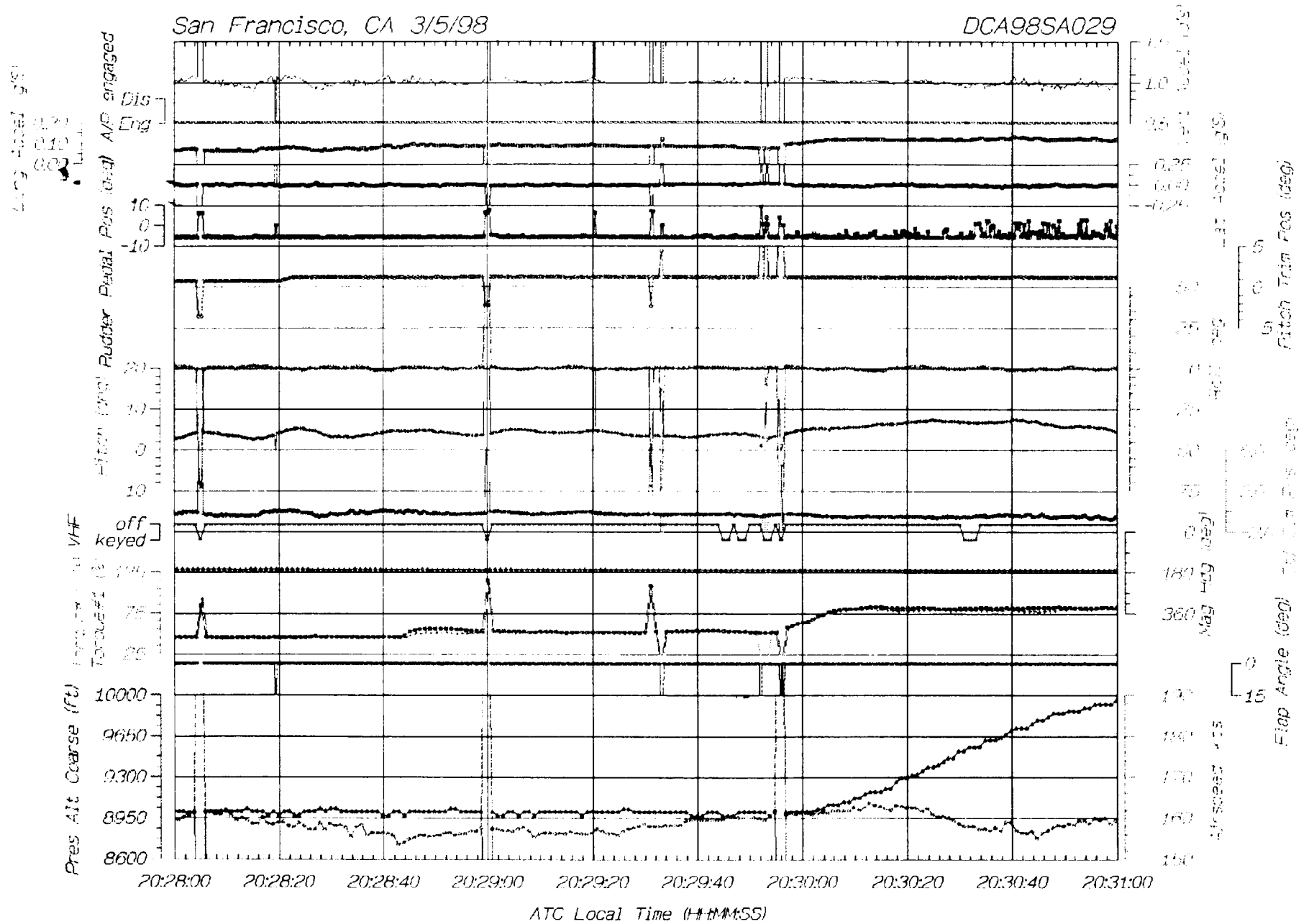
ATTACHMENTS Section III

FDR Data

Westair EMB-120

San Francisco, CA 3/5/98

DCA98SA029



Airspd3 3minutes

Revised: May 6, 1998

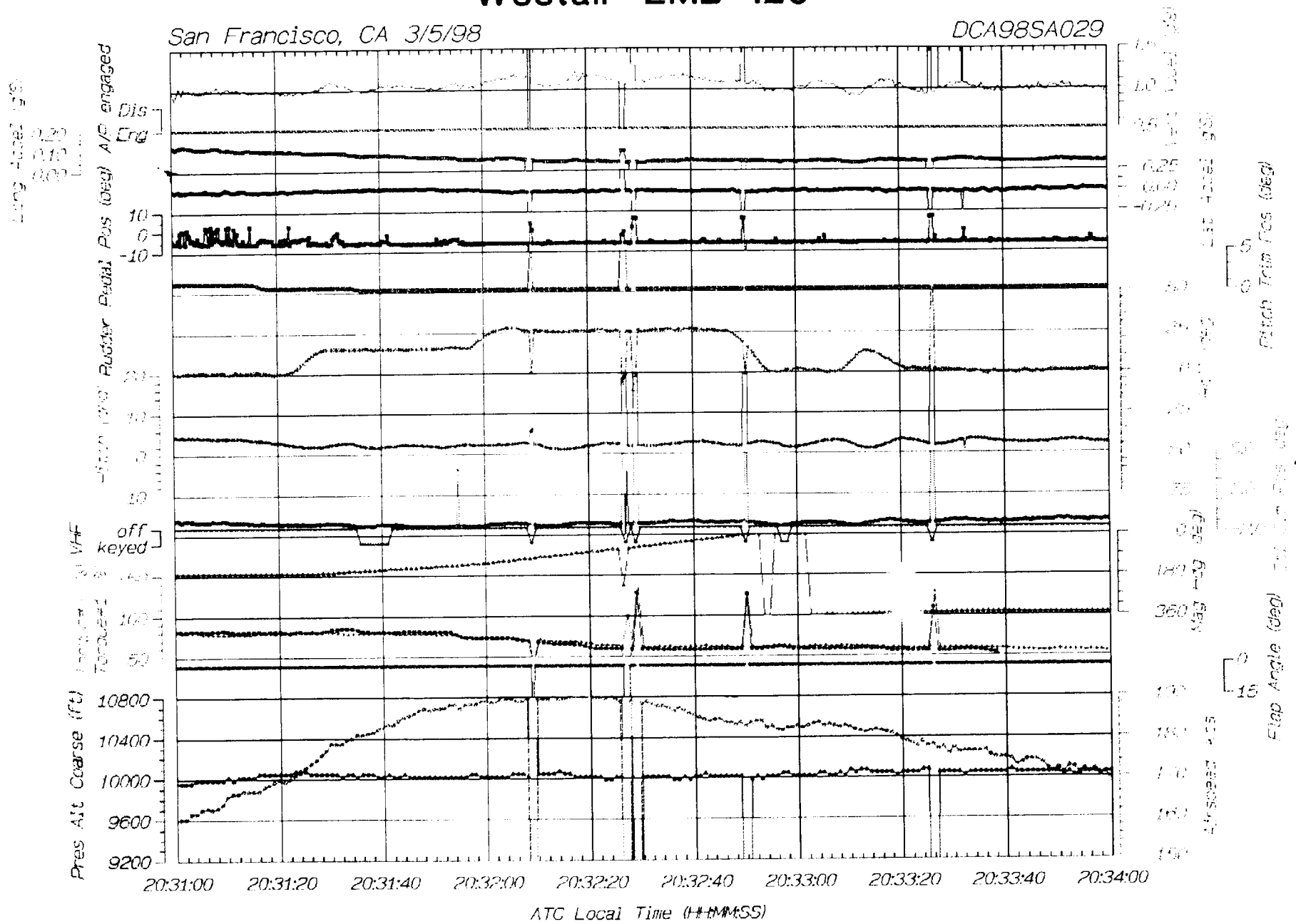
National Transportation Safety Board

1-III

Westair EMB-120

San Francisco, CA 3/5/98

DCA98SA029



020

Long Level (g)

0.20
0.10
0.00

VHF
off
keyed

Indicated Airspeed (IAS)

Pres Alt Coarse (ft)

20:31:00 20:31:20 20:31:40 20:32:00 20:32:20 20:32:40 20:33:00 20:33:20 20:33:40 20:34:00

ATC Local Time (H:MM:SS)

100
110
120
130
140
150
160
170
180
360
Mag (deg)

0
10
20
30
40
50
60
70
80
90
100
110
120
130
140
150
160
170
180
360
Mag (deg)

0
10
20
30
40
50
60
70
80
90
100
110
120
130
140
150
160
170
180
360
Mag (deg)

0
10
20
30
40
50
60
70
80
90
100
110
120
130
140
150
160
170
180
360
Mag (deg)

0
10
20
30
40
50
60
70
80
90
100
110
120
130
140
150
160
170
180
360
Mag (deg)

III-2

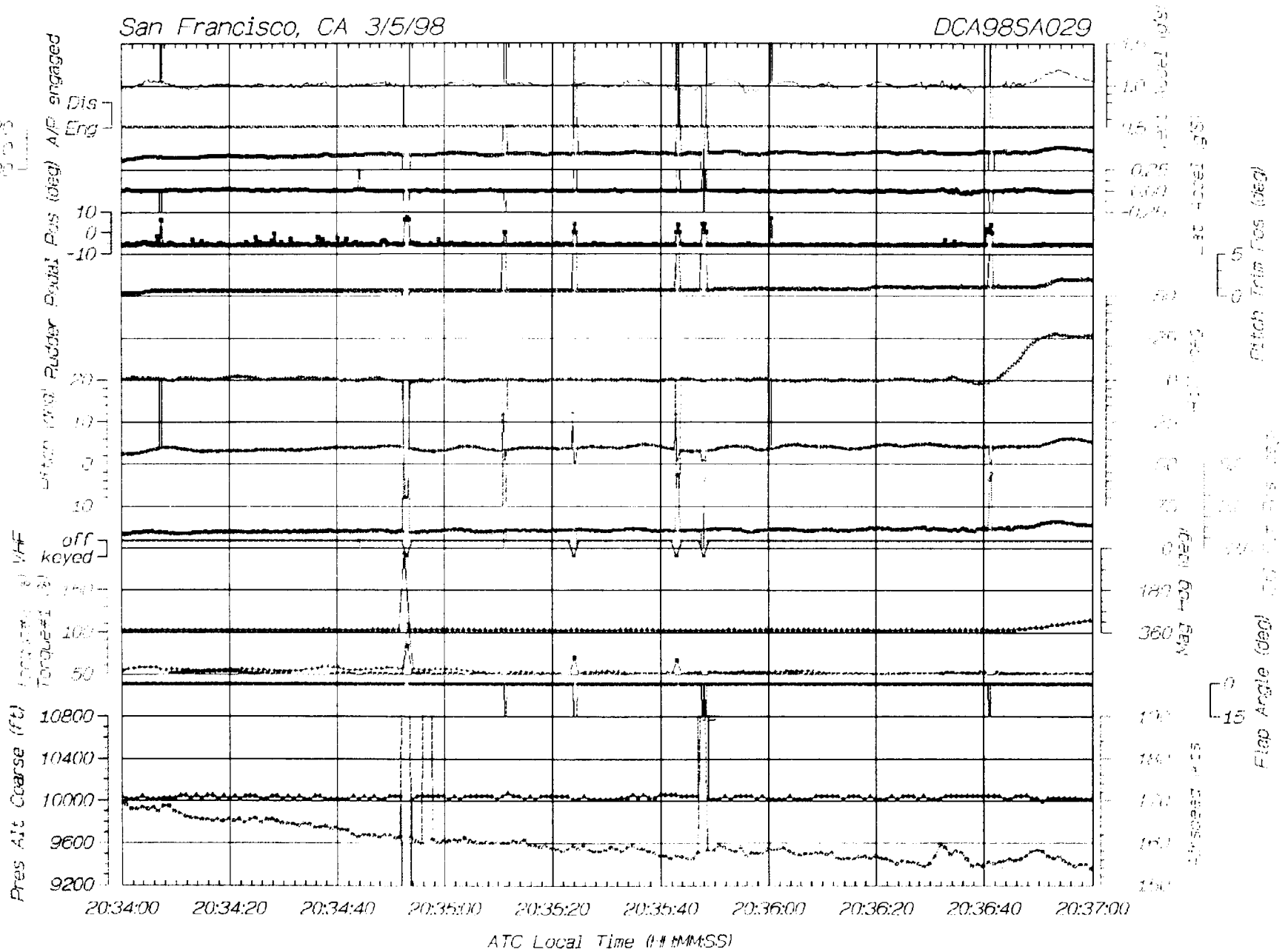
Airspd2 3 minutes
Created: May 06, 1998

National Transportation Safety Board

Westair EMB-120

San Francisco, CA 3/5/98

DCA98SA029



Airspd1 3 minutes
Revised: May 06, 1998

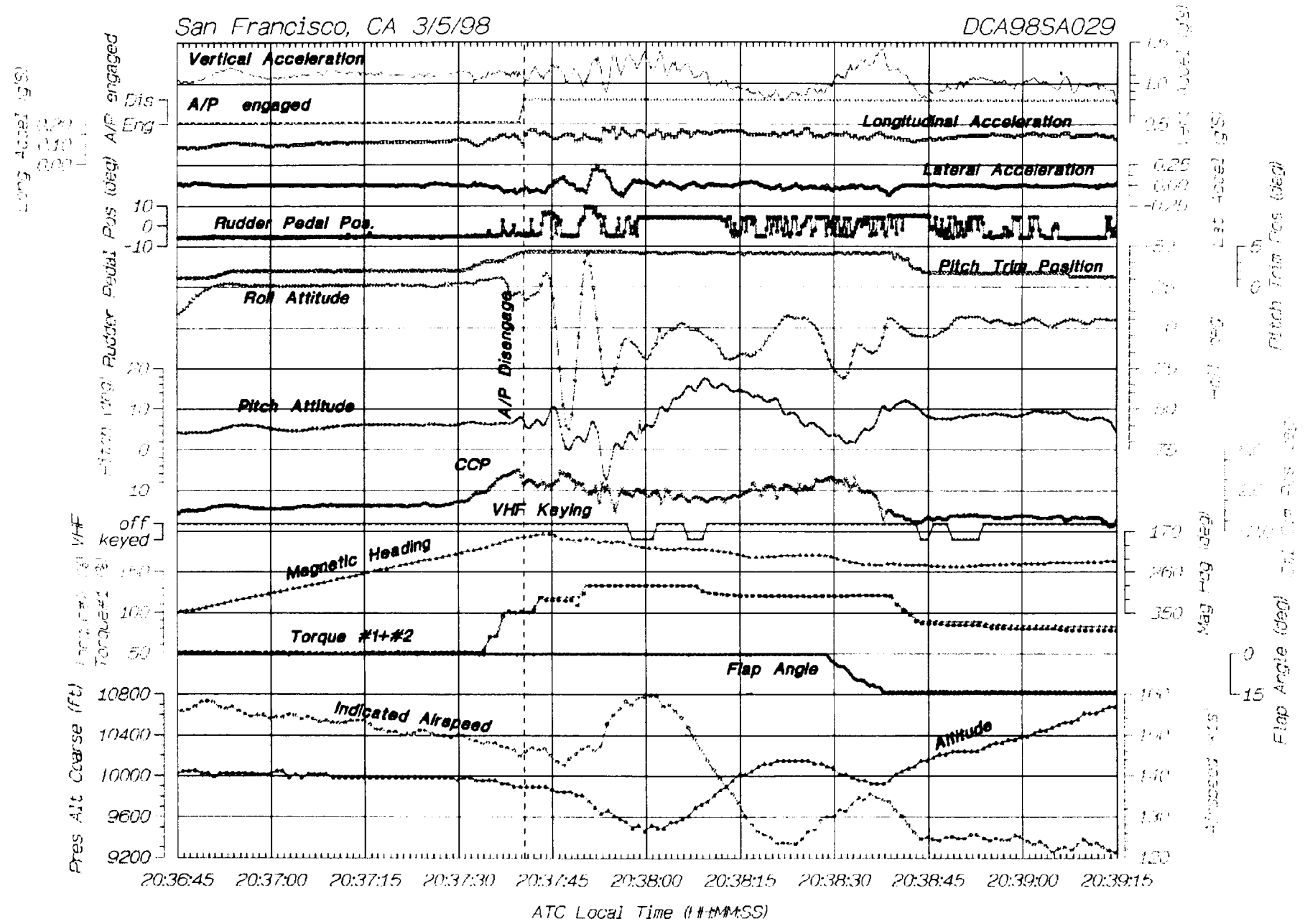
National Transportation Safety Board

III-3

Westair EMB-120

San Francisco, CA 3/5/98

DCA98SA029



Plot1, 160 seconds

Revised: April 23, 1998

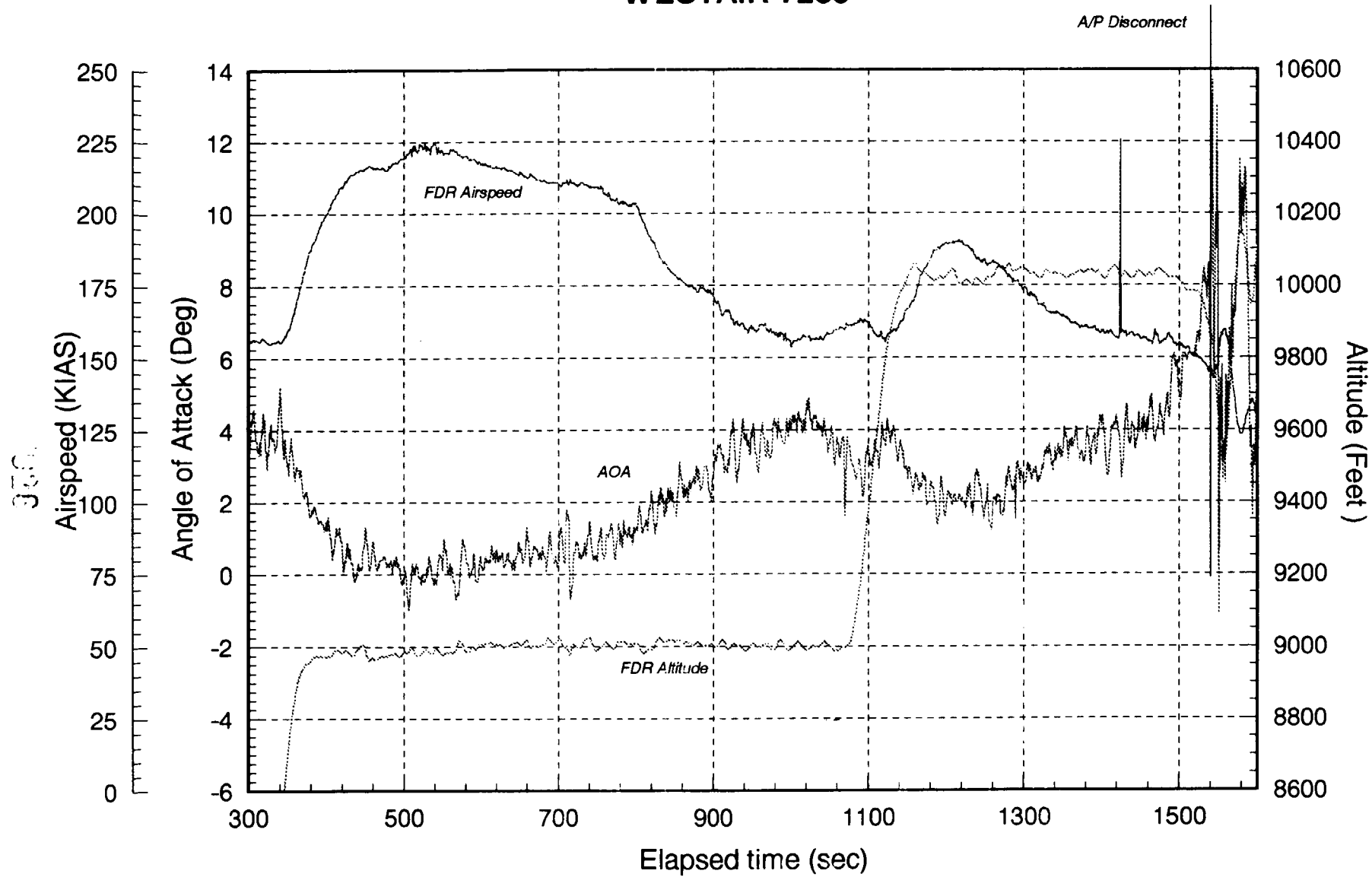
National Transportation Safety Board

A-III

ATTACHMENTS Section IV

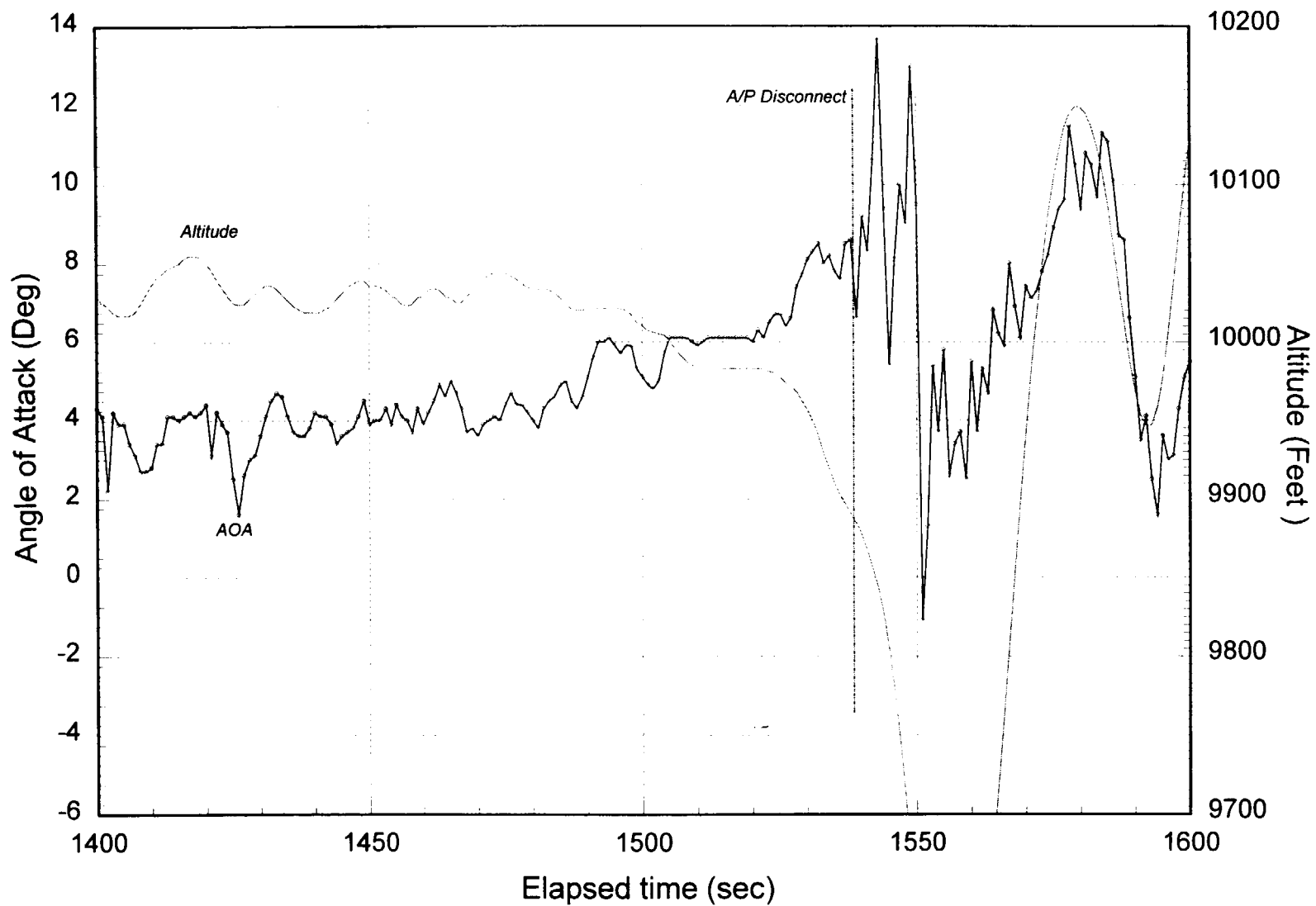
Angle of Attack
Indicated Airspeed

Calculated Angle of Attack WESTAIR 7233



14.1

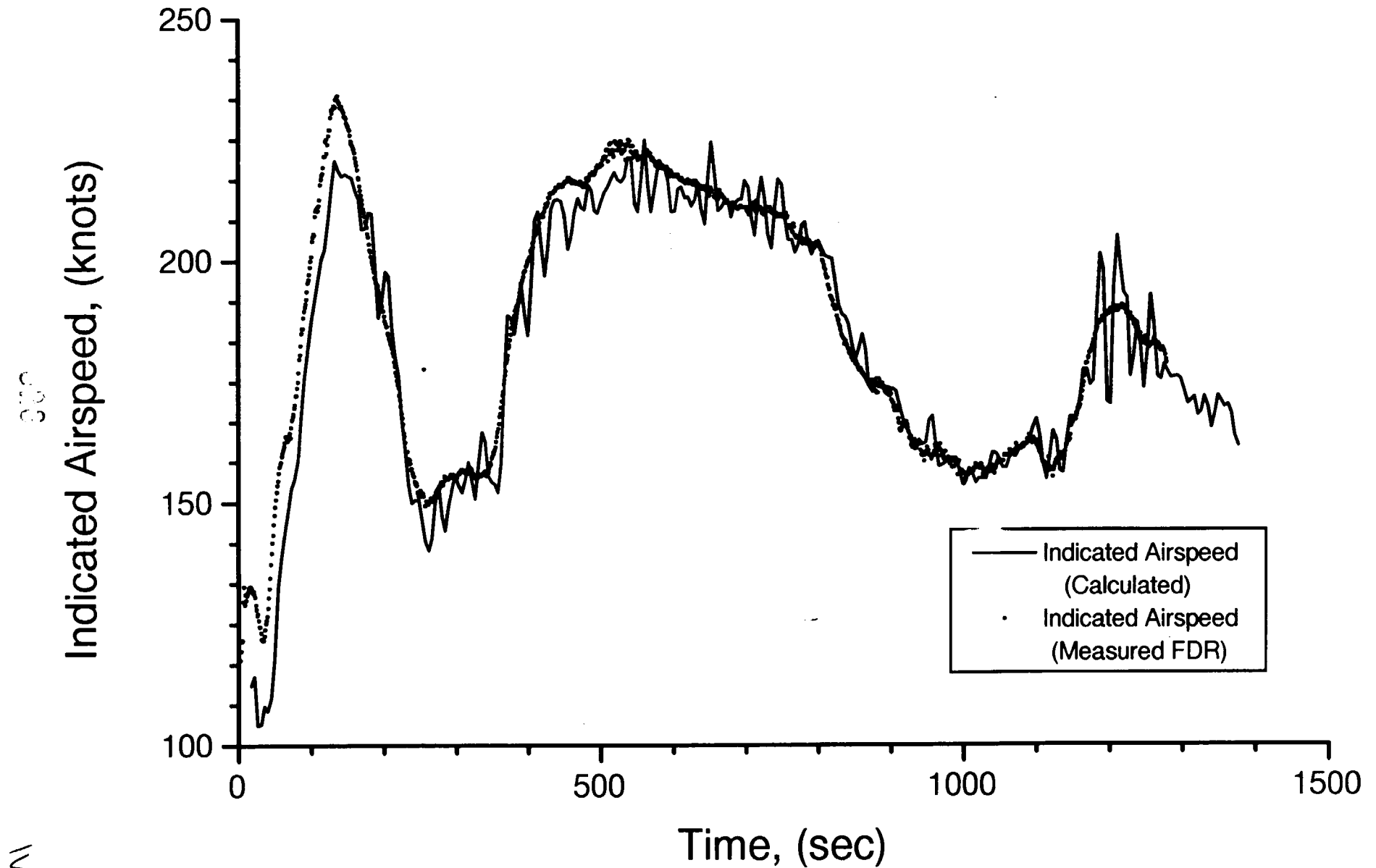
Calculated Angle of Attack WESTAIR 233



027

W-2

Calculated and Measured Indicated Airspeed WESTAIR Flight 233

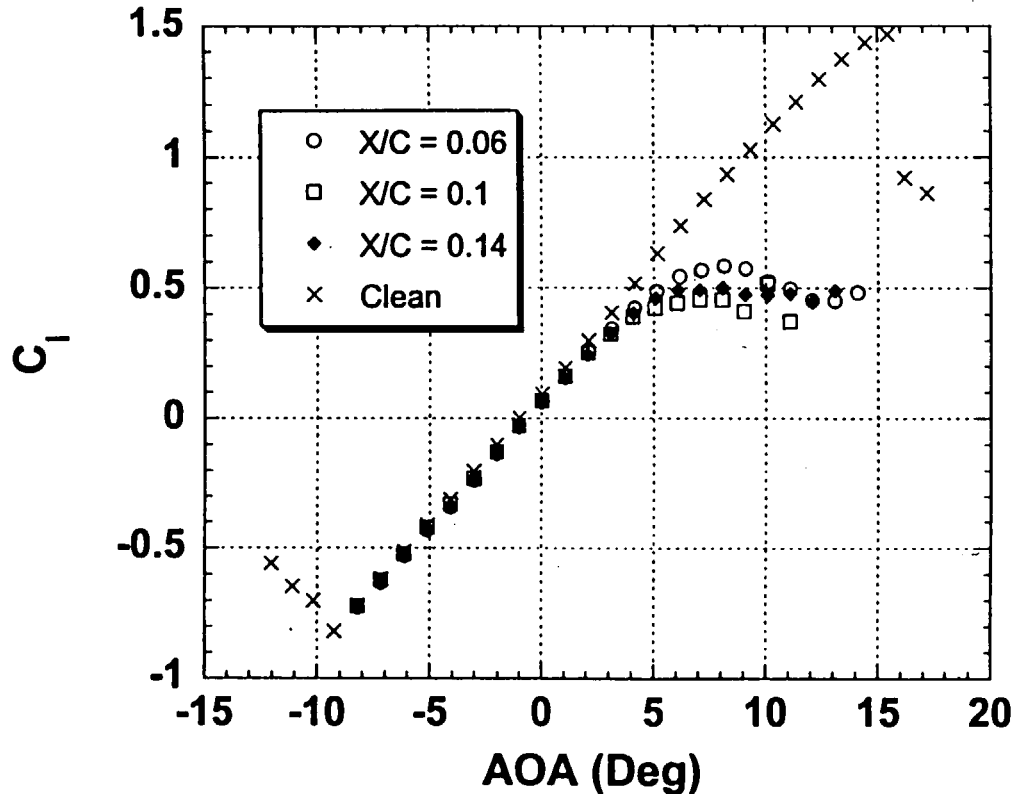


14-3

ATTACHMENTS Section V

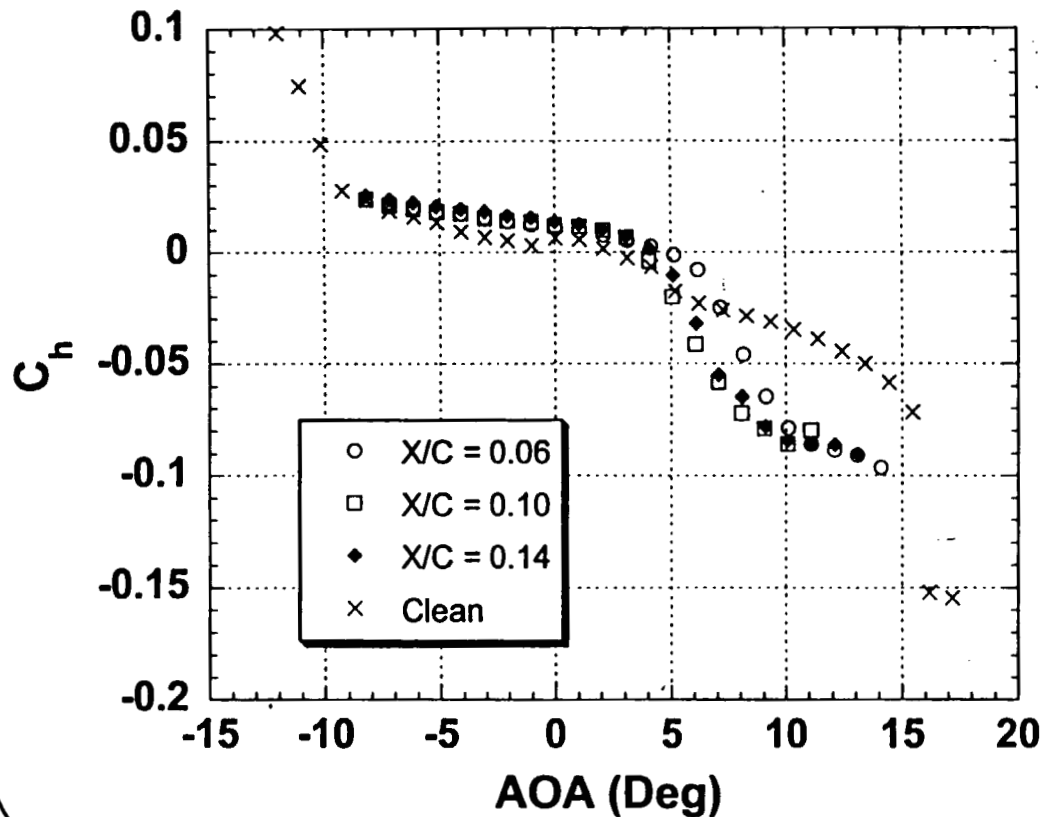
FAA/University of Illinois Data

Effect of Ice Ridge Location on Lift Coefficients



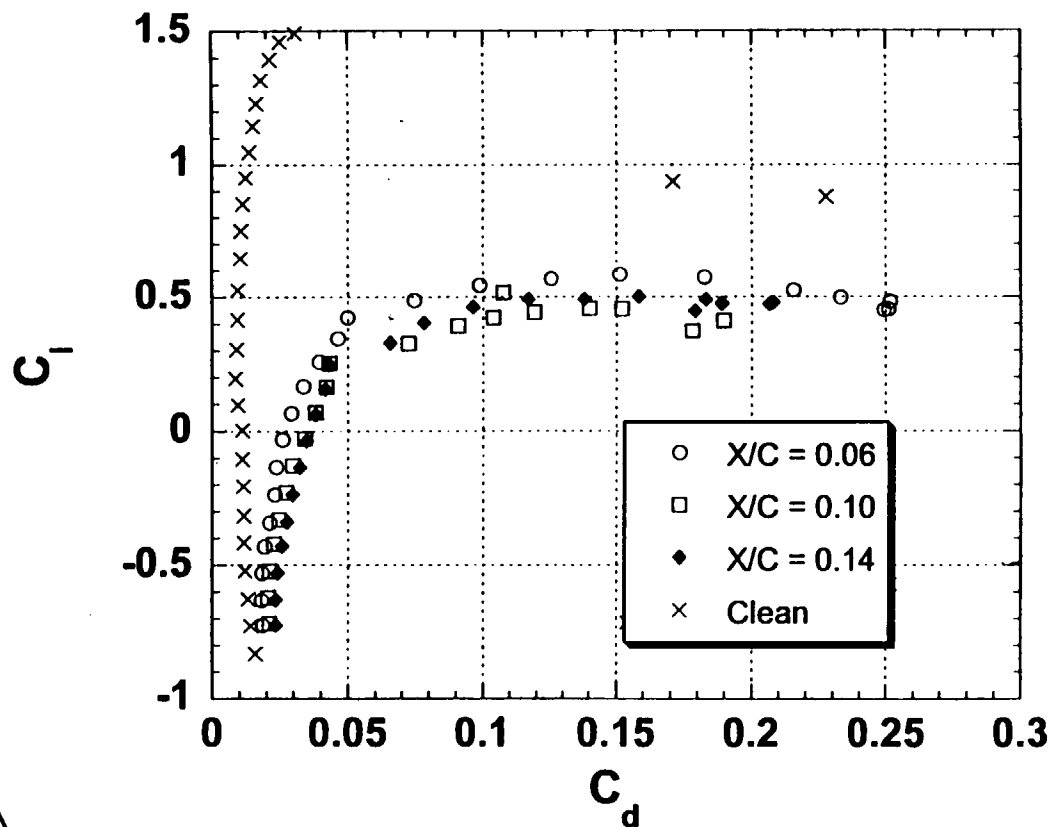
- **0.15" forward facing quarter round on upper surface.**
- **0° flap deflection**
- **Re = 1.8×10^6**
- **Boundary-layer trip at $x/c = 0.05$, upper and lower surface**

Effect of Ice Ridge Location on Flap Hinge Moment Coefficients



- 0.15" forward facing quarter round on upper surface.
- 0° flap deflection
- $Re = 1.8 \times 10^6$
- Boundary-layer trip at $x/c = 0.05$, upper and lower surface

Effect of Ice Ridge Location on Drag



- 0.15" forward facing quarter round on upper surface.
- 0° flap deflection
- $Re = 1.8 \times 10^6$
- Boundary-layer trip at $x/c = 0.05$, upper and lower surface

ATTACHMENTS Section VI

NASA Testing Results
LEWICE Results
IRT Ice Shapes
IRT Drag Measurements

LEWICE Results

	case#	Lower x Limit (in)	Upper x Limit (in)
0	1	3.75	0.25
1	5	4.50	0.25
2	9	2.25	0.75
3	13	3.50	0.50
4	17	3.75	0.25
5	21	3.50	0.25
6	25	3.75	0.75
7	2	12.00	1.25
8	3	12.00	1.00
9	6	13.50	1.00
10	7	13.00	0.50
11	10	7.00	2.00
12	11	7.00	1.50
13	14	11.50	1.50
14	15	11.00	1.00
15	18	11.50	1.00
16	19	11.50	0.50
17	22	11.50	0.75
18	23	11.50	0.75
19	26	12.00	1.25
20	27	11.50	1.00
21	4	18.50	2.00
22	8	20.00	1.00
23	12	16.00	3.00
24	16	18.00	2.00
25	20	18.50	1.50
26	24	18.50	1.50
27	28	18.50	1.50

20 μ, LWC = 0.8

LWC = 0.8

LWC = 0.52

LWC = 0.8

LWC = 0.52

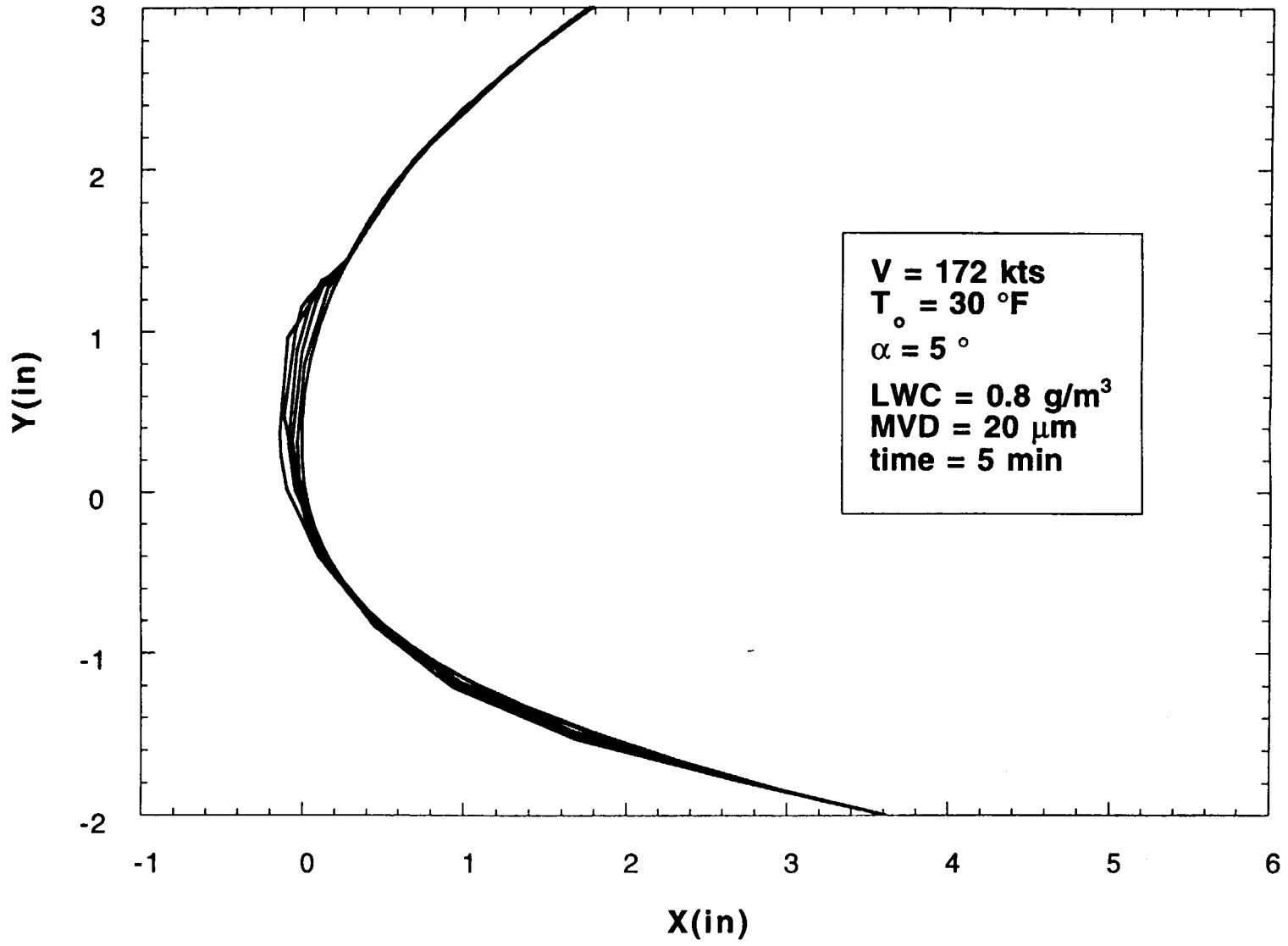
40 μ

70 μ, LWC = 0.58

U35

VI-1

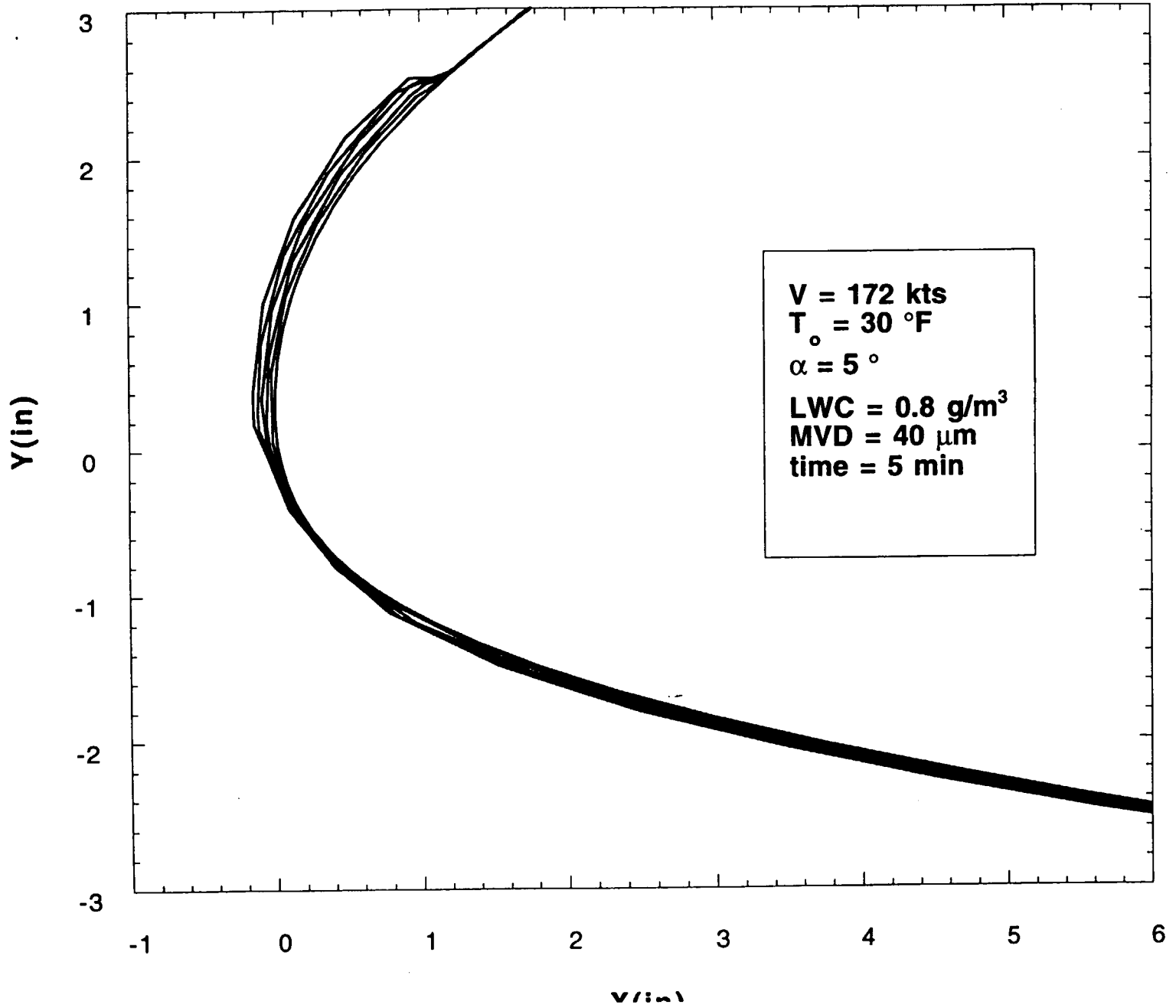
**Ice Shapes for Tunnel Conditions
Case #1**



086

V1-2

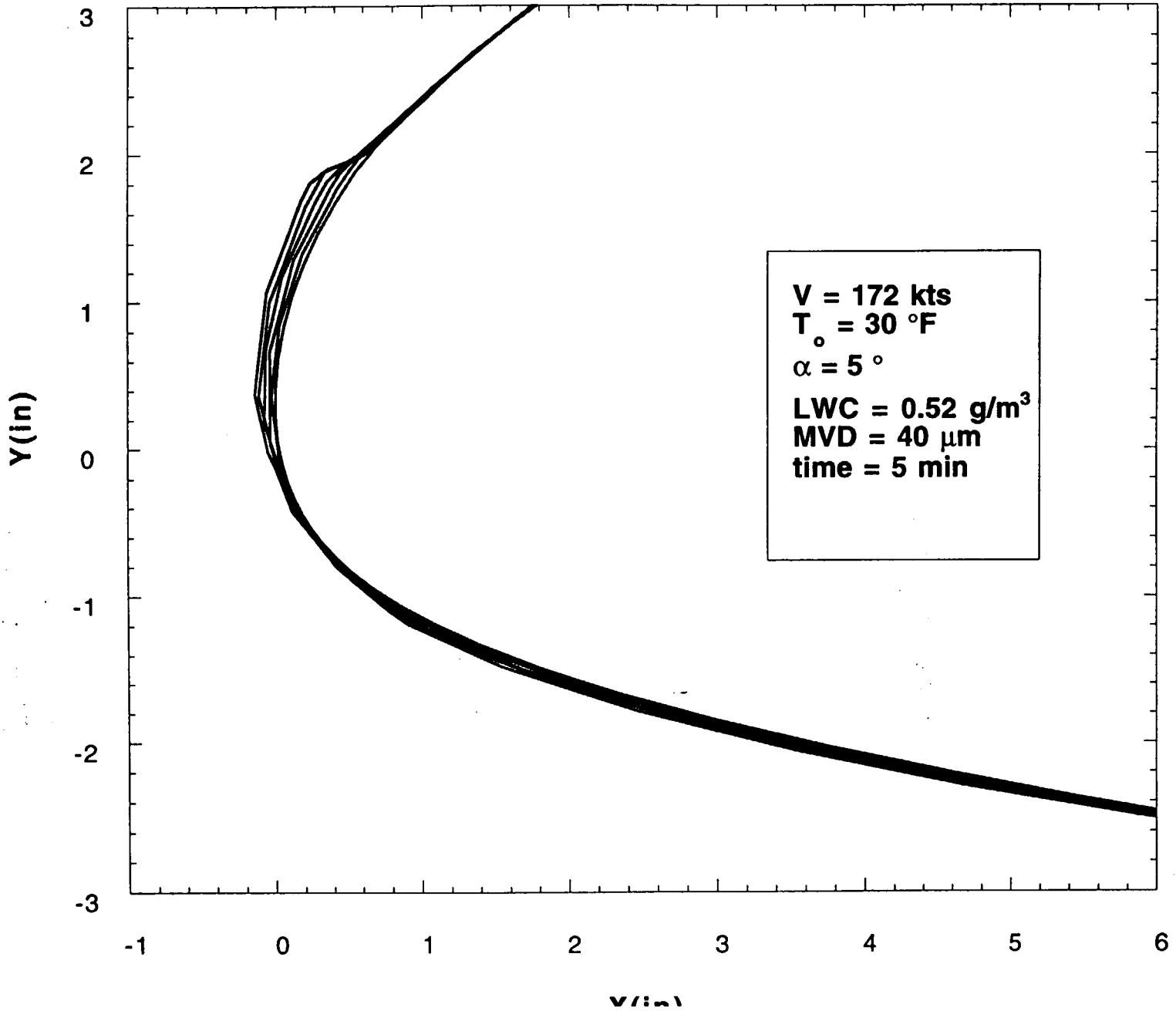
**Ice Shapes for Tunnel Conditions
Case #2**



0.87

M-3

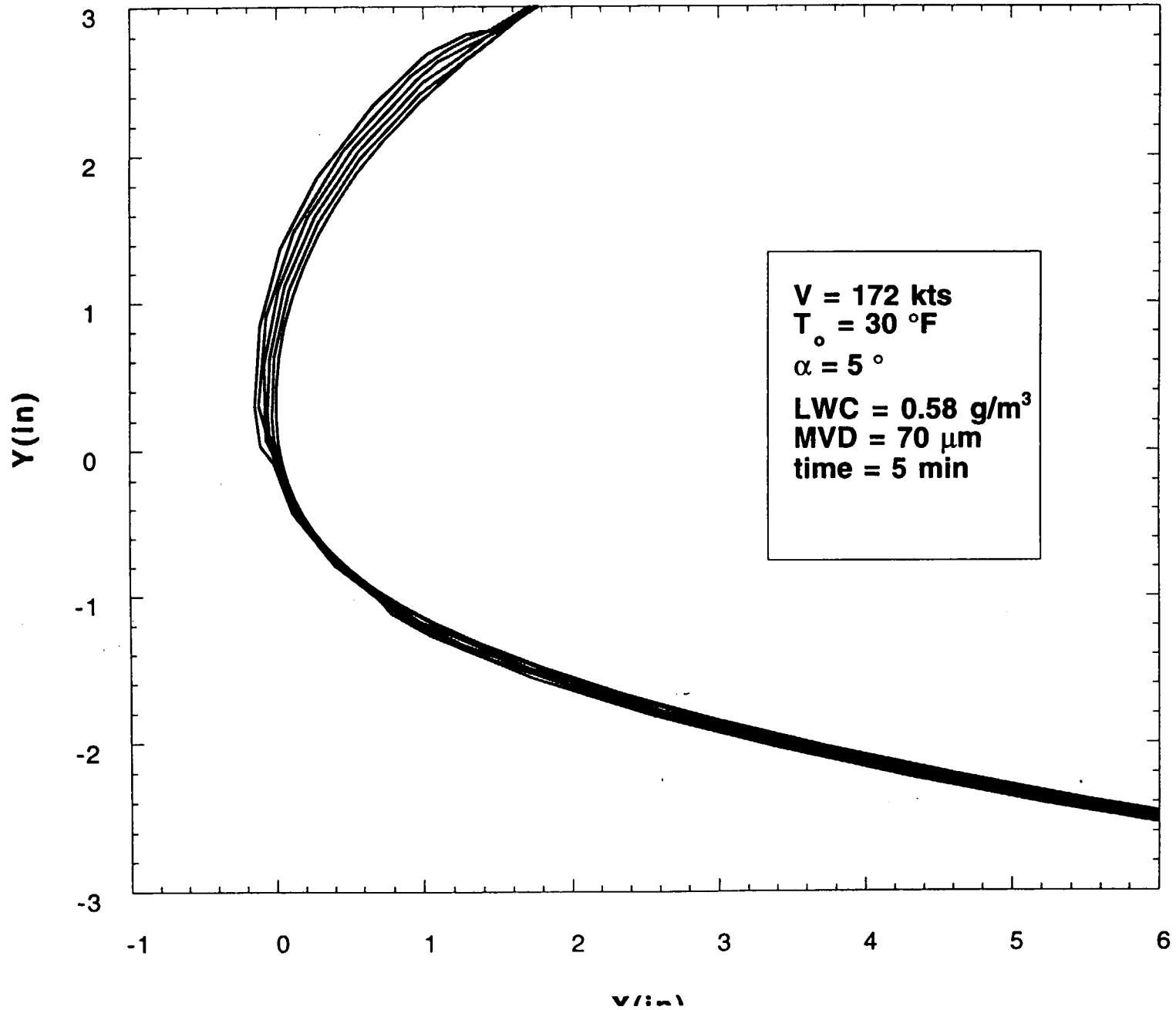
**Ice Shapes for Tunnel Conditions
Case #3**



056

1-4

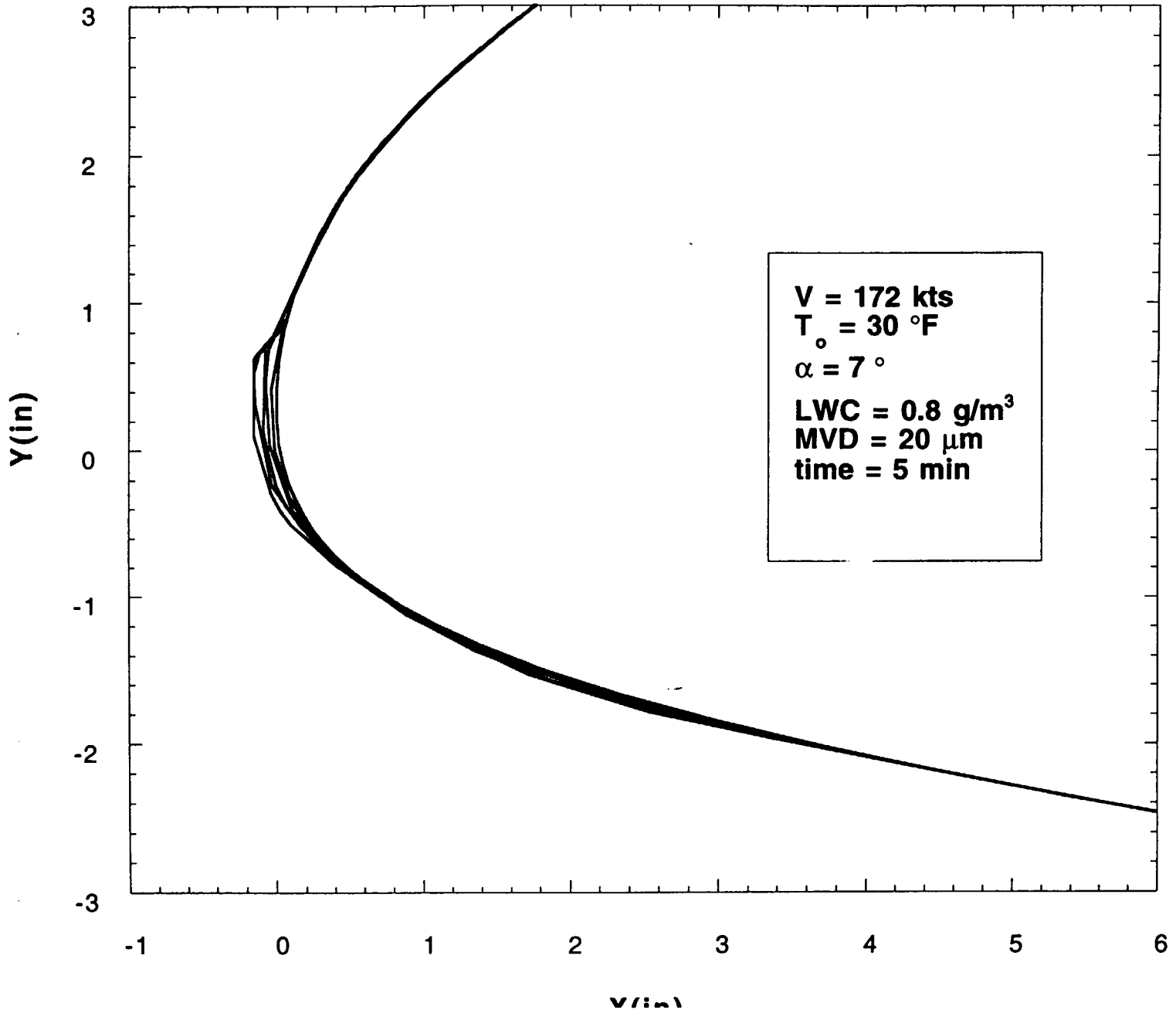
Ice Shapes for Tunnel Conditions Case #4



980

W-5

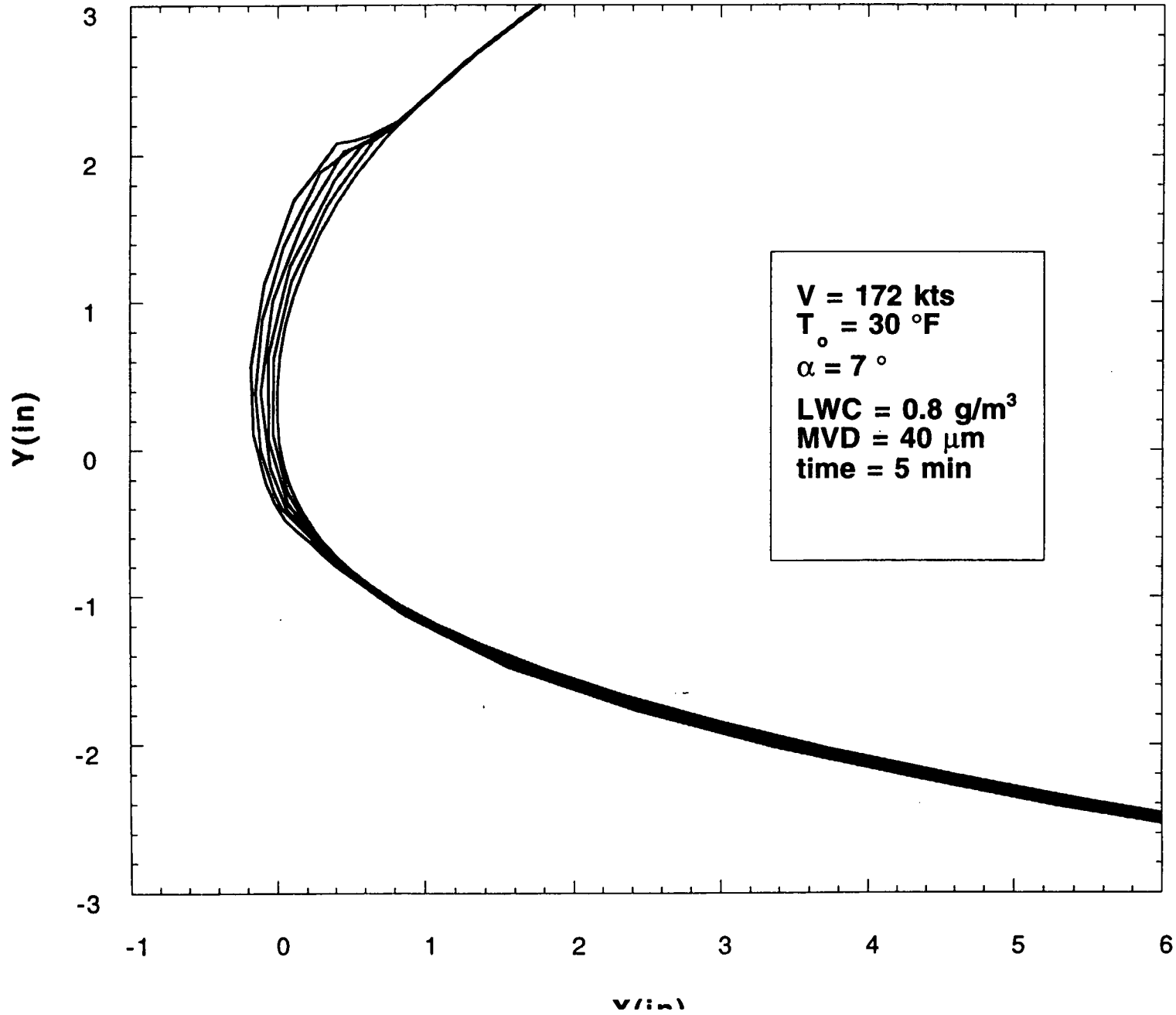
**Ice Shapes for Tunnel Conditions
Case #5**



040

9-16

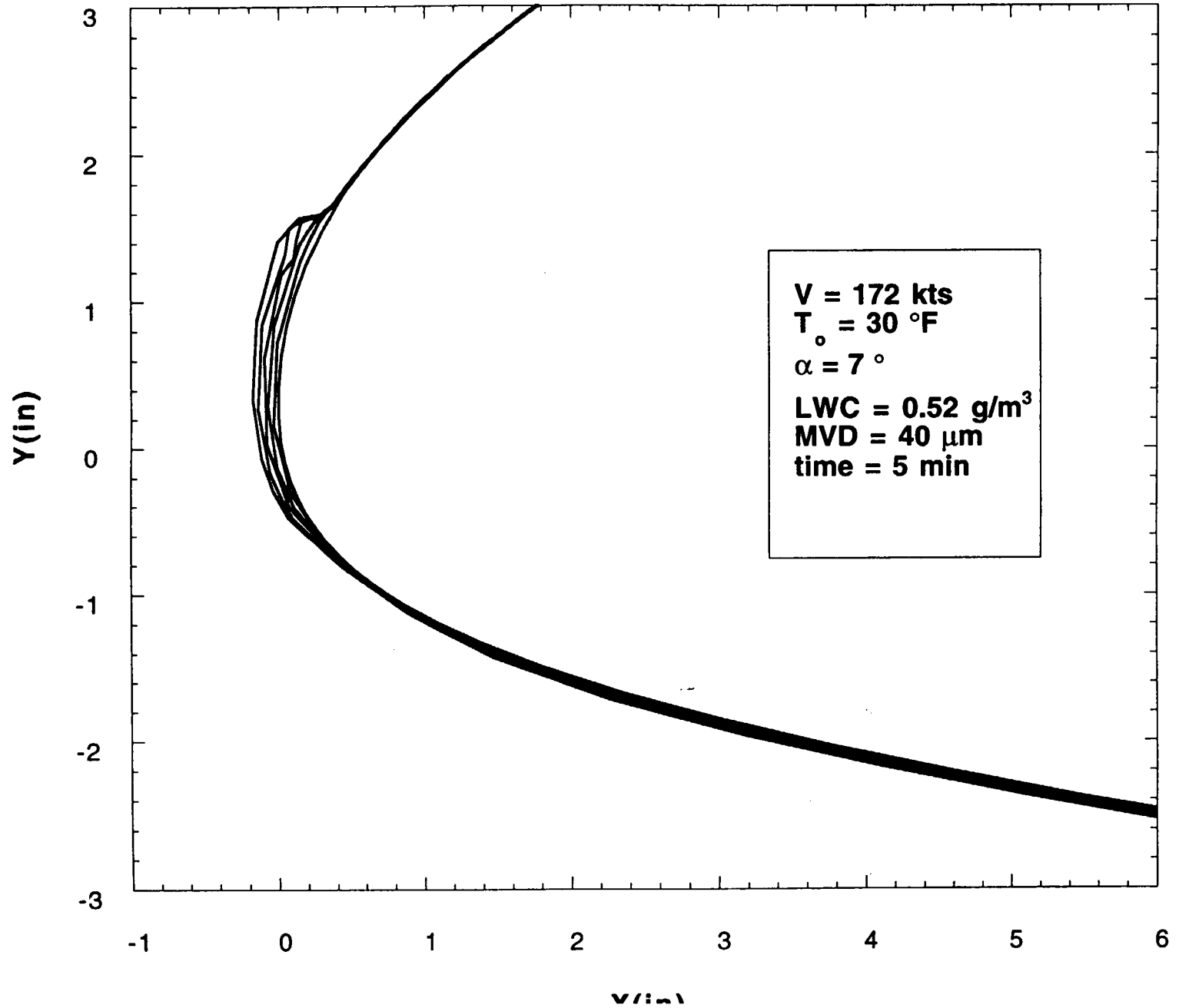
**Ice Shapes for Tunnel Conditions
Case #6**



041

W-7

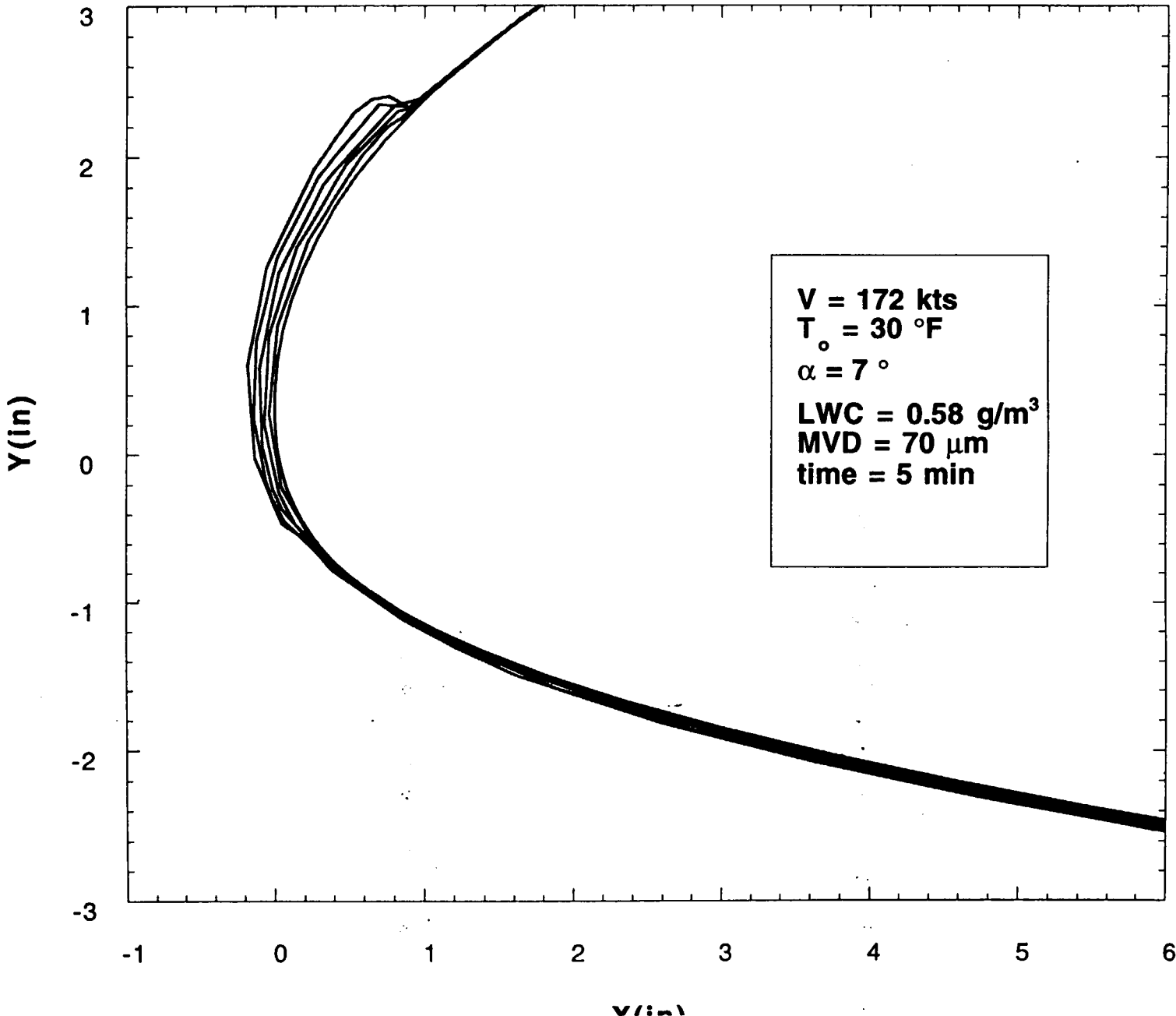
**Ice Shapes for Tunnel Conditions
Case #7**



U42

V1-8

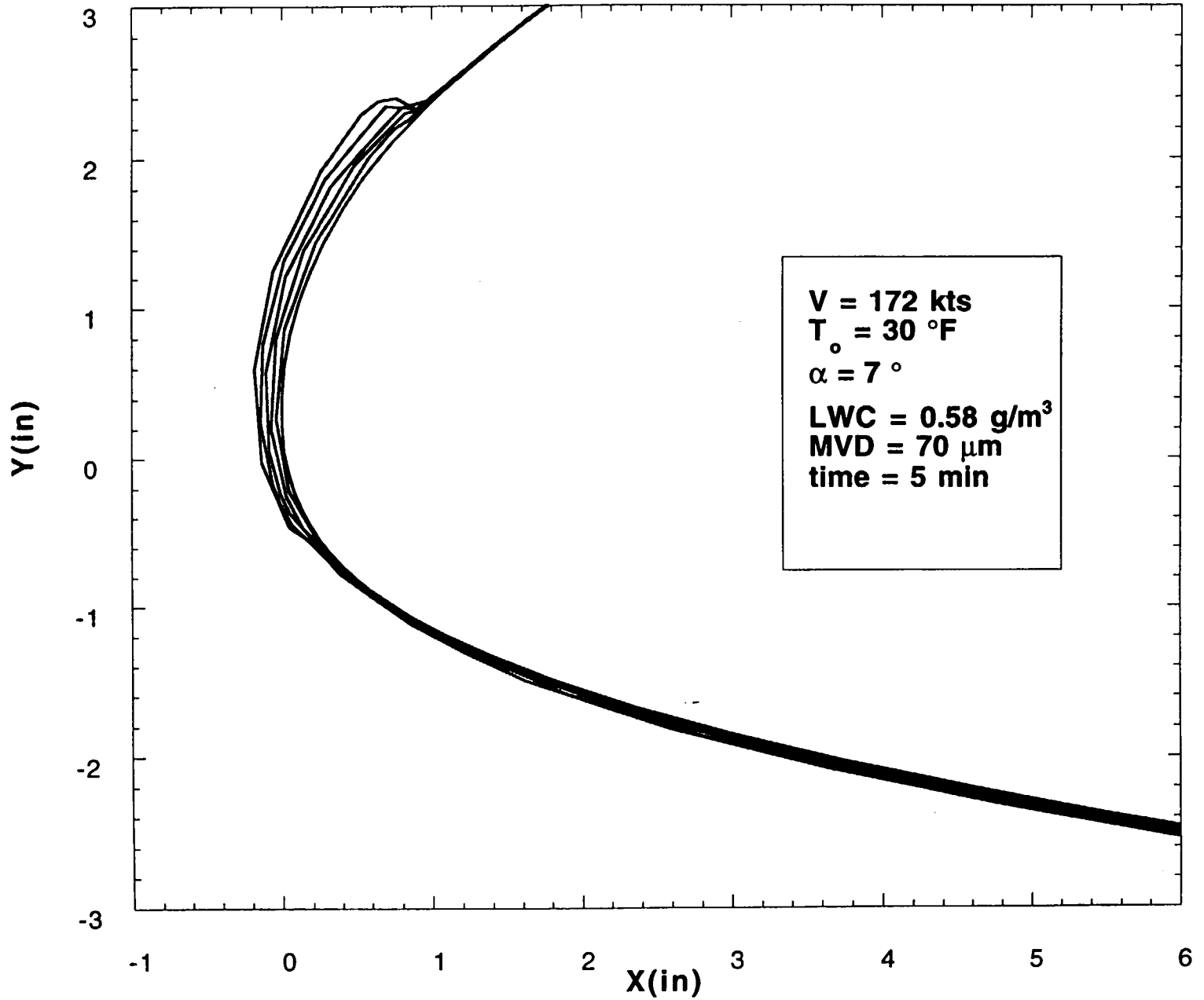
**Ice Shapes for Tunnel Conditions
Case #8**



043

11-9

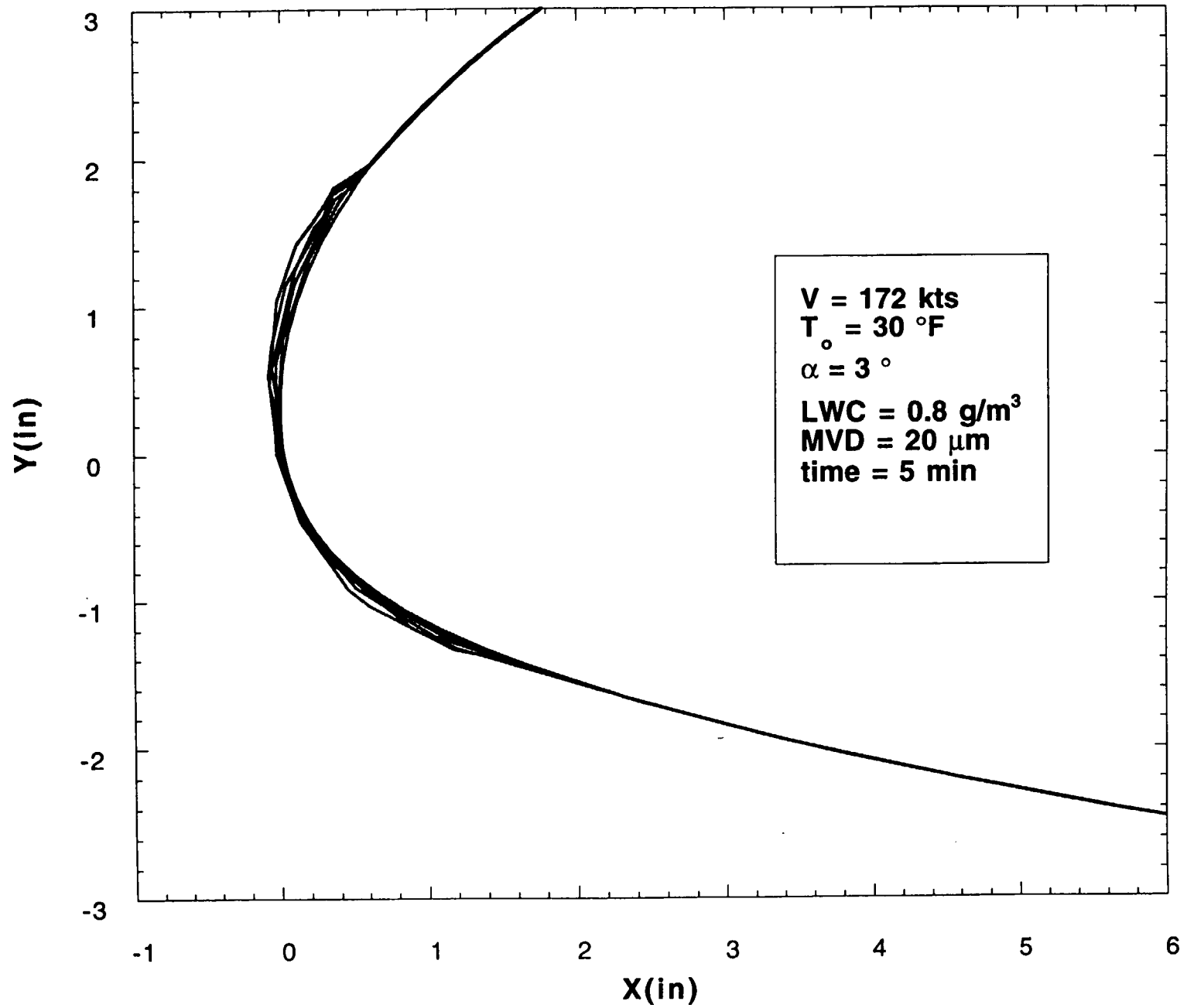
**Ice Shapes for Tunnel Conditions
Case #8**



044

VI-10

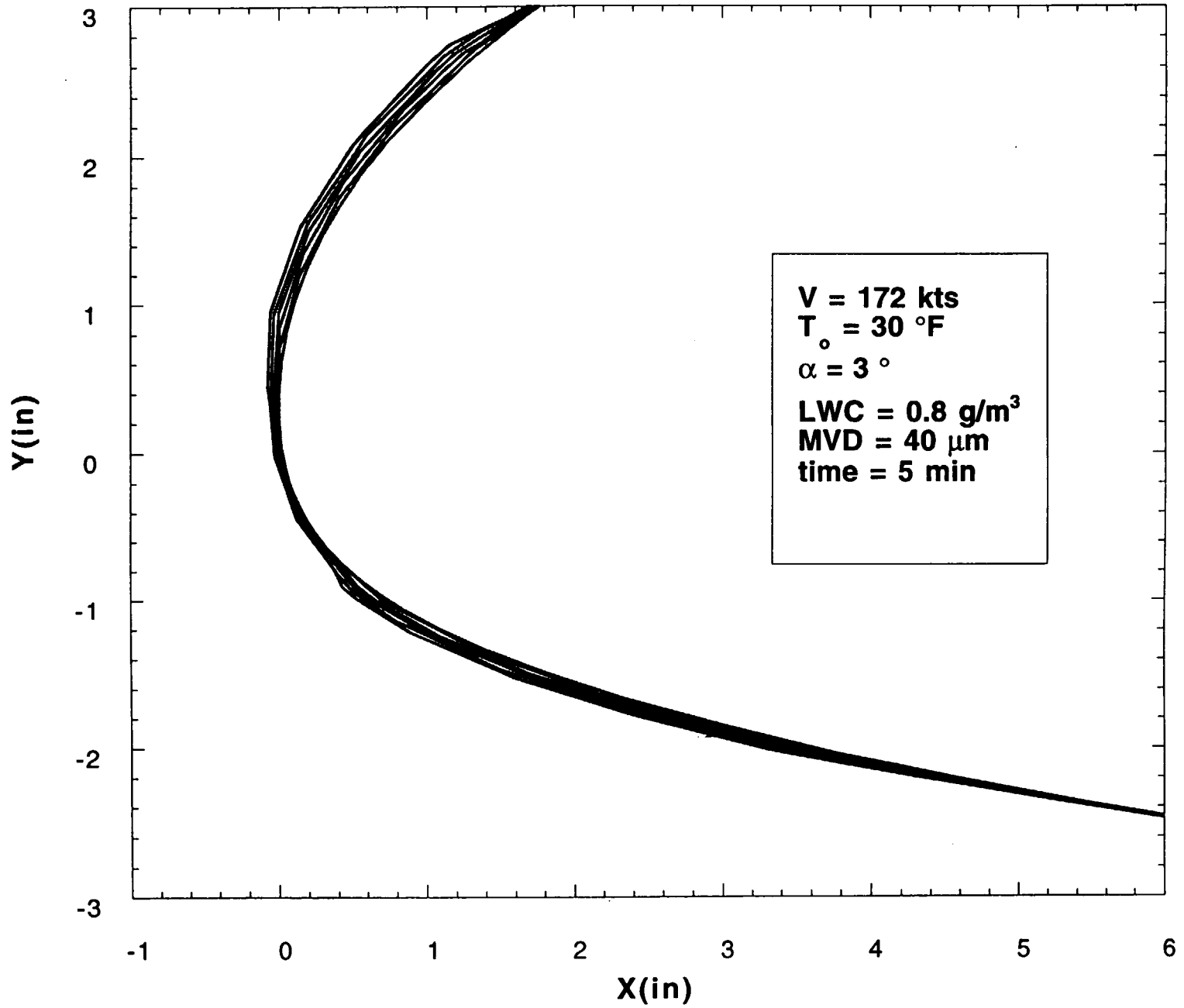
**Ice Shapes for Tunnel Conditions
Case #9**



0.5

VI-11

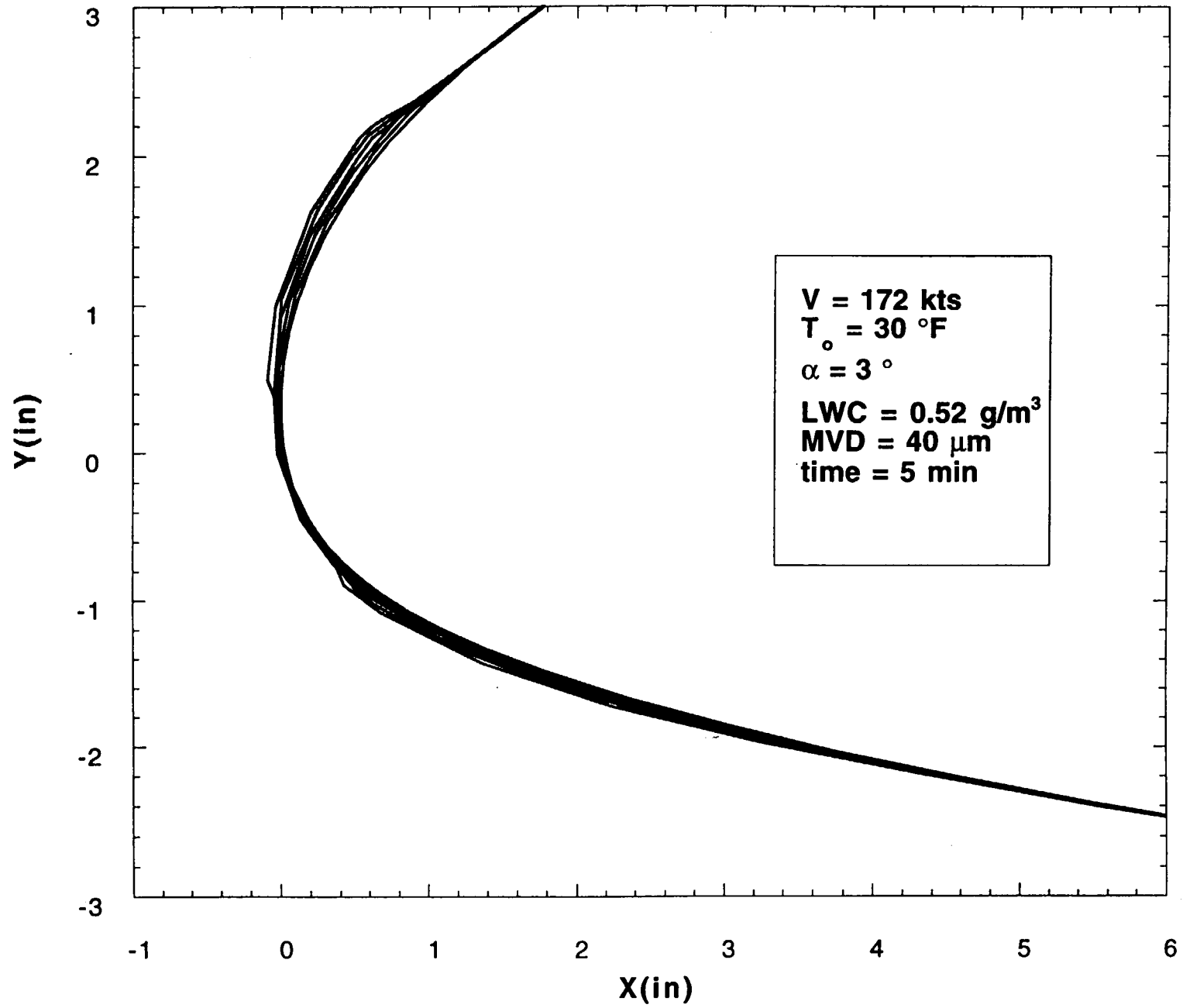
**Ice Shapes for Tunnel Conditions
Case #10**



046

V-12

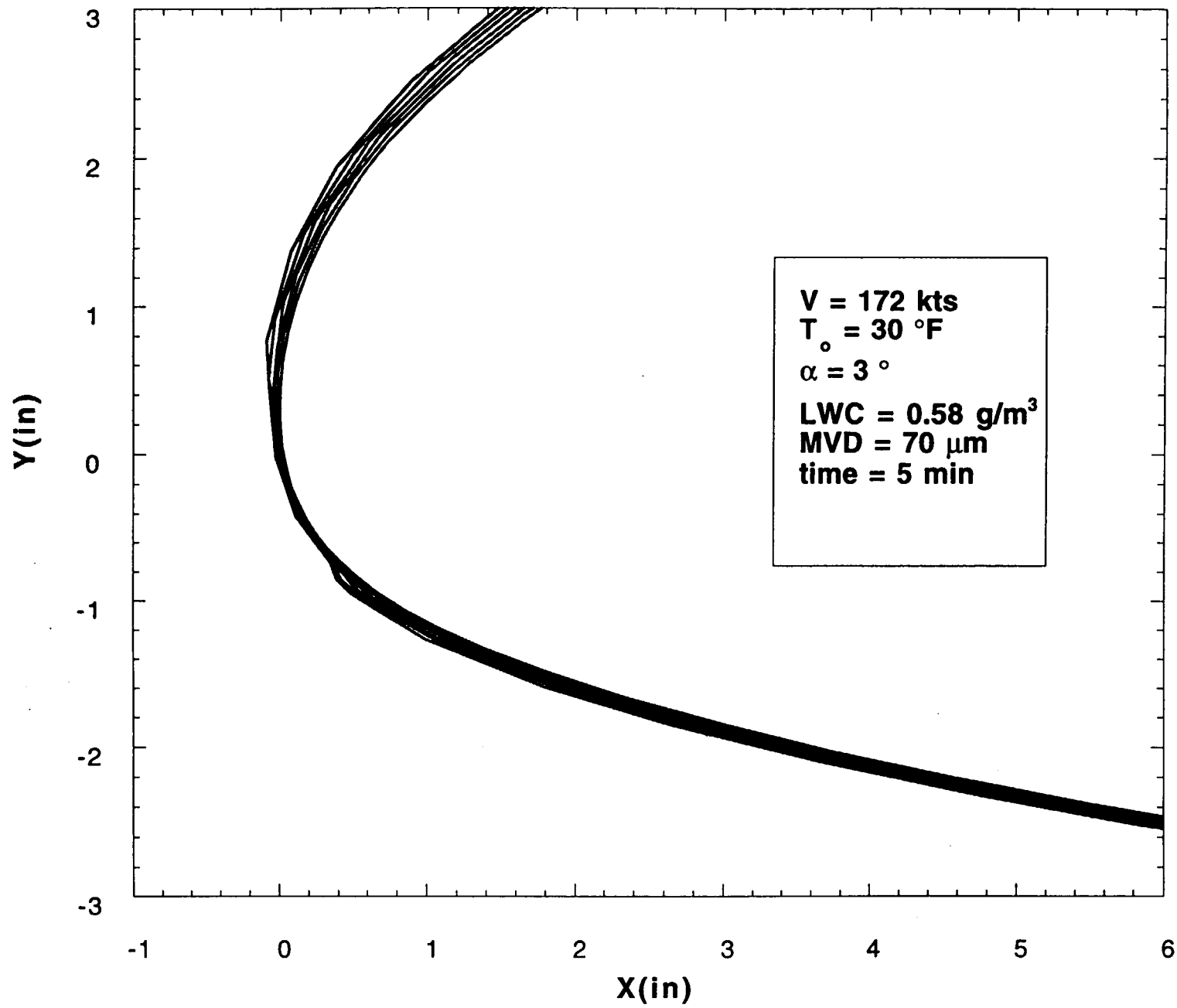
**Ice Shapes for Tunnel Conditions
Case #11**



047

M-13

**Ice Shapes for Tunnel Conditions
Case #12**



0.8

M-14

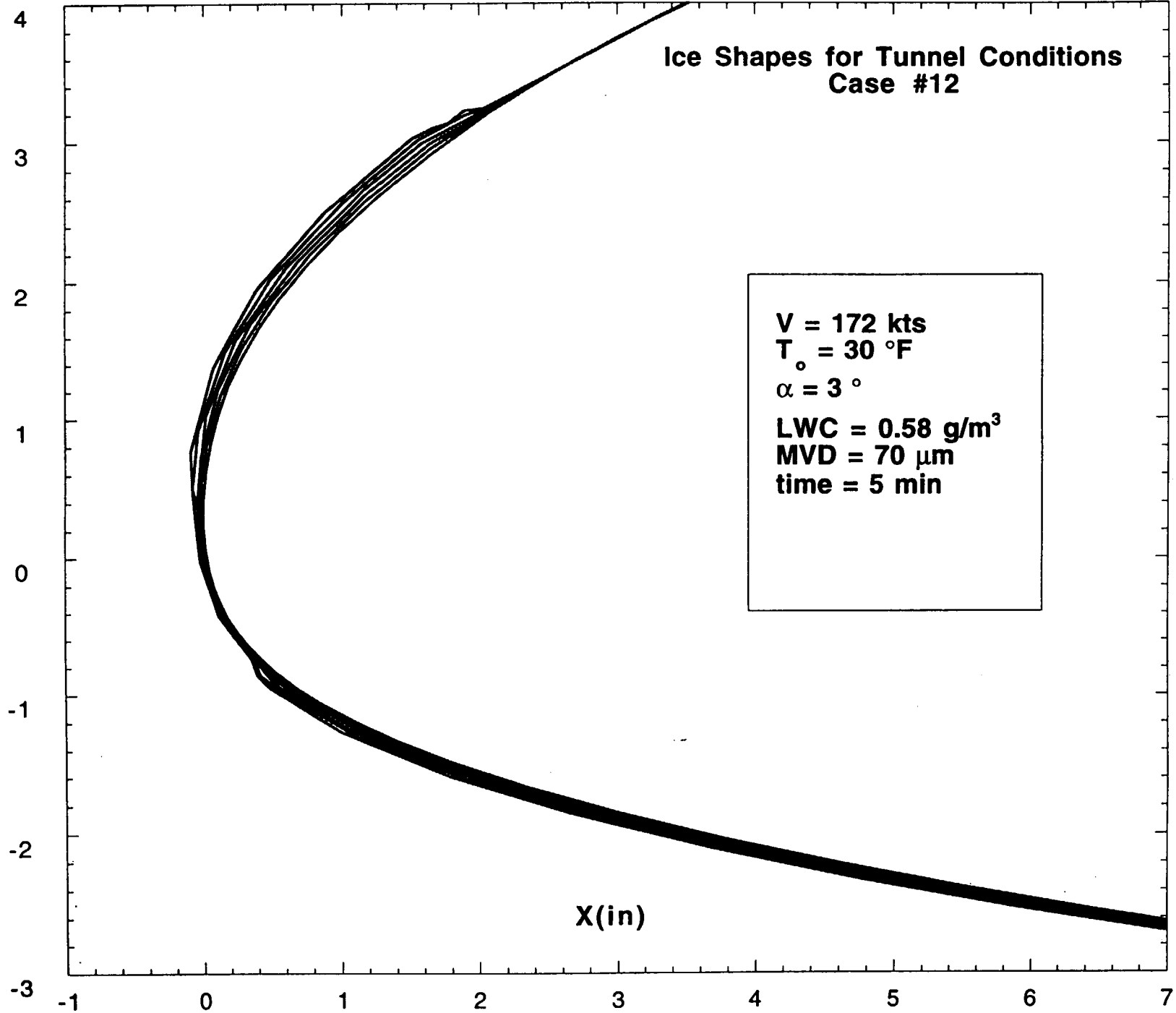
048

M-15

Y(in)

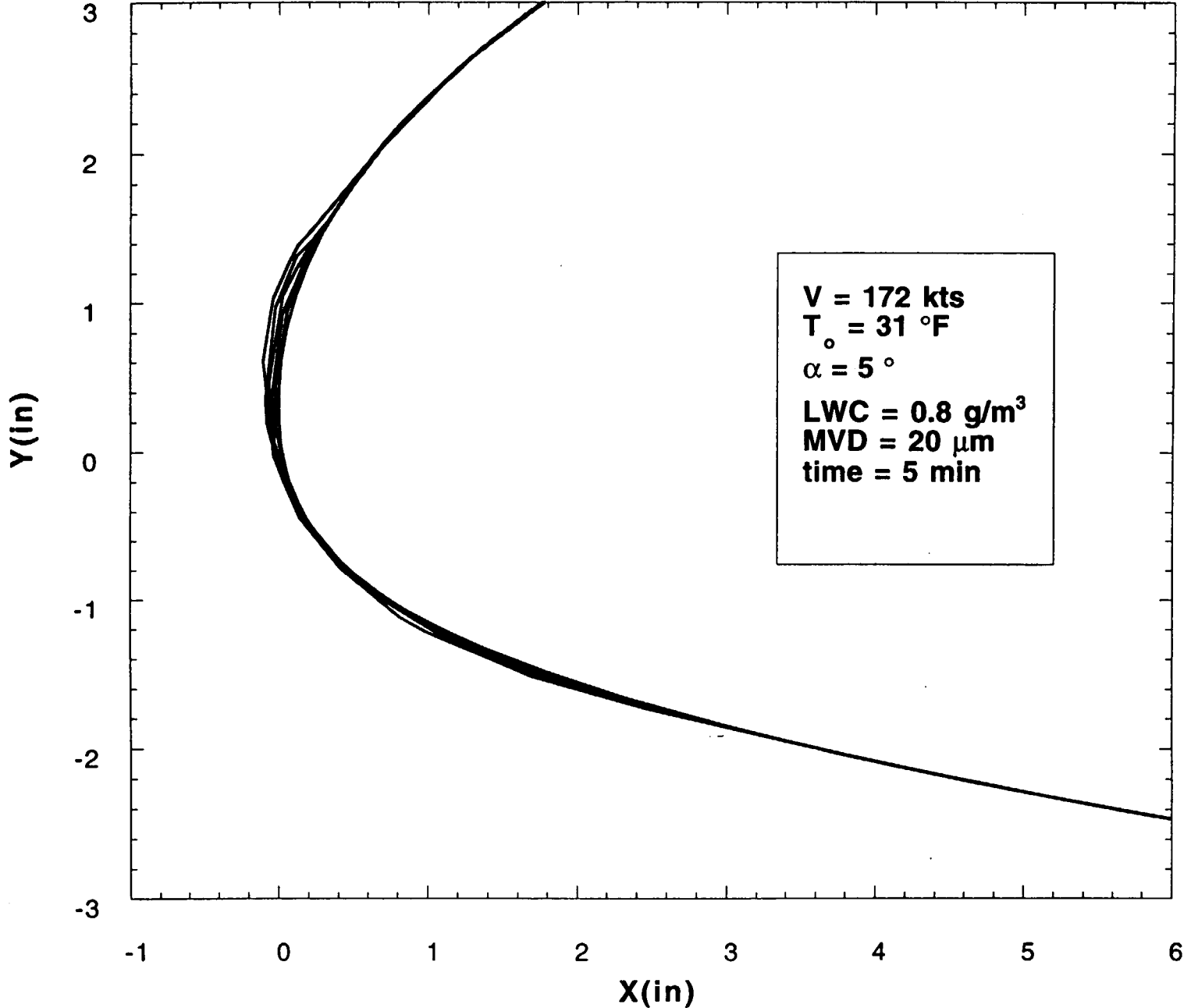
Ice Shapes for Tunnel Conditions Case #12

V = 172 kts
T_o = 30 °F
α = 3 °
LWC = 0.58 g/m³
MVD = 70 μm
time = 5 min



X(in)

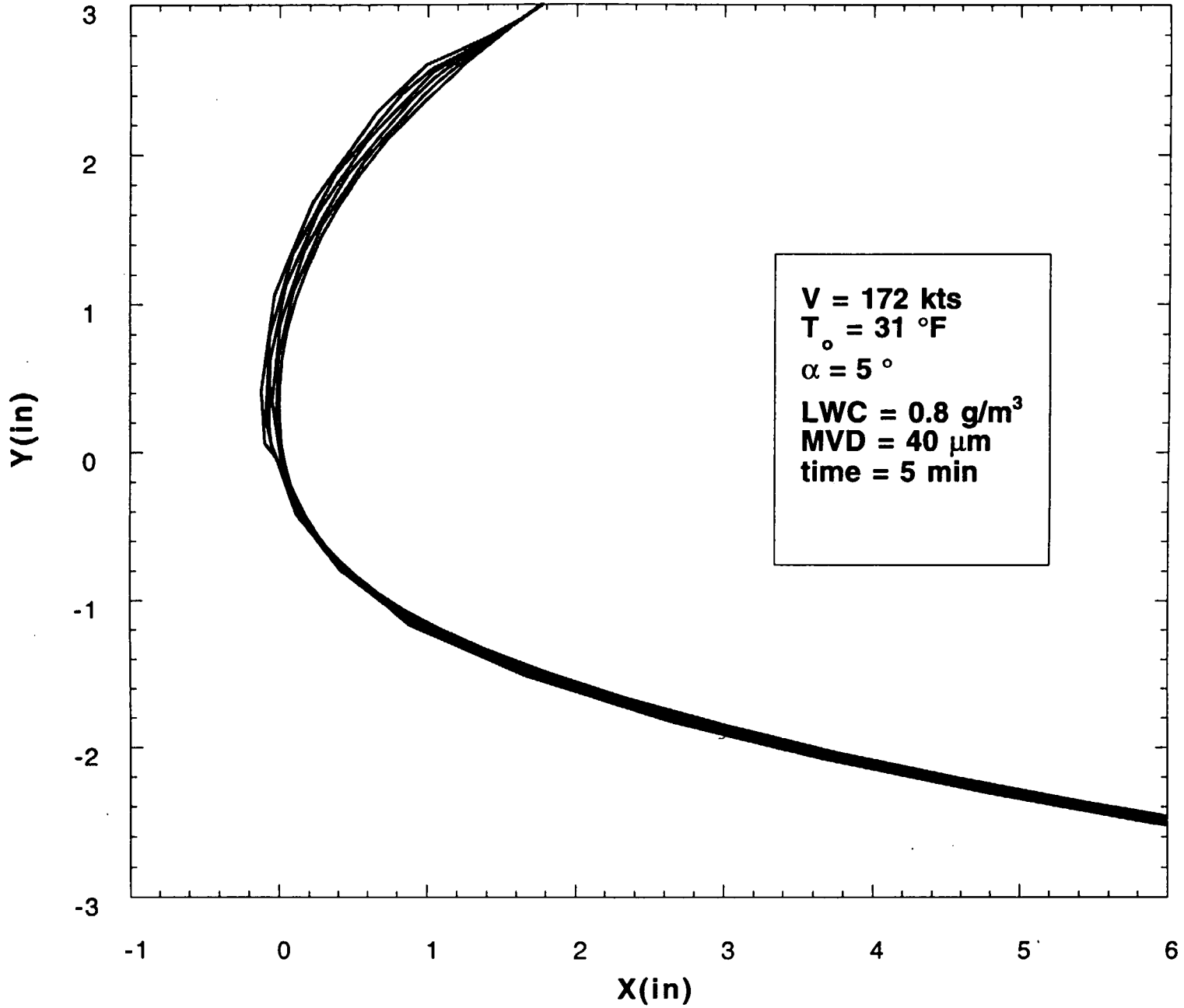
**Ice Shapes for Tunnel Conditions
Case #13**



050

VI-16

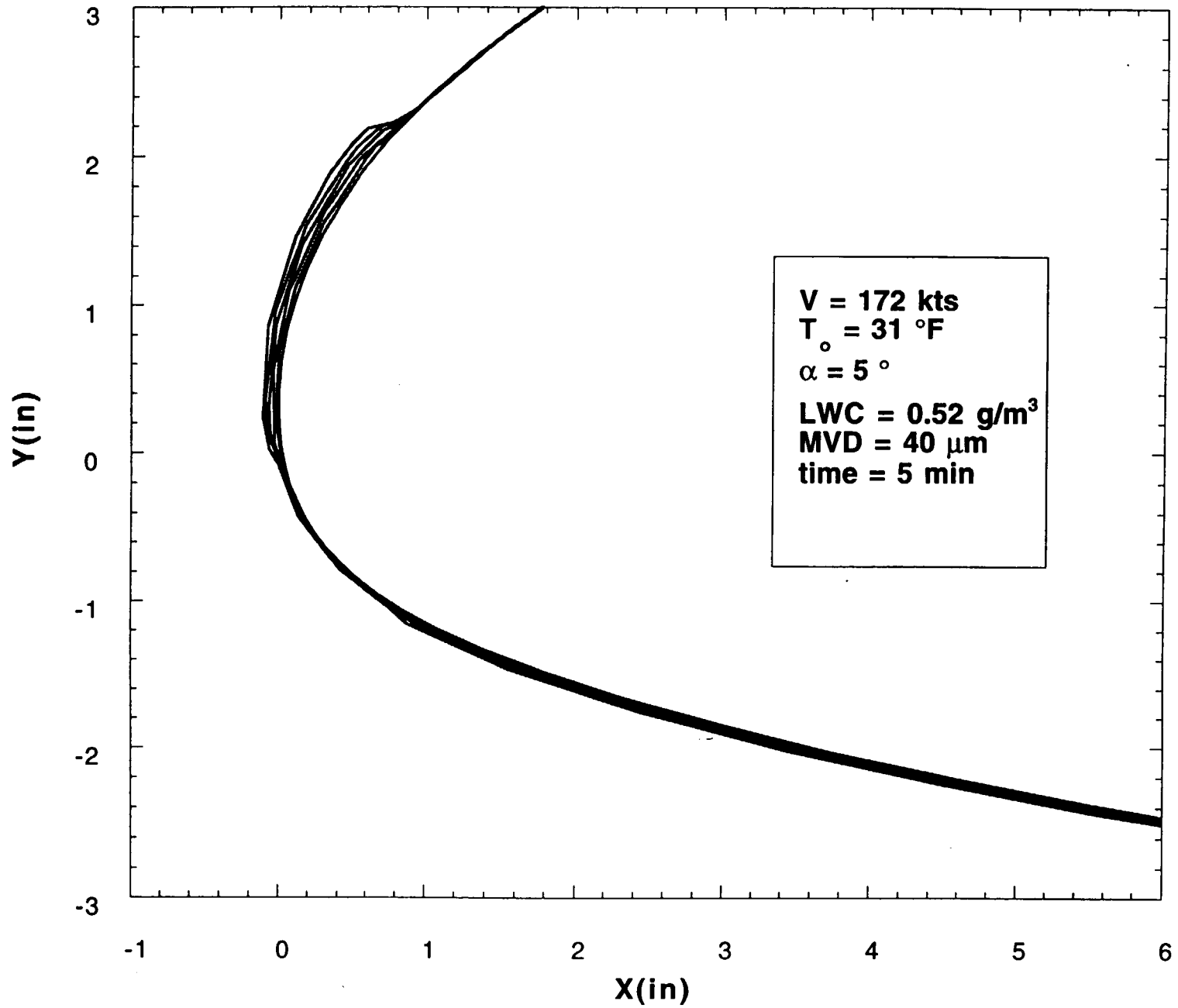
**Ice Shapes for Tunnel Conditions
Case #14**



051

VI-17

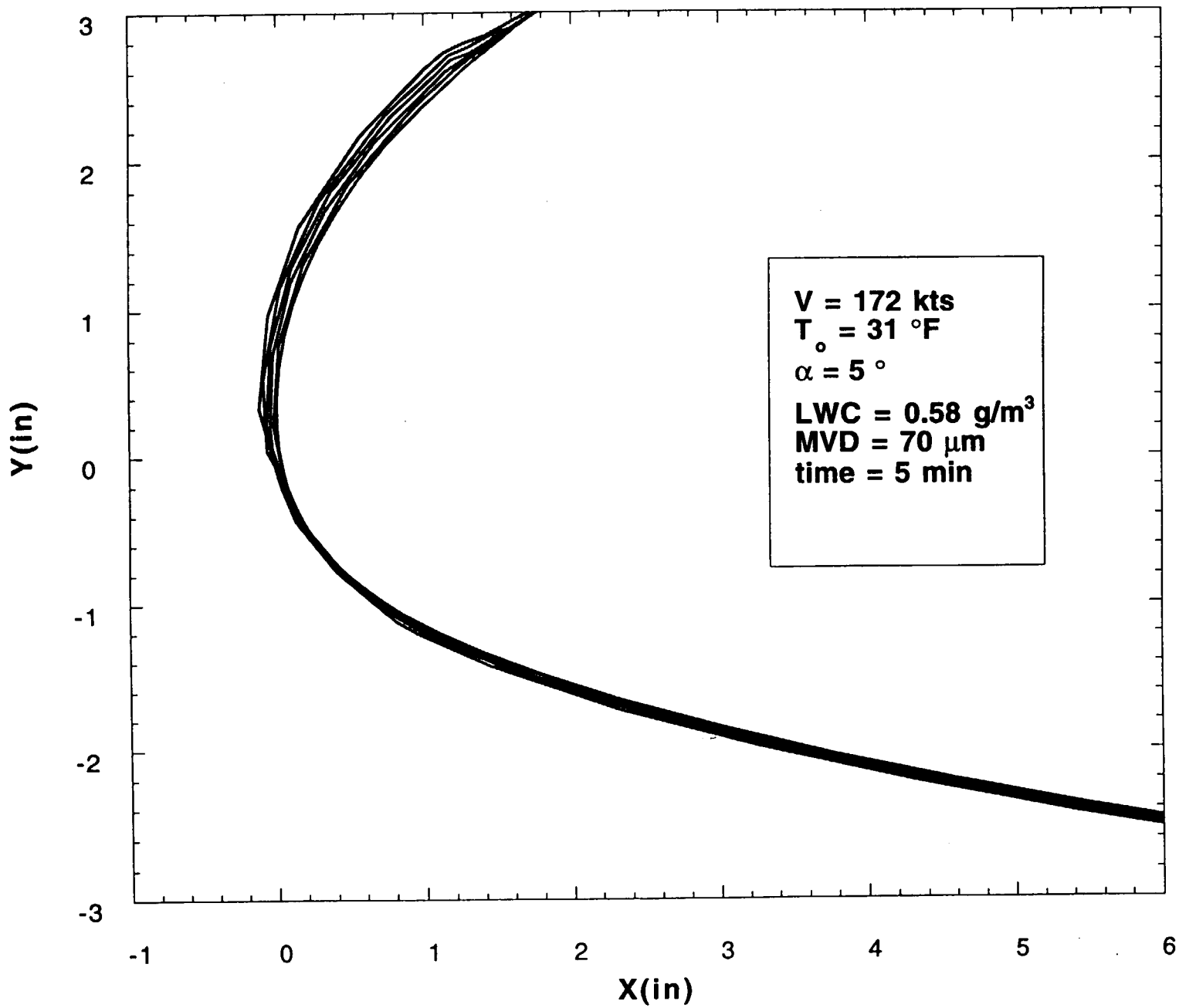
**Ice Shapes for Tunnel Conditions
Case #15**



052

VI-18

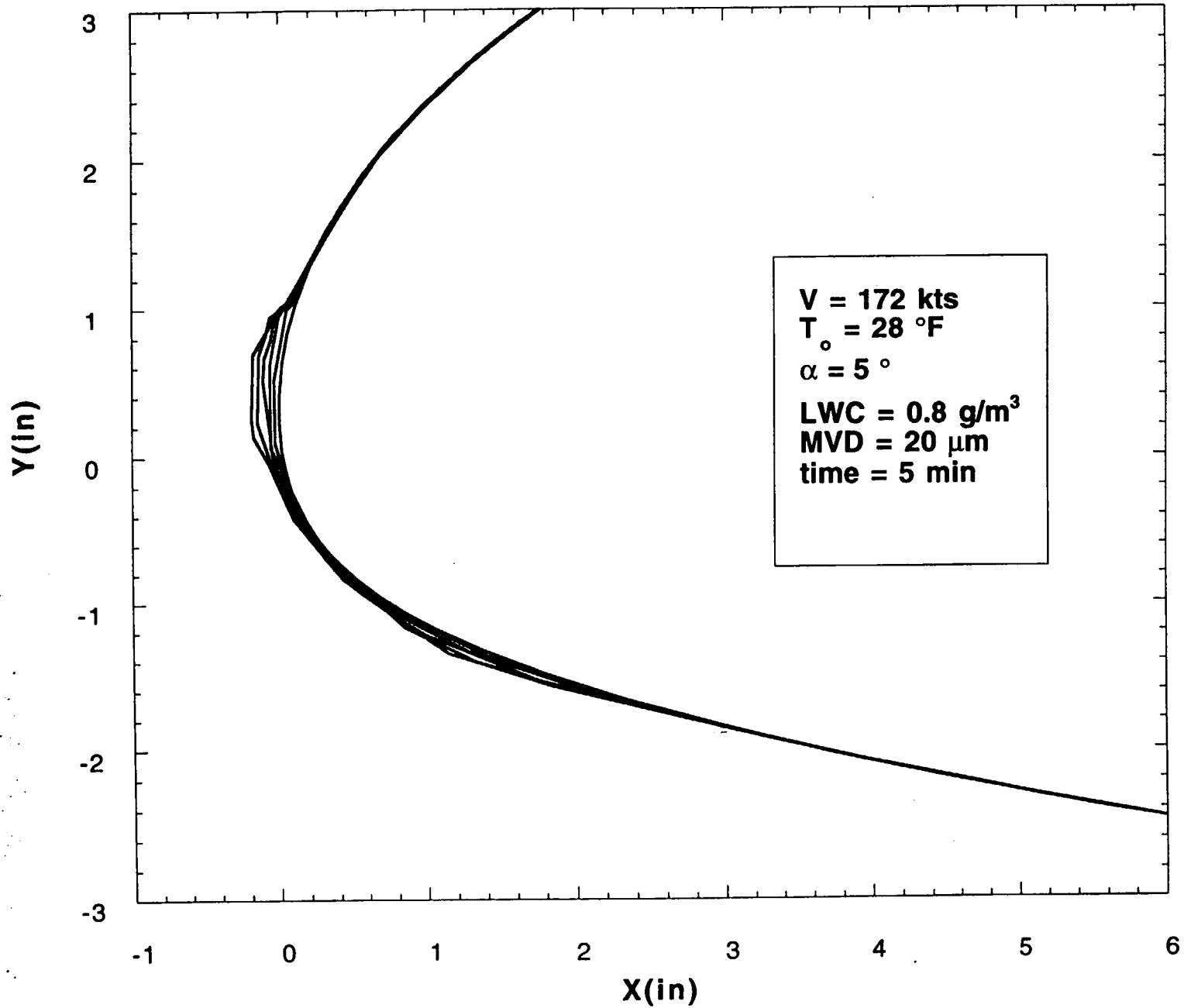
**Ice Shapes for Tunnel Conditions
Case #16**



US3

VI-19

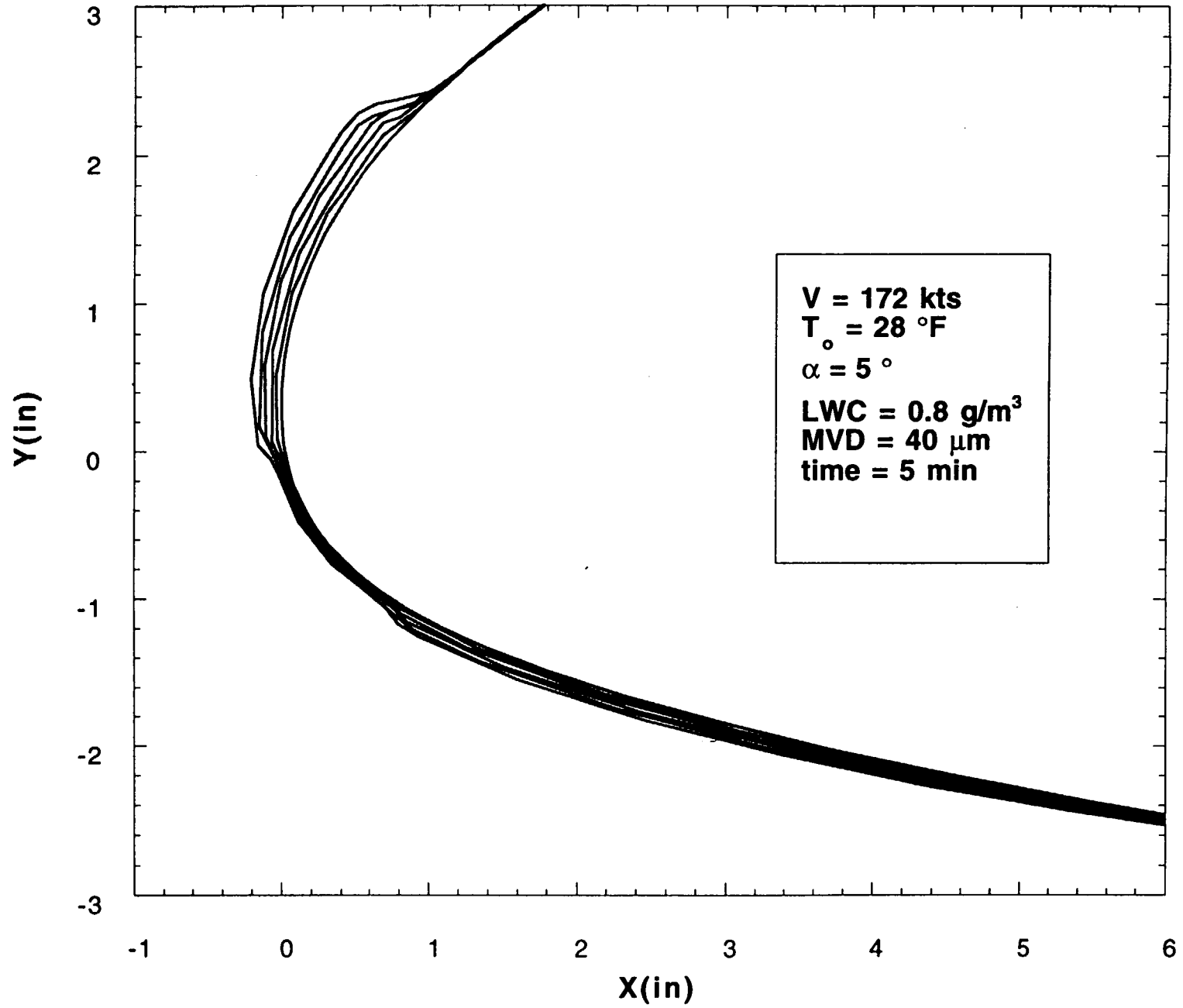
**Ice Shapes for Tunnel Conditions
Case #17**



U34

V1-20

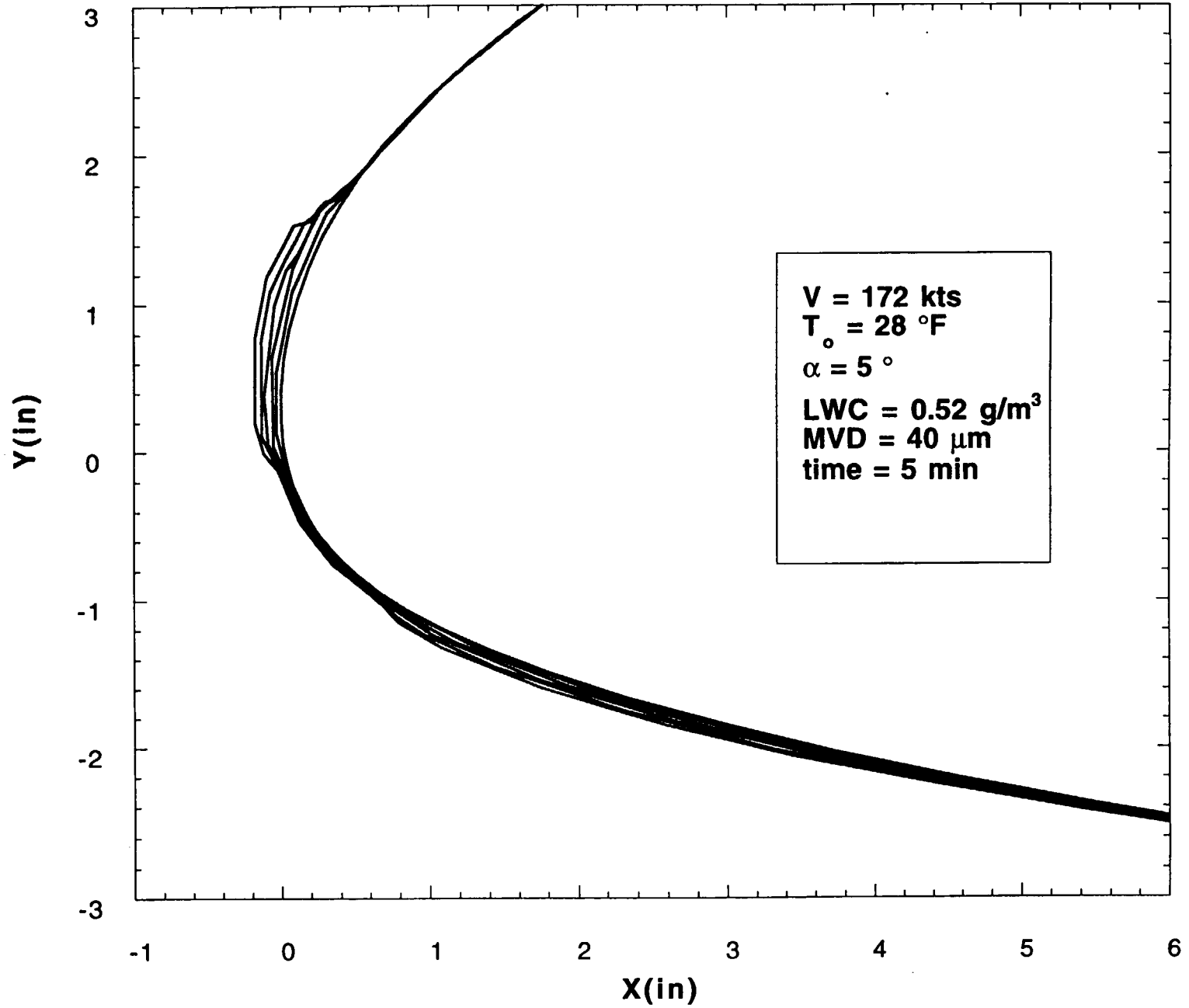
**Ice Shapes for Tunnel Conditions
Case #18**



U35

VI-21

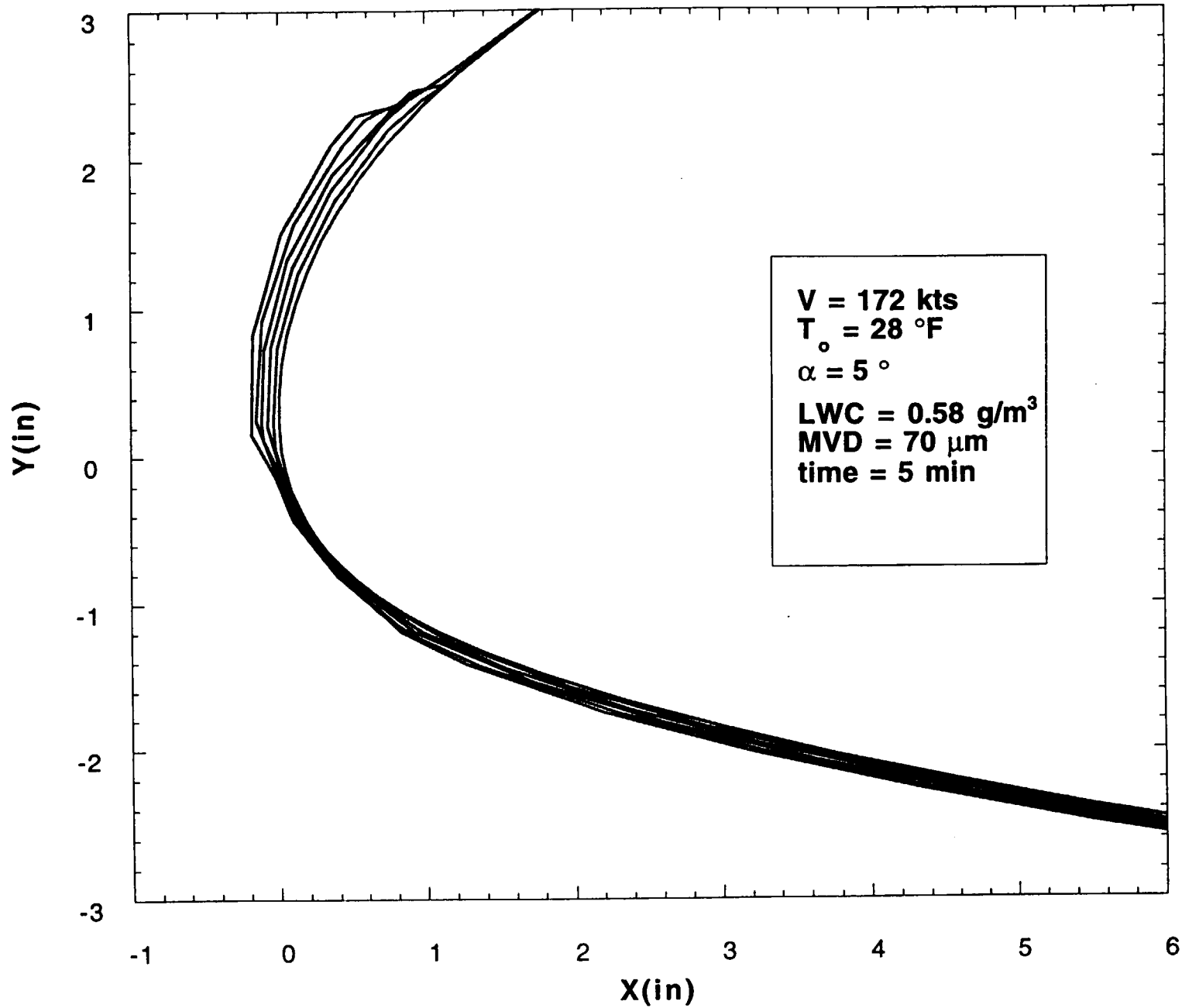
**Ice Shapes for Tunnel Conditions
Case #19**



056

V-22

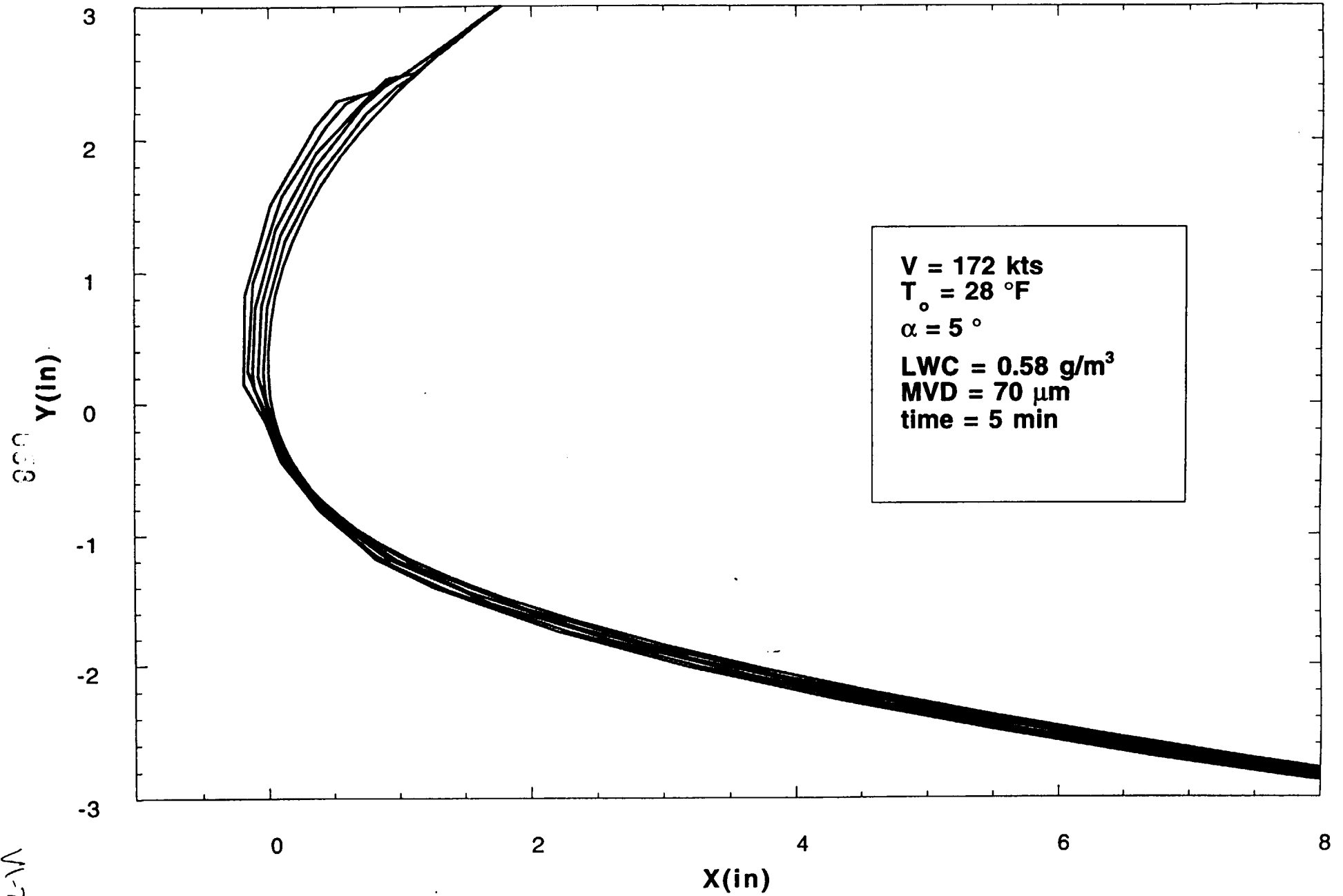
**Ice Shapes for Tunnel Conditions
Case #20**



U57

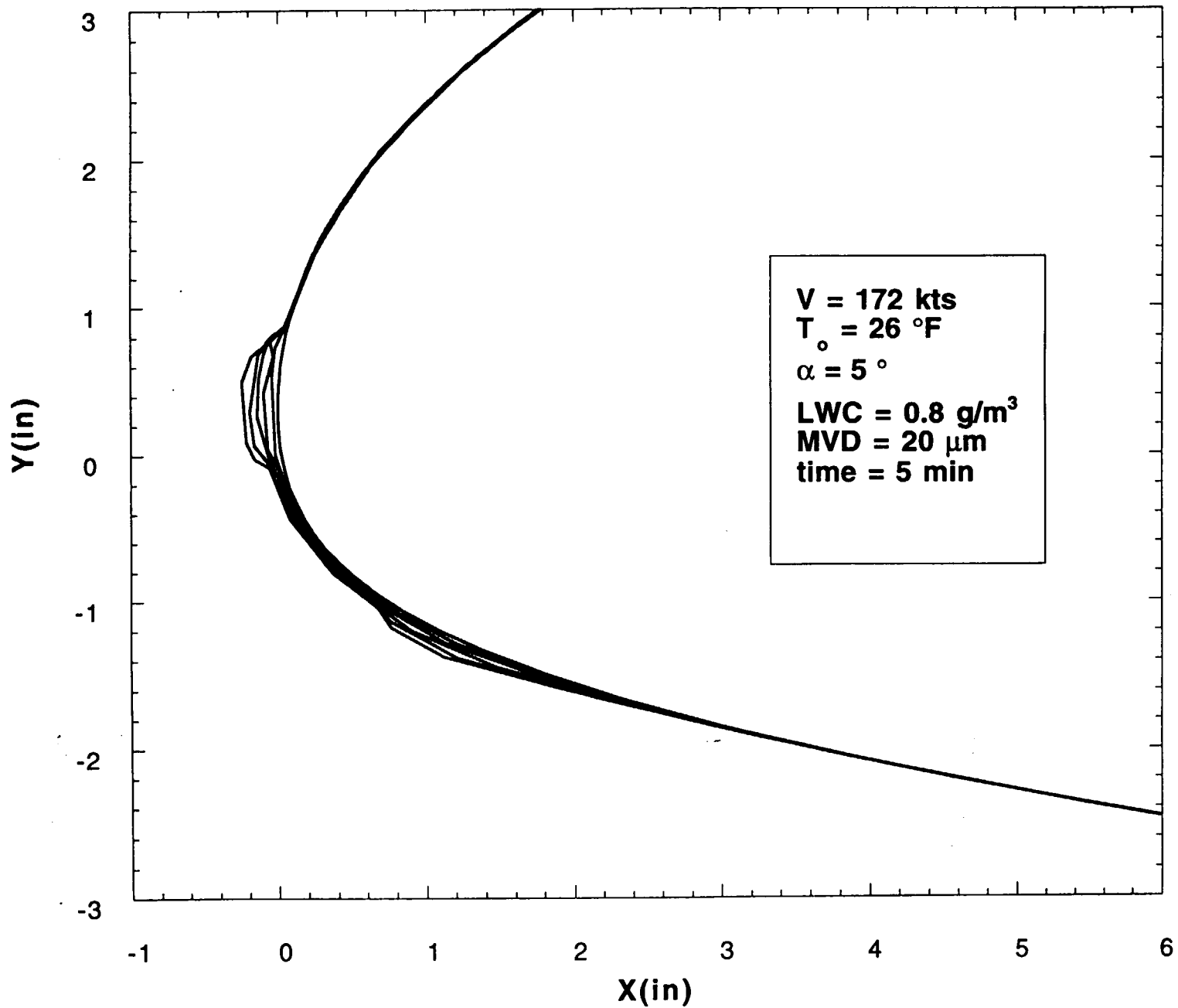
V-23

**Ice Shapes for Tunnel Conditions
Case #20**



W-24

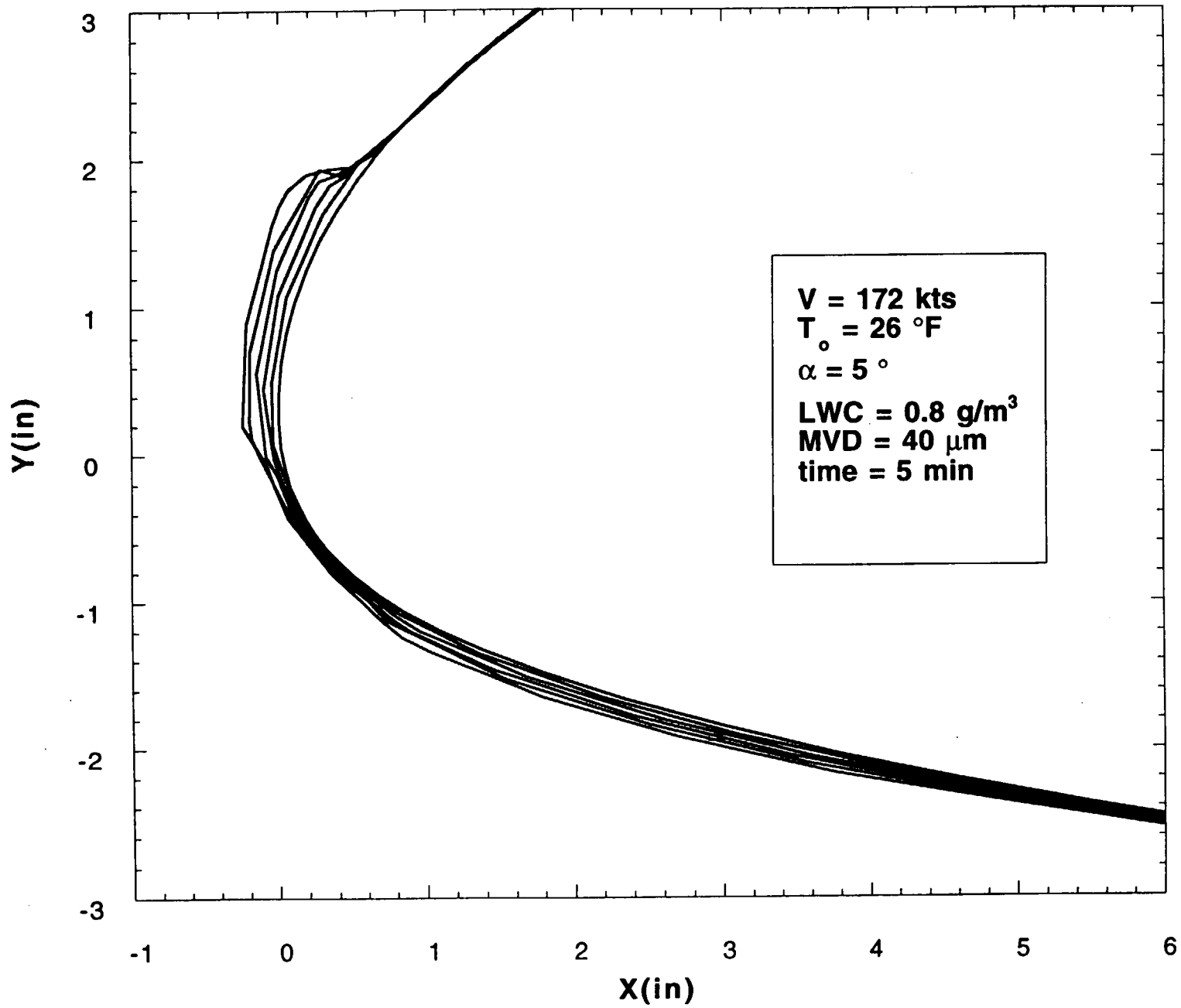
**Ice Shapes for Tunnel Conditions
Case #21**



658

M-25

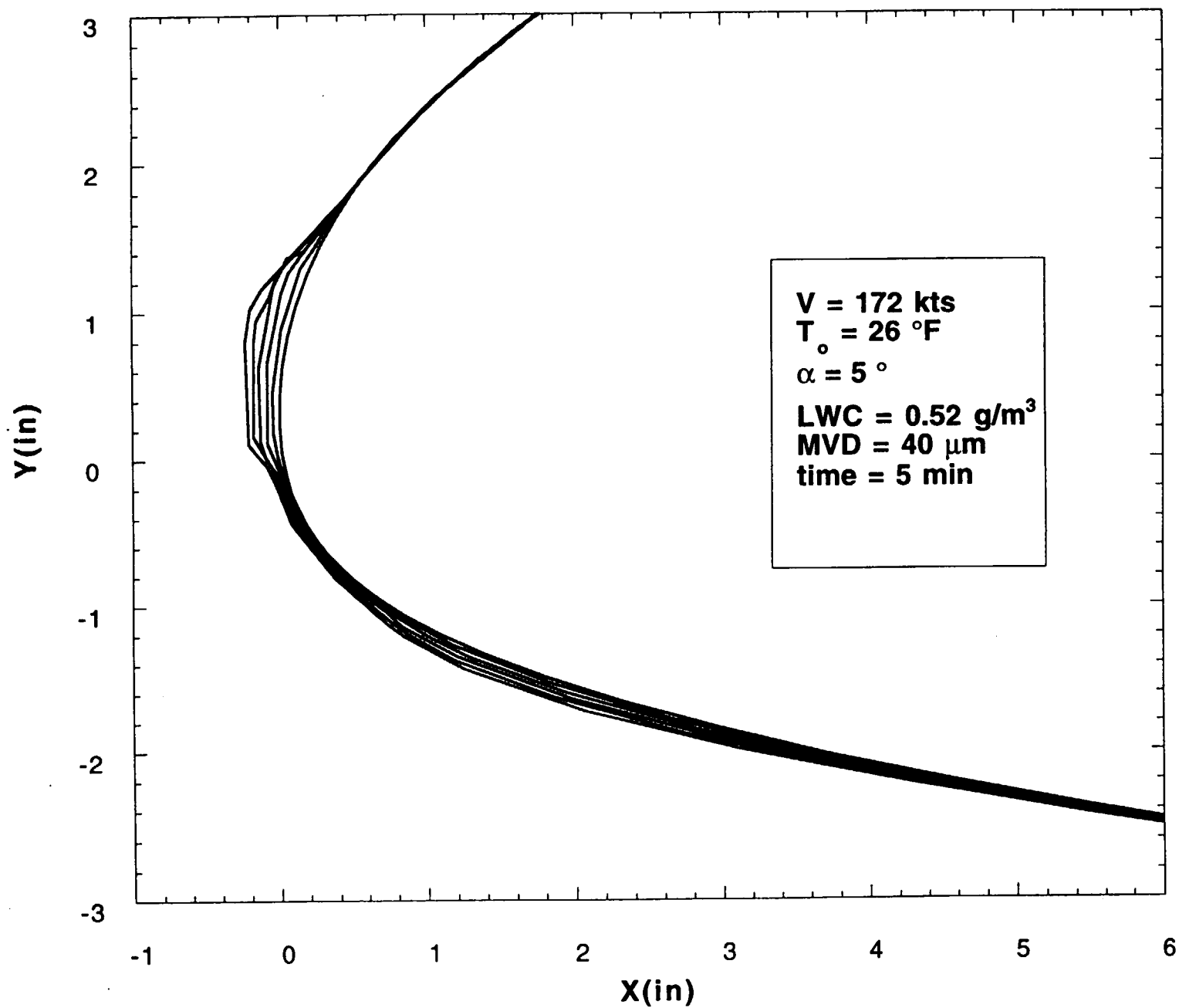
**Ice Shapes for Tunnel Conditions
Case #22**



030

V1-26

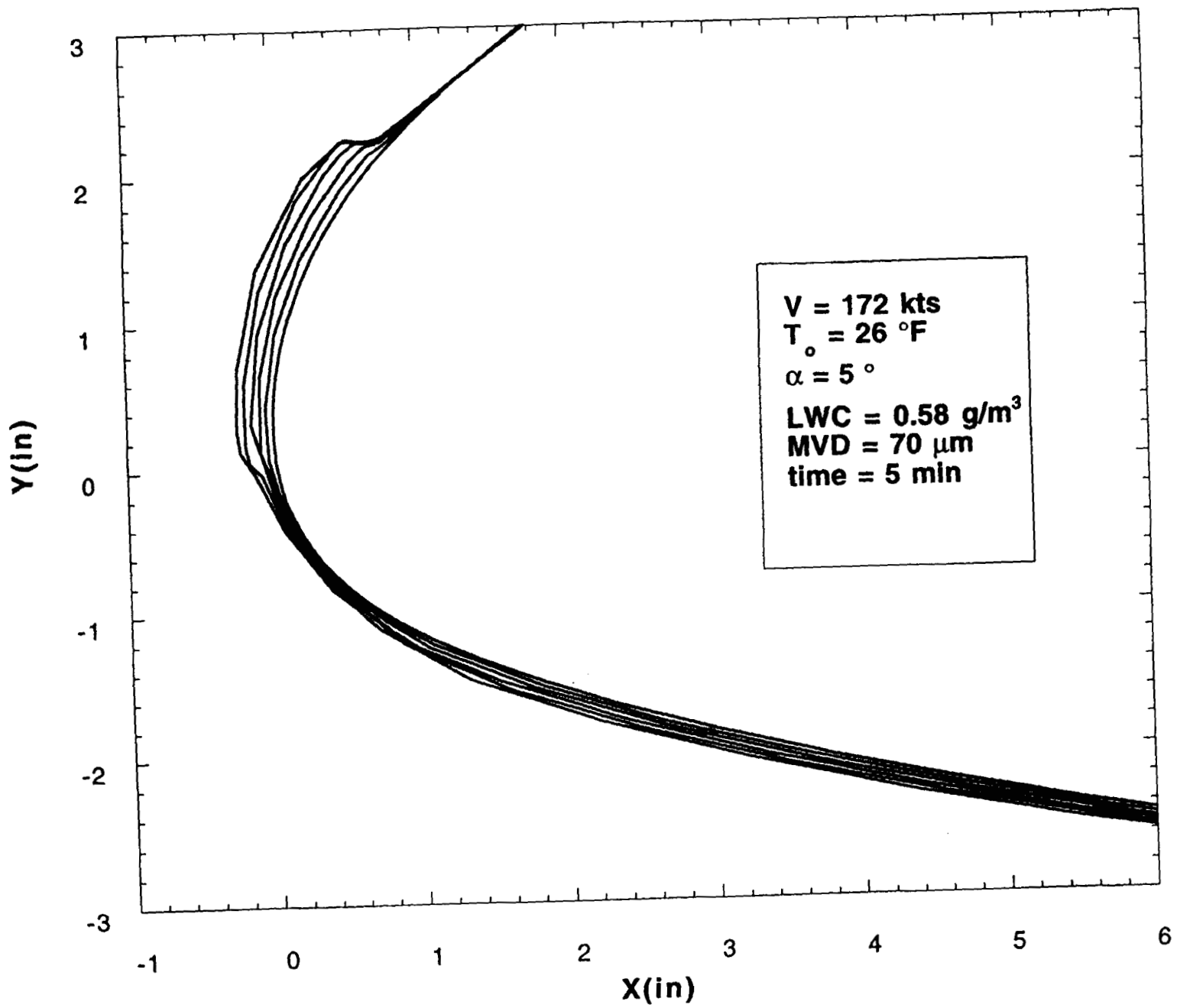
**Ice Shapes for Tunnel Conditions
Case #23**



031

W-27

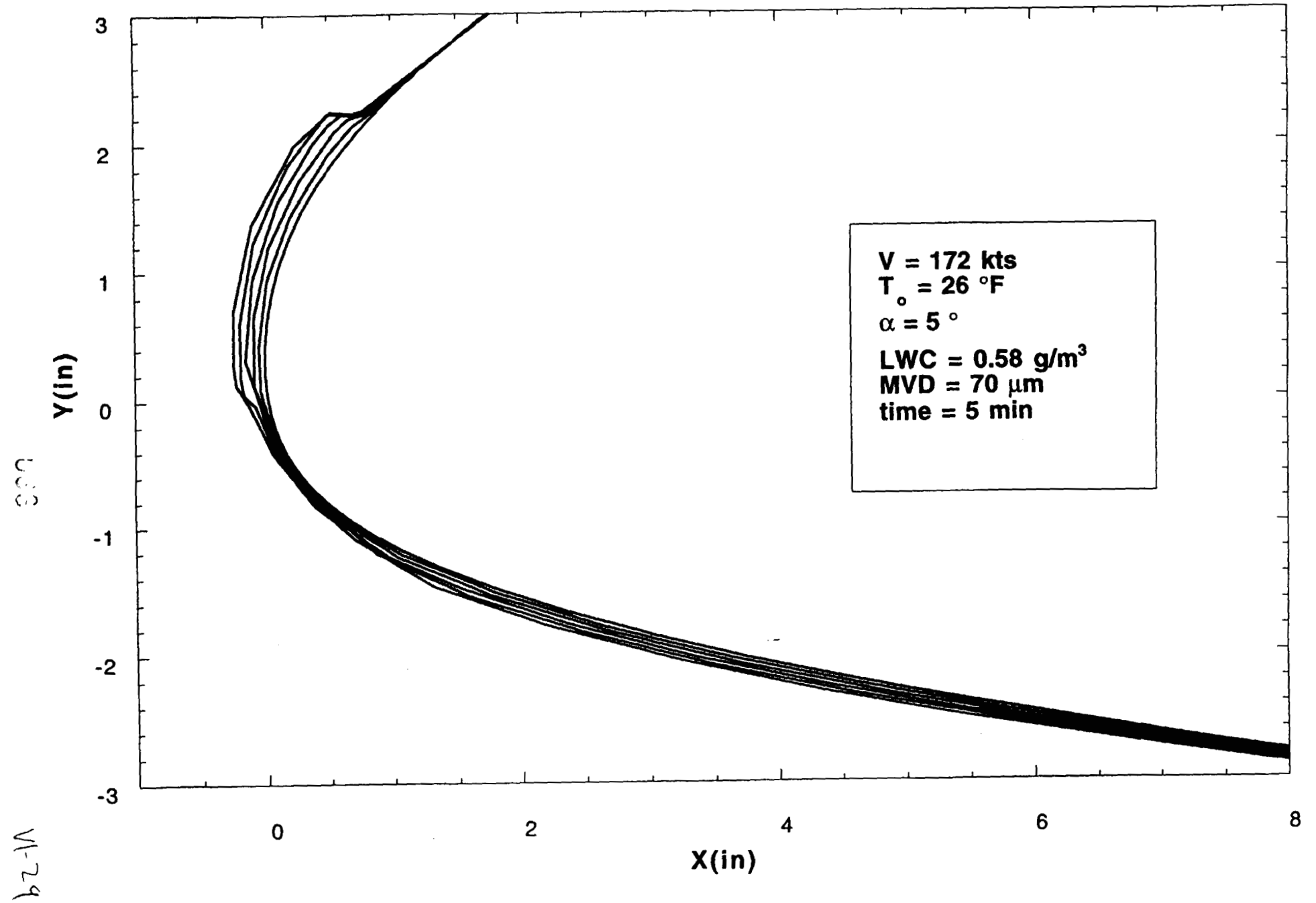
**Ice Shapes for Tunnel Conditions
Case #24**



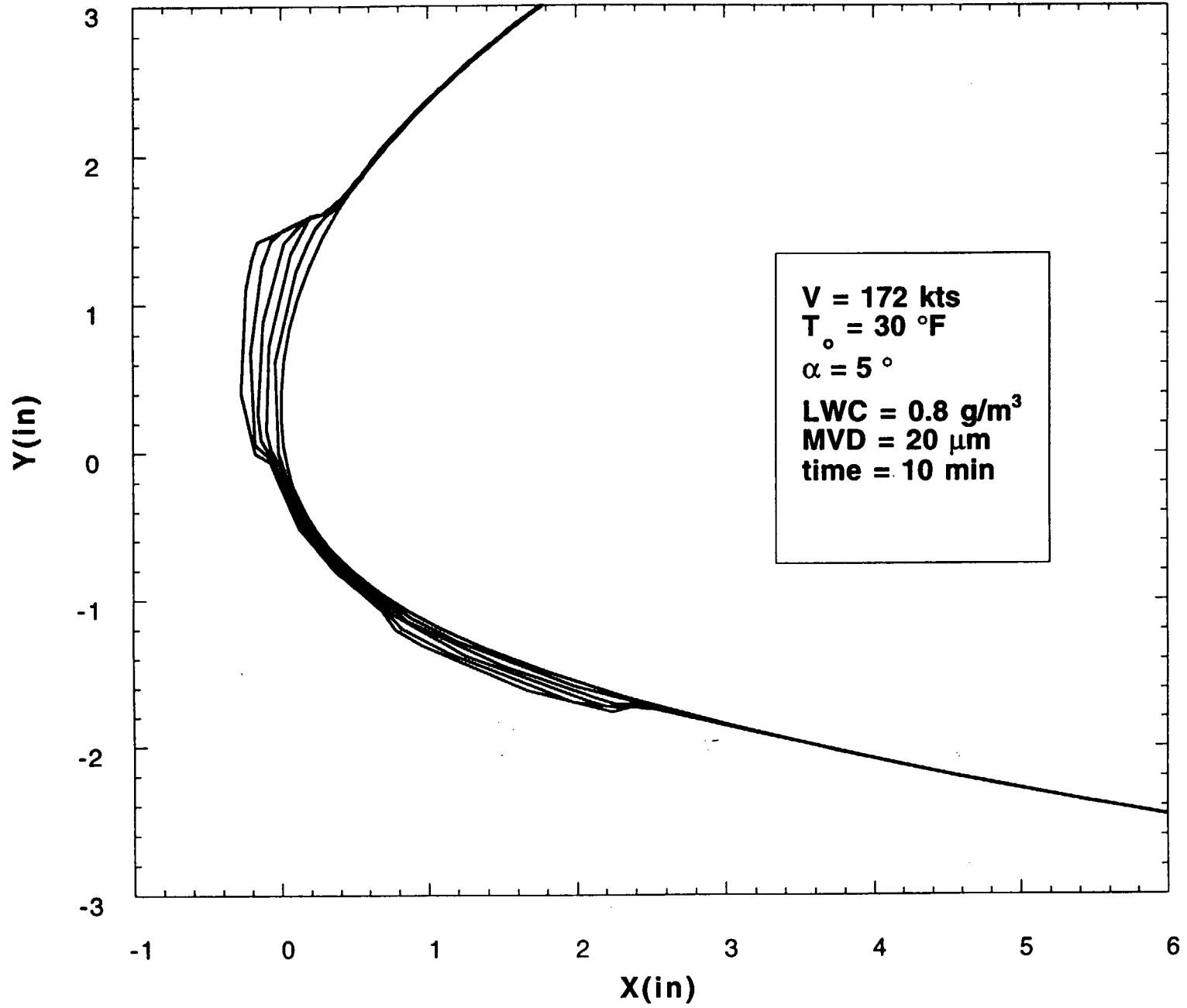
UG2

V-28

**Ice Shapes for Tunnel Conditions
Case #24**



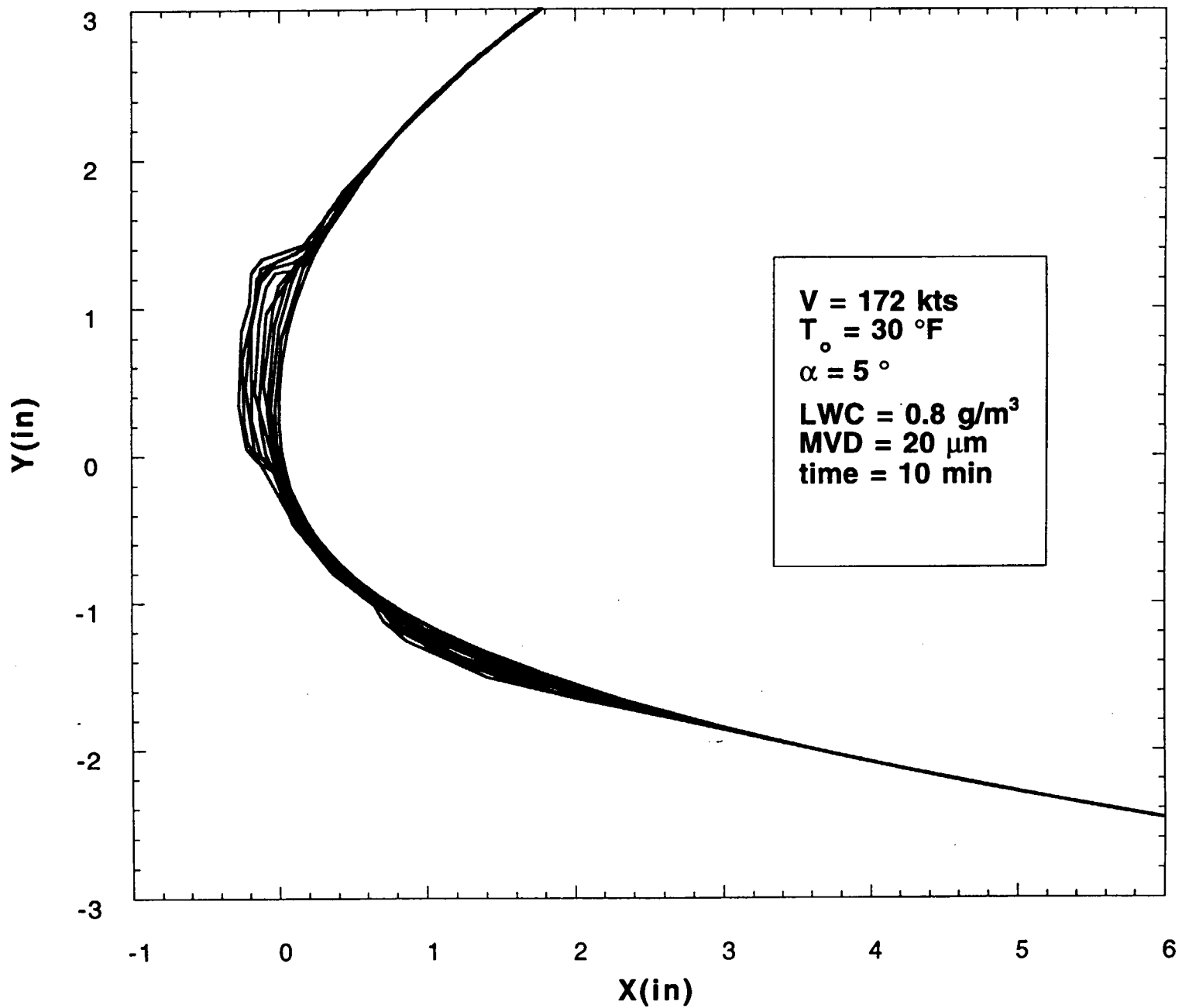
**Ice Shapes for Tunnel Conditions
Case #25**



024

V1-30

**Ice Shapes for Tunnel Conditions
Case #25**



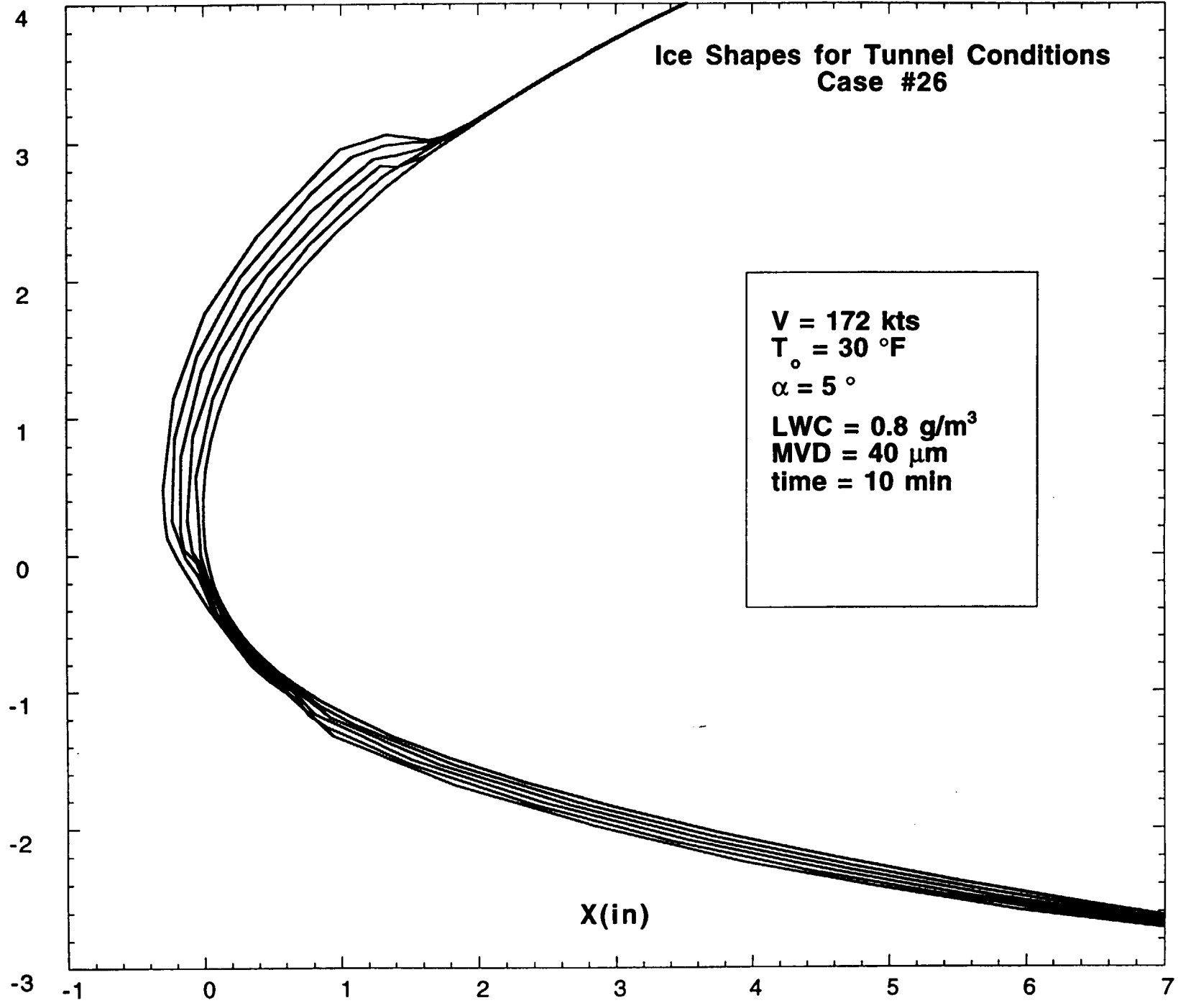
005

VI-31

906

V-32

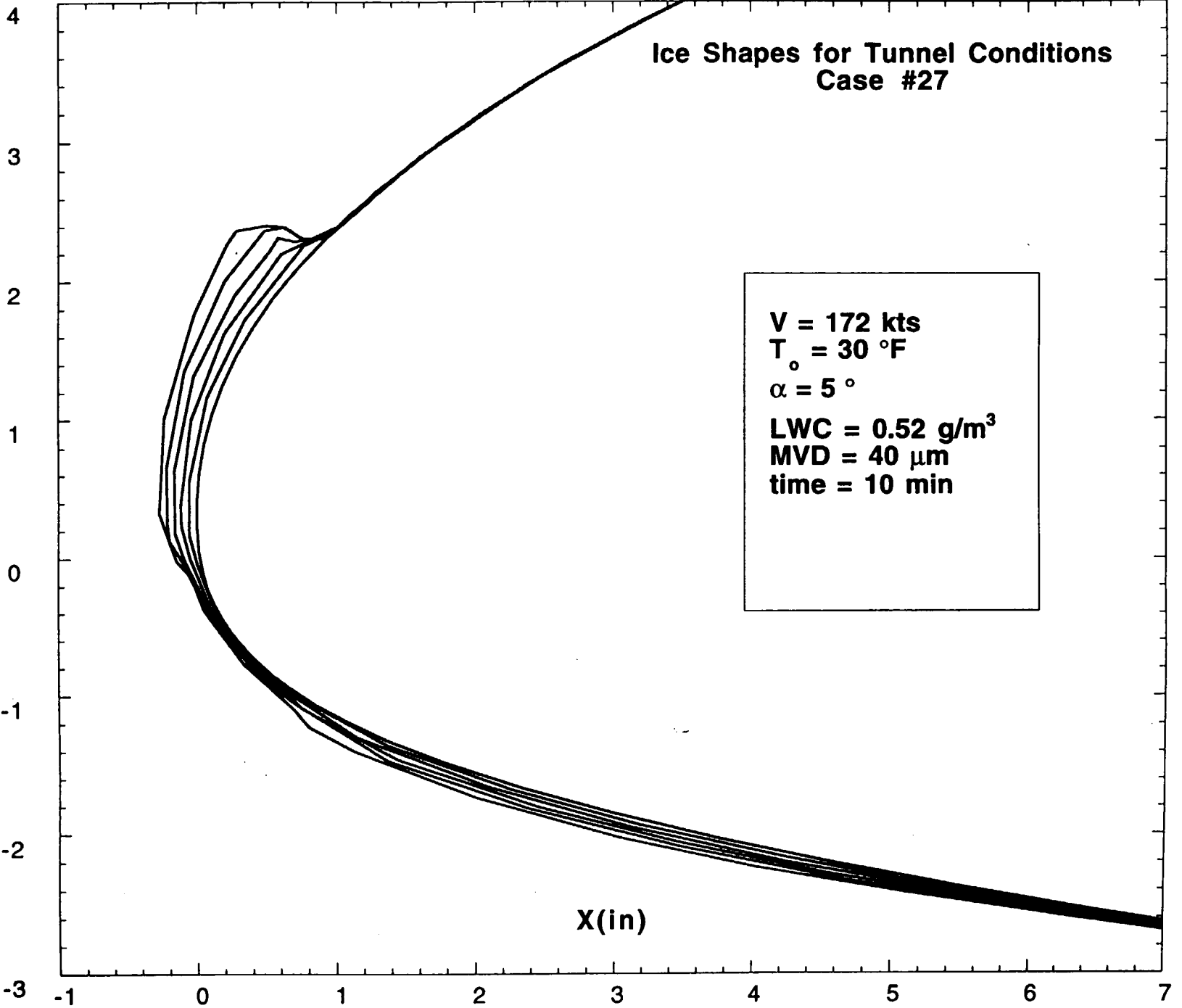
Y(in)



087

VI-33

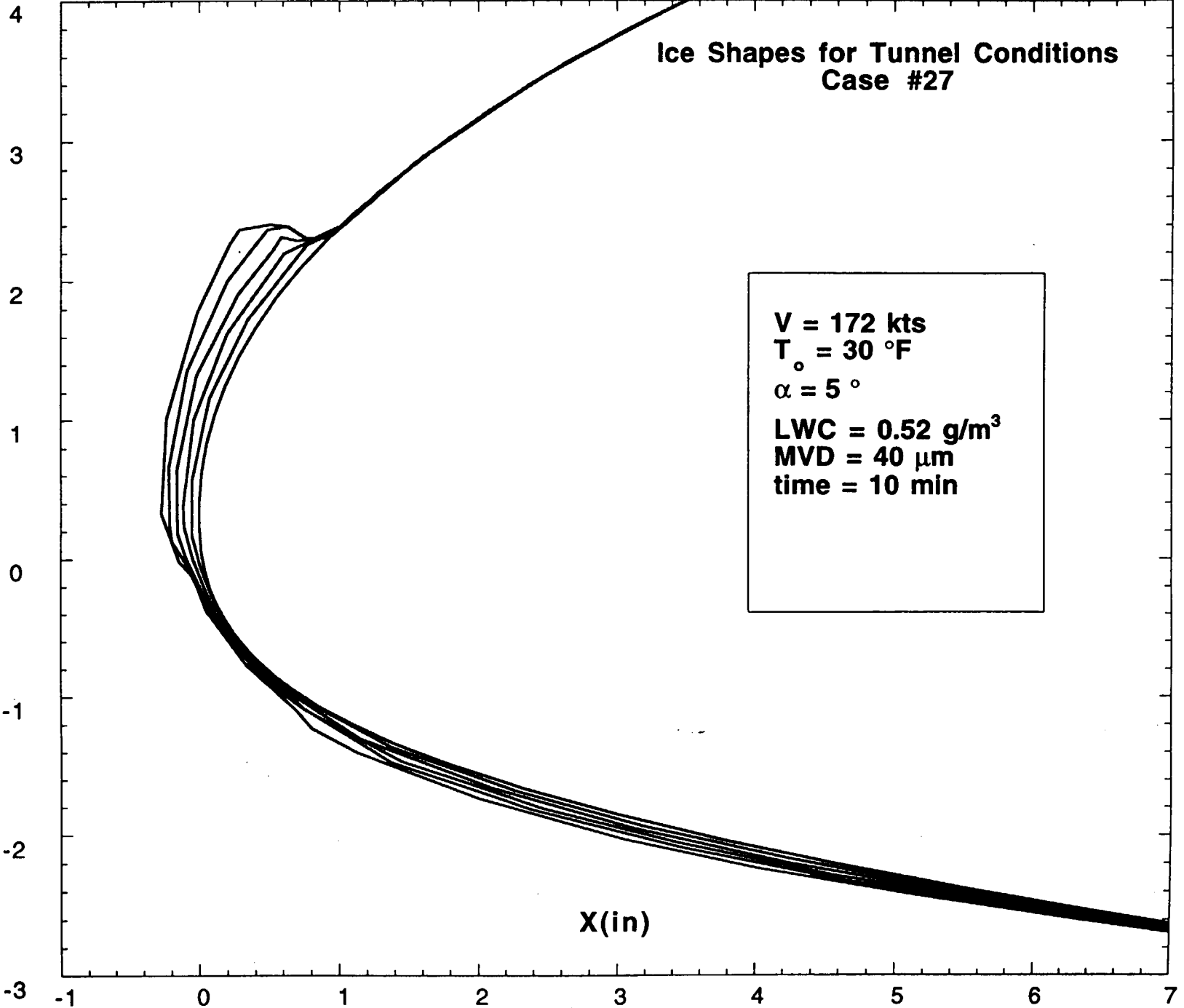
Y(in)



006

VI-34

Y(in)



Ice Shapes for Tunnel Conditions
Case #27

**Ice Shapes for Tunnel Conditions
Case #27**

V = 172 kts

T_o = 30 °F

α = 5 °

LWC = 0.52 g/m³

MVD = 40 μm

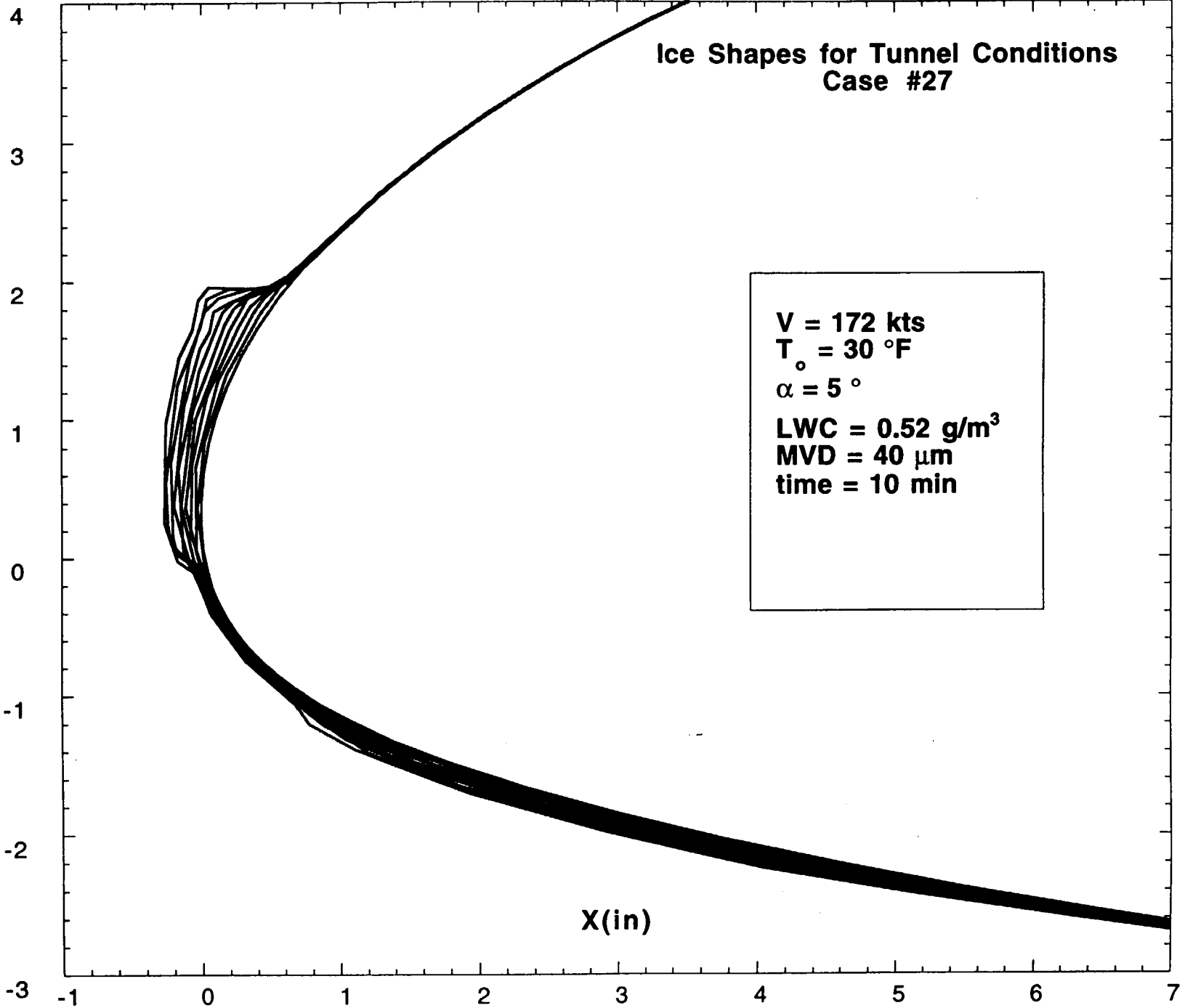
time = 10 min

Y(in)

X(in)

600

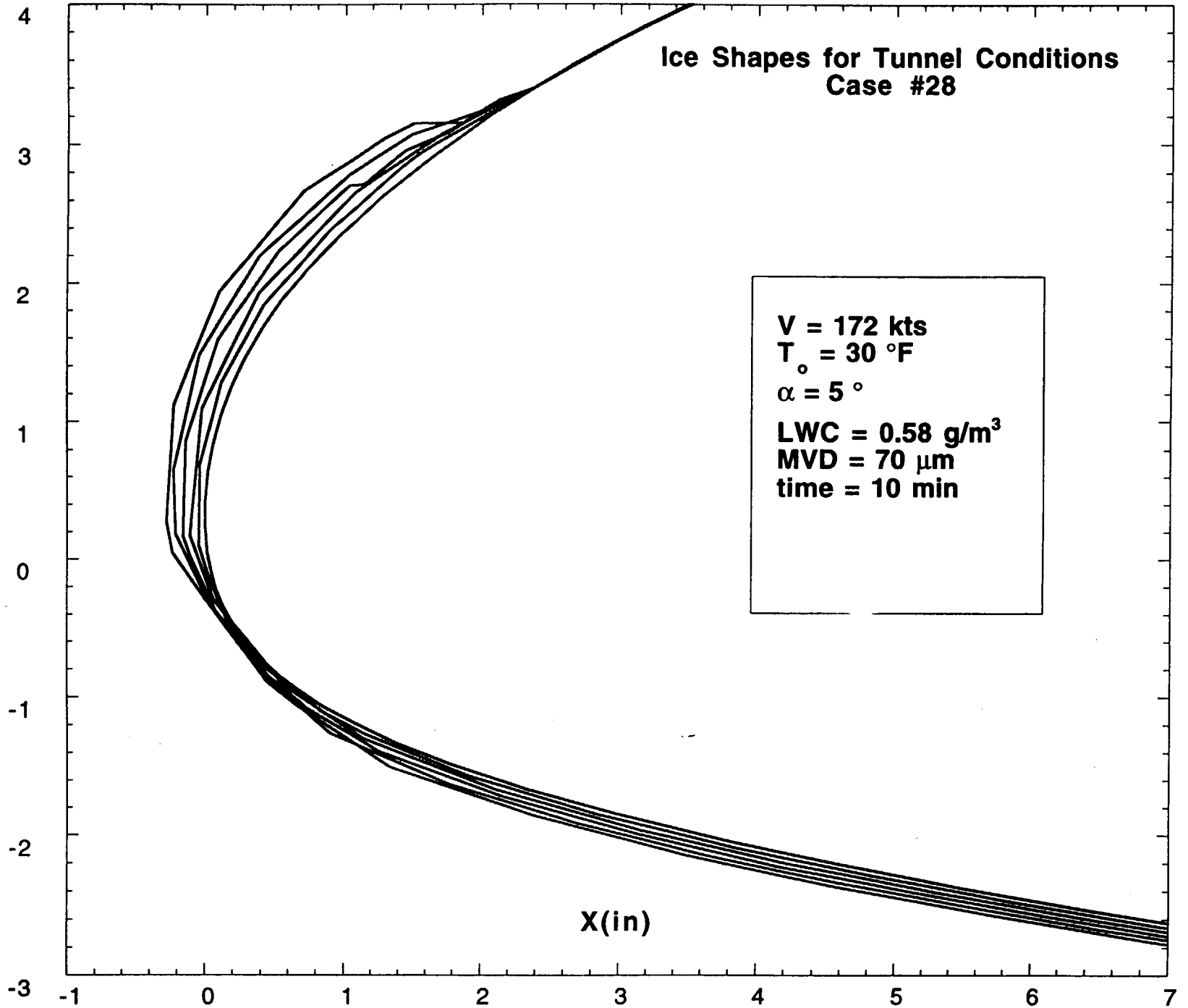
W-35



V1-36

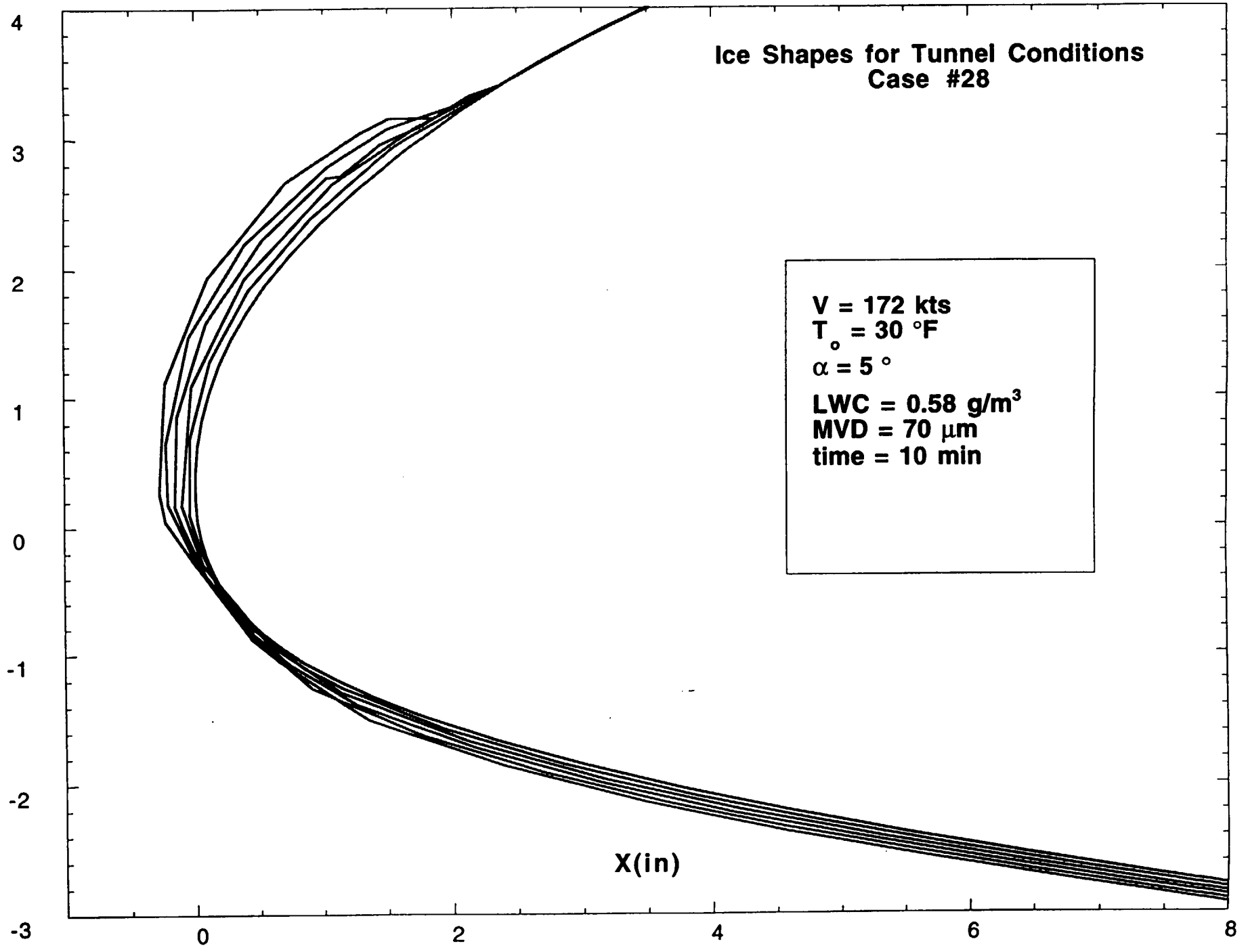
U70

Y(in)



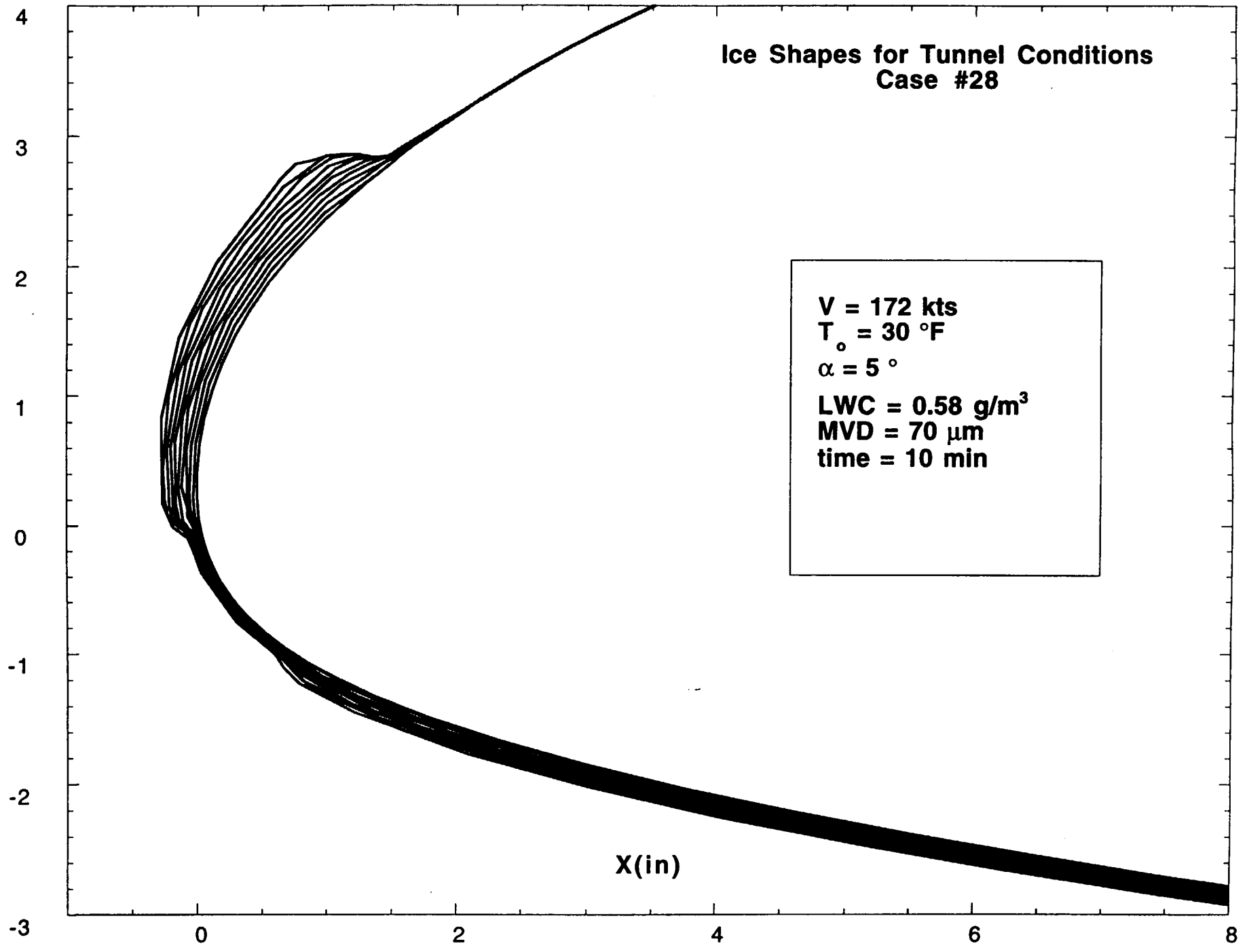
TLC
071

V1-37



**Ice Shapes for Tunnel Conditions
Case #28**

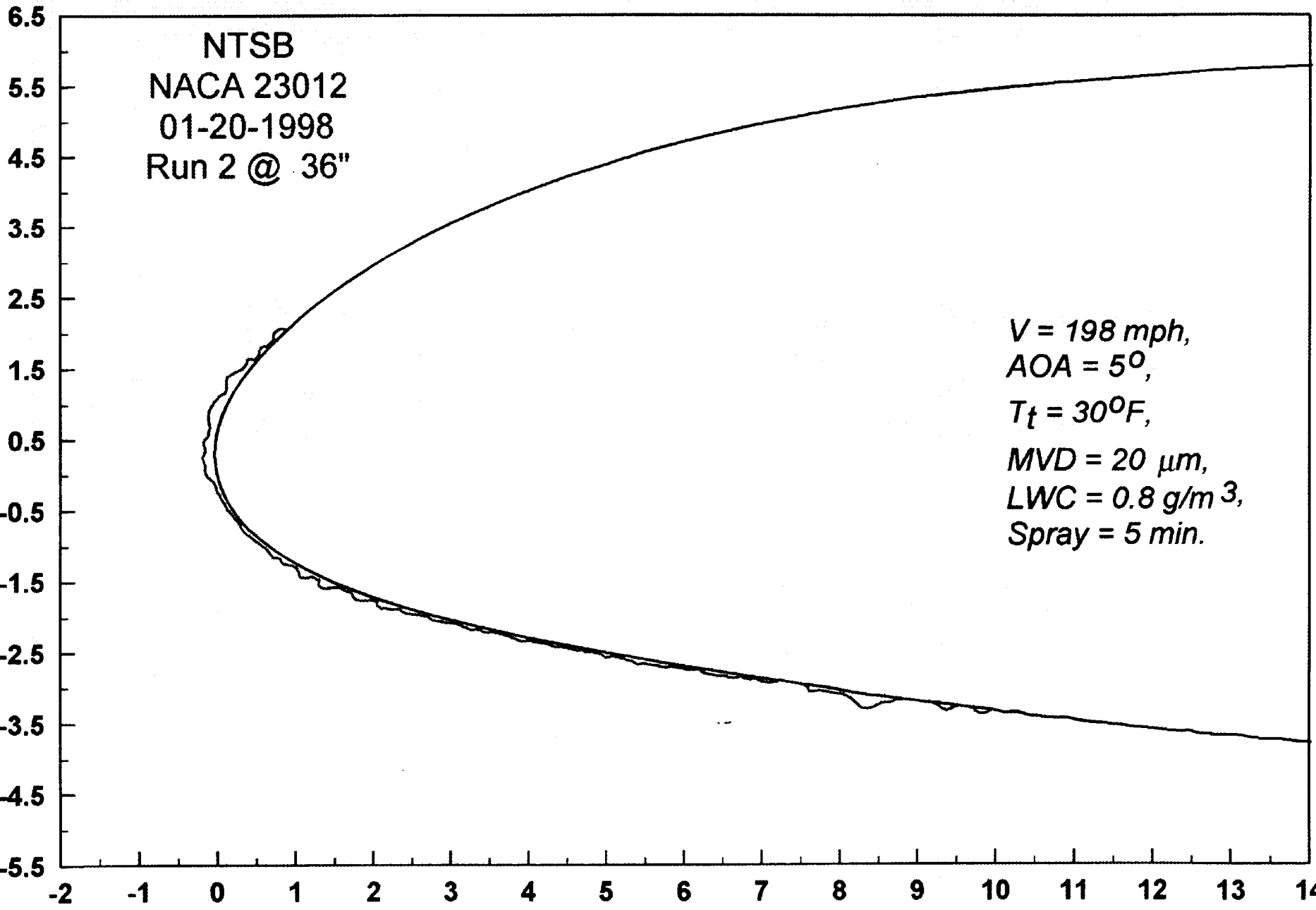
**V = 172 kts
T_o = 30 °F
α = 5 °
LWC = 0.58 g/m³
MVD = 70 μm
time = 10 min**



Z12
U72
Y(in)

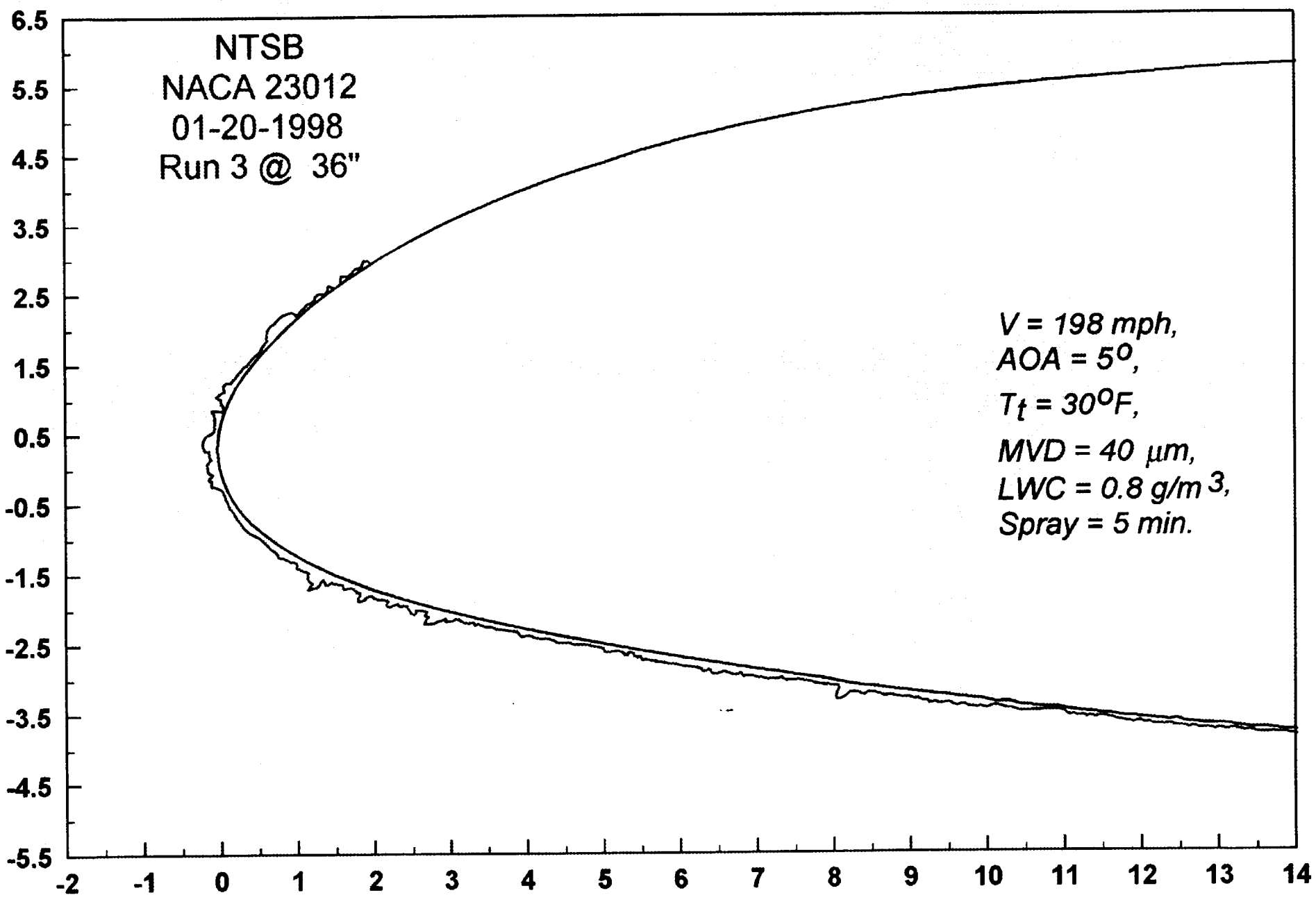
V-38

IRT Ice Shape Results

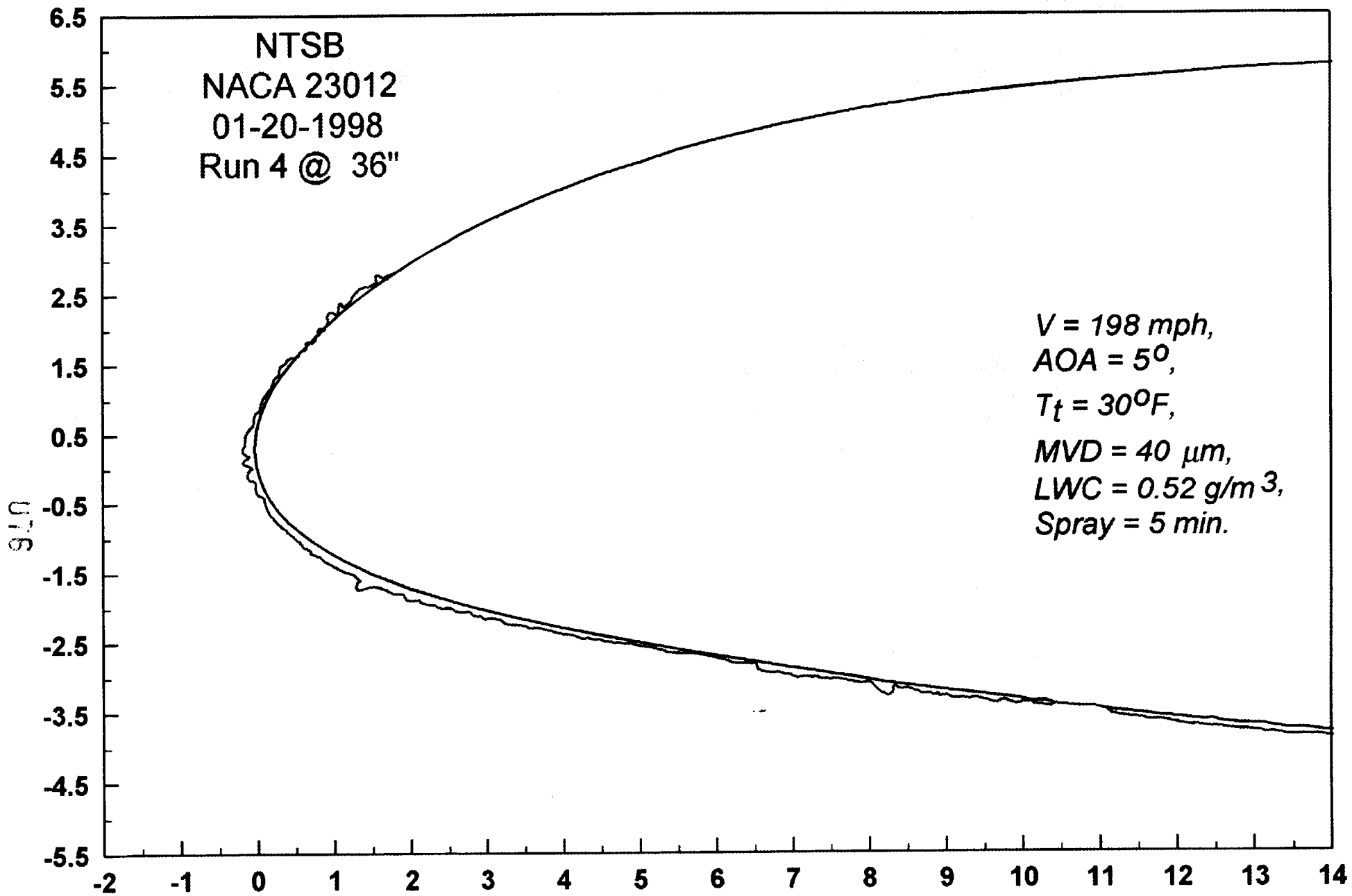


0h-11

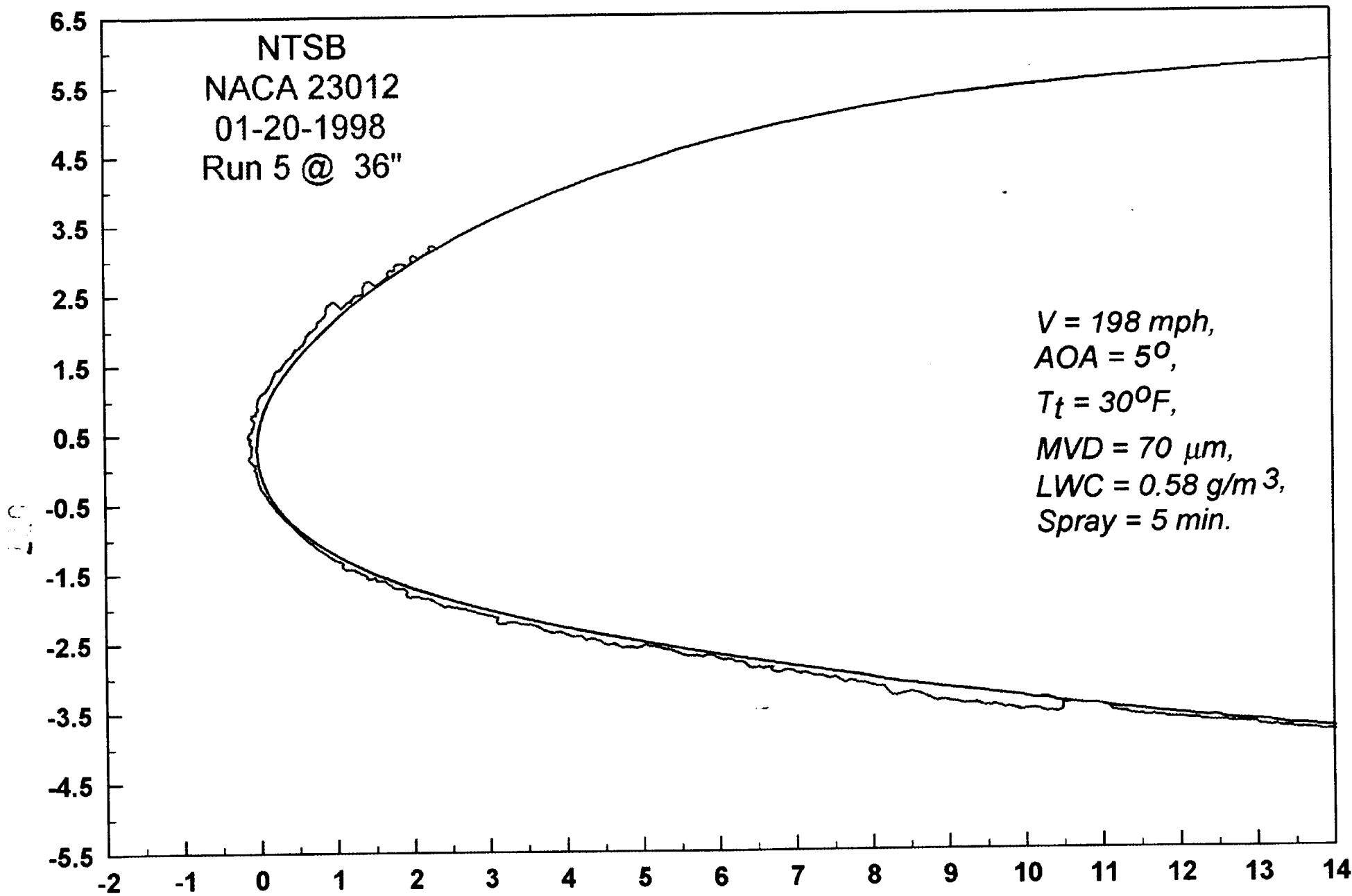
075



M-41



VI-42

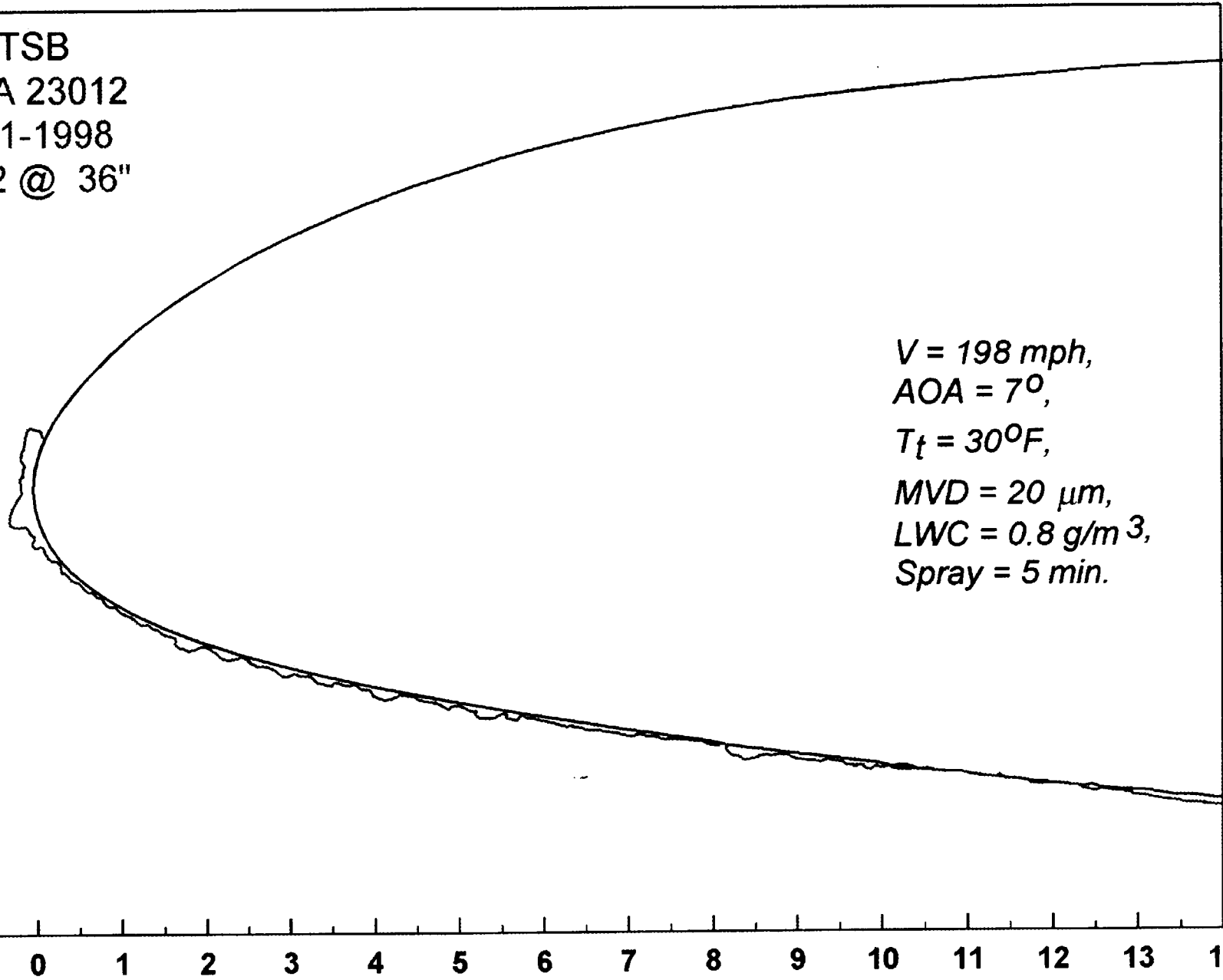


V1-43

6.5
5.5
4.5
3.5
2.5
1.5
0.5
-0.5
-1.5
-2.5
-3.5
-4.5
-5.5

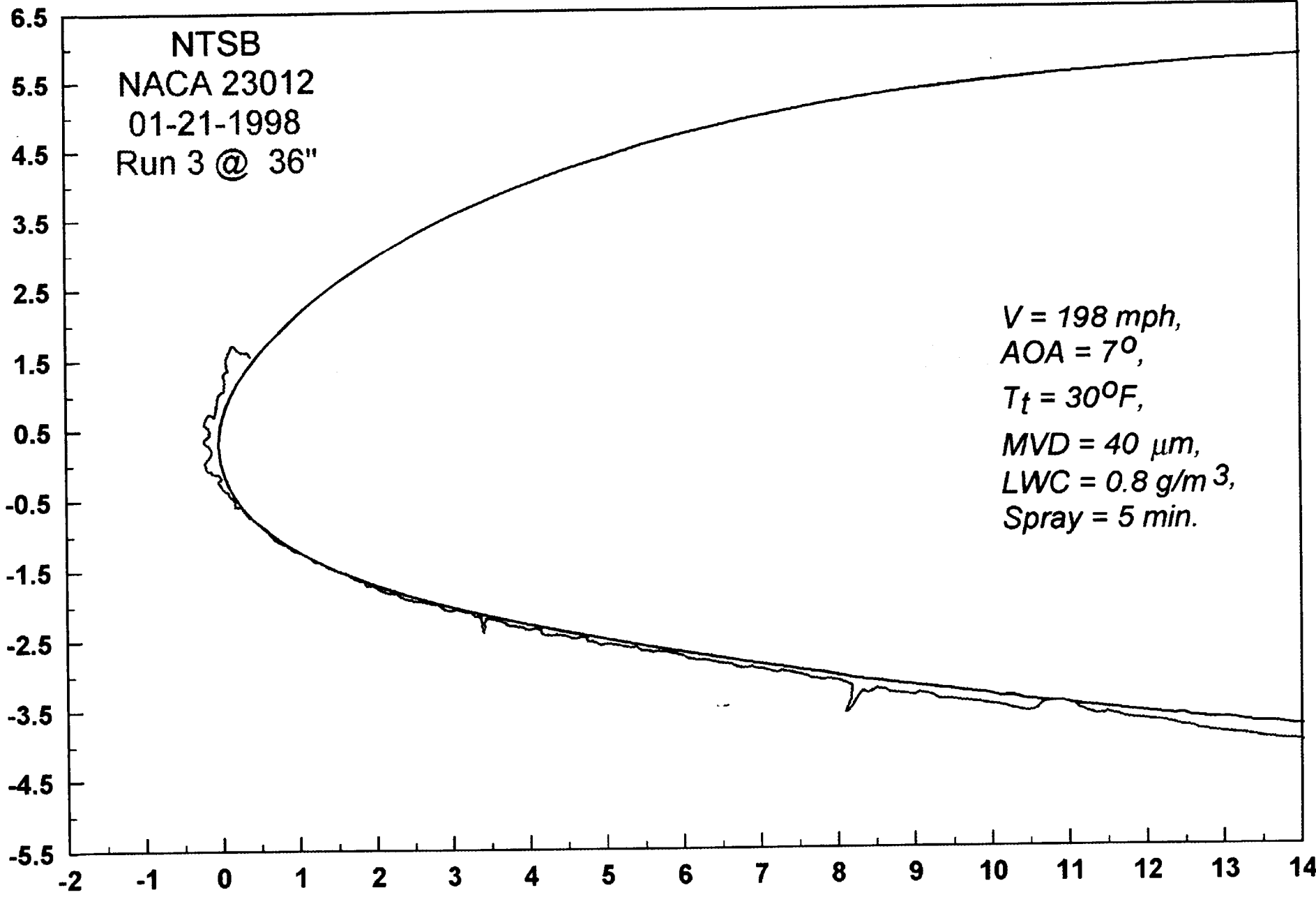
NTSB
NACA 23012
01-21-1998
Run 2 @ 36"

V = 198 mph,
AOA = 7°,
T_t = 30°F,
MVD = 20 μm,
LWC = 0.8 g/m³,
Spray = 5 min.



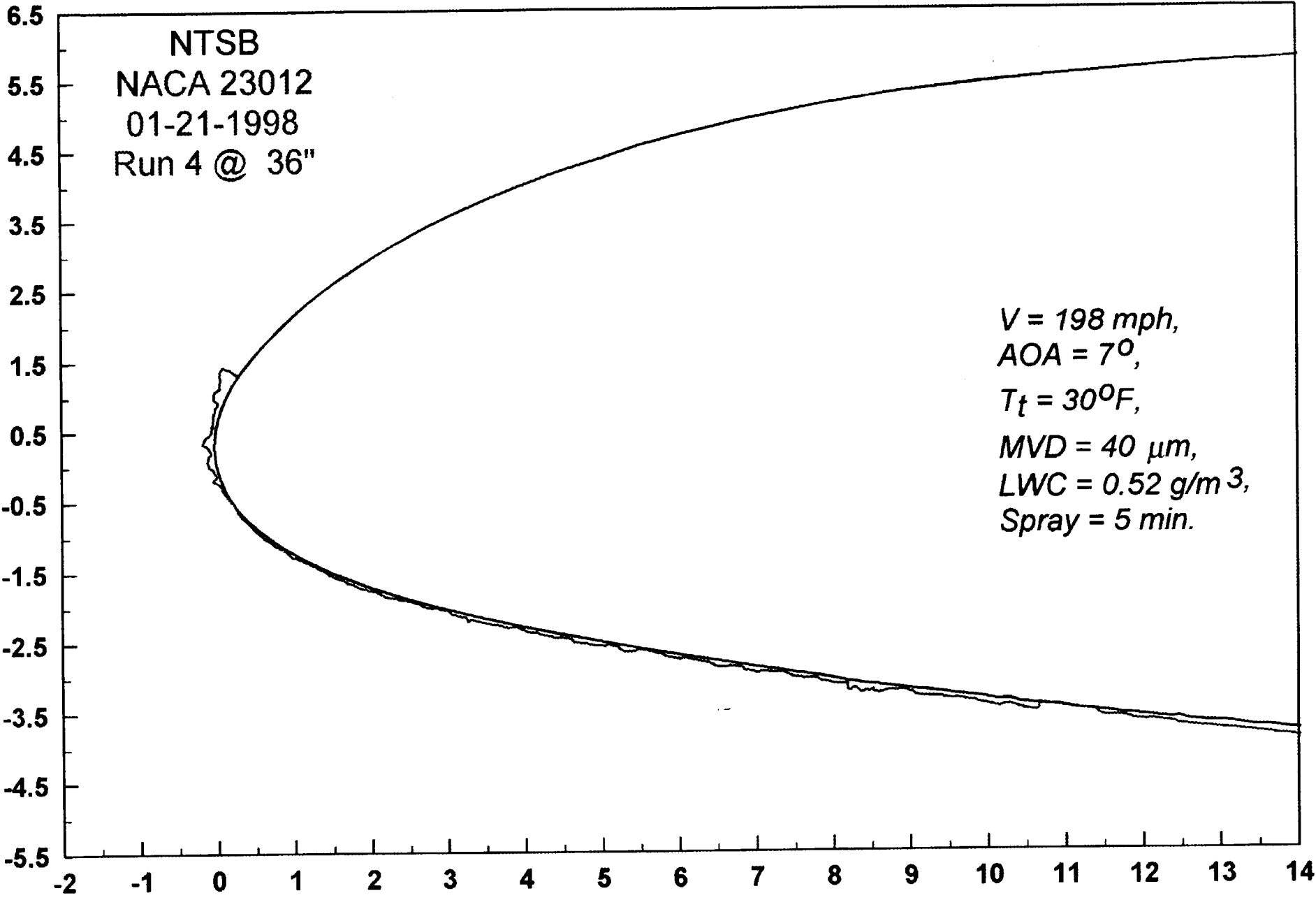
078

11-11



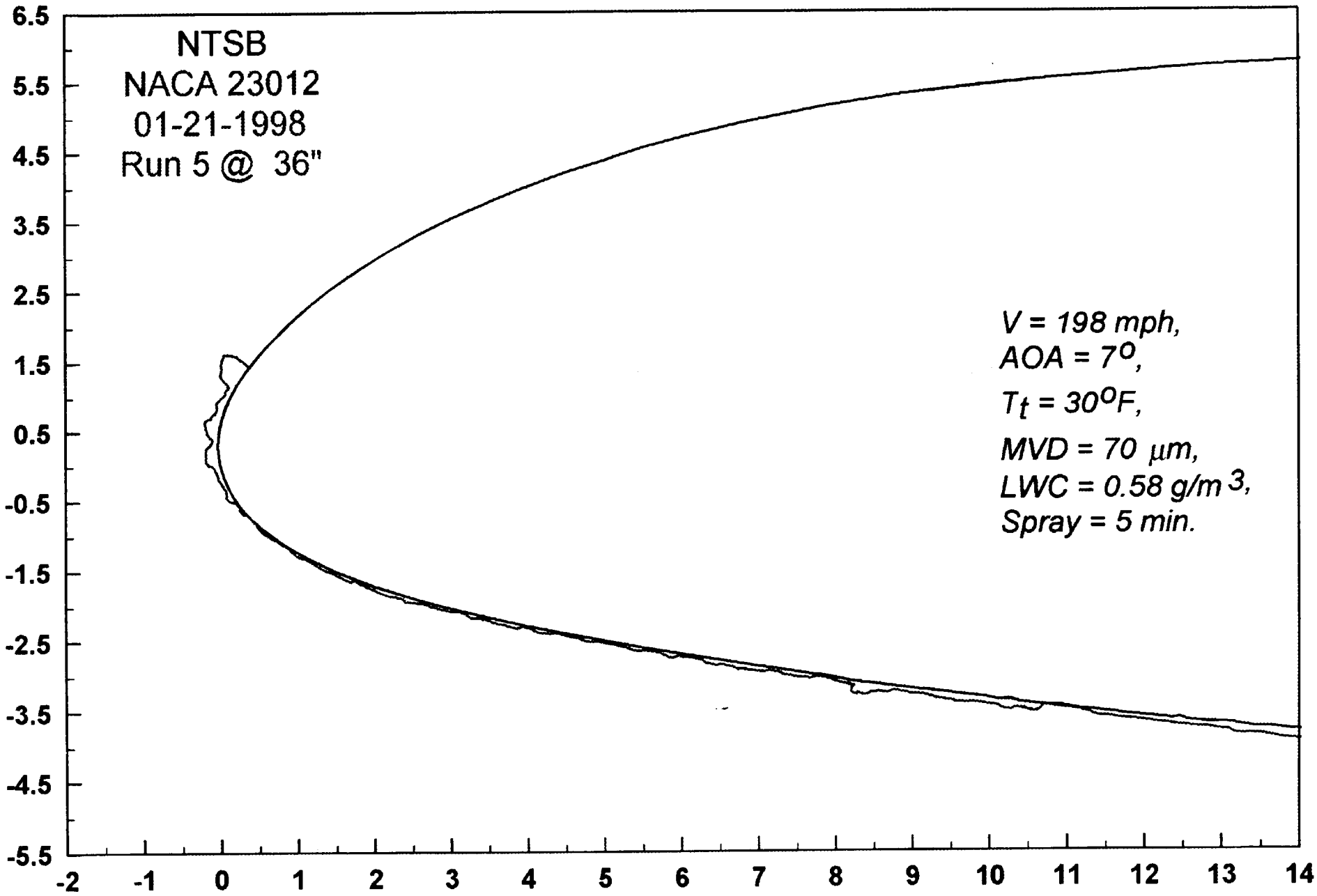
079

M-45

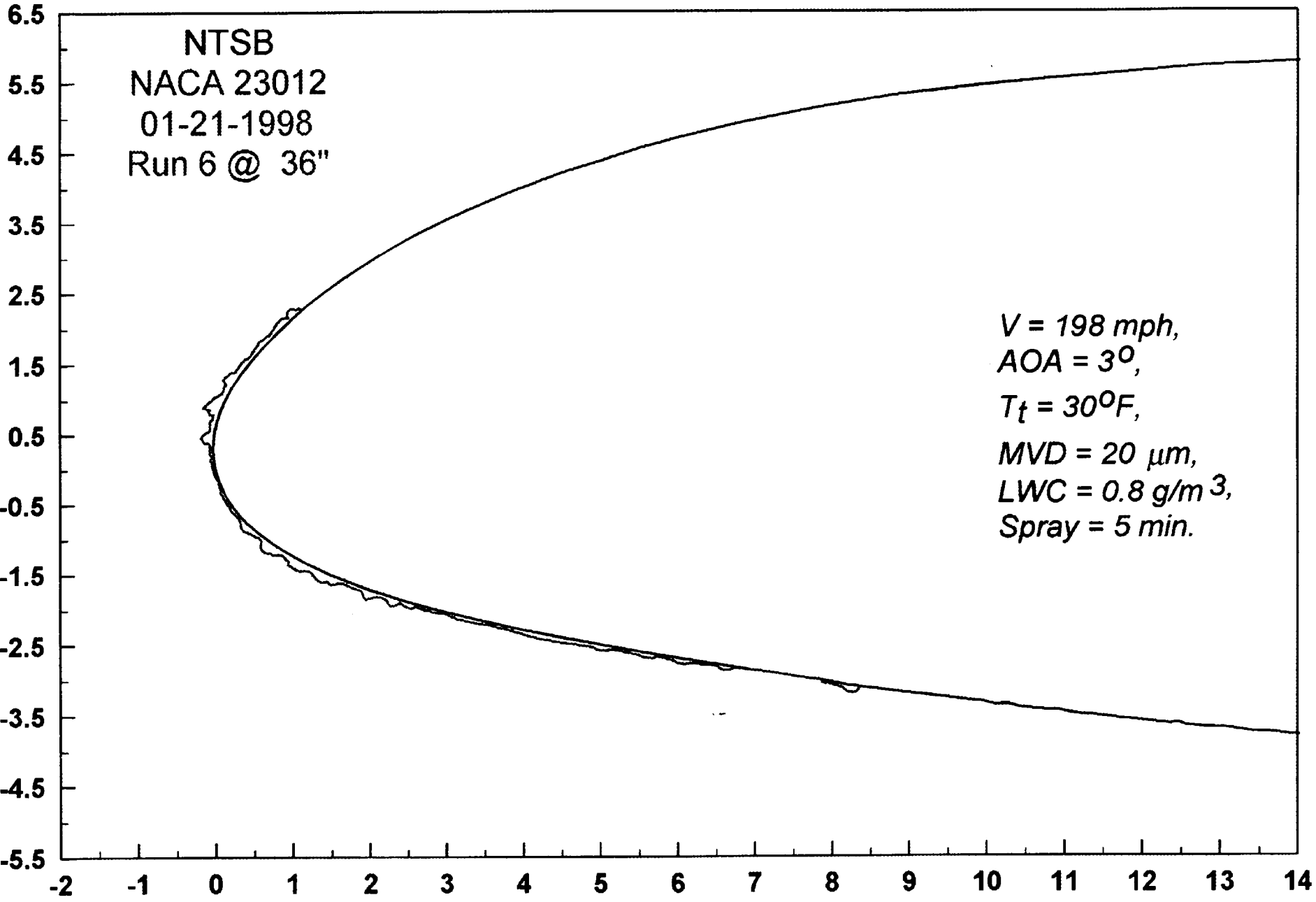


030

VI-46

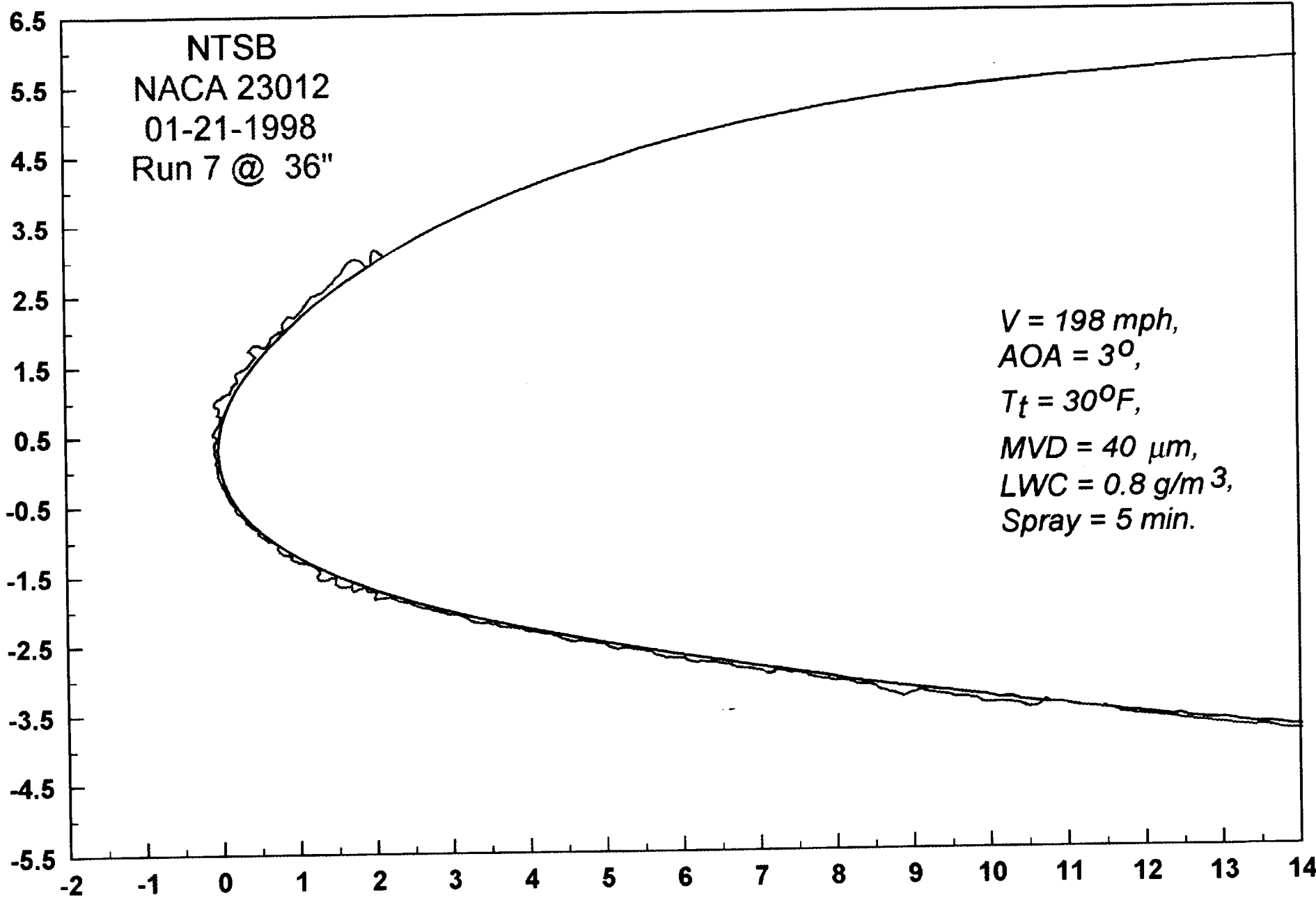


LH-11



W-48

CSD

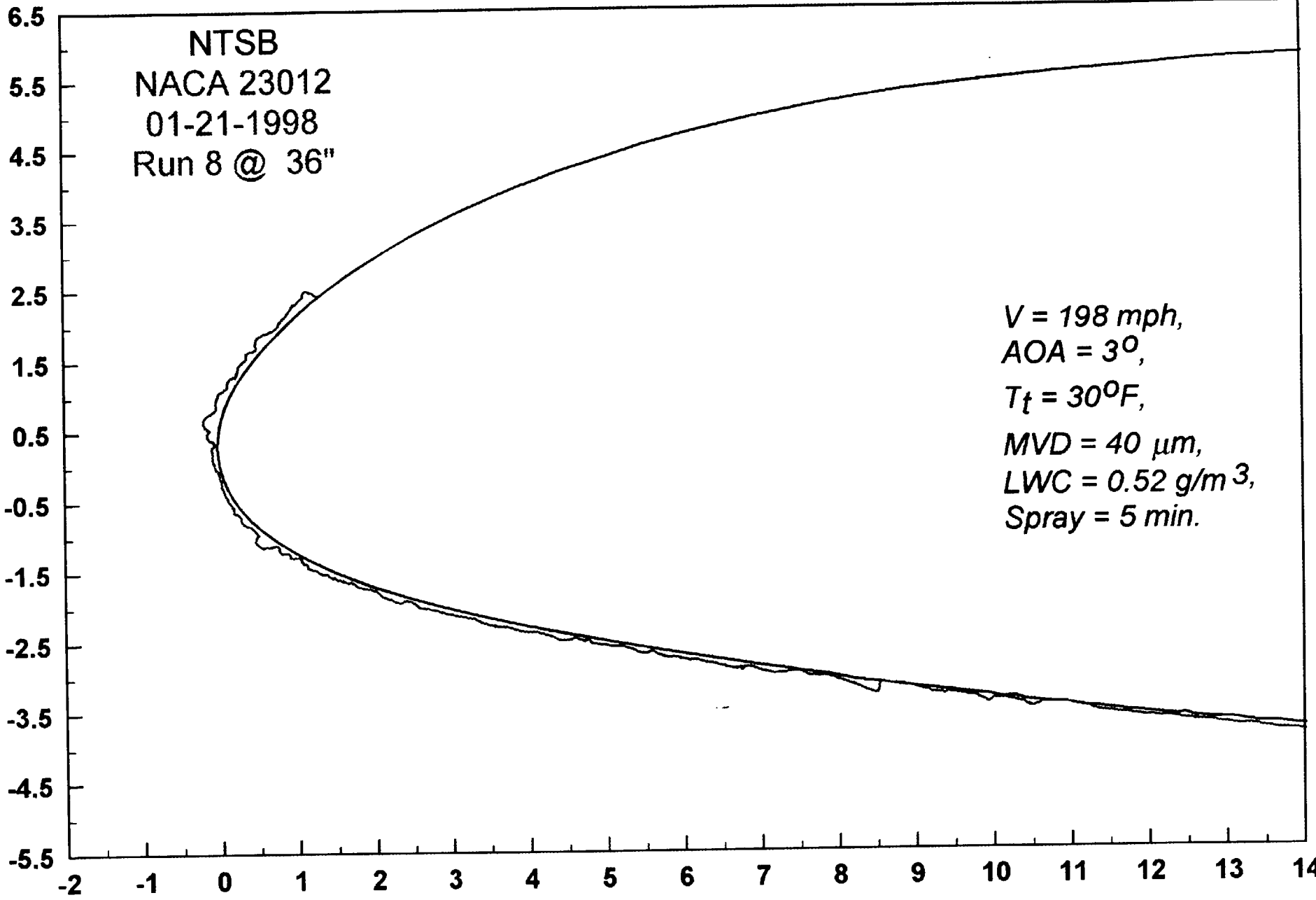


080

W-49

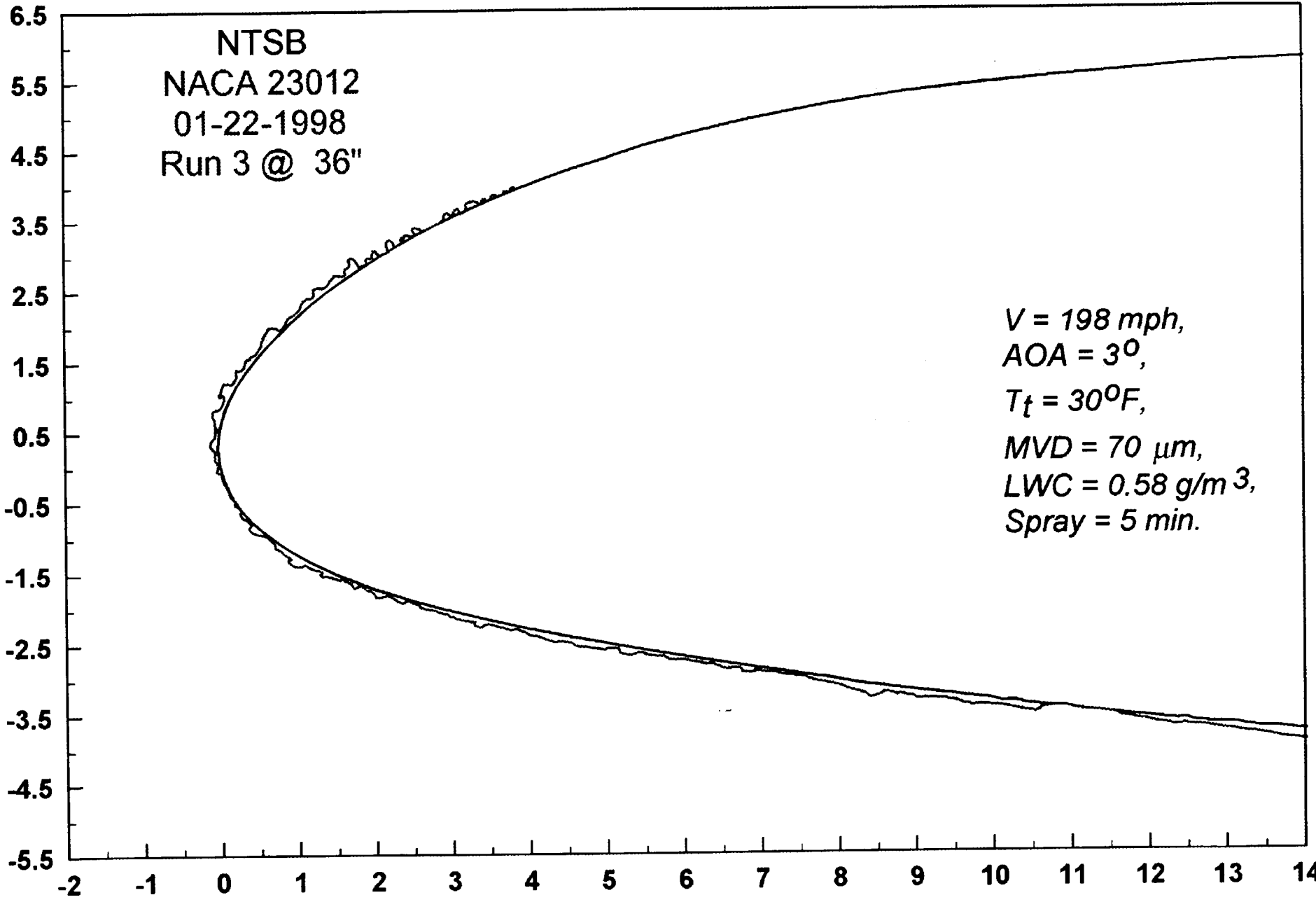
400

N-50



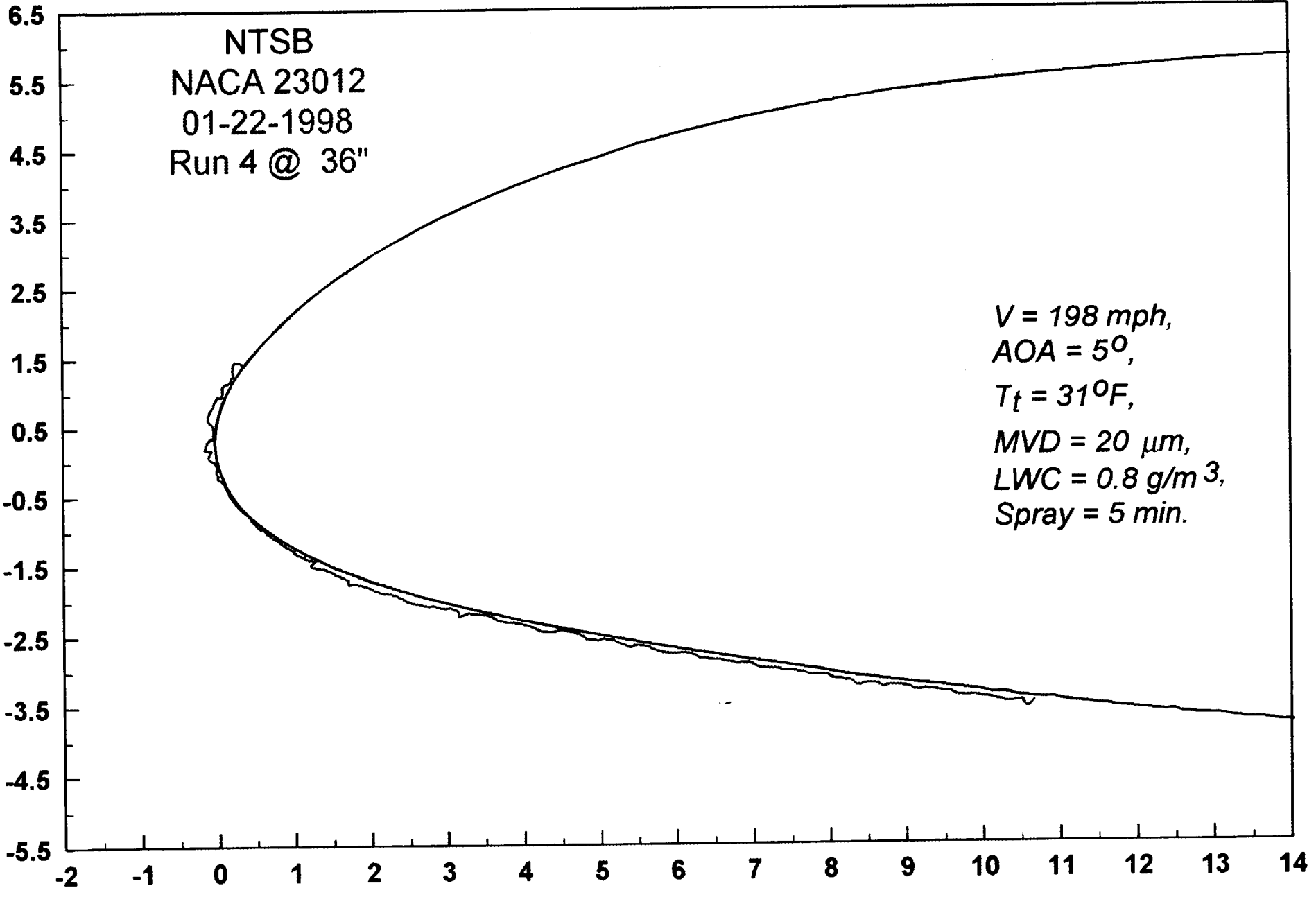
M-51

900



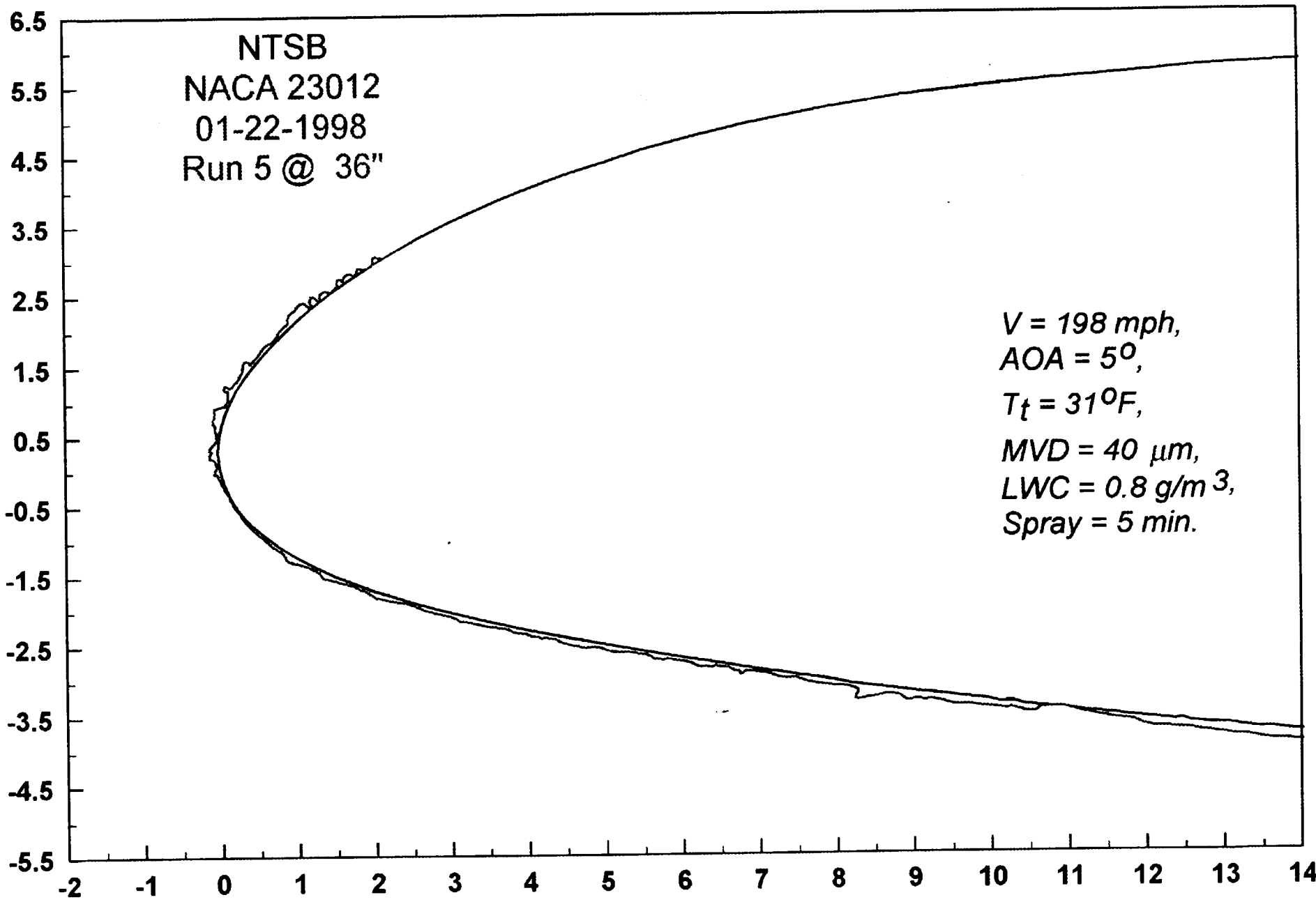
056

M-52



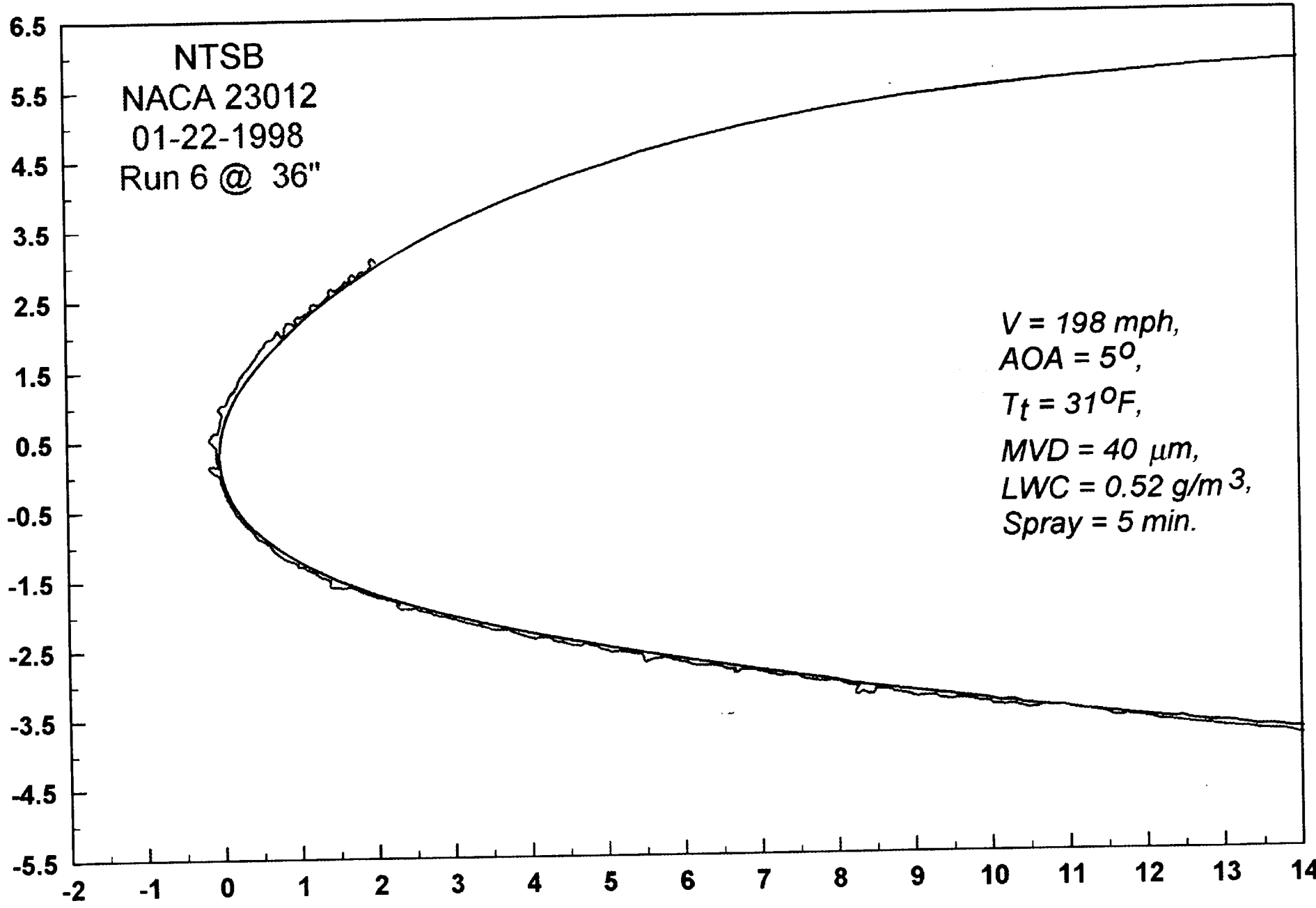
067

N-53



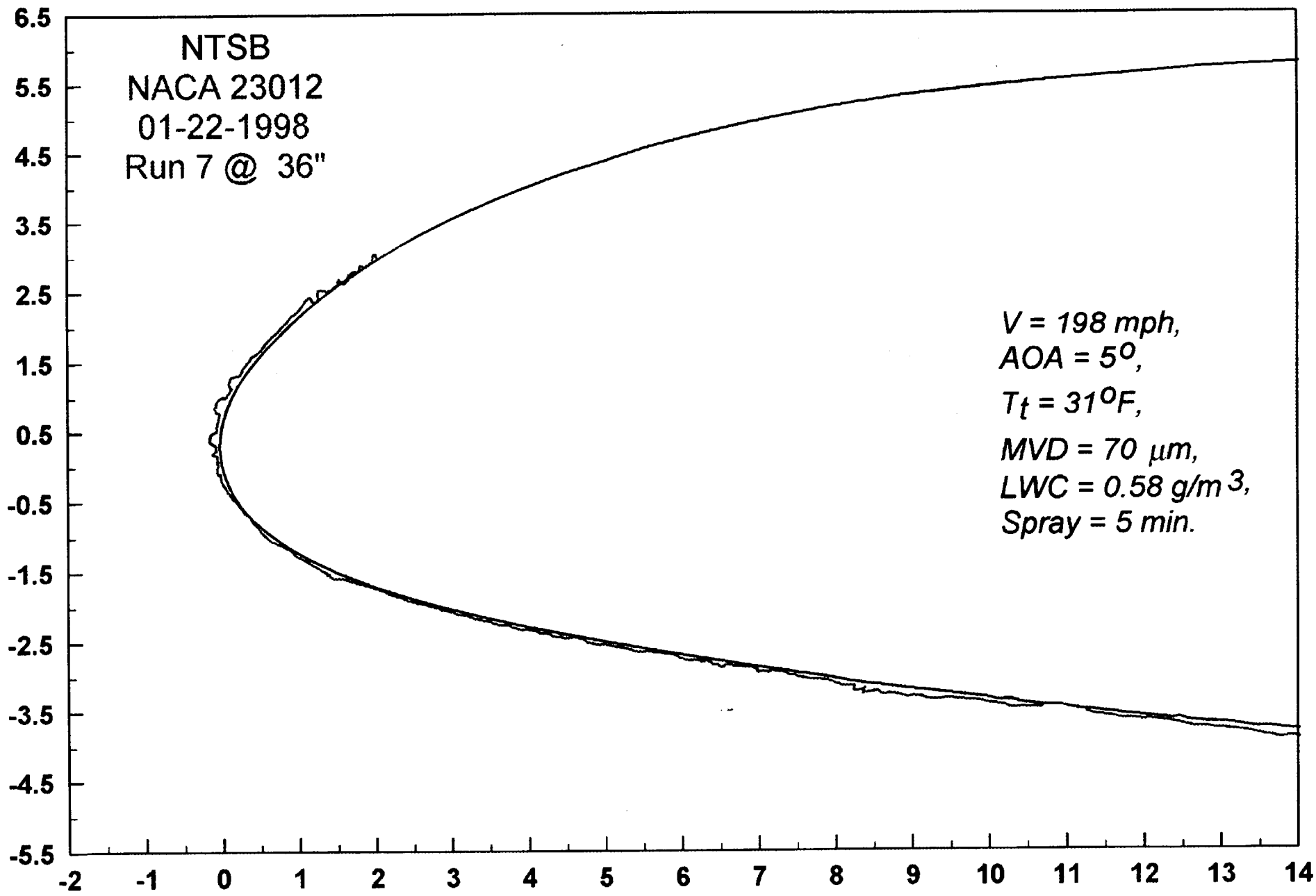
888

VI-54



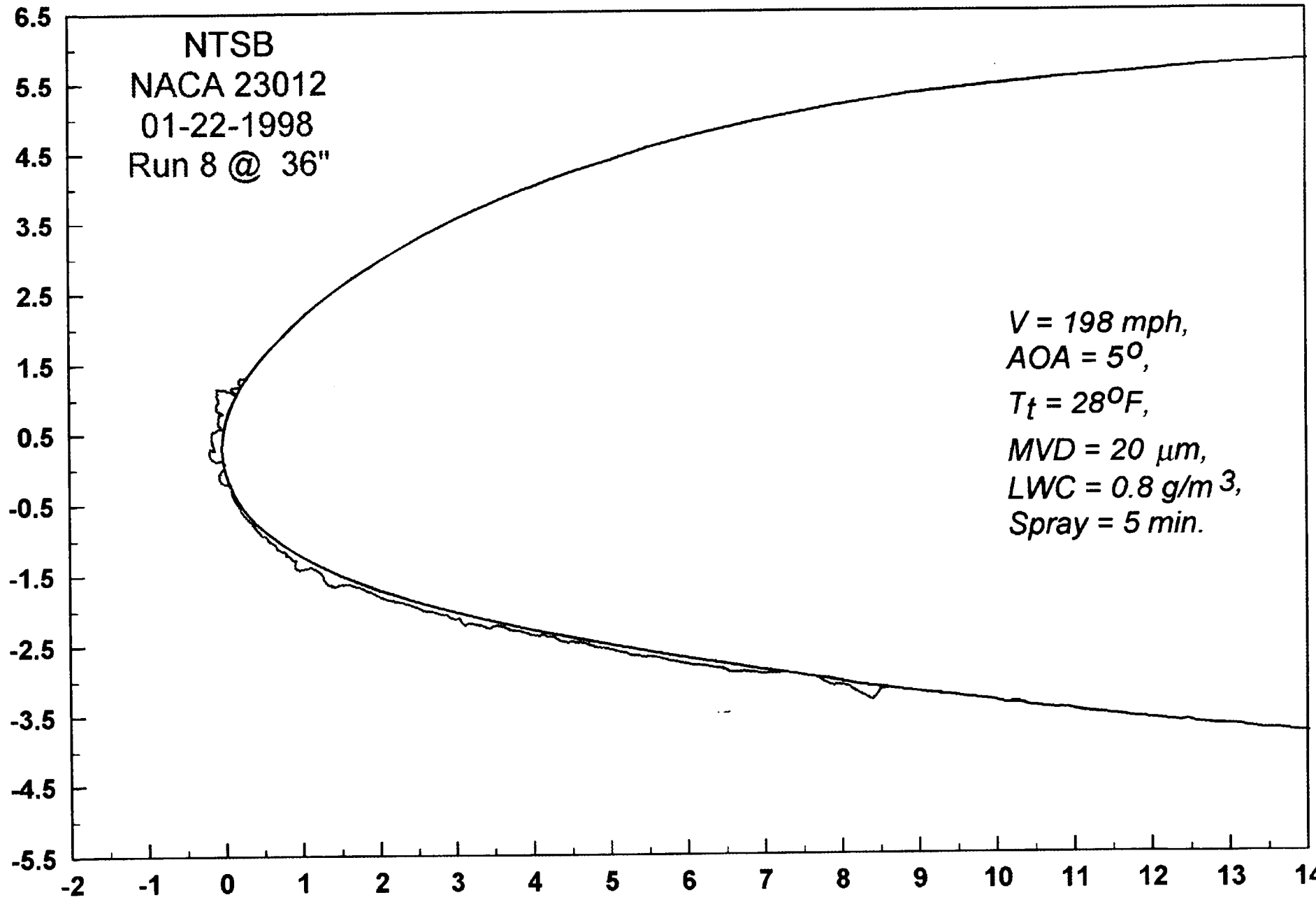
590.

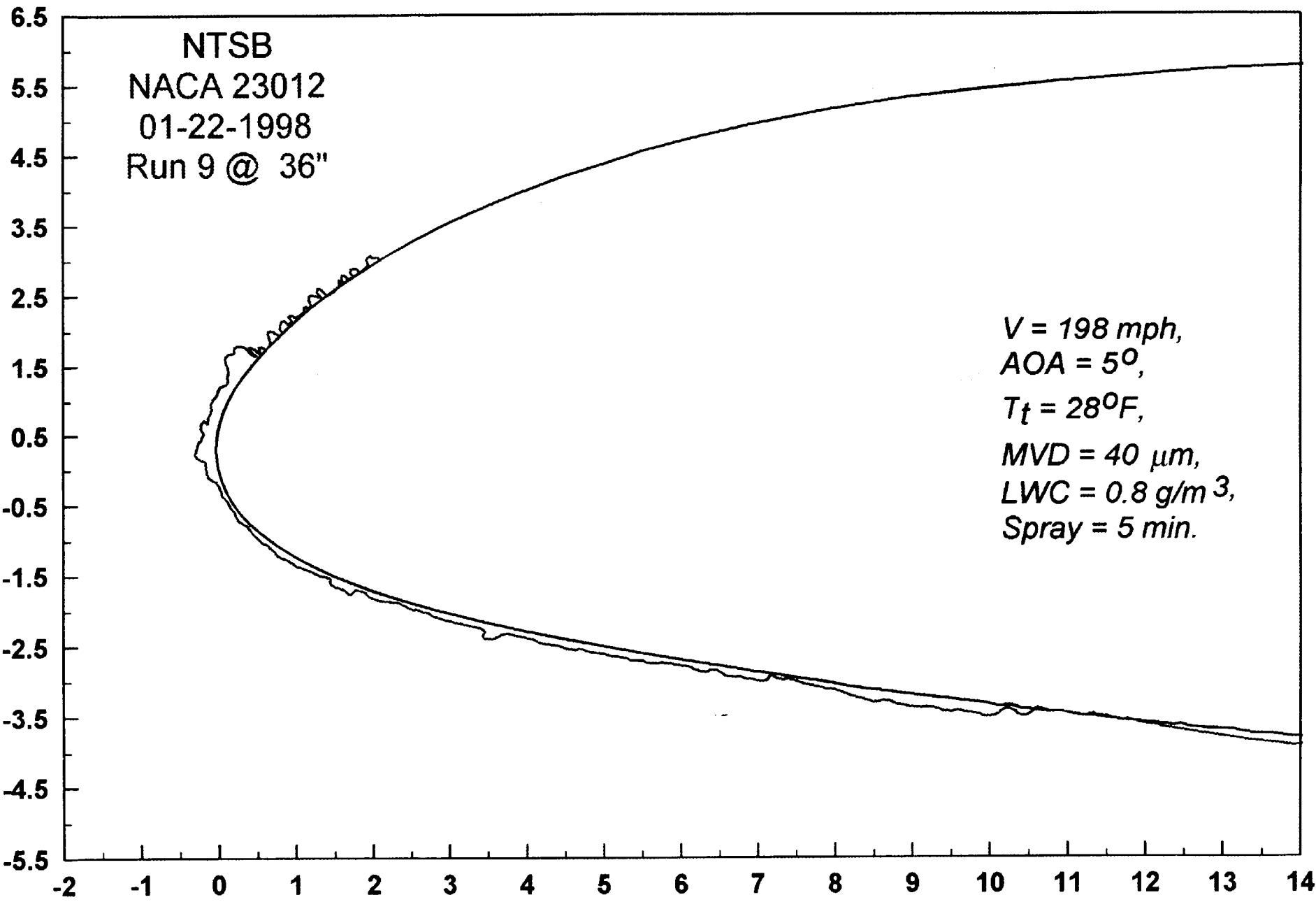
55-55



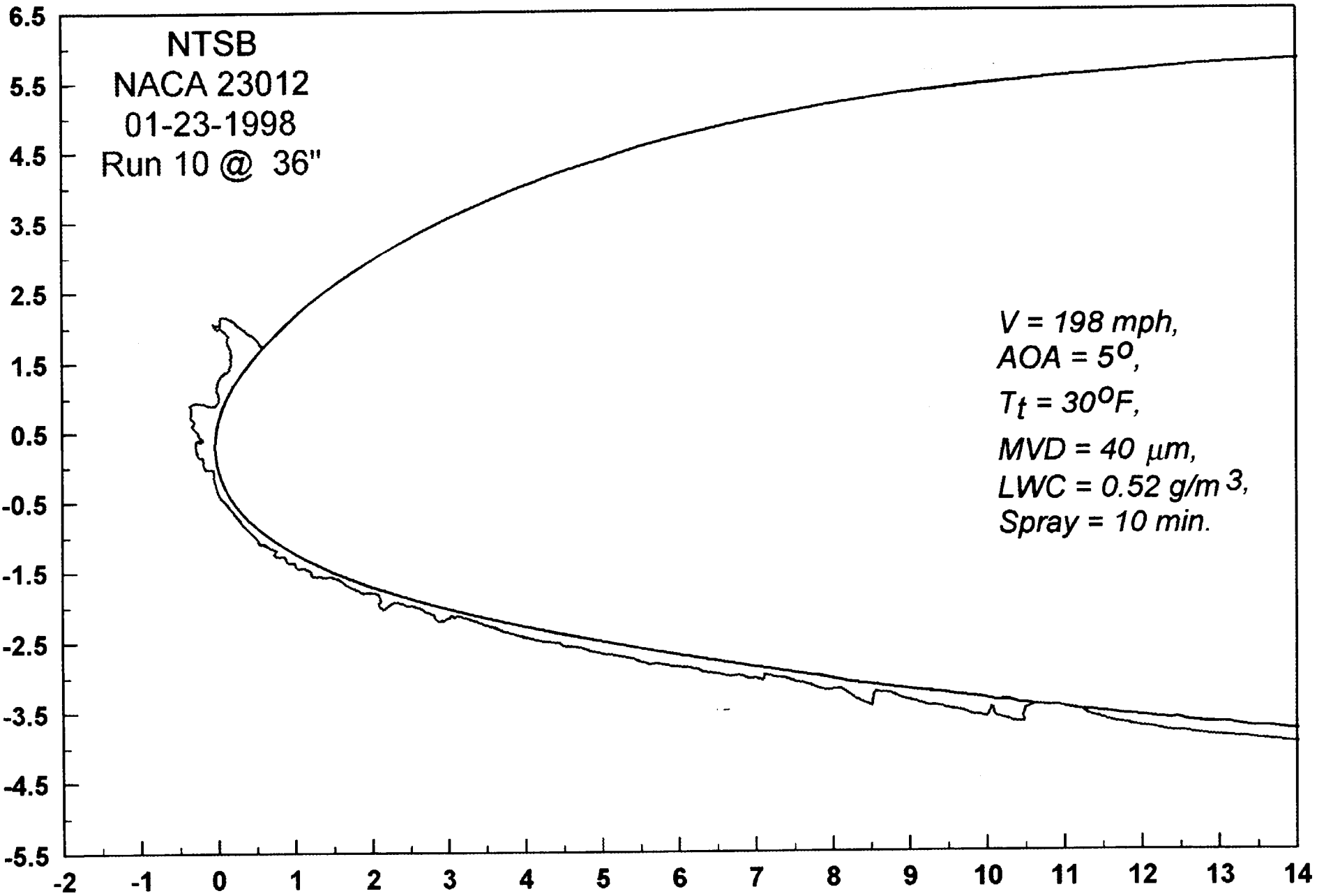
080

VI-56

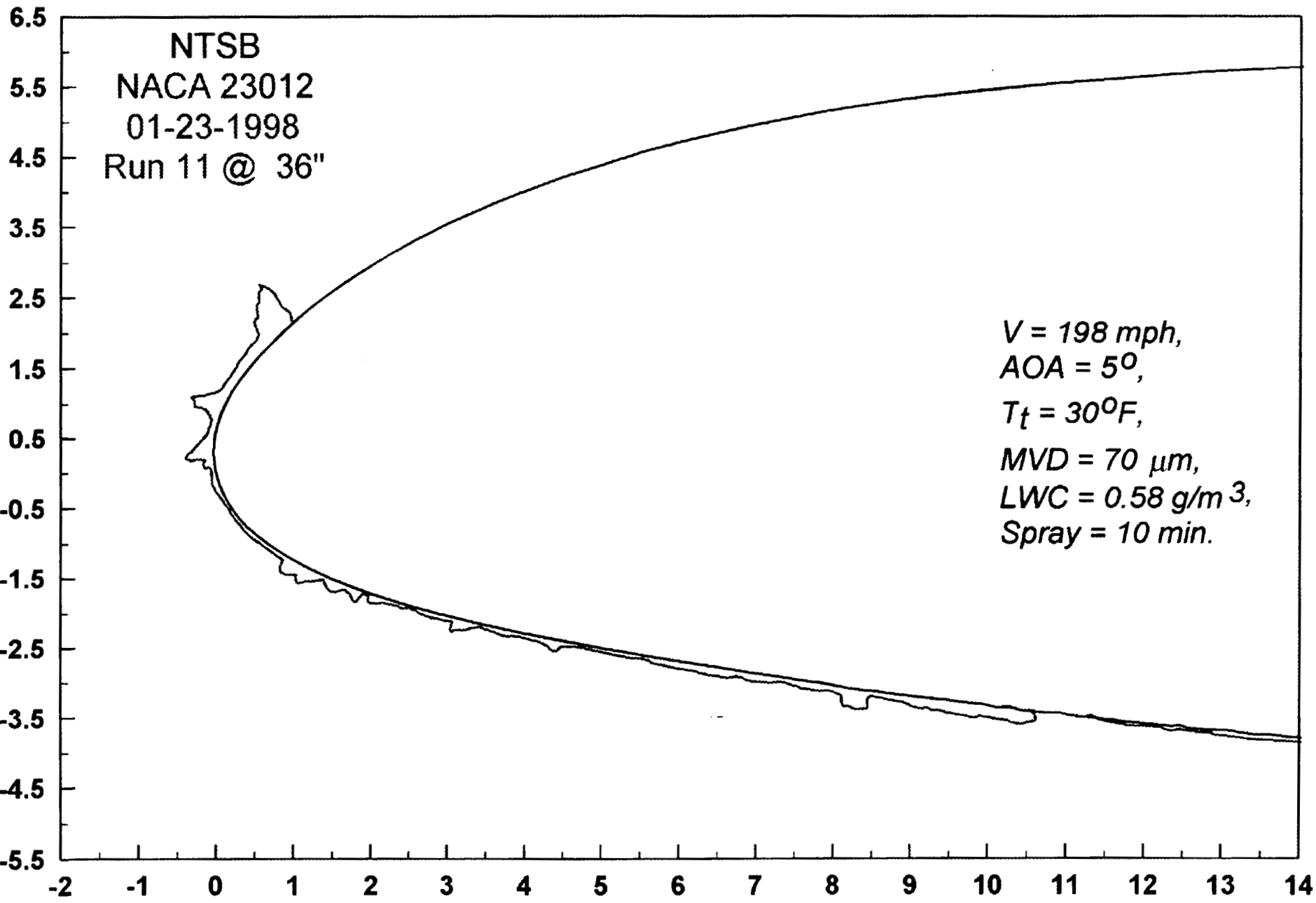


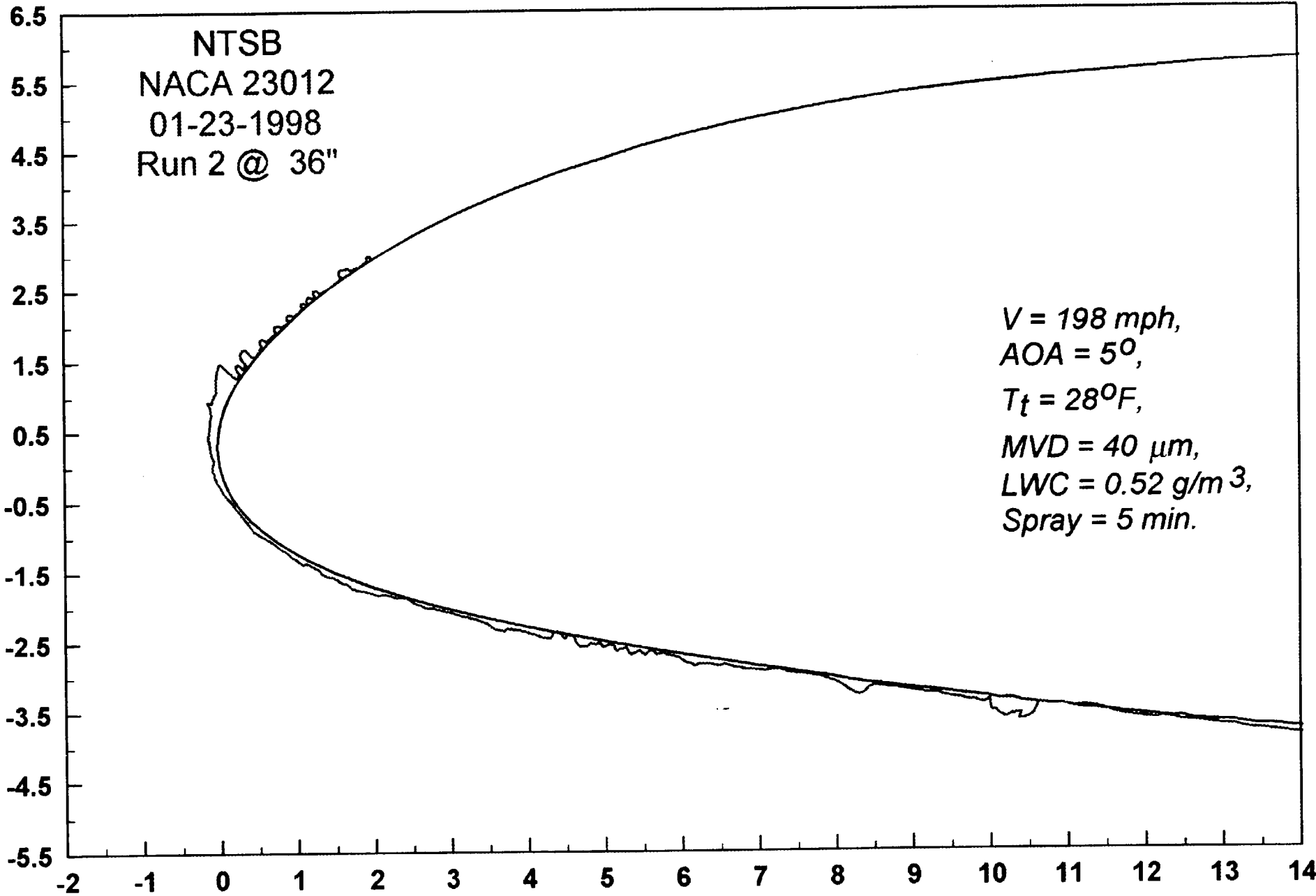


W-57



V1-58





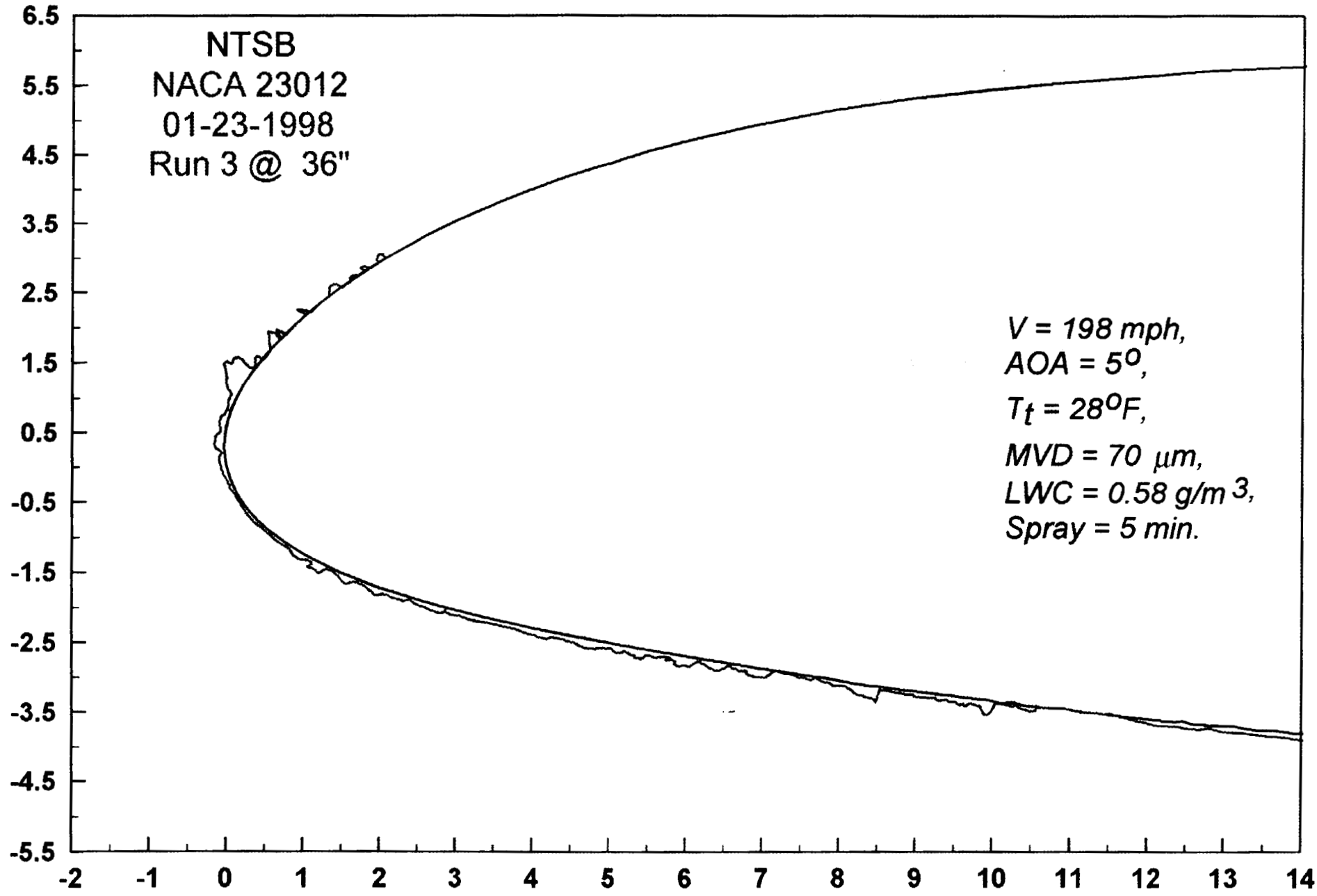
09-11

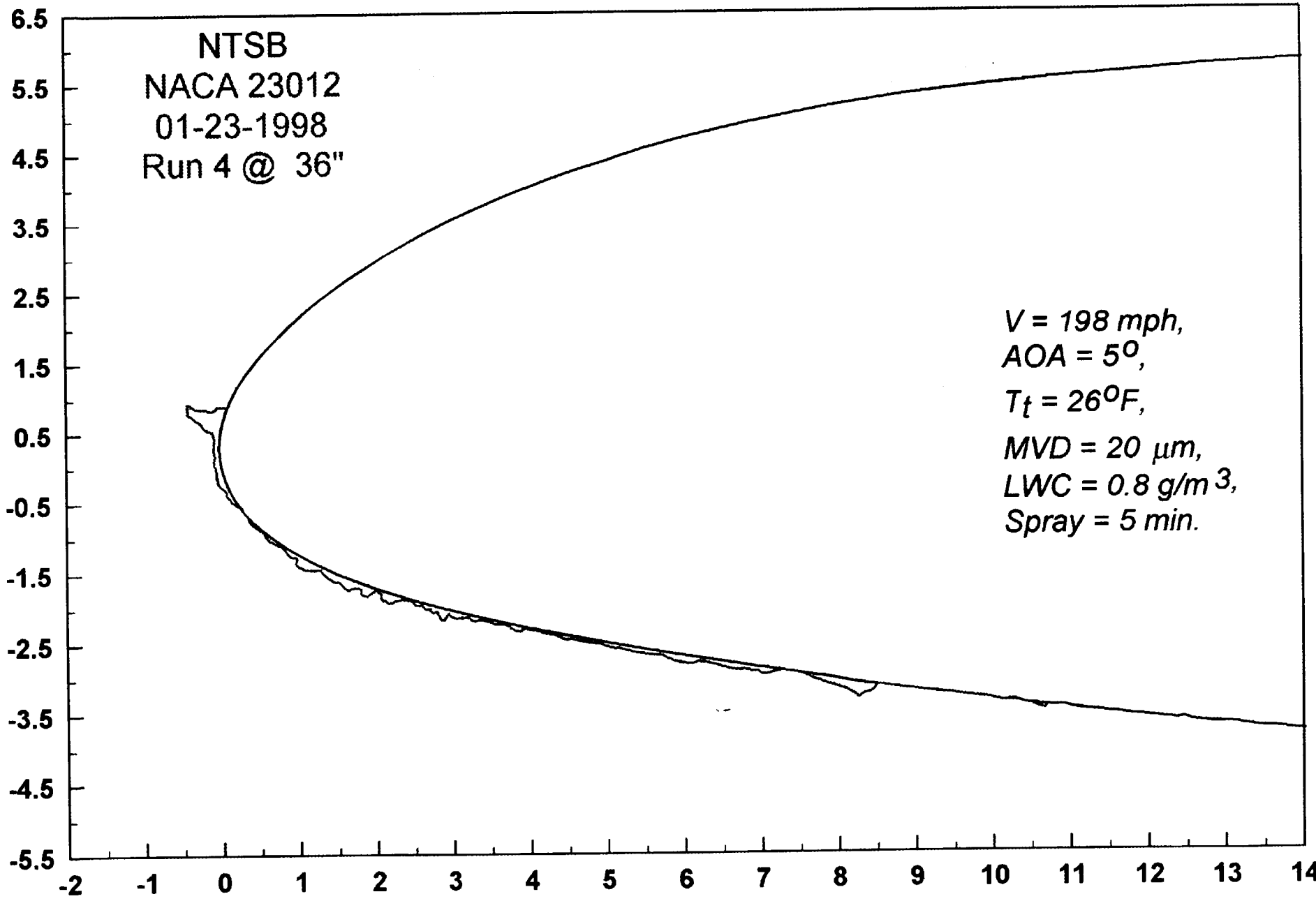
NTSB
NACA 23012
01-23-1998
Run 3 @ 36"

V = 198 mph,
AOA = 5°,
T_t = 28°F,
MVD = 70 μm,
LWC = 0.58 g/m³,
Spray = 5 min.

095

19-61





0.96

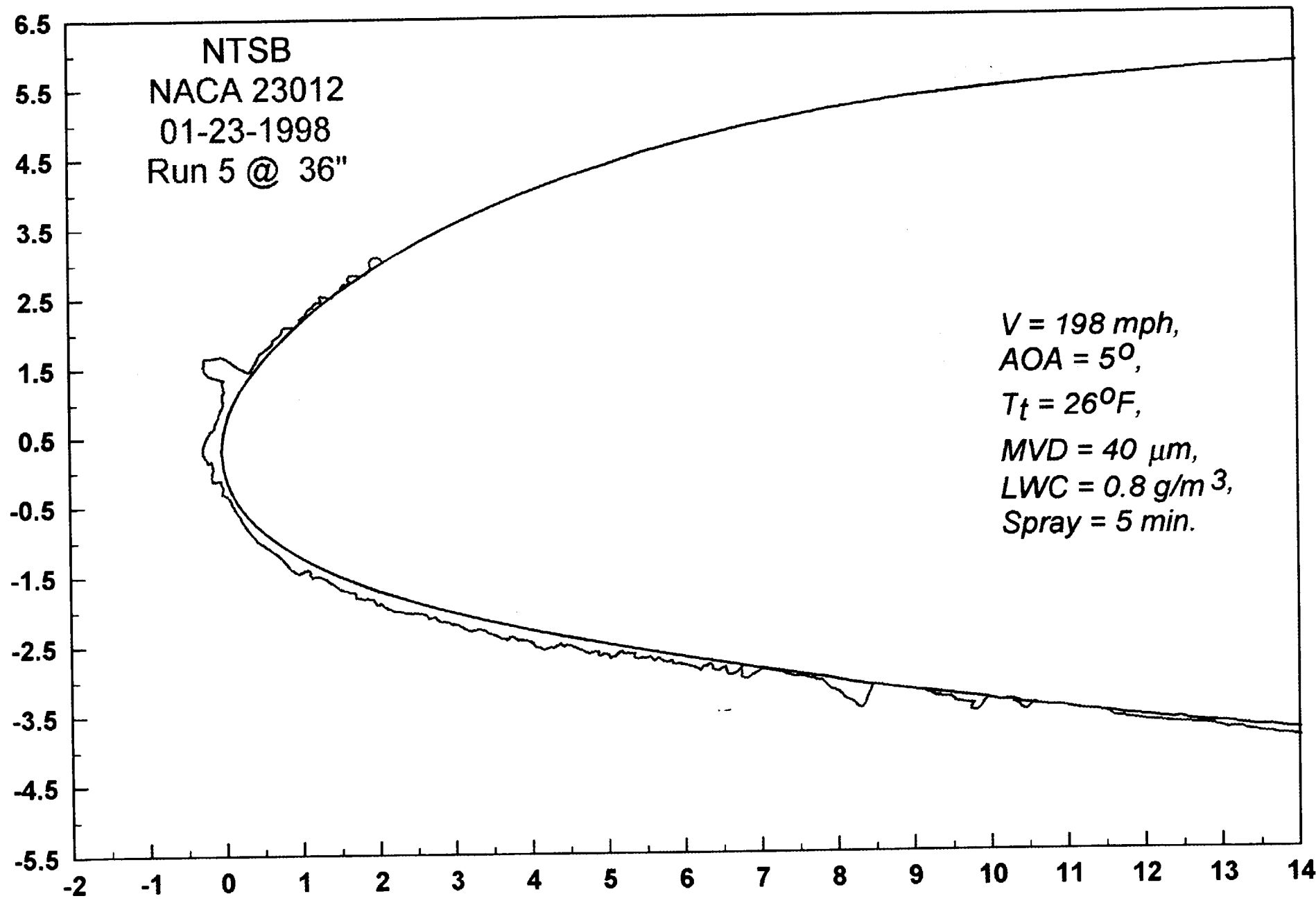
VI-62

NTSB
NACA 23012
01-23-1998
Run 5 @ 36"

$V = 198 \text{ mph}$,
 $AOA = 5^\circ$,
 $T_t = 26^\circ F$,
 $MVD = 40 \mu m$,
 $LWC = 0.8 \text{ g/m}^3$,
Spray = 5 min.

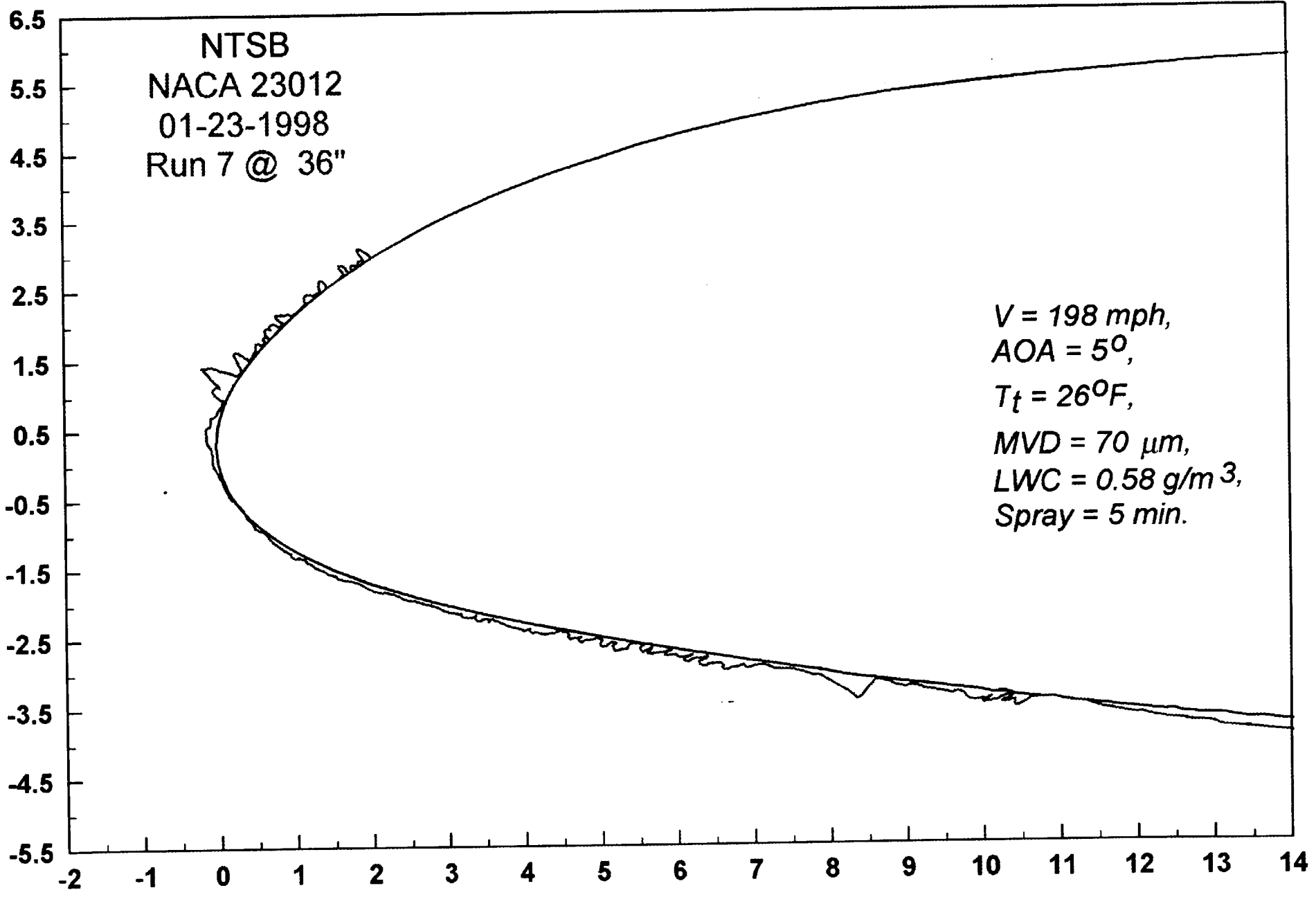
087

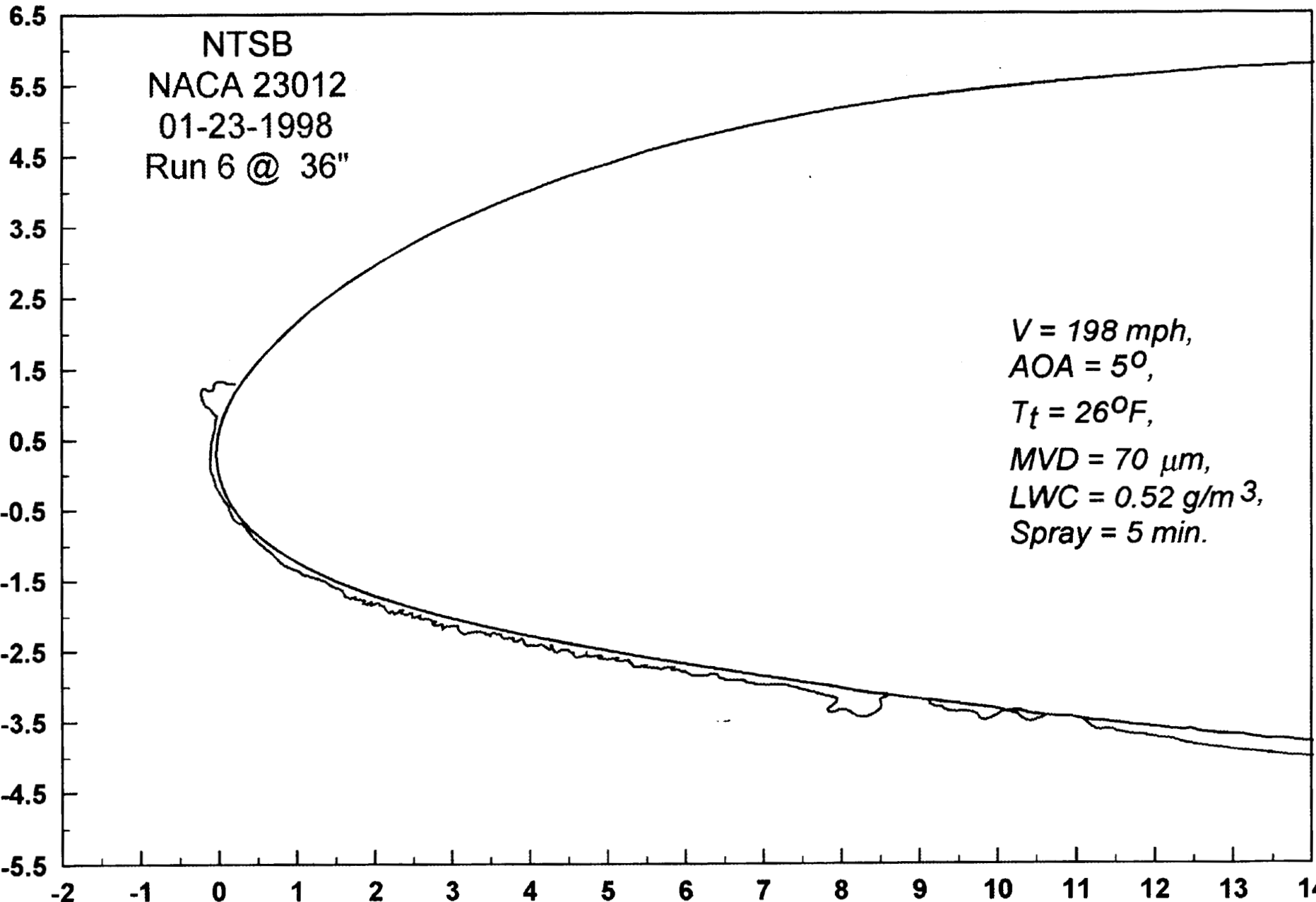
W-63



11-614

098



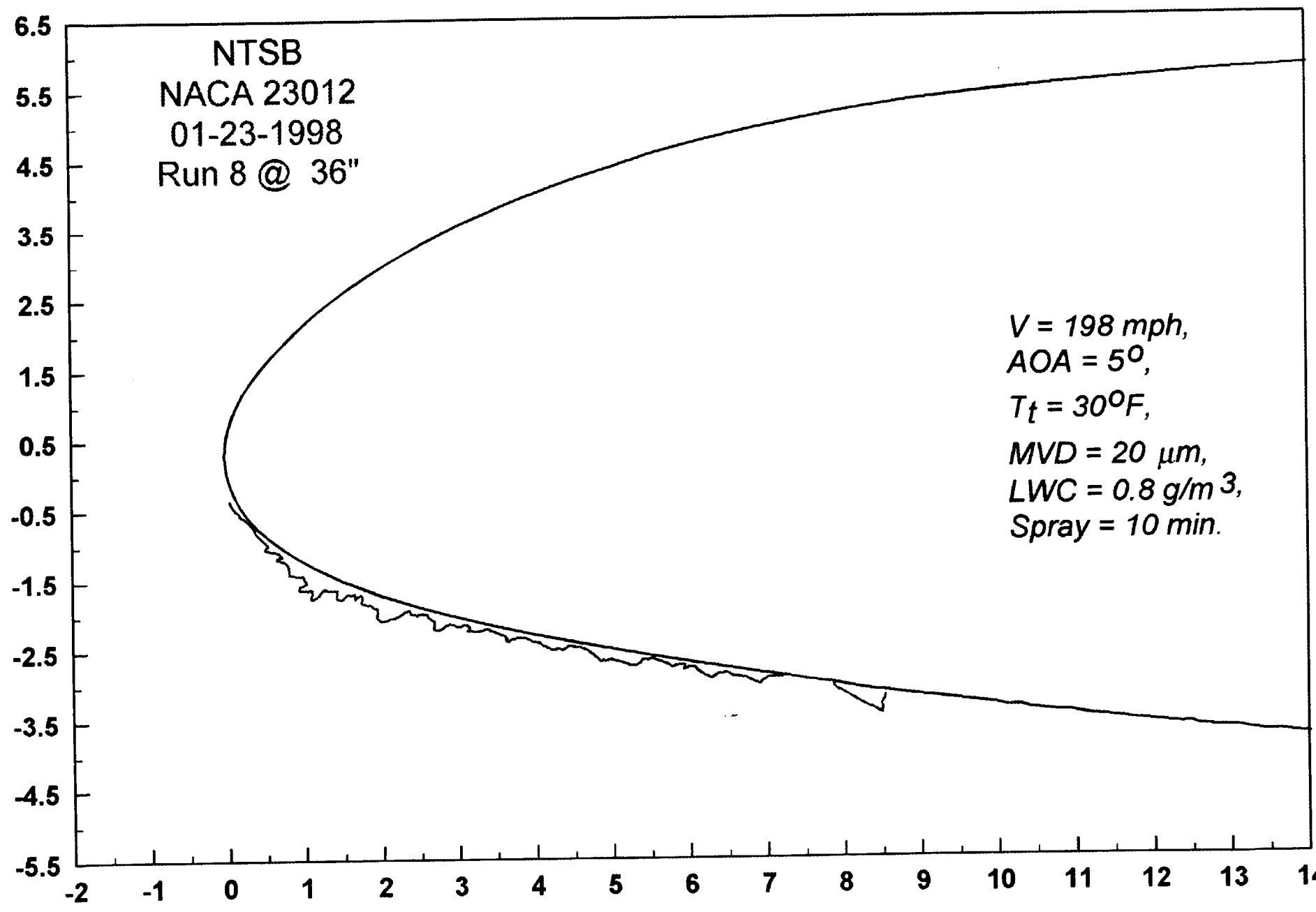


069

M-65

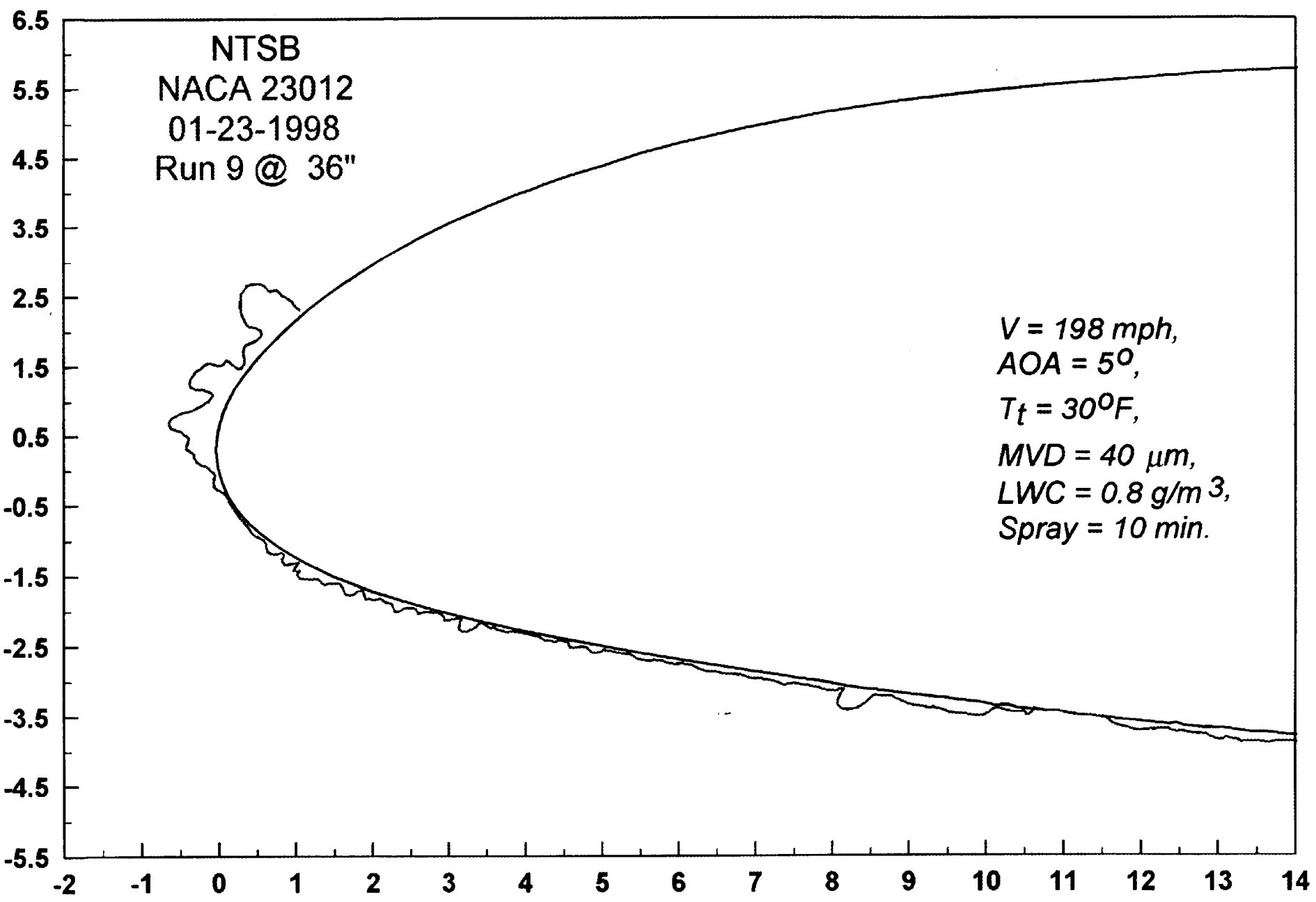
99-66

100



19-11

TCT

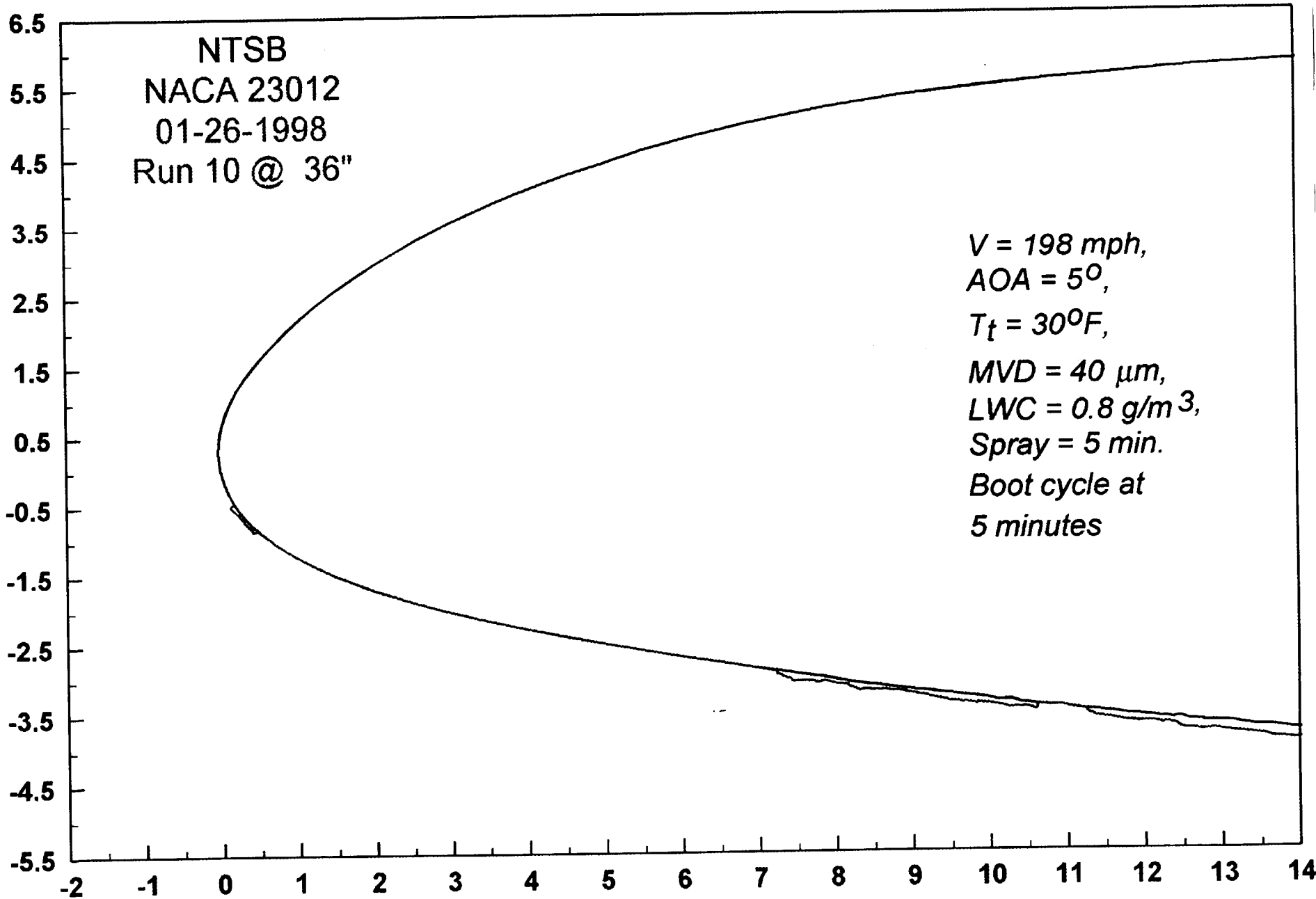


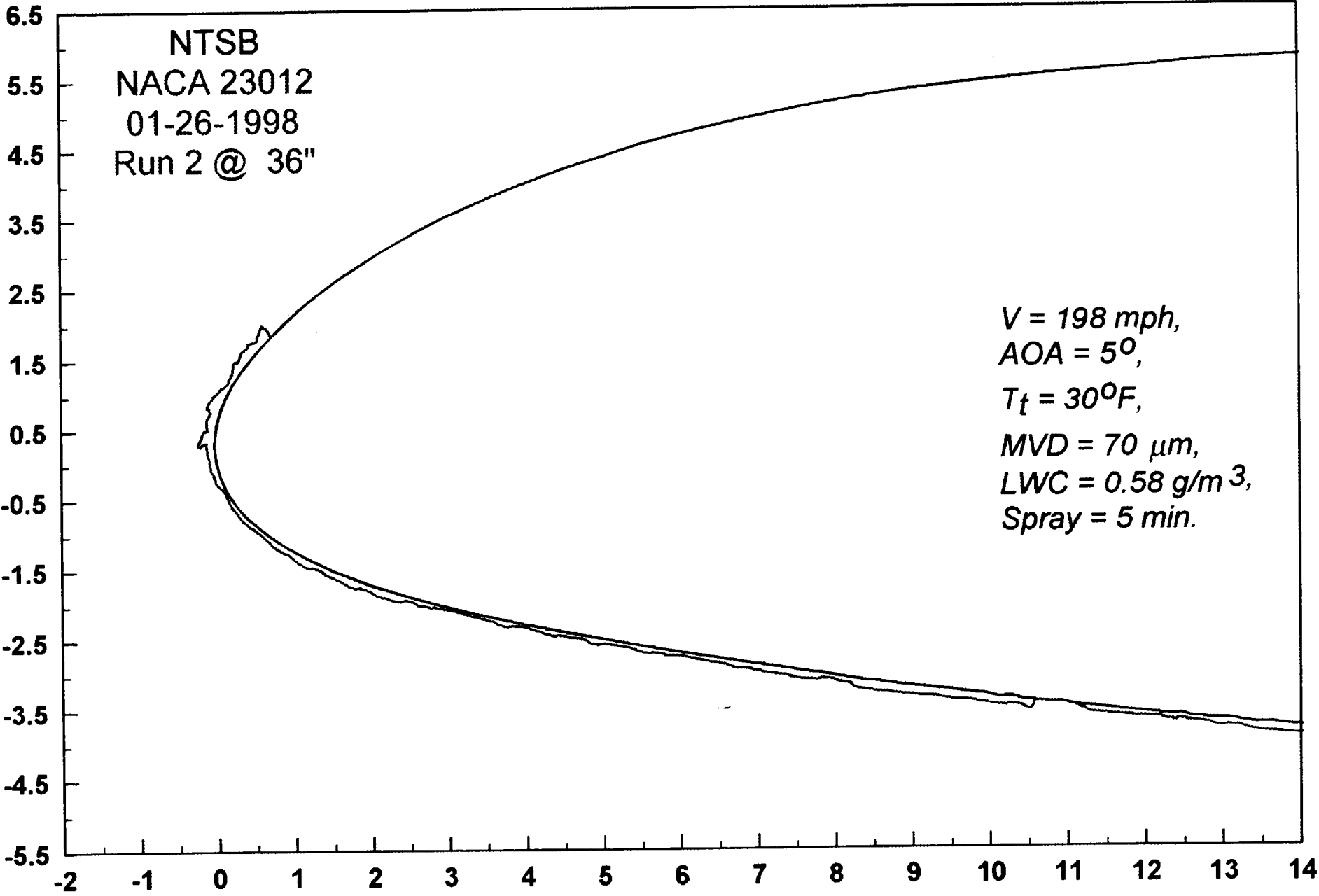
NTSB
NACA 23012
01-26-1998
Run 10 @ 36"

*V = 198 mph,
AOA = 5°,
T_t = 30°F,
MVD = 40 μm,
LWC = 0.8 g/m³,
Spray = 5 min.
Boot cycle at
5 minutes*

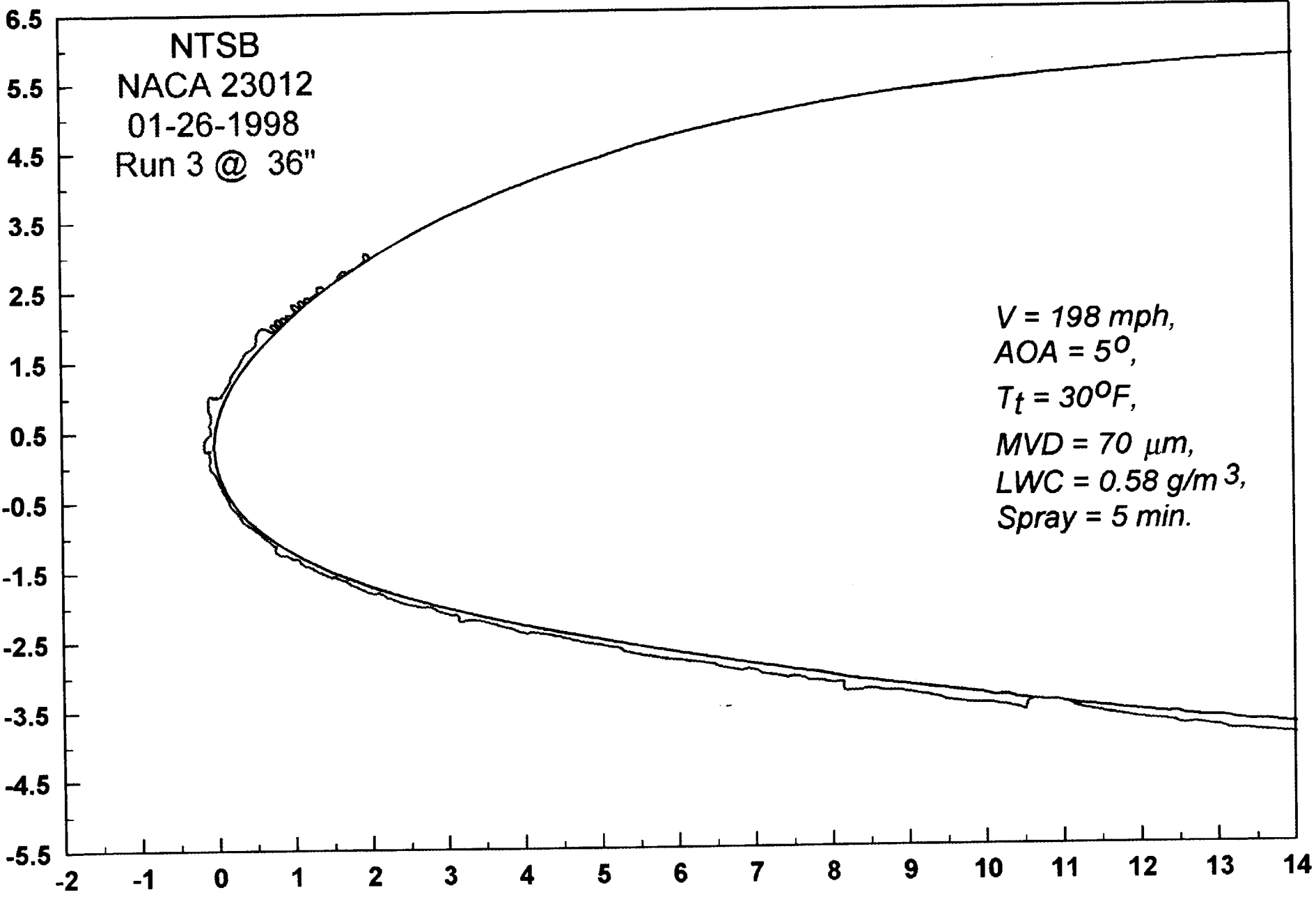
IS2

N-68





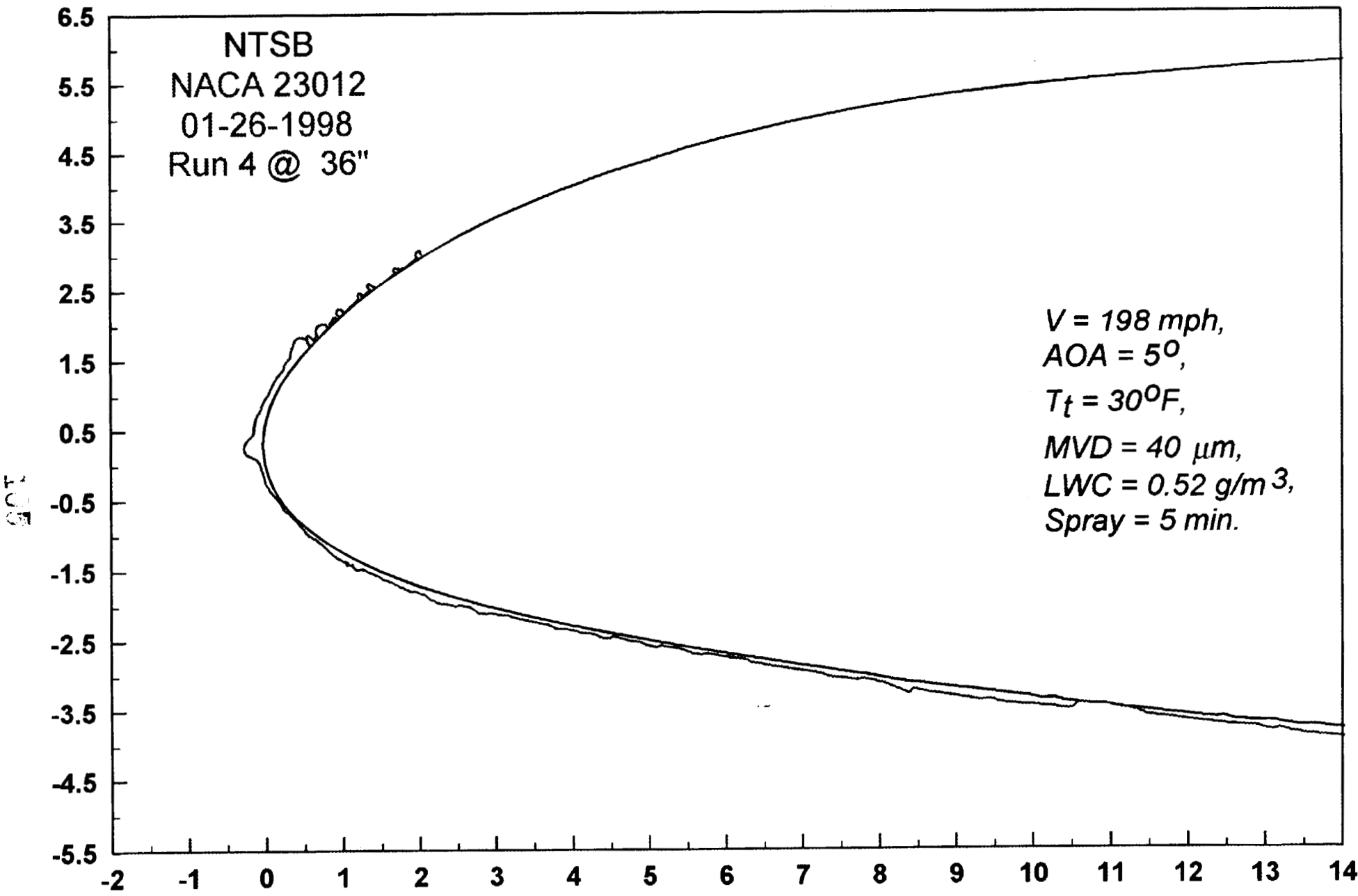
M-69



104

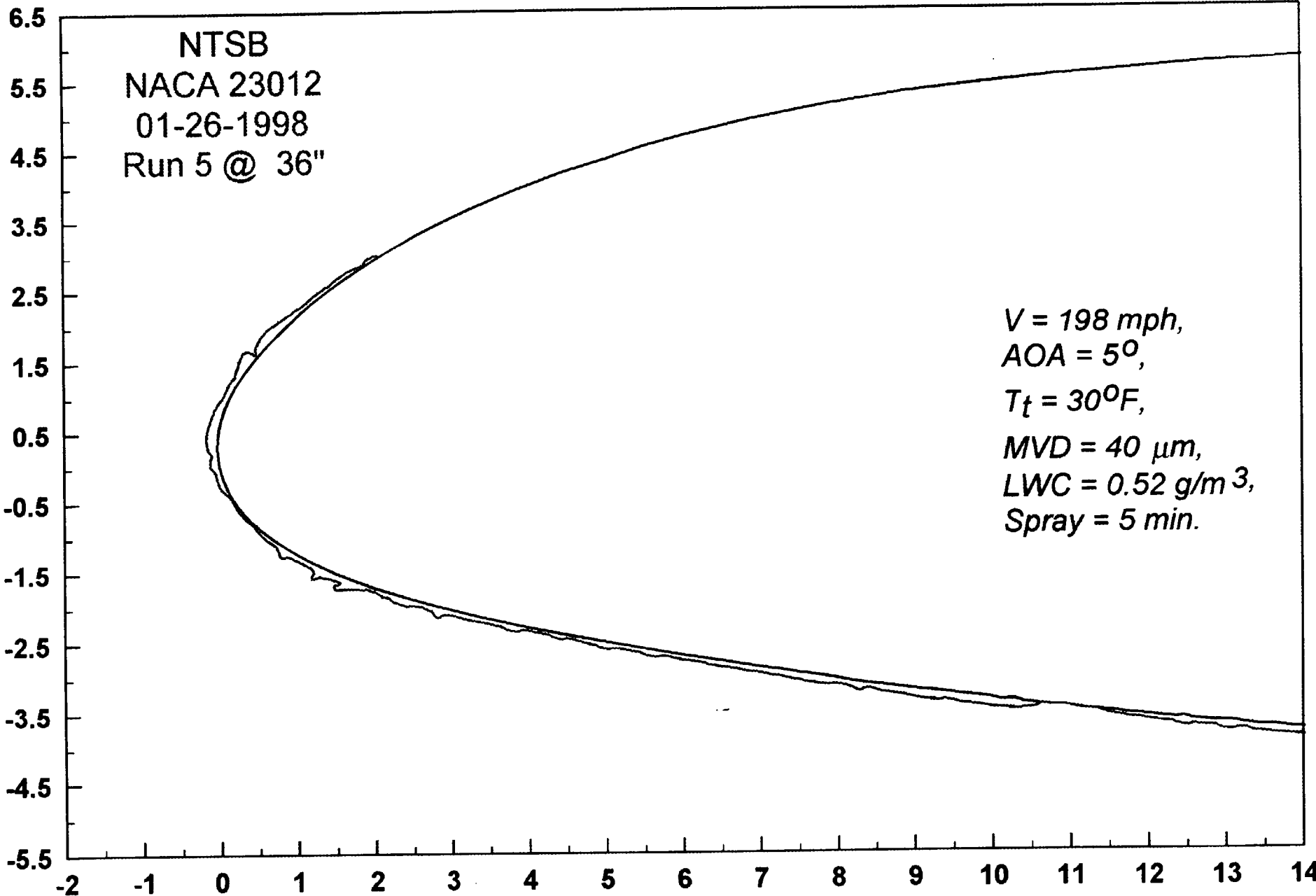
VI-70

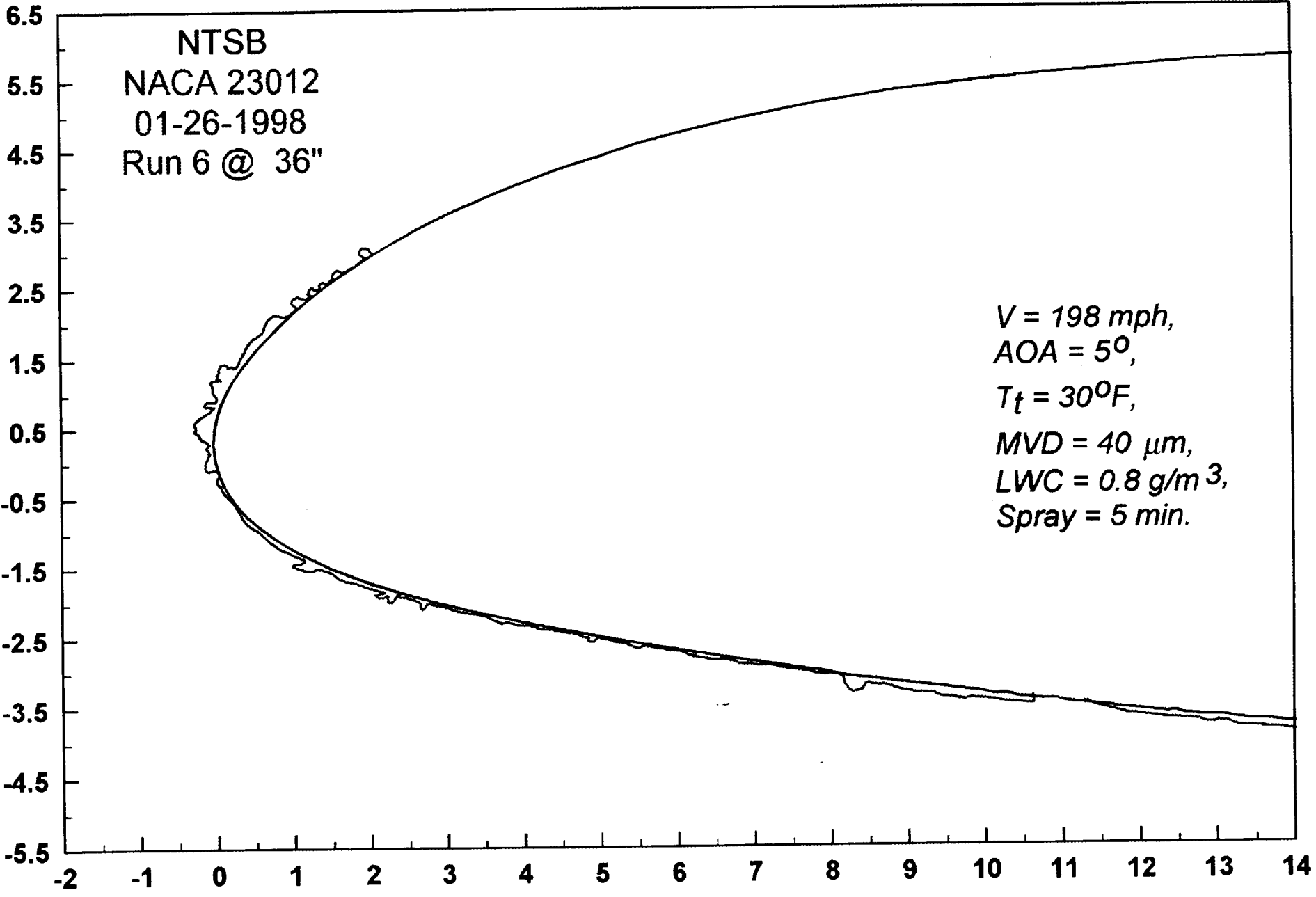
12-11

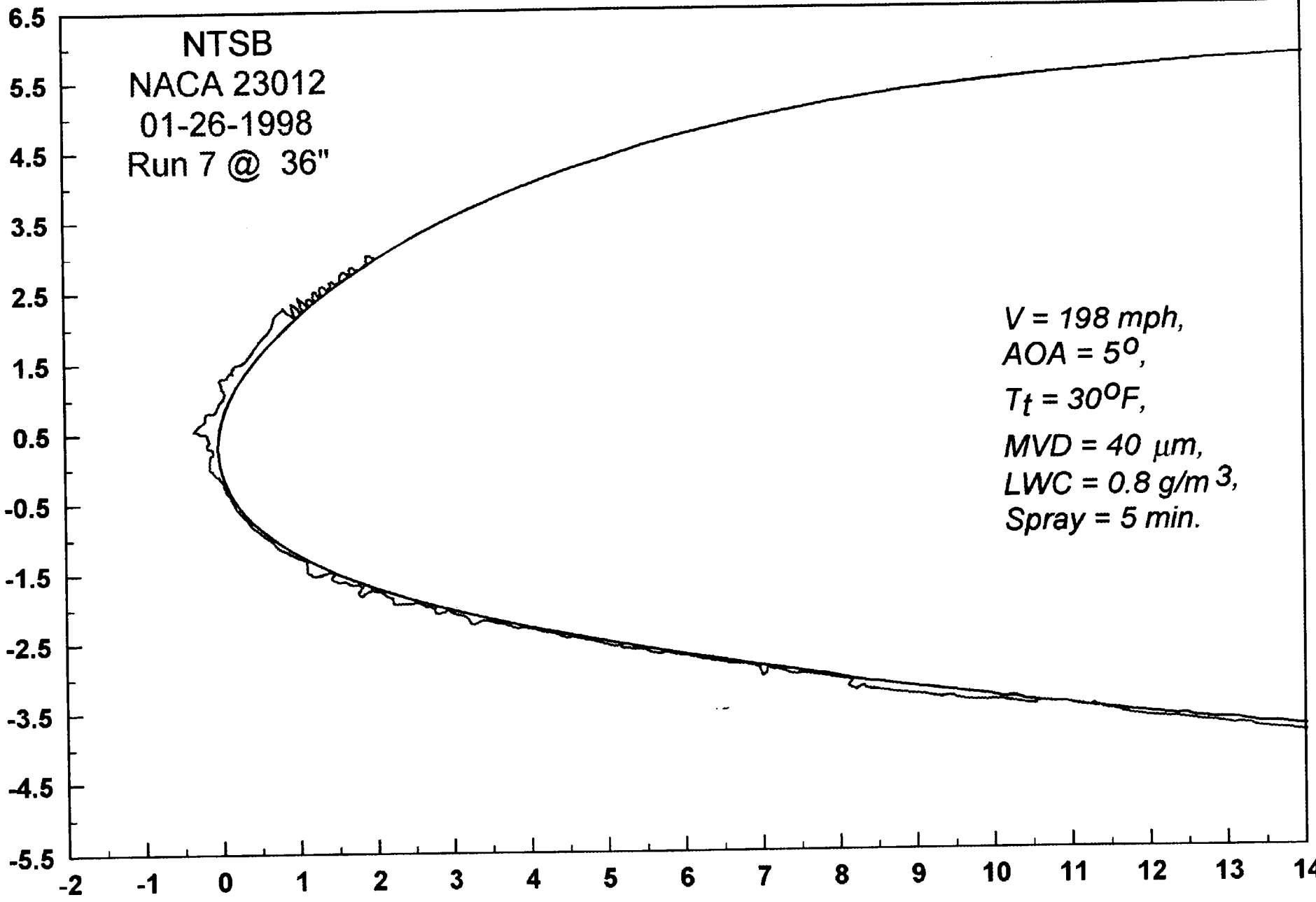


907

W-72

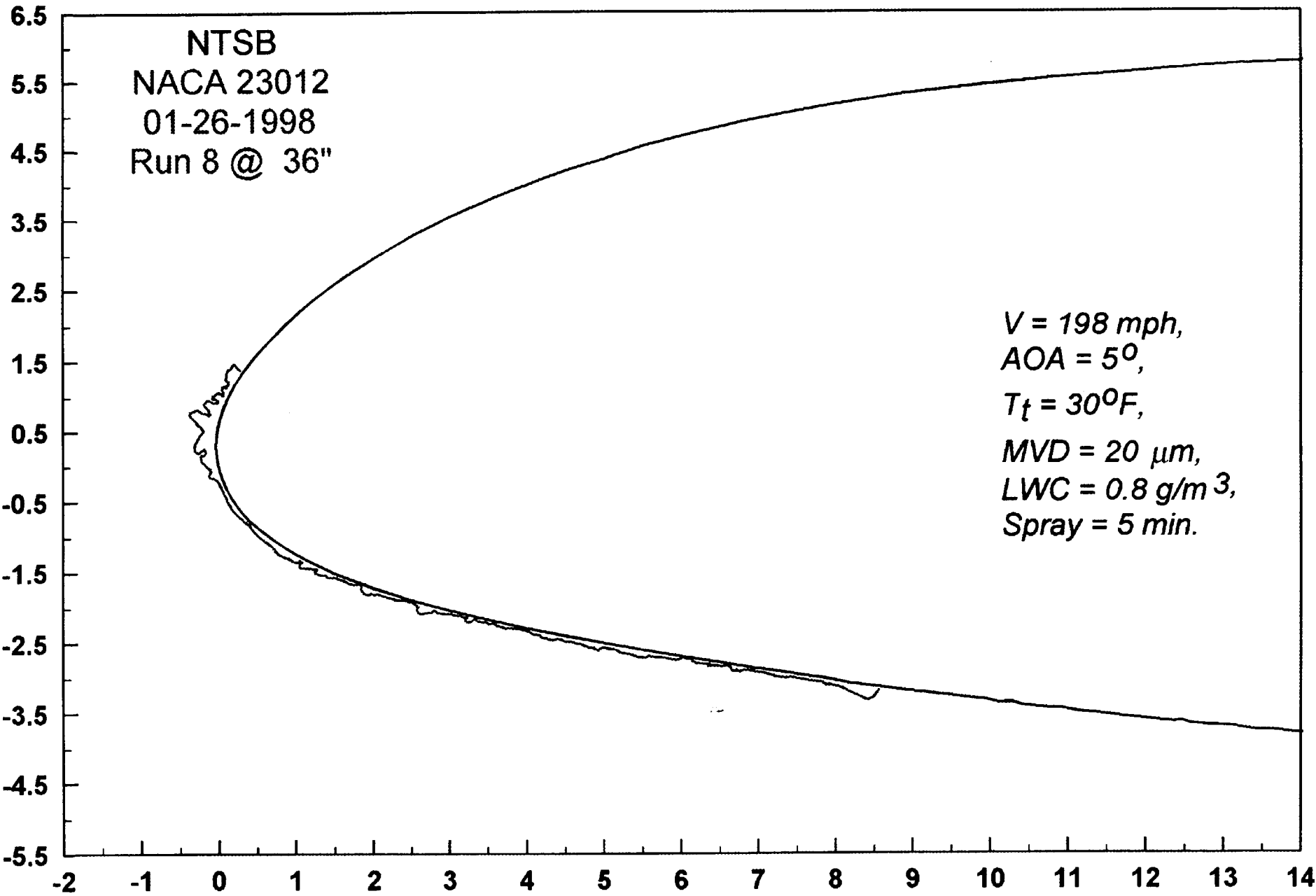






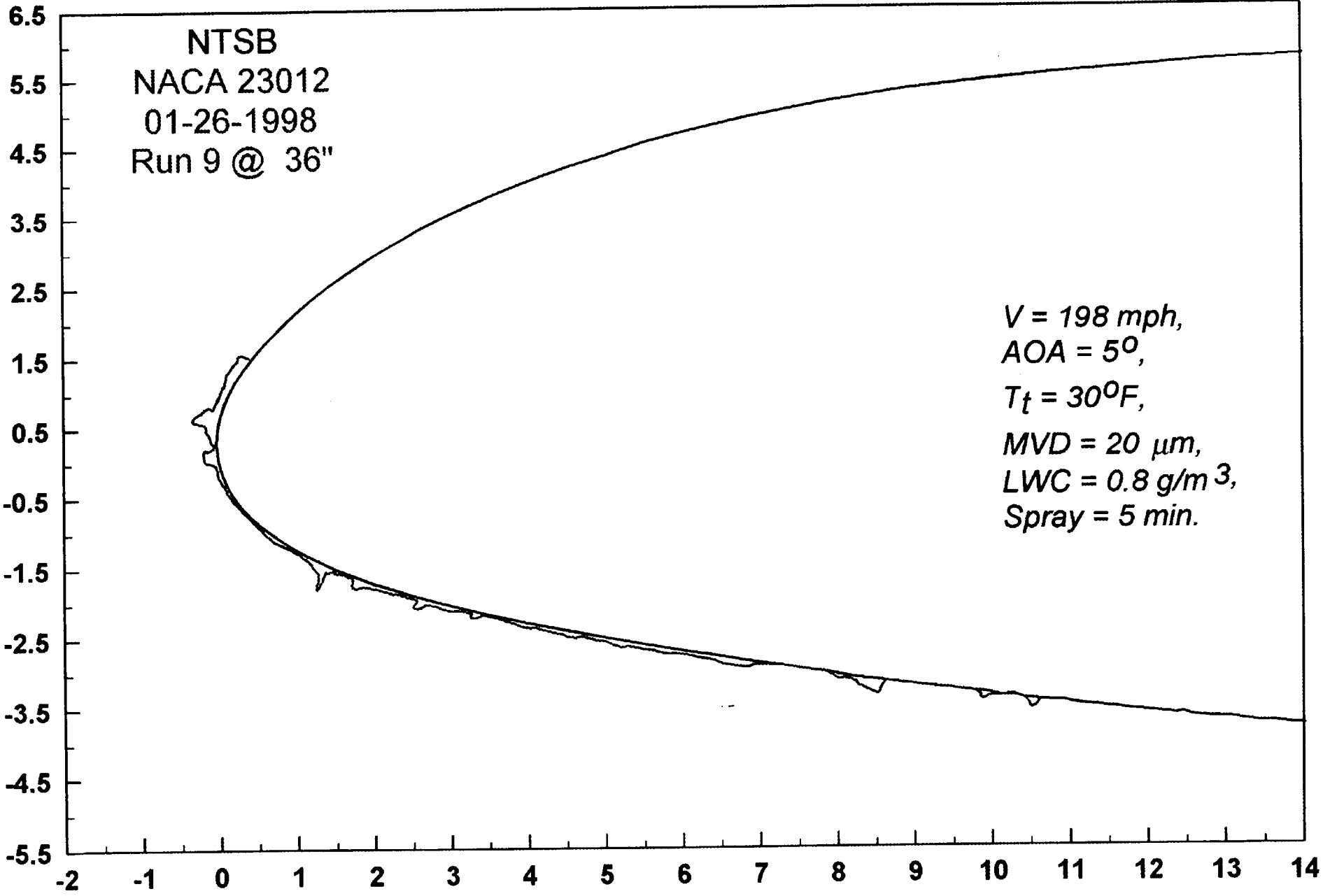
003

W-74

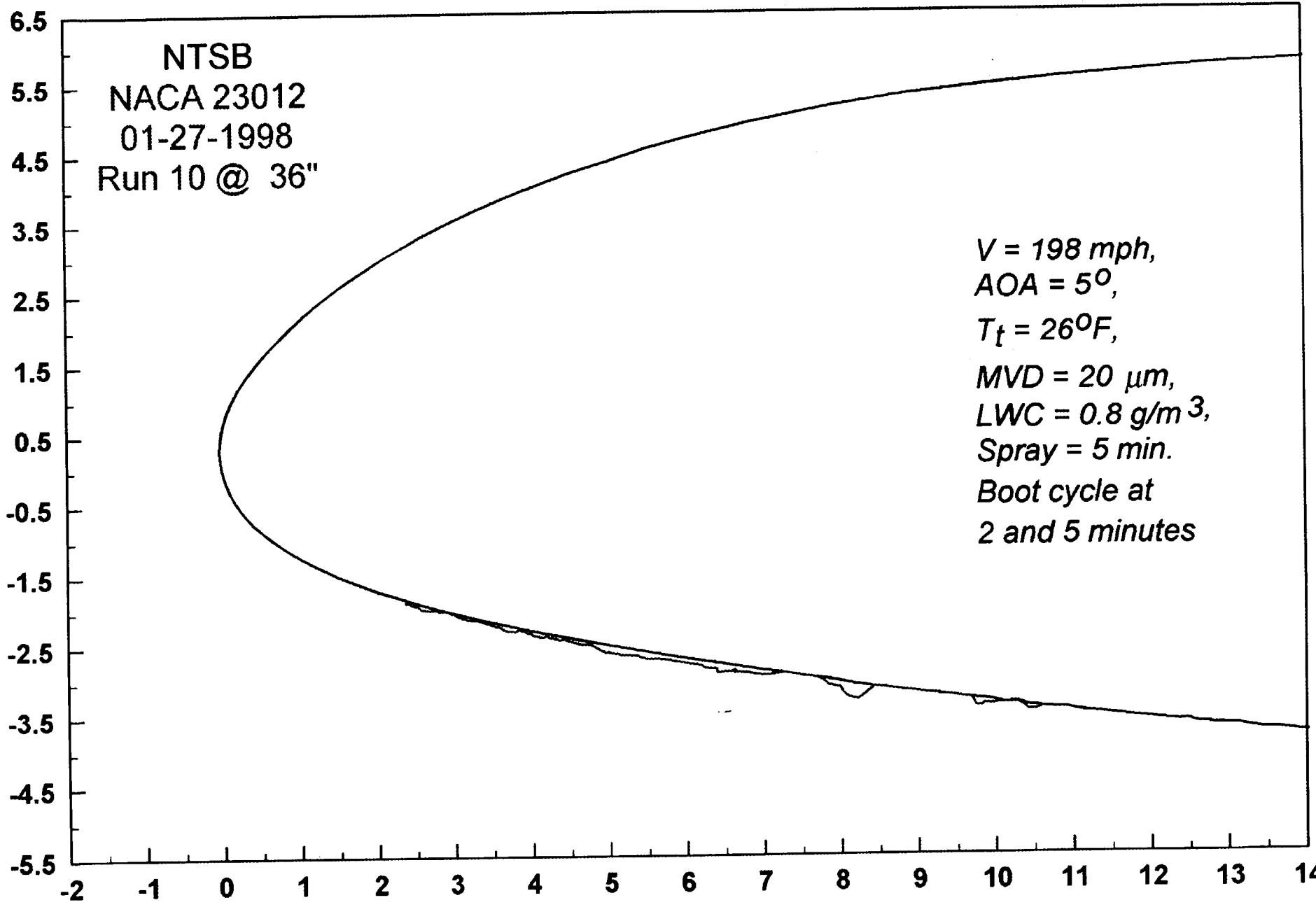


607

11-75



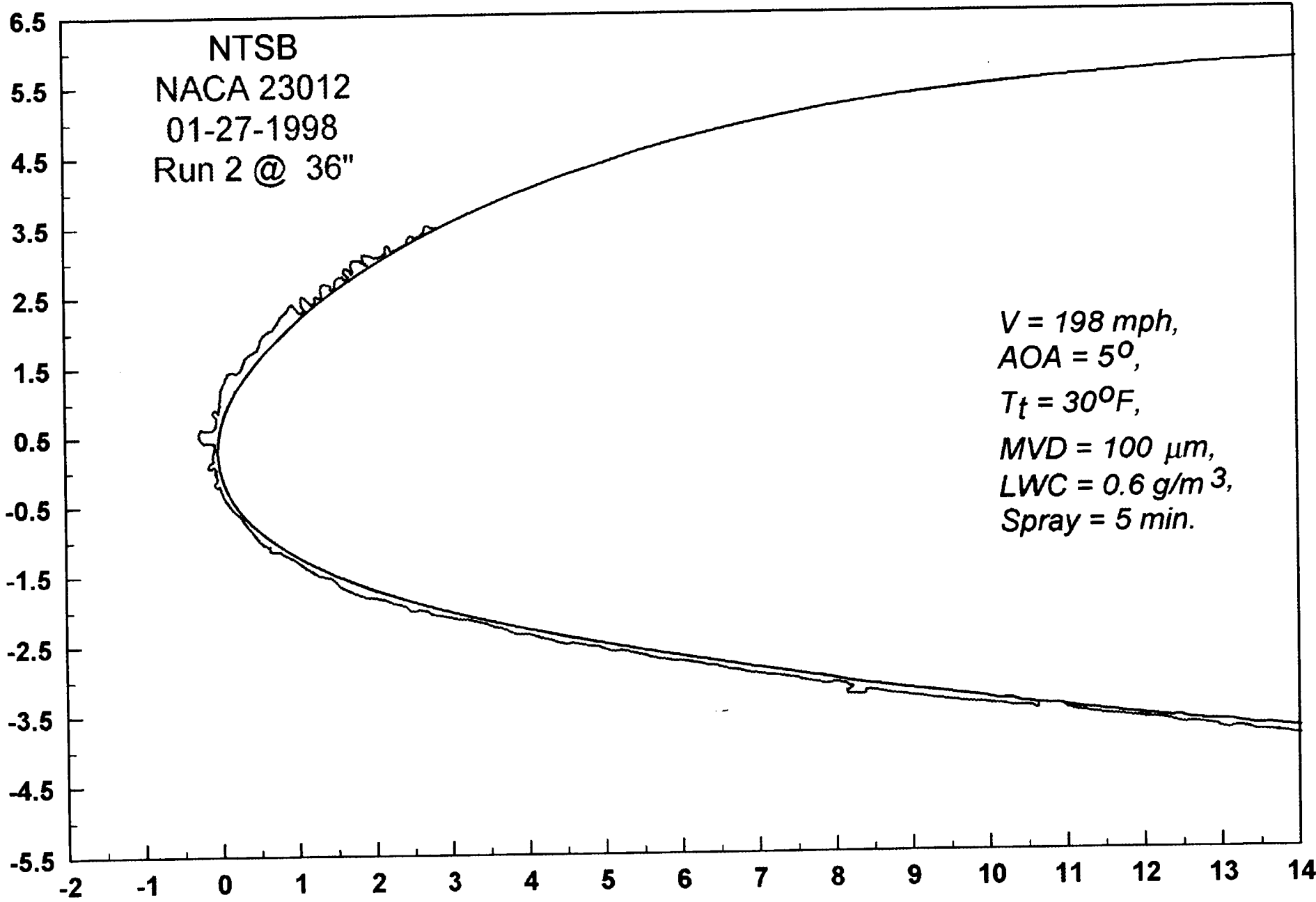
9L-76

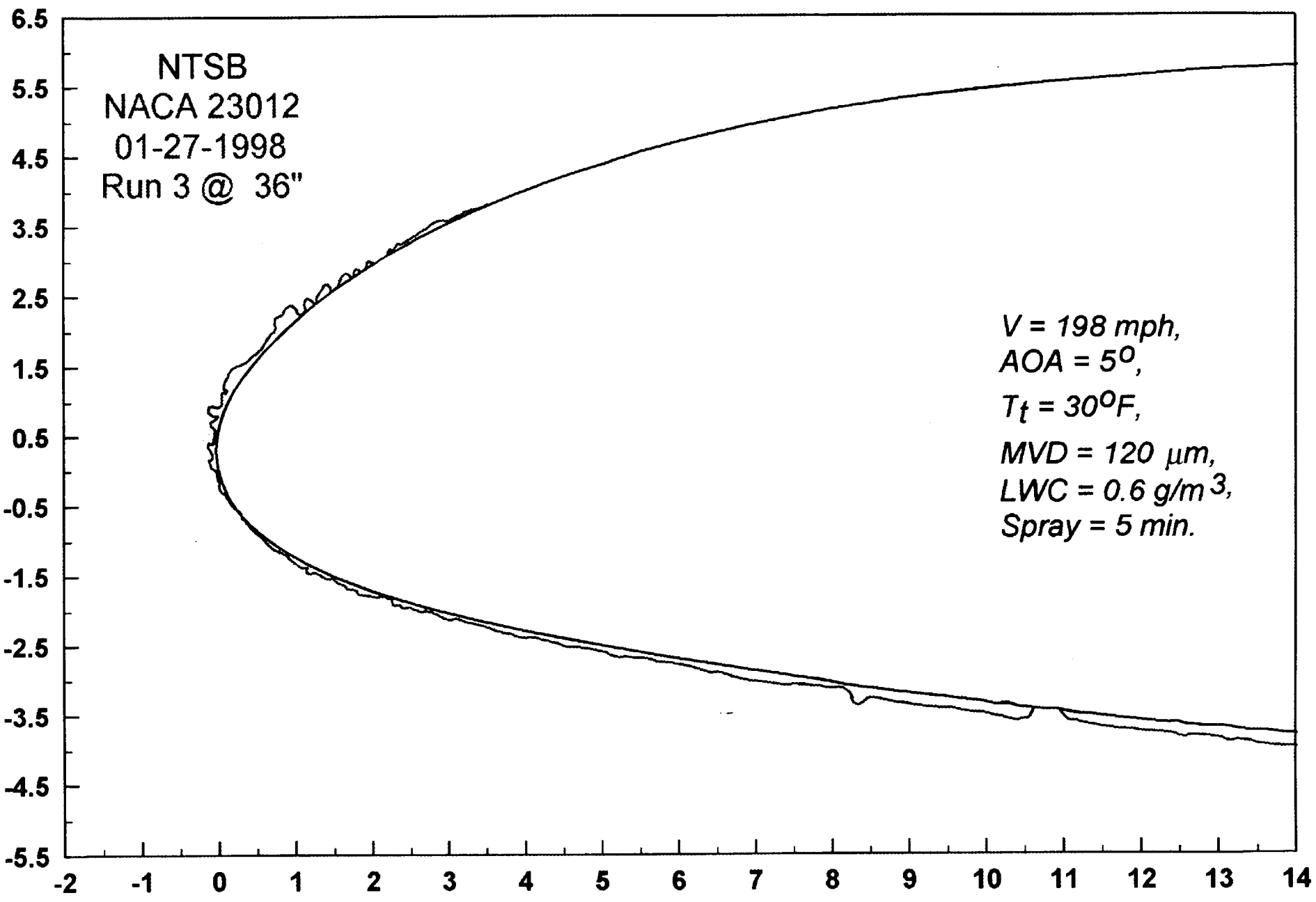


LL-11

11-11

112
V1-78





218

VI-79

6.5
5.5
4.5
3.5
2.5
1.5
0.5
-0.5
-1.5
-2.5
-3.5
-4.5
-5.5

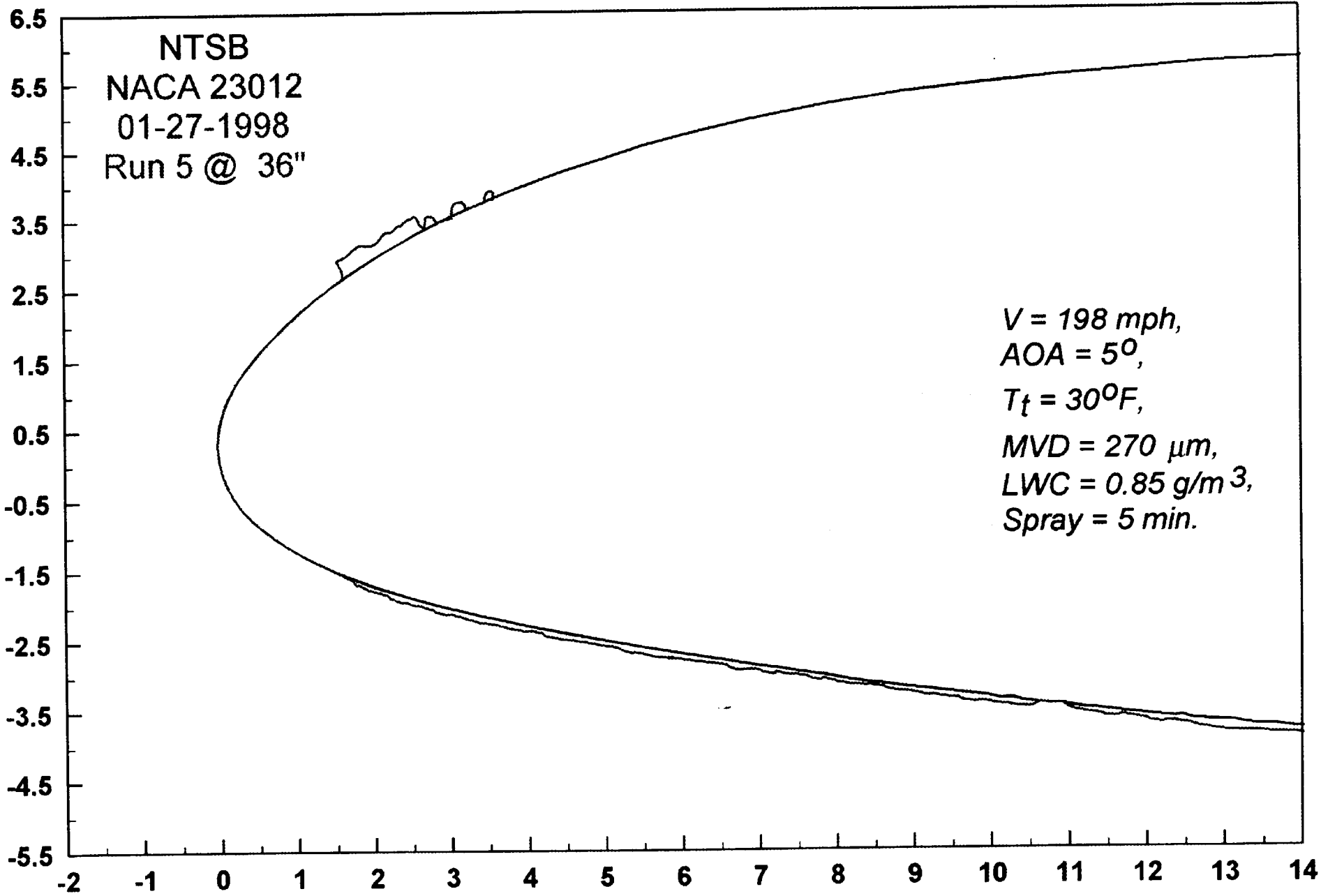
NTSB
NACA 23012
01-27-1998
Run 4 @ 36"

$V = 198 \text{ mph}$,
 $AOA = 5^\circ$,
 $T_t = 30^\circ\text{F}$,
 $MVD = 175 \mu\text{m}$,
 $LWC = 0.85 \text{ g/m}^3$,
 $\text{Spray} = 5 \text{ min.}$

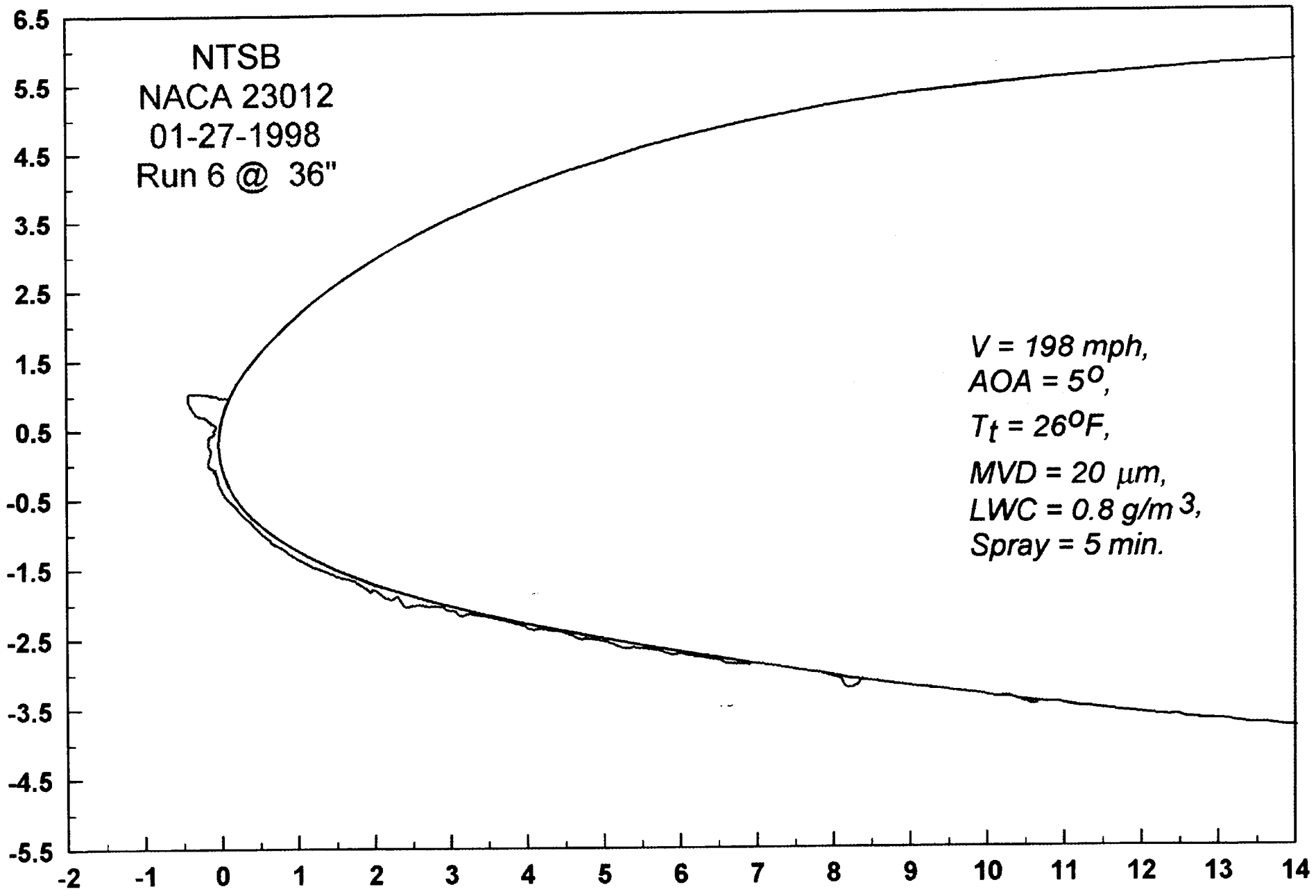
-2 -1 0 1 2 3 4 5 6 7 8 9 10 11 12 13 14

4.4

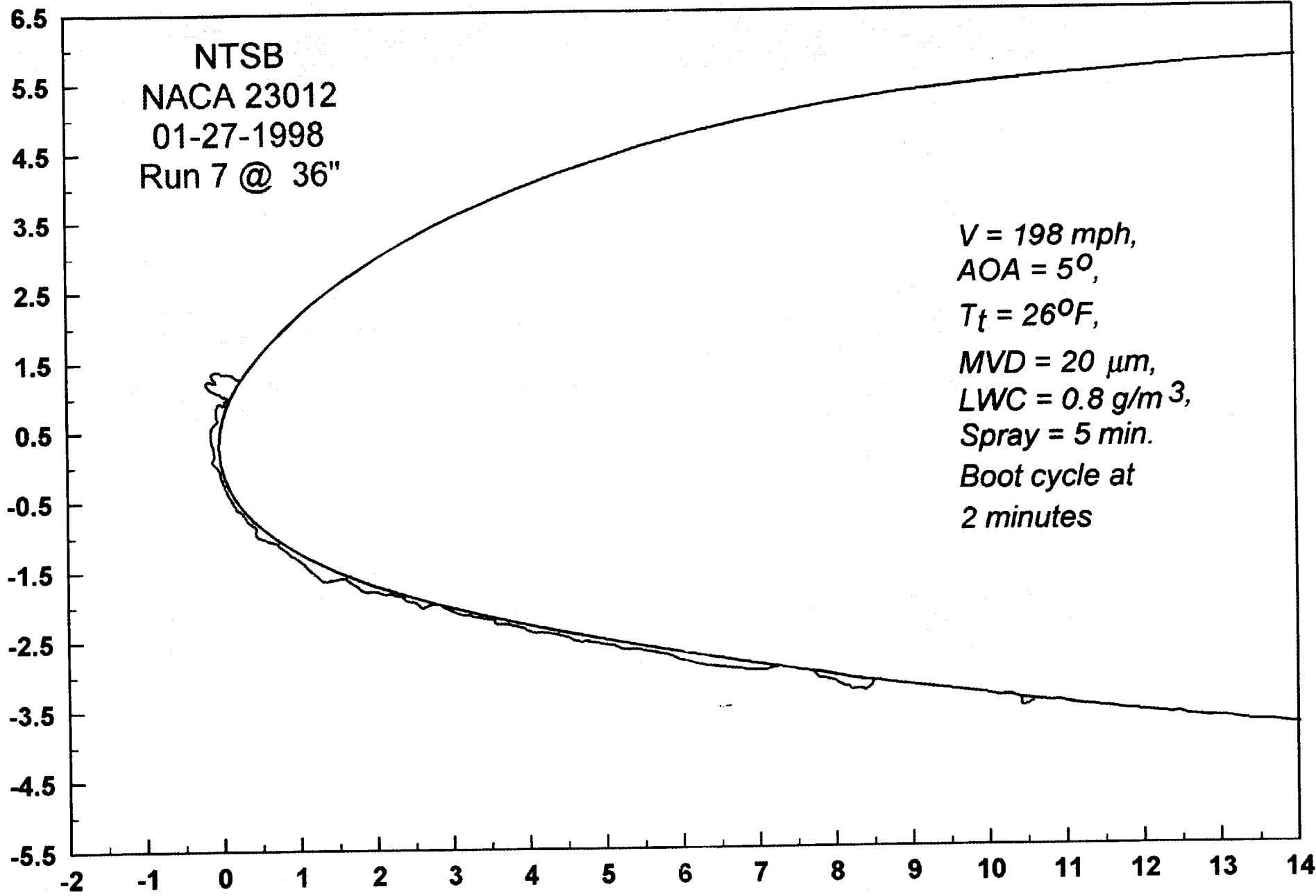
11-80



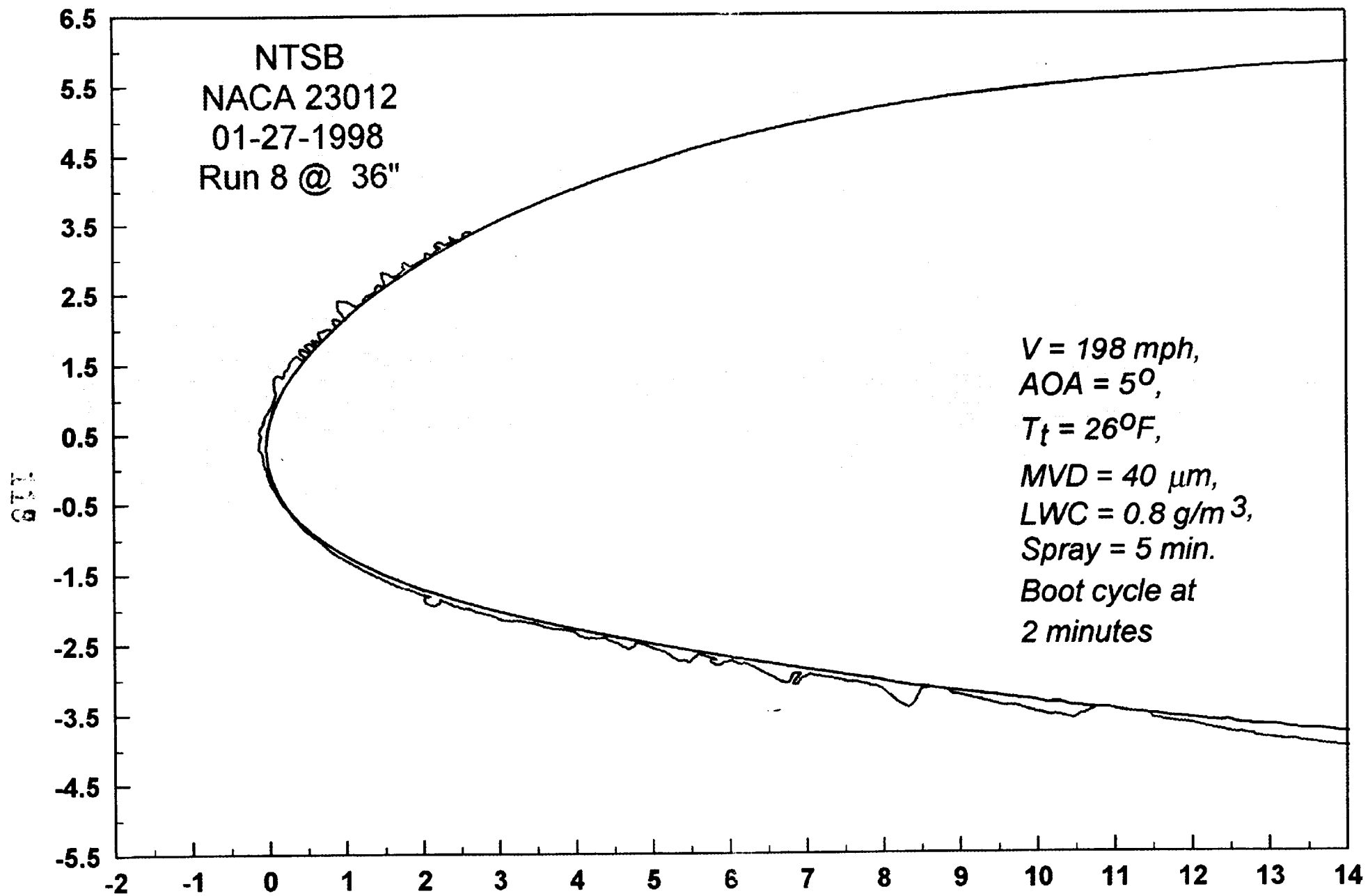
18-81



28-82

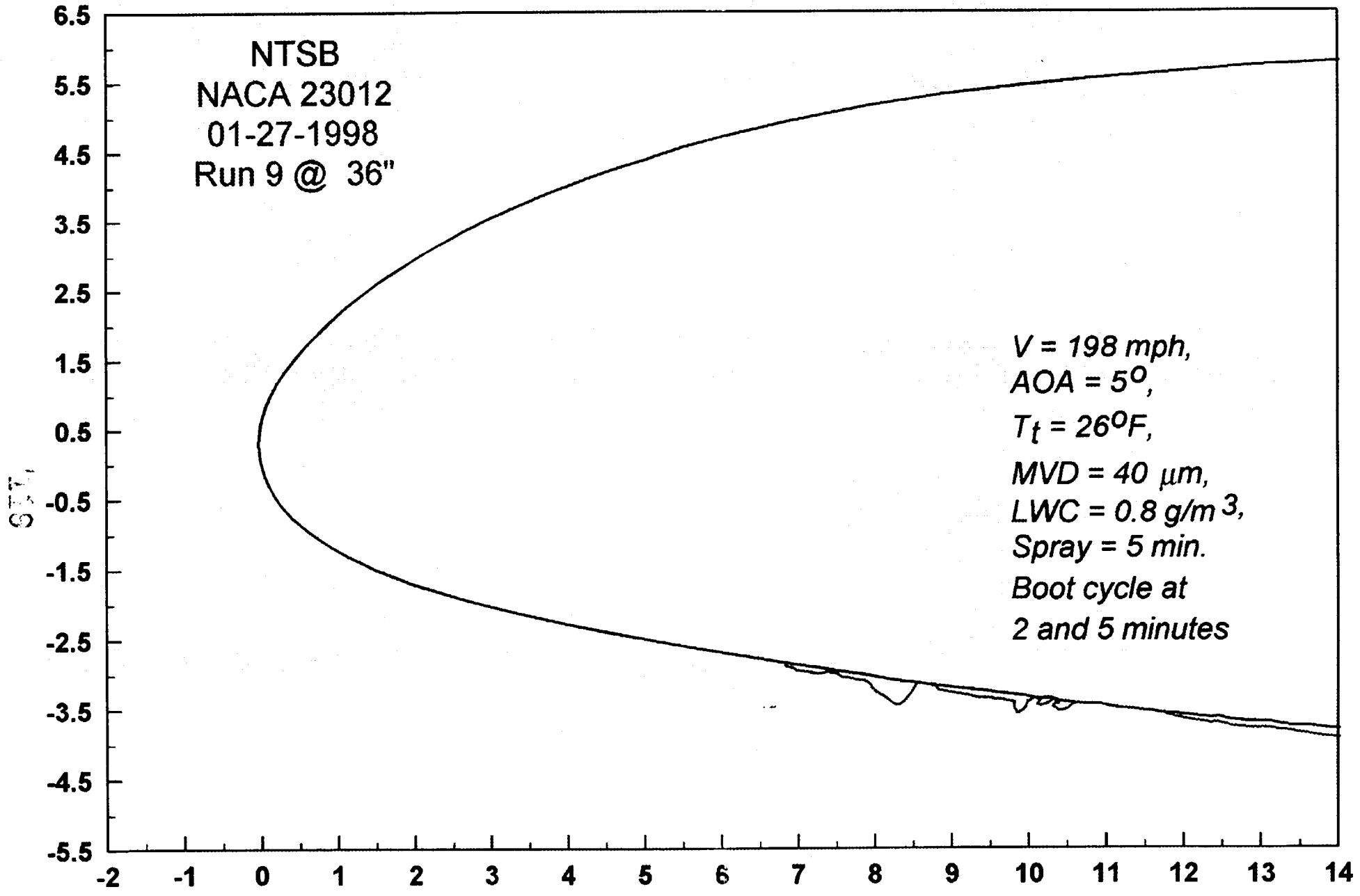


1183



VI-89

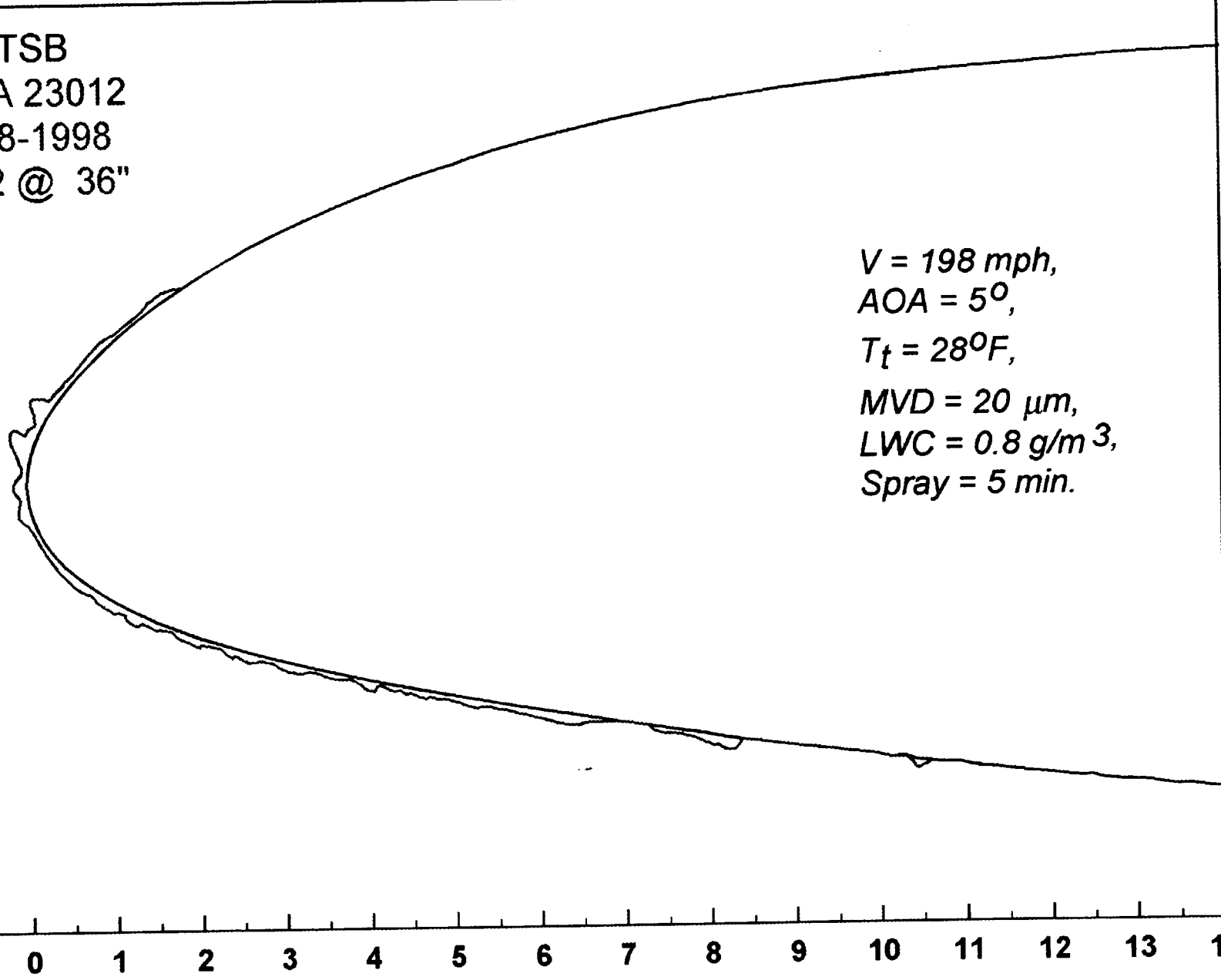
58-11



6.5
5.5
4.5
3.5
2.5
1.5
0.5
-0.5
-1.5
-2.5
-3.5
-4.5
-5.5

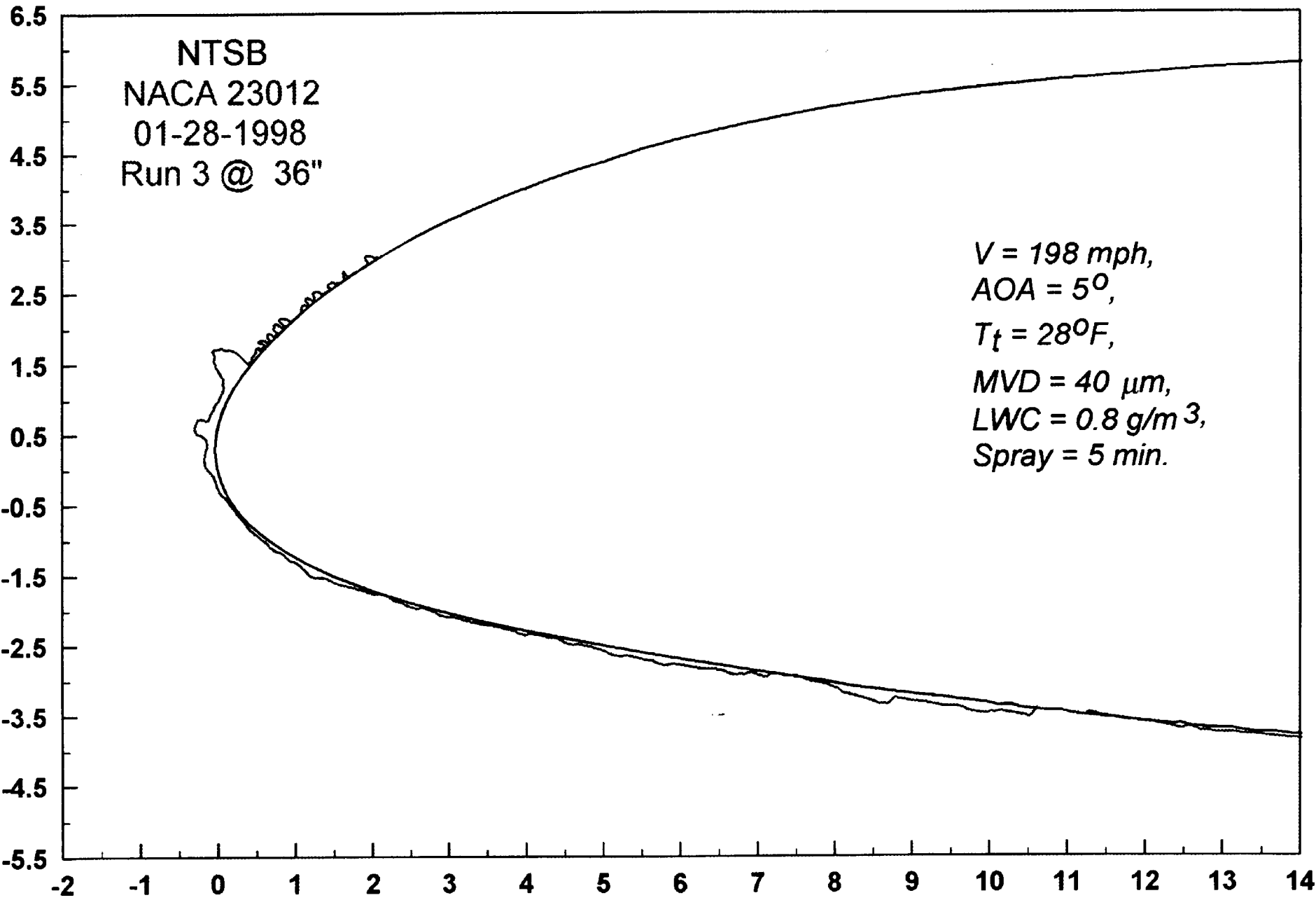
NTSB
NACA 23012
01-28-1998
Run 2 @ 36"

V = 198 mph,
AOA = 5°,
T_t = 28°F,
MVD = 20 μm,
LWC = 0.8 g/m³,
Spray = 5 min.



126

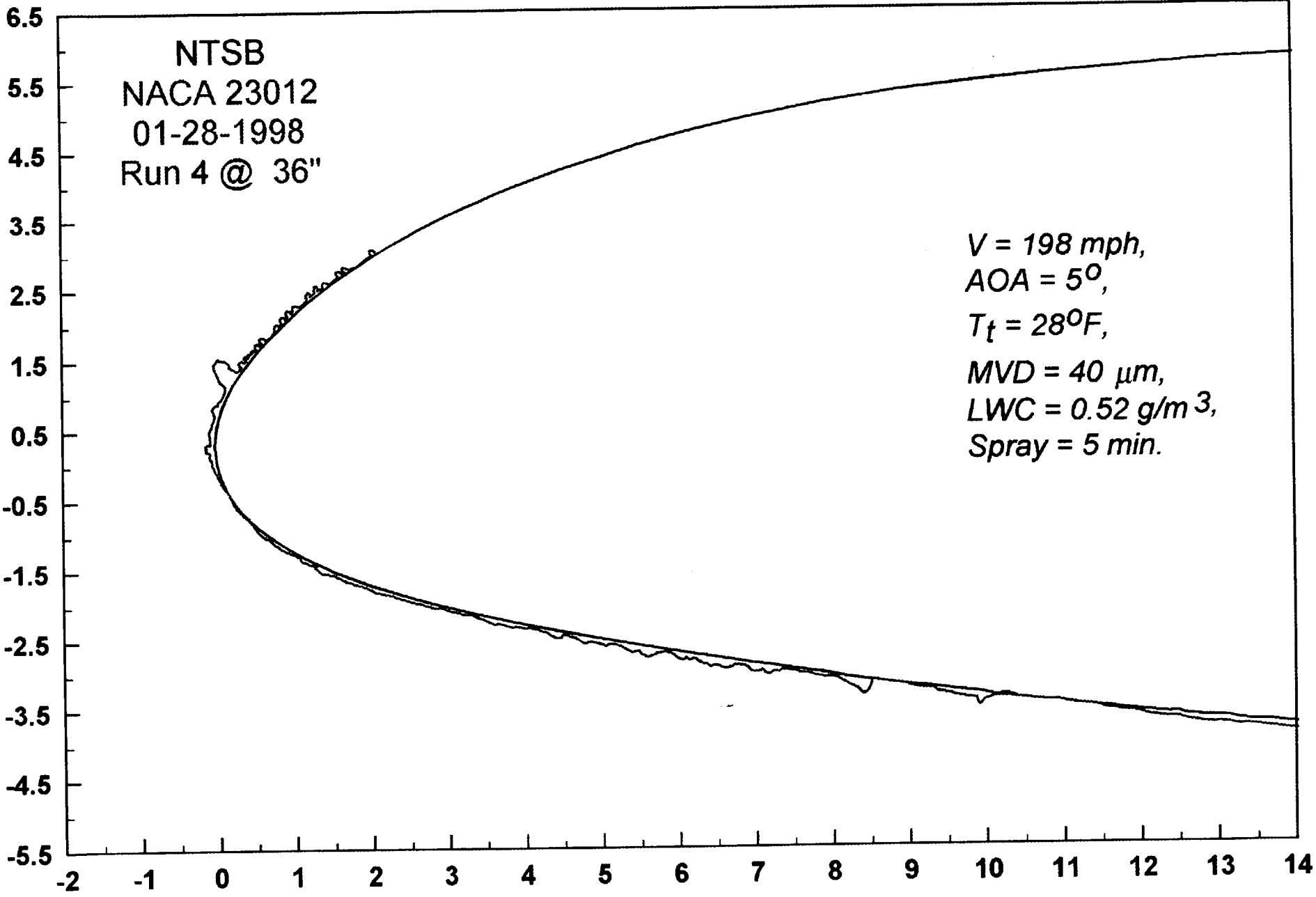
M-86

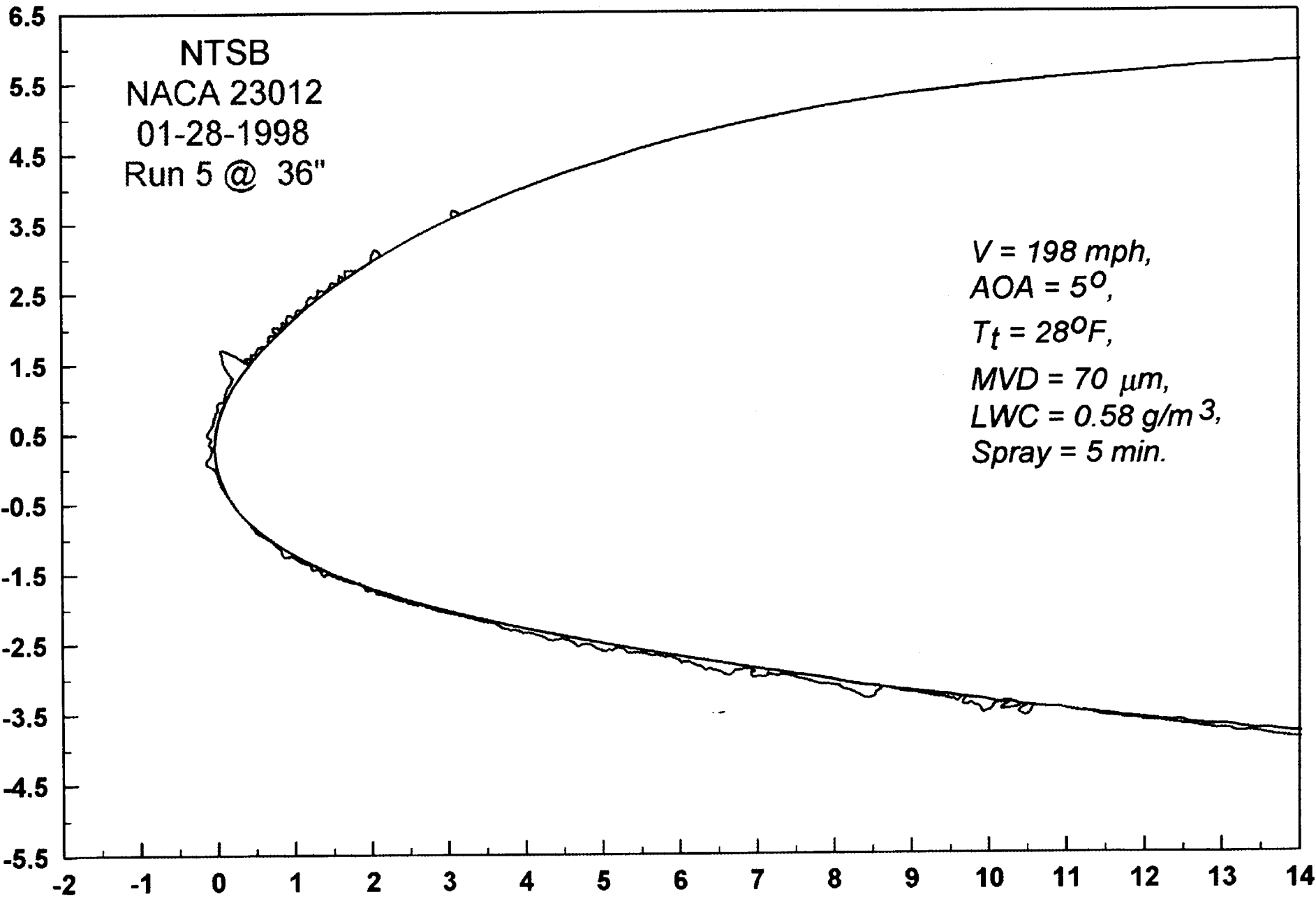


M-87

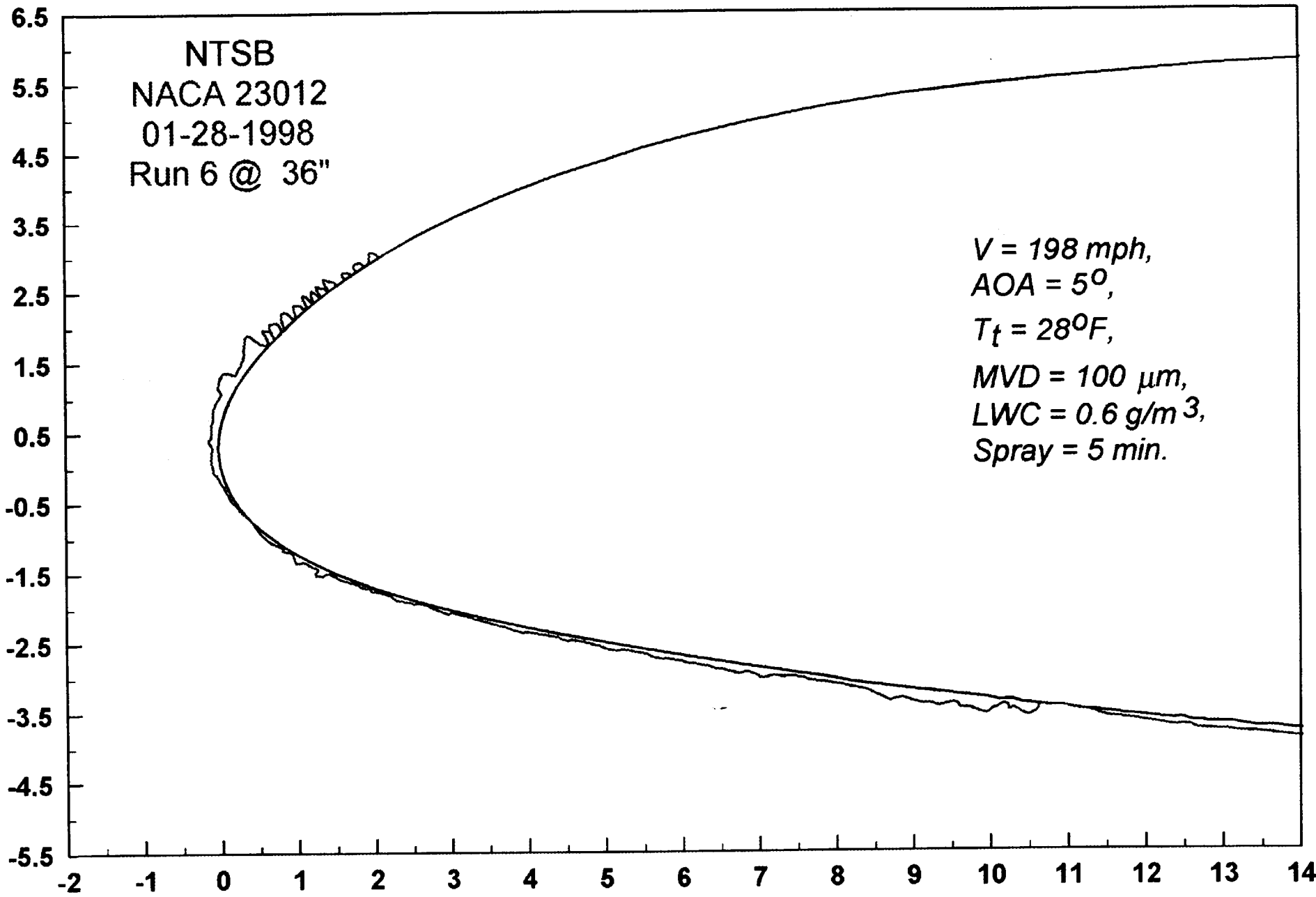
1222

M-58

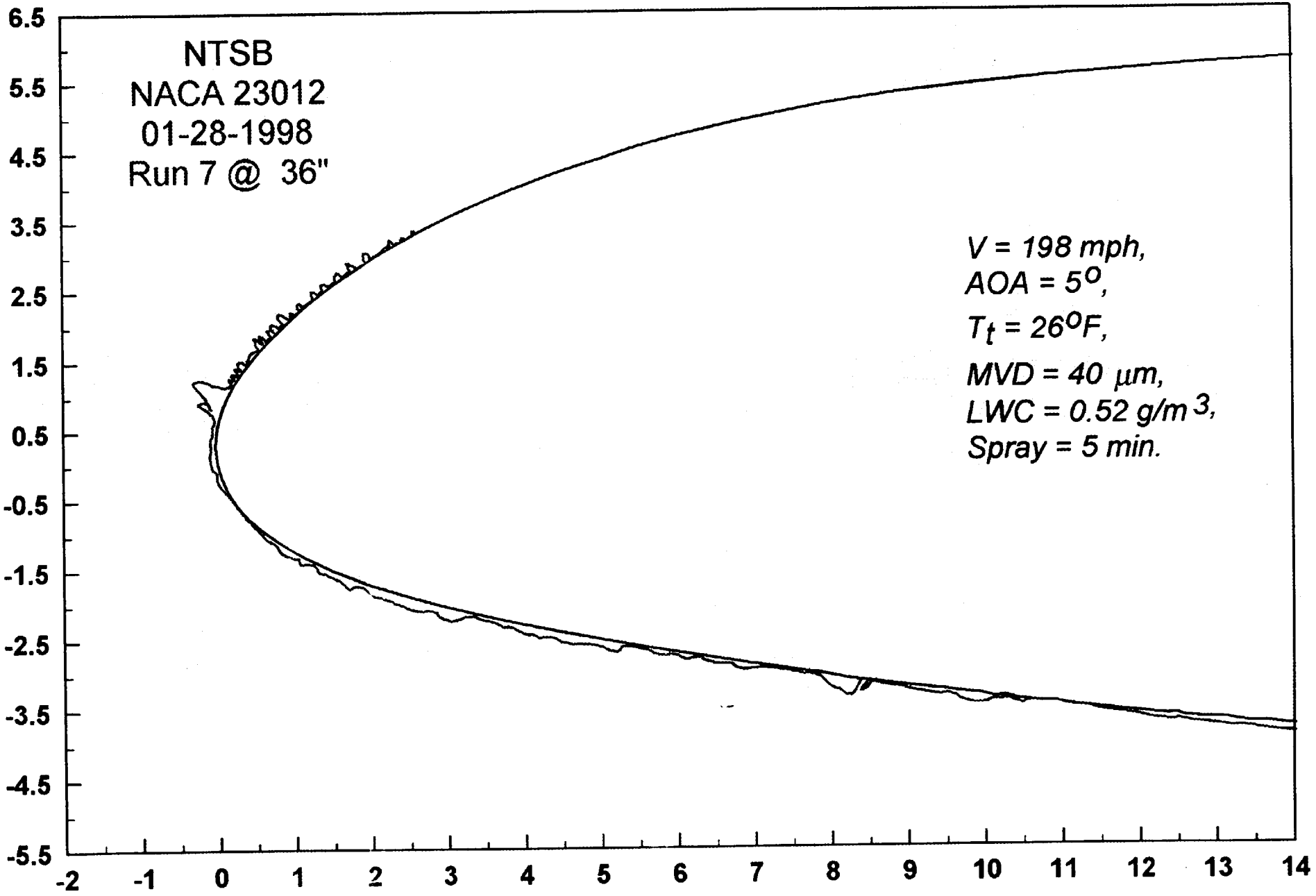




11-89



11-90

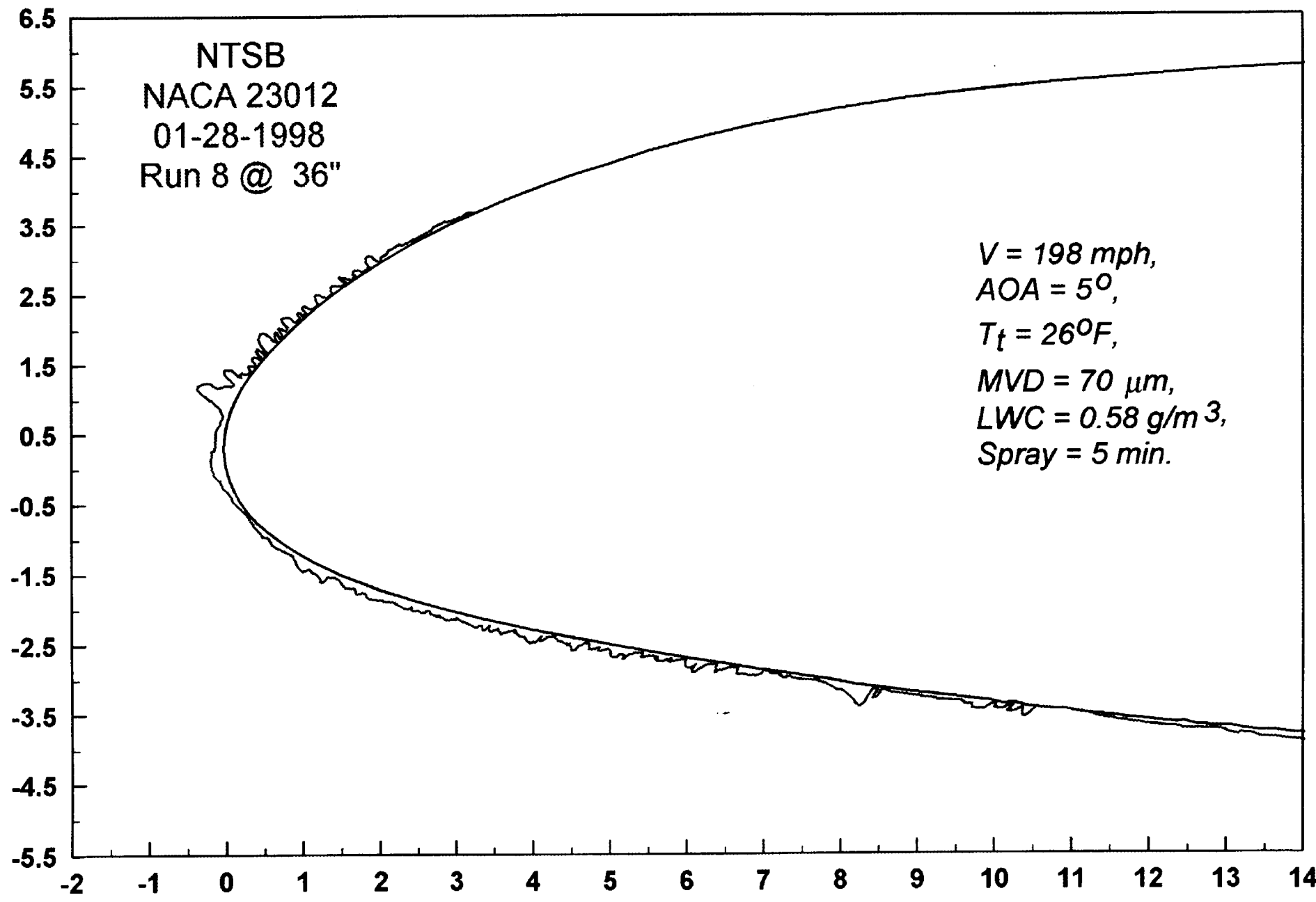


1285

11-91

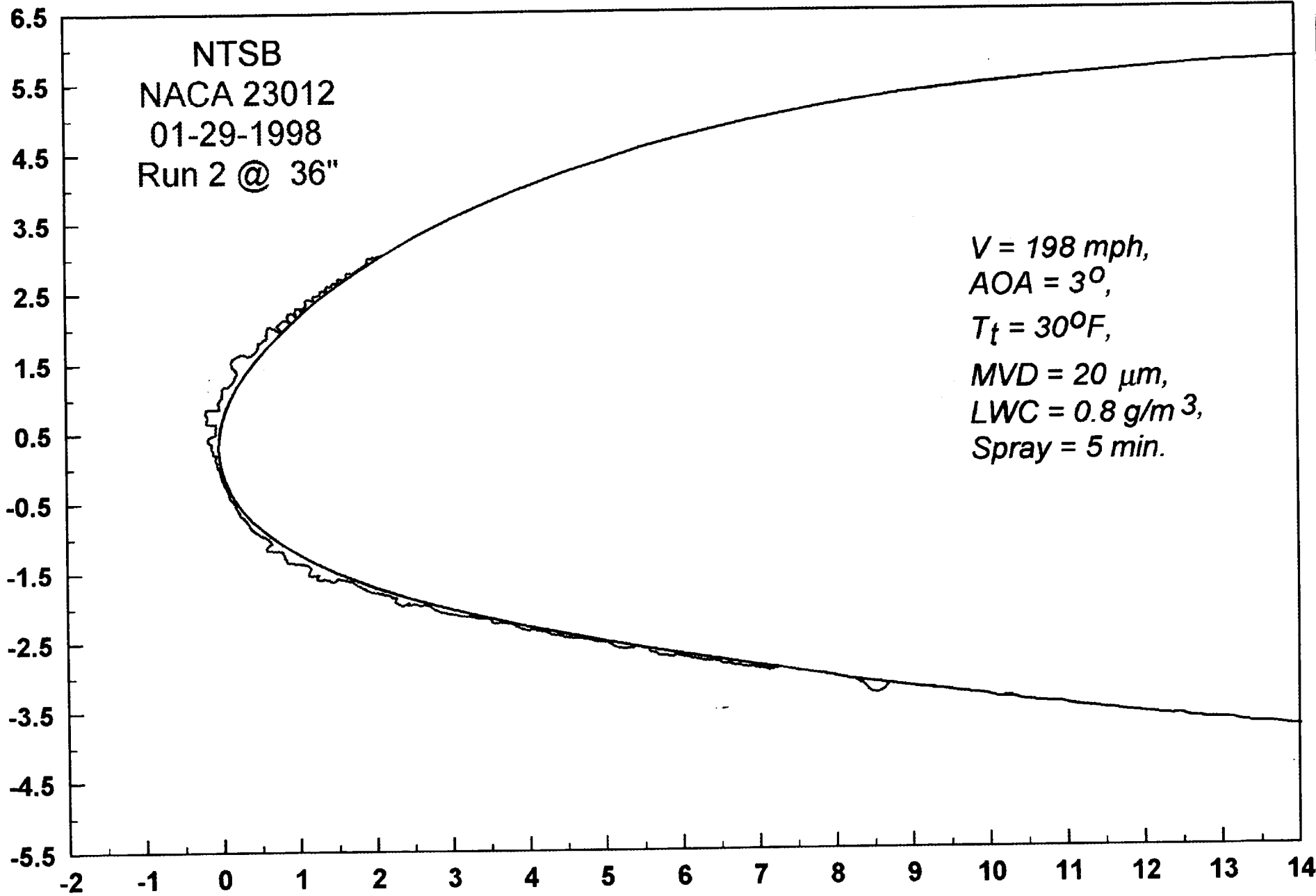
NTSB
NACA 23012
01-28-1998
Run 8 @ 36"

$V = 198 \text{ mph}$,
 $AOA = 5^\circ$,
 $T_t = 26^\circ\text{F}$,
 $MVD = 70 \mu\text{m}$,
 $LWC = 0.58 \text{ g/m}^3$,
Spray = 5 min.



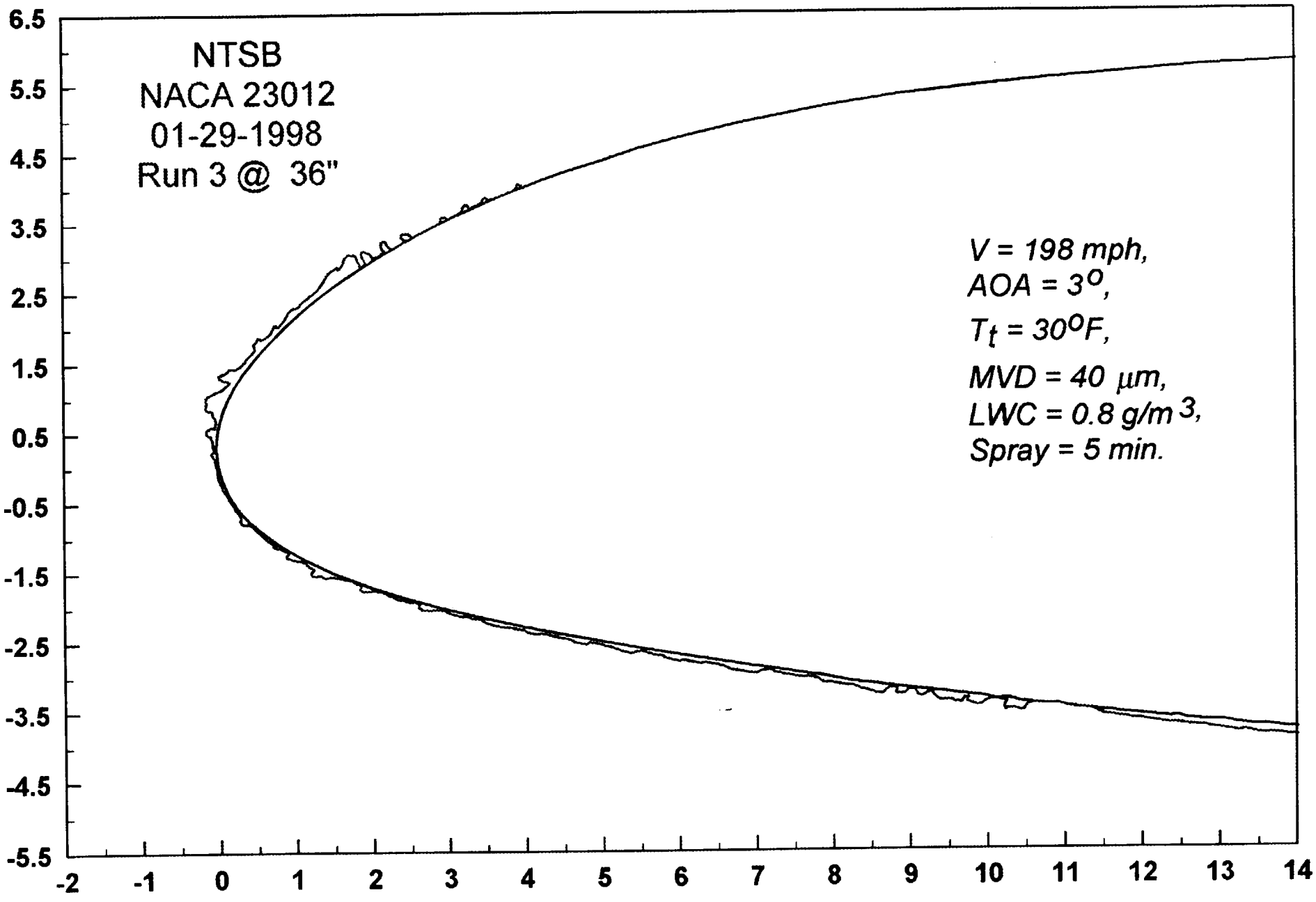
926

11-972

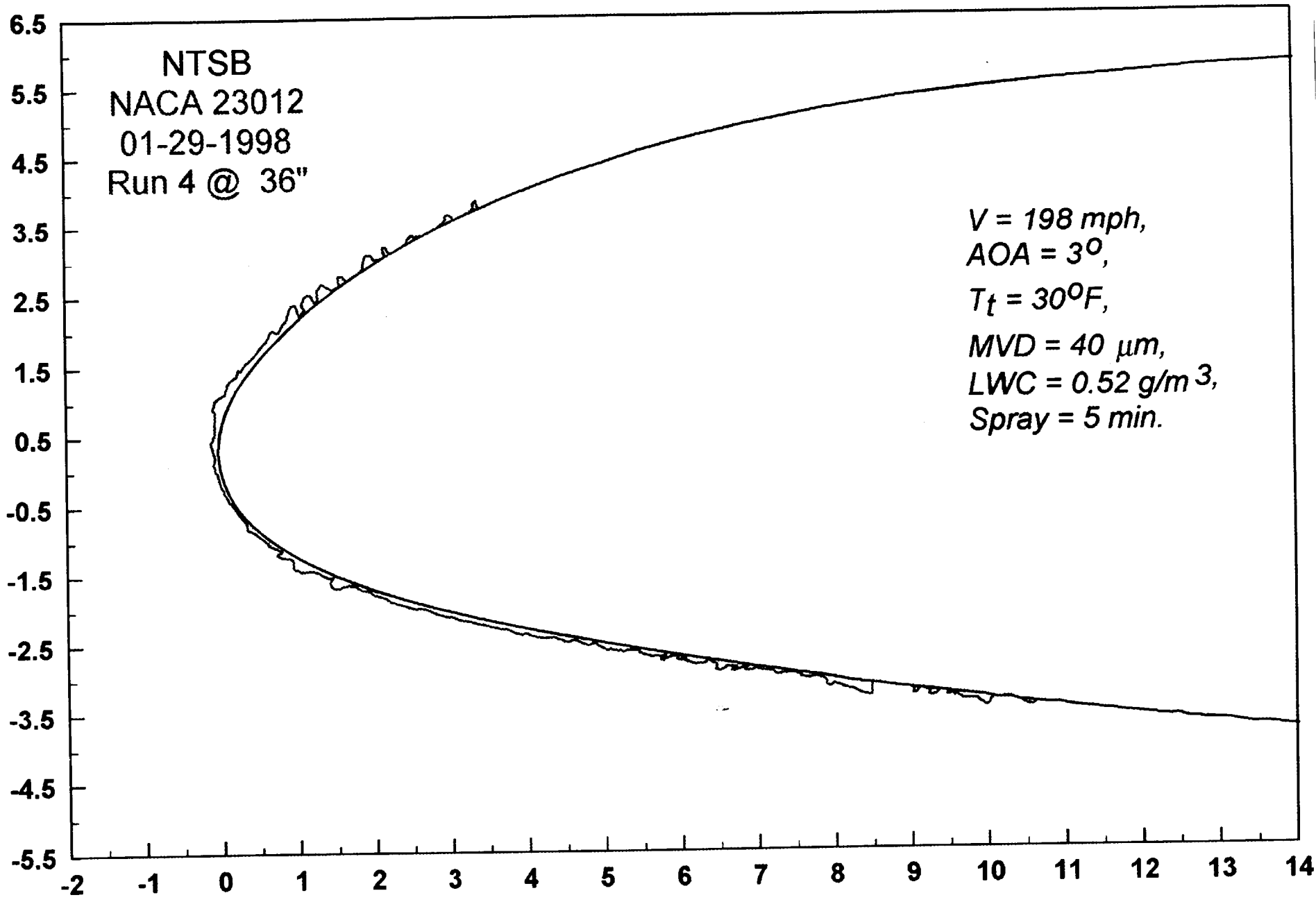


1-27

W-93



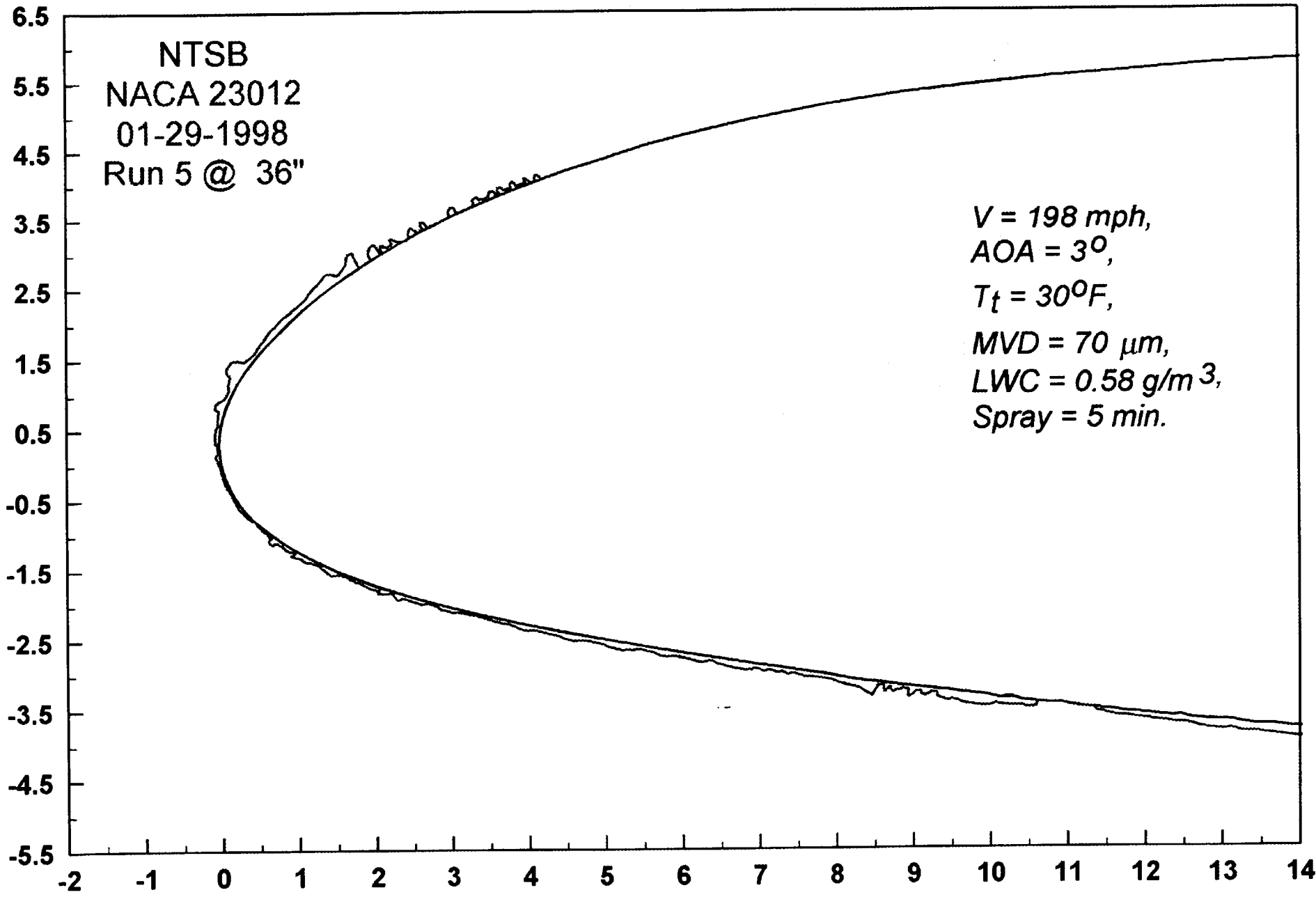
nb-N



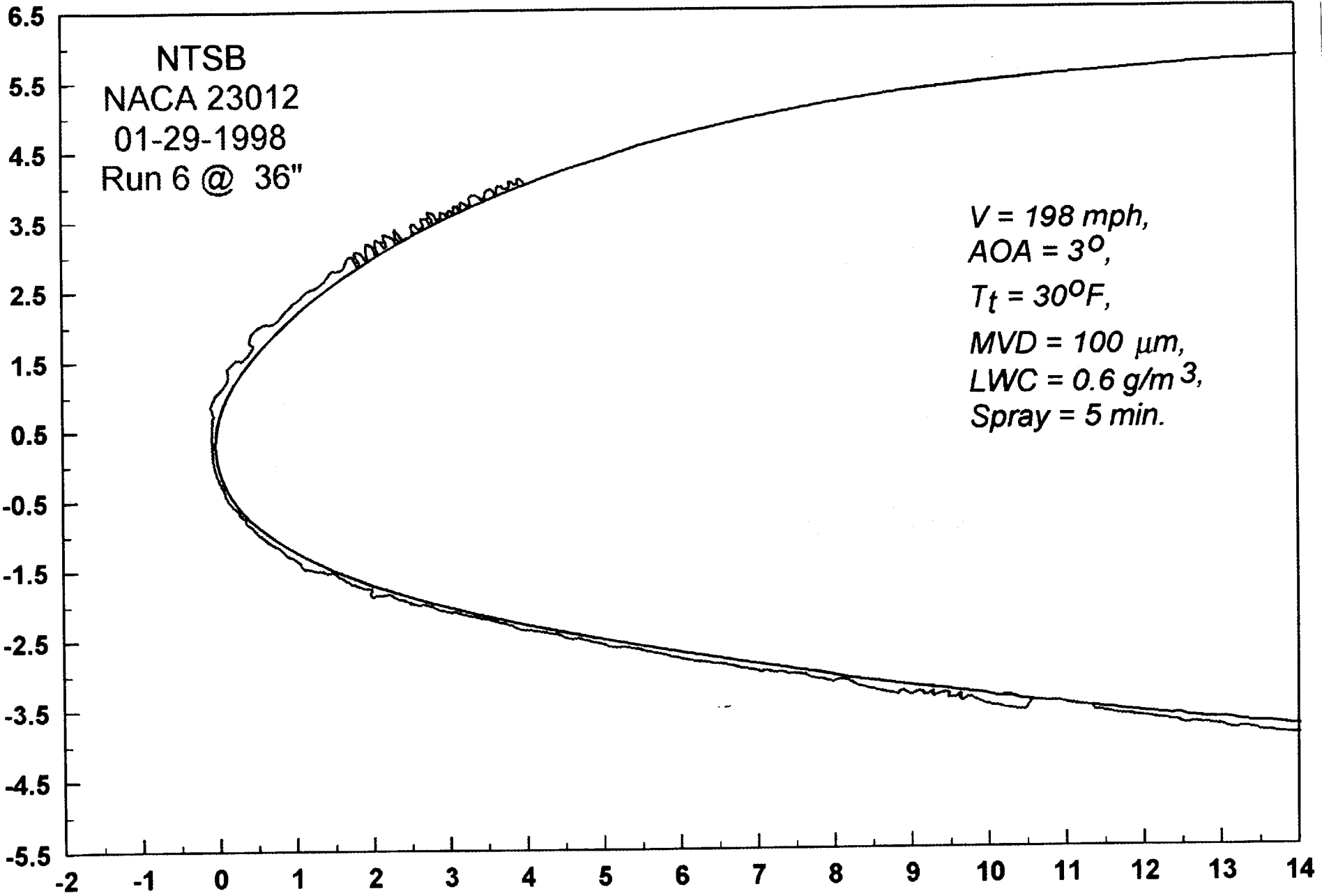
229

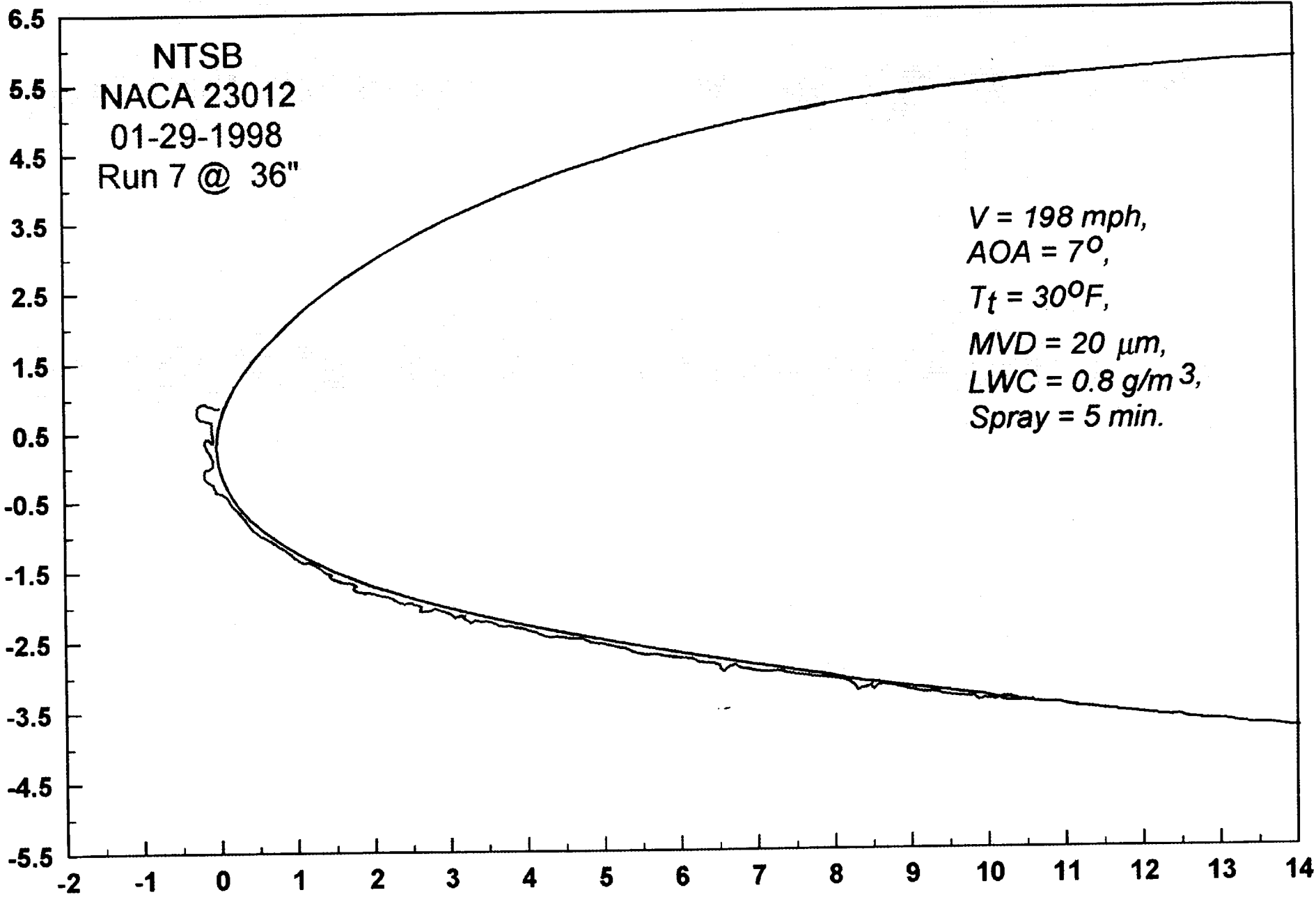
W-95

30



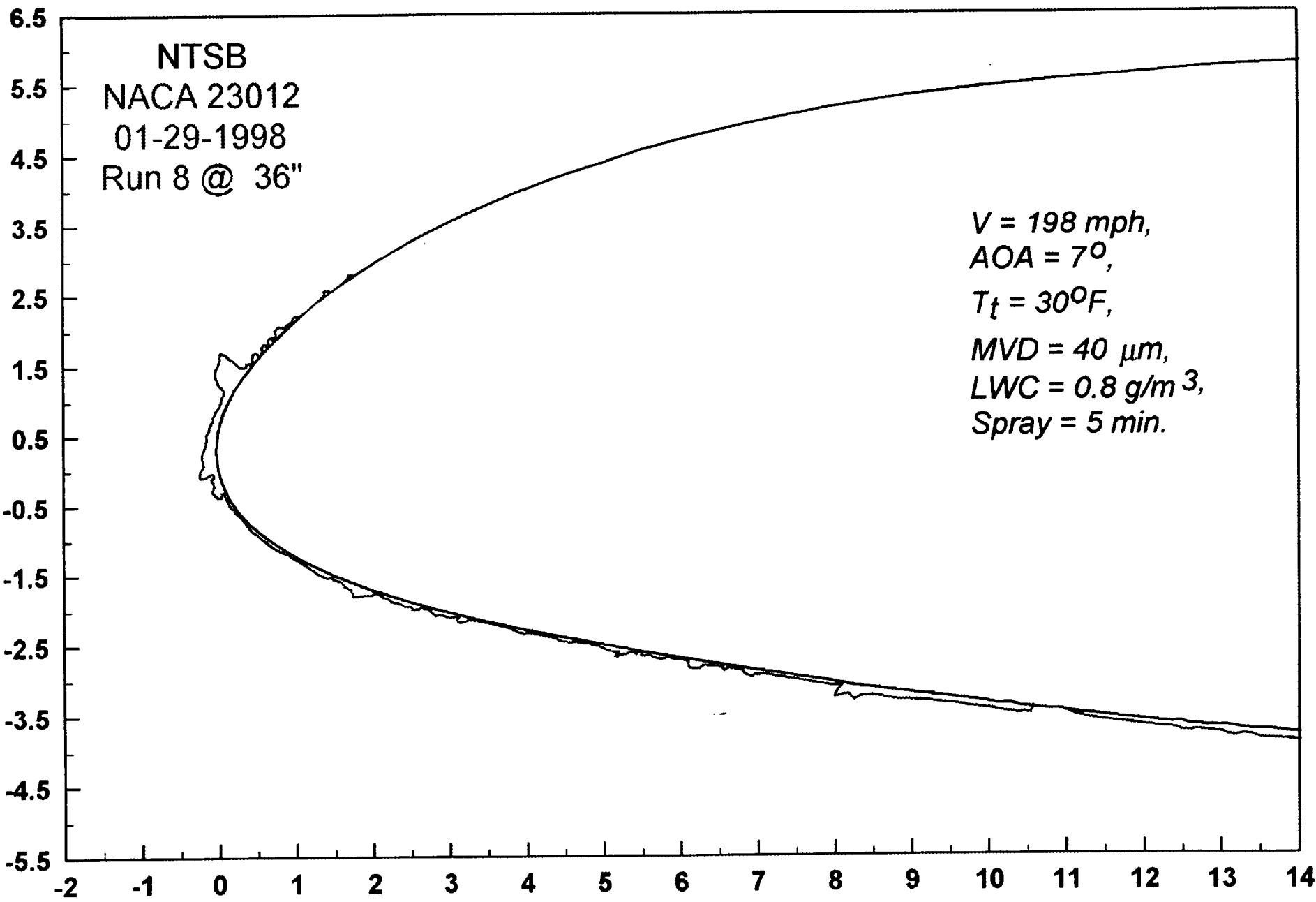
96





32

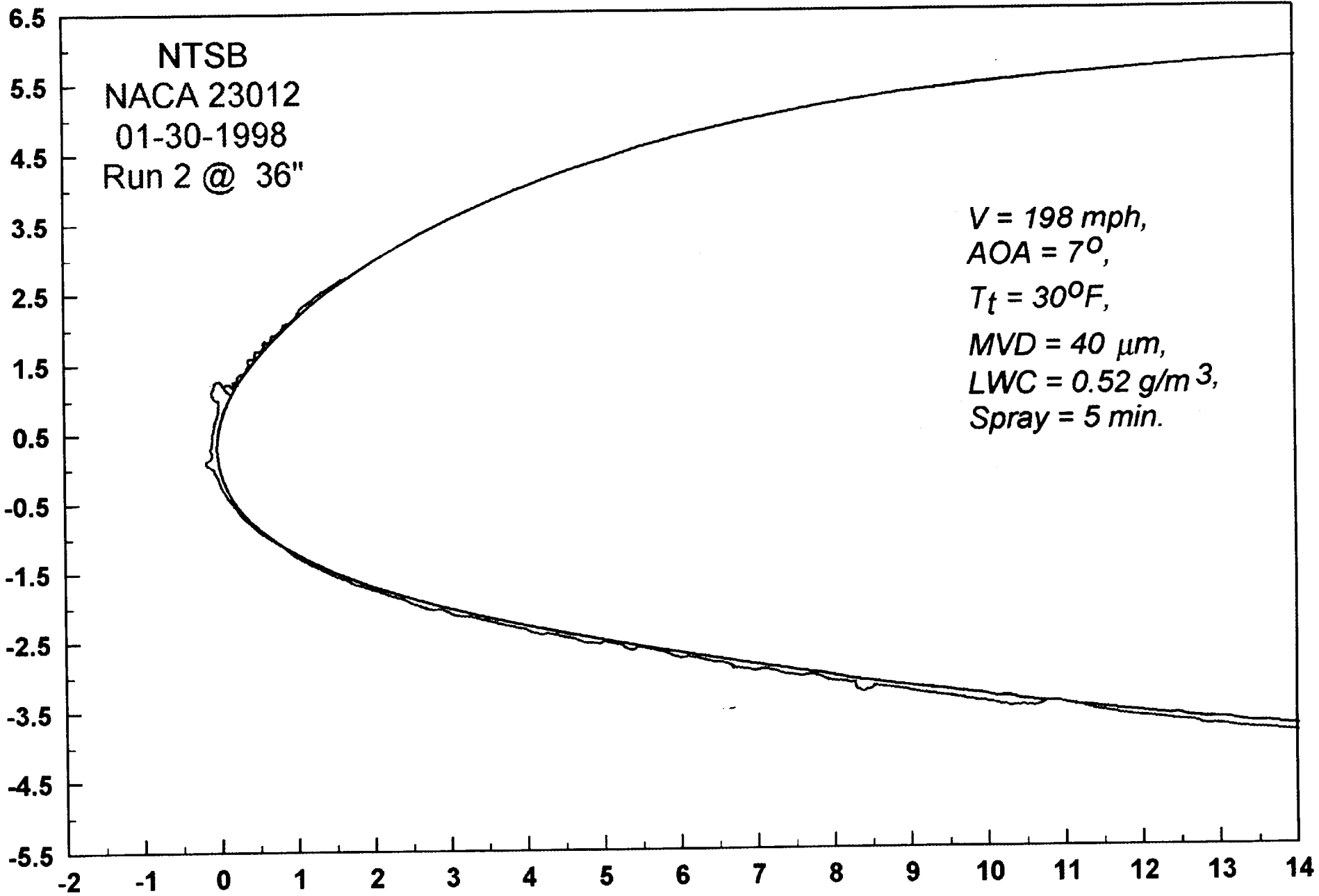
11-98



11-99

487

W-100



6.5

5.5

4.5

3.5

2.5

1.5

0.5

-0.5

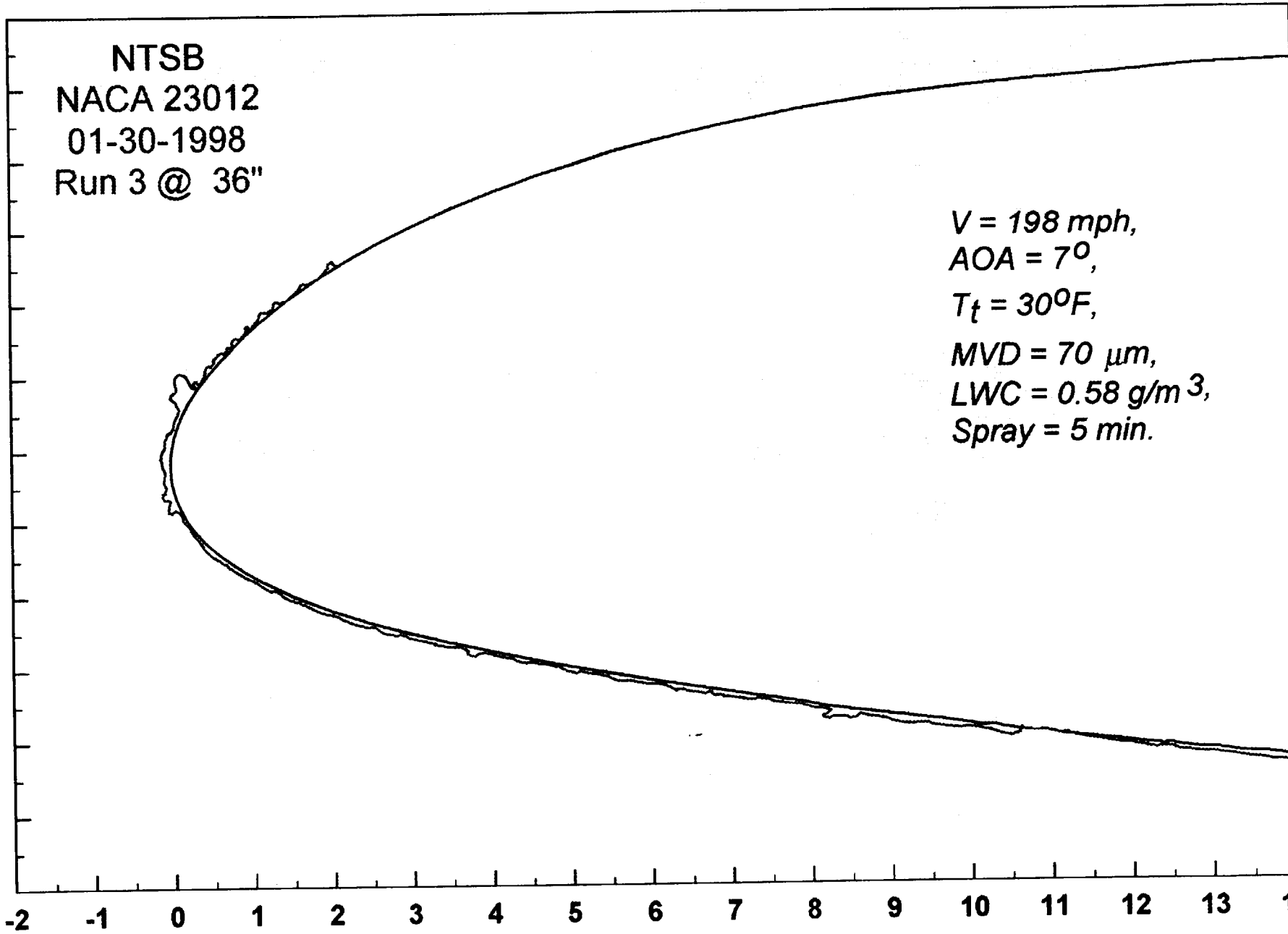
-1.5

-2.5

-3.5

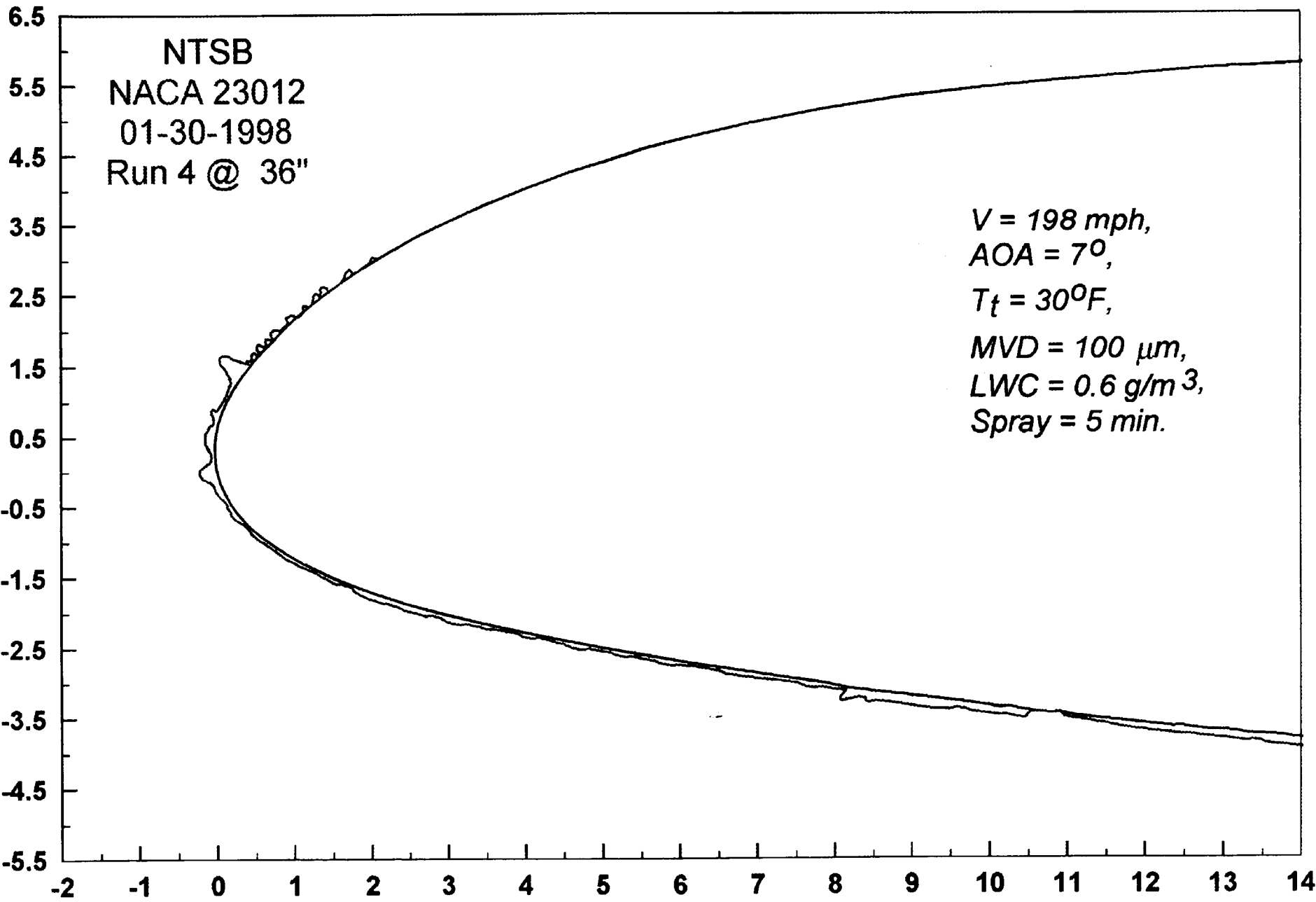
-4.5

-5.5

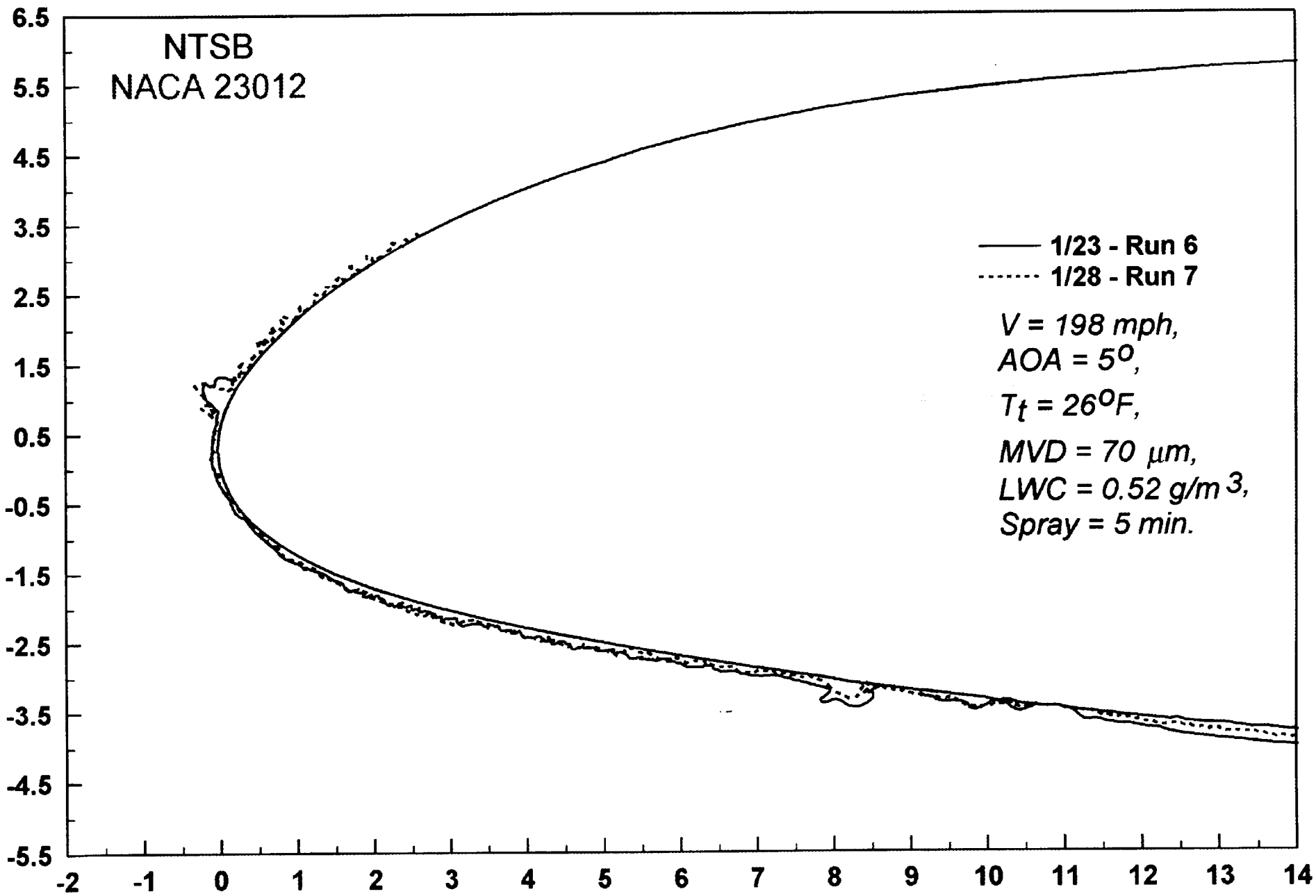


987

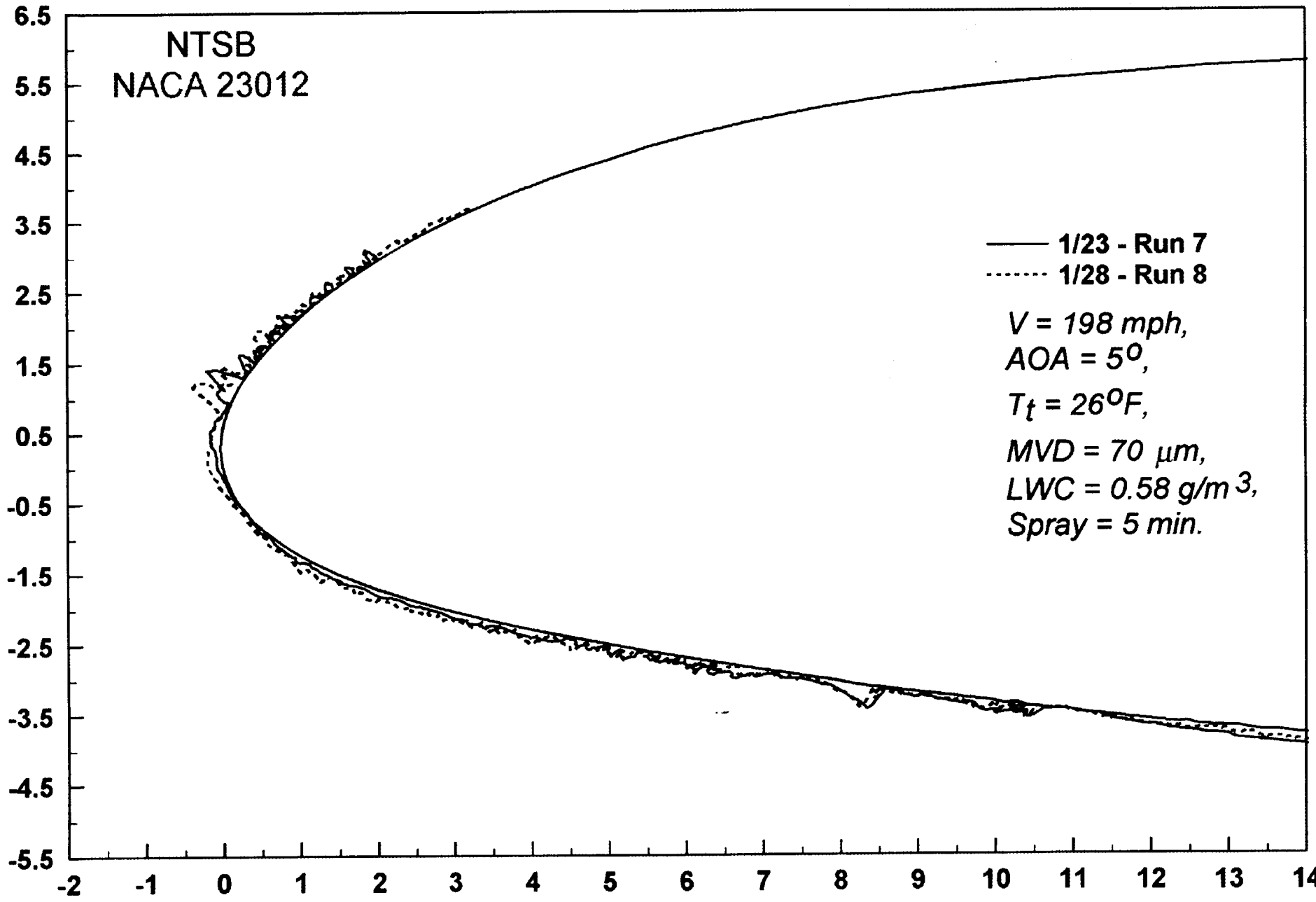
VI-101



201-102



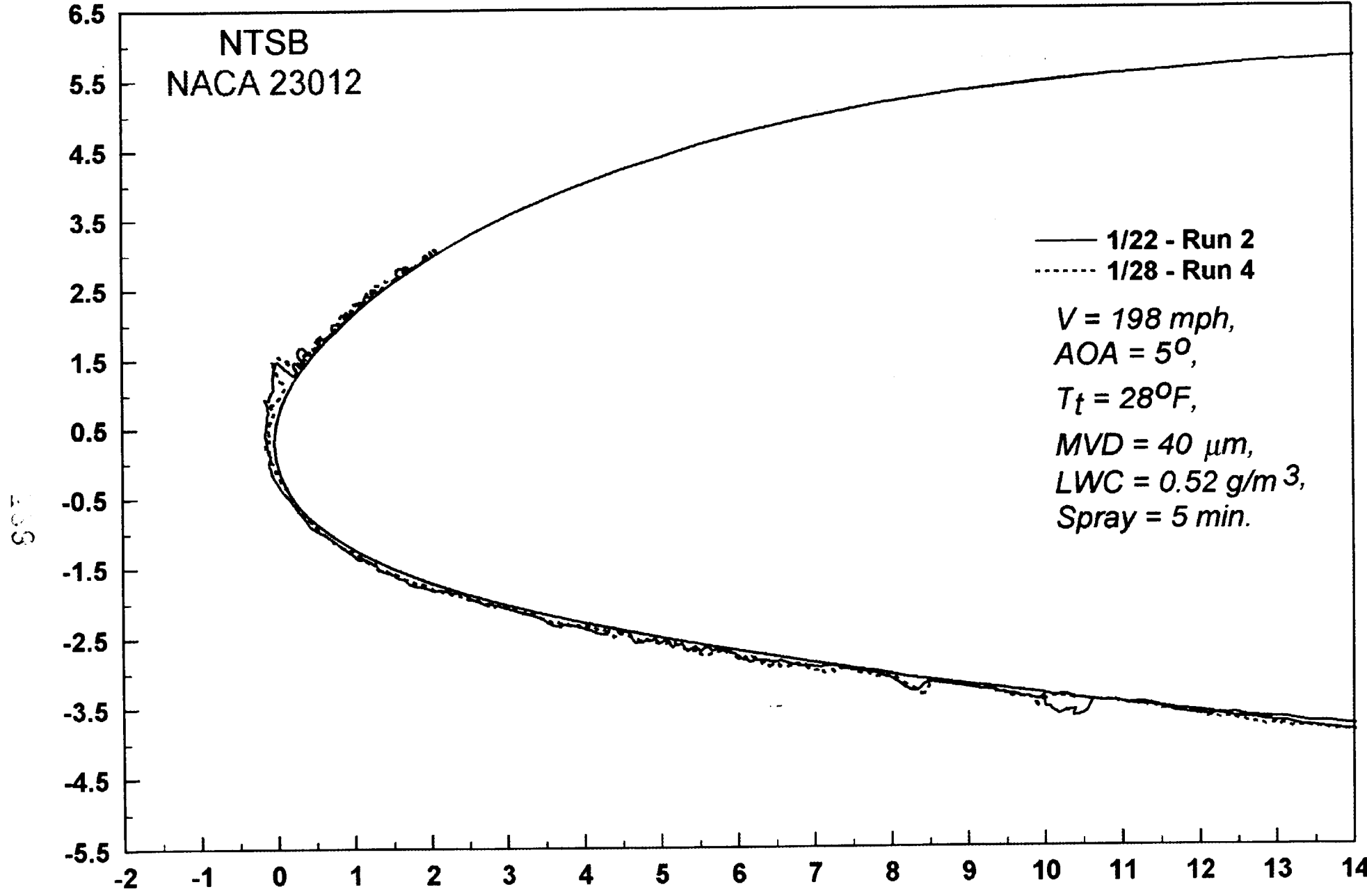
NTSB
NACA 23012



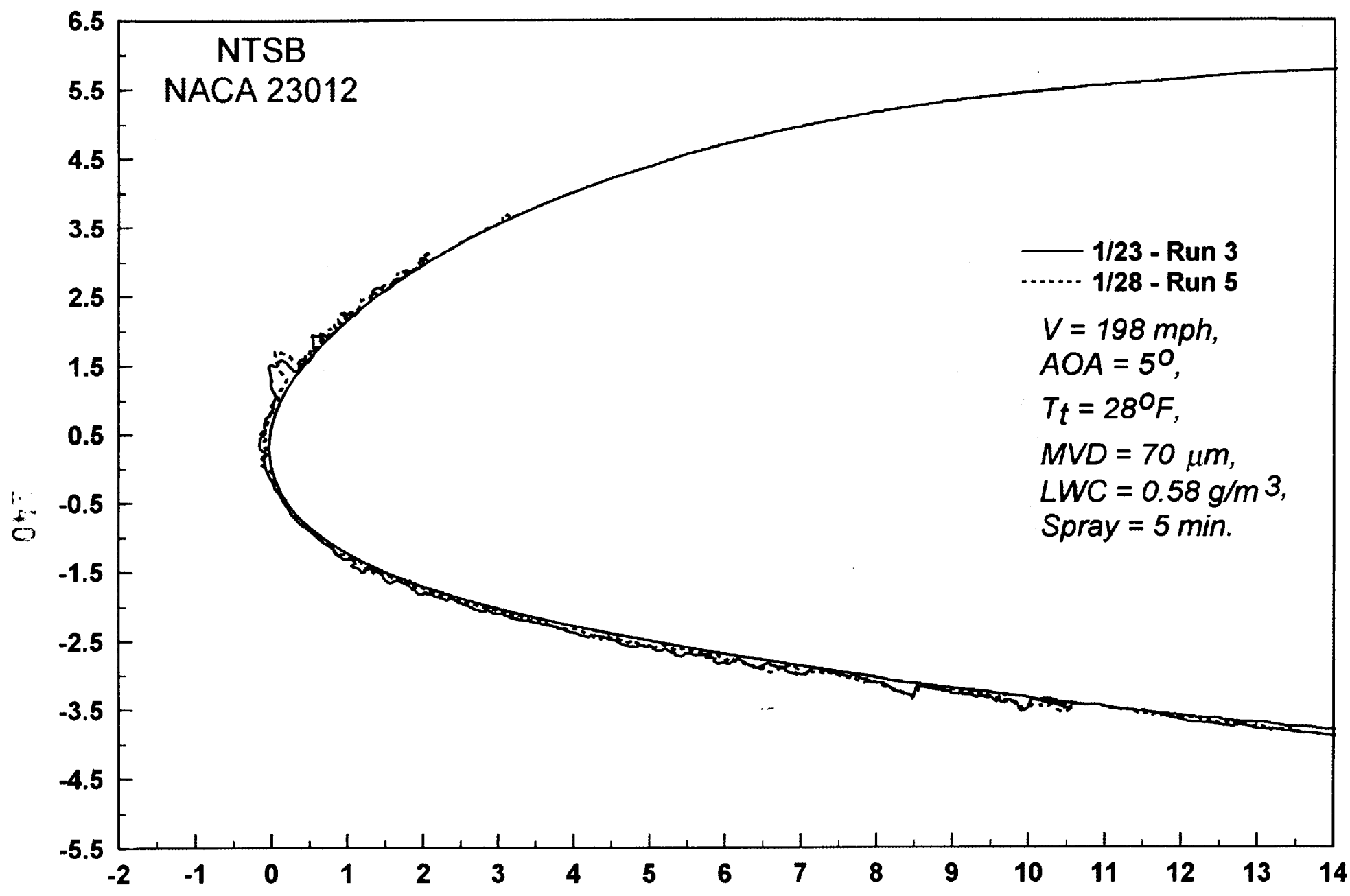
CL

VI-104

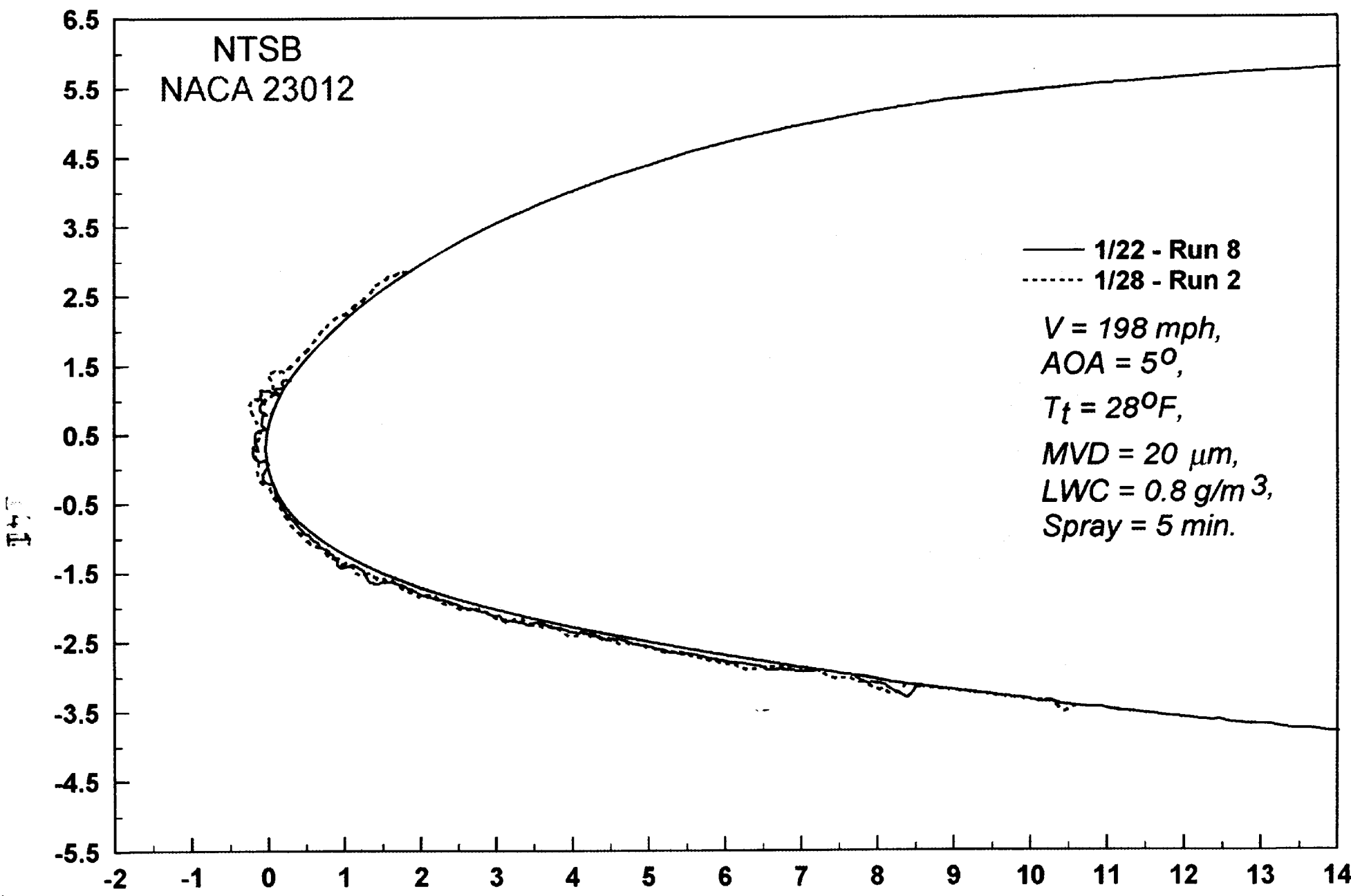
NTSB
NACA 23012



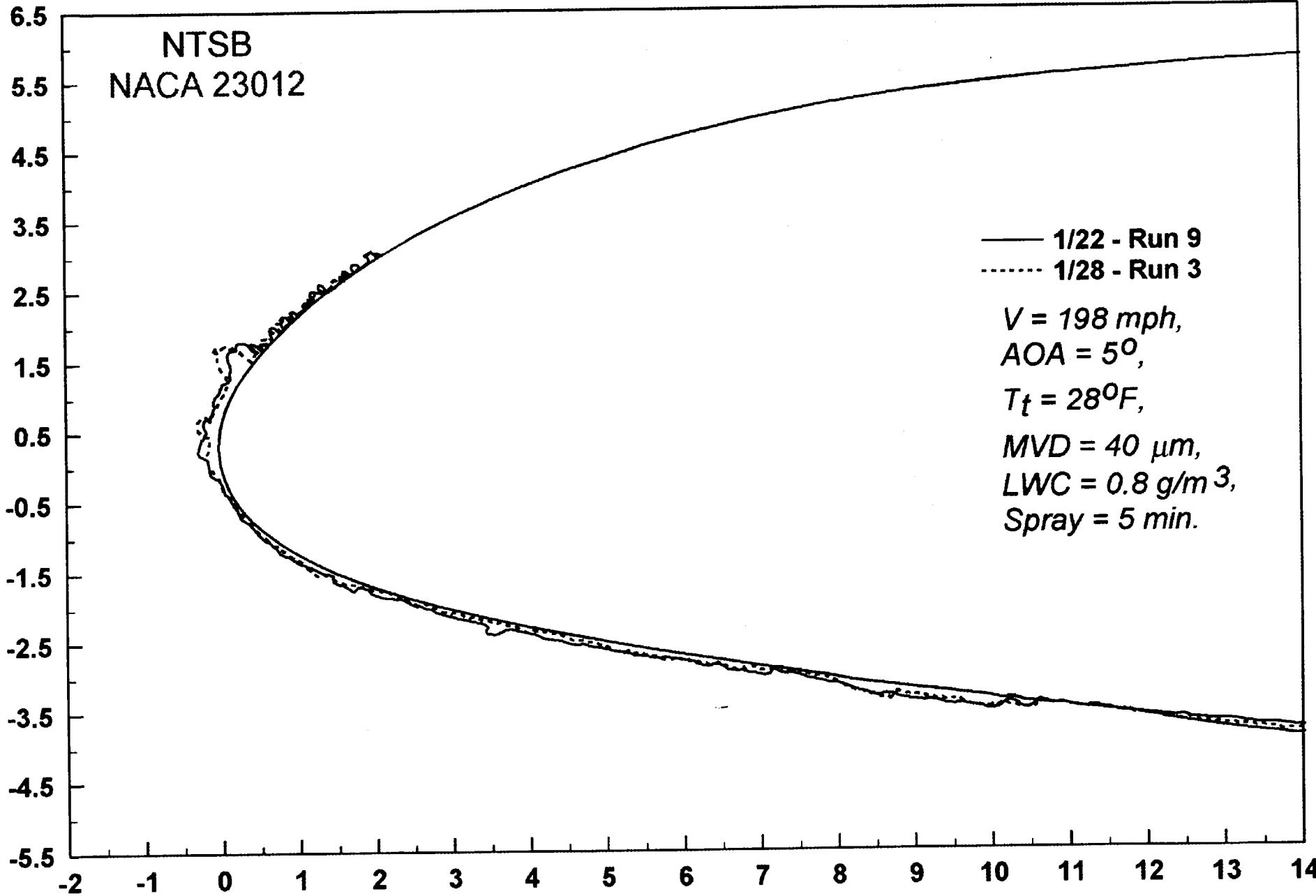
VI-105



NTSB
NACA 23012

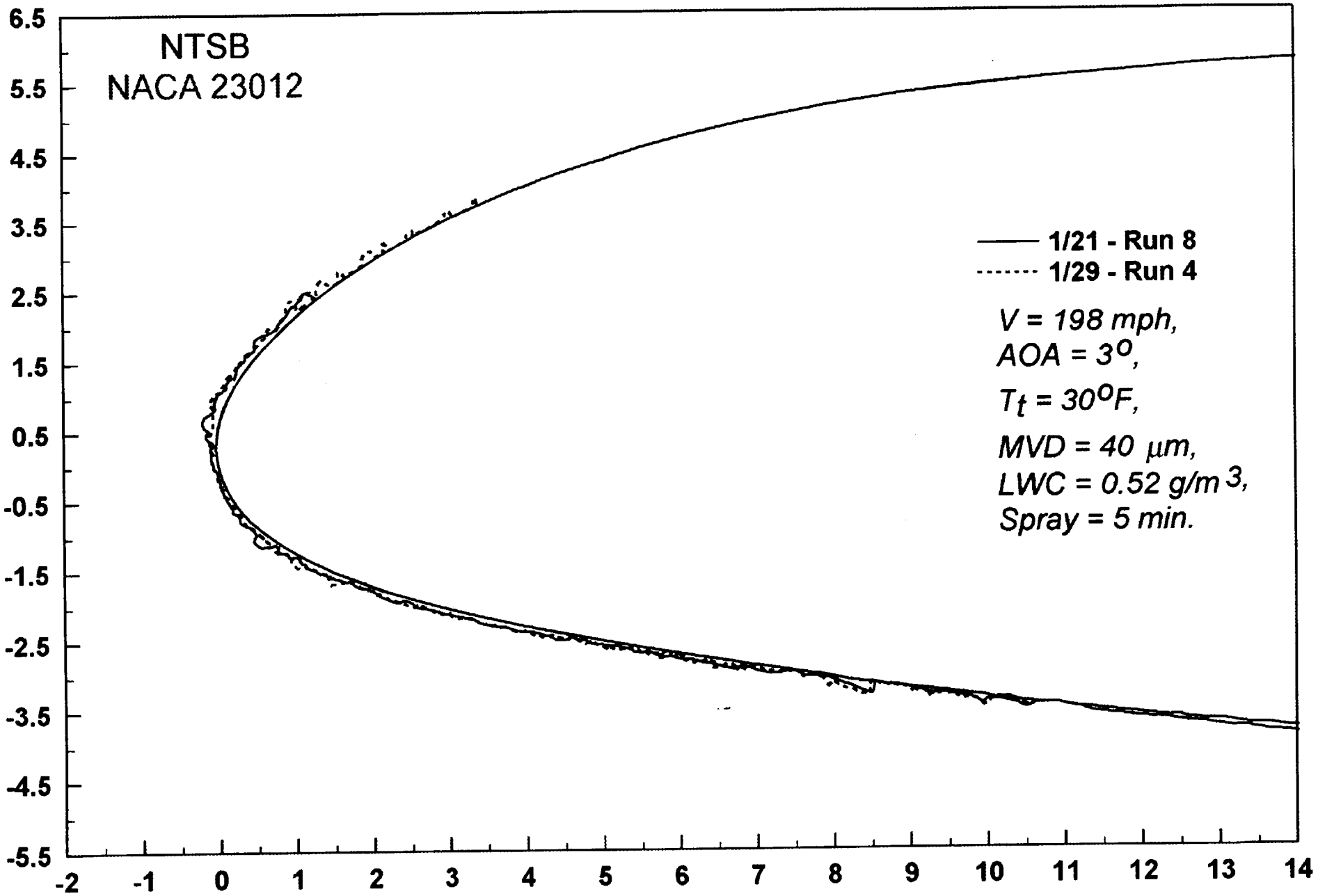


11-107

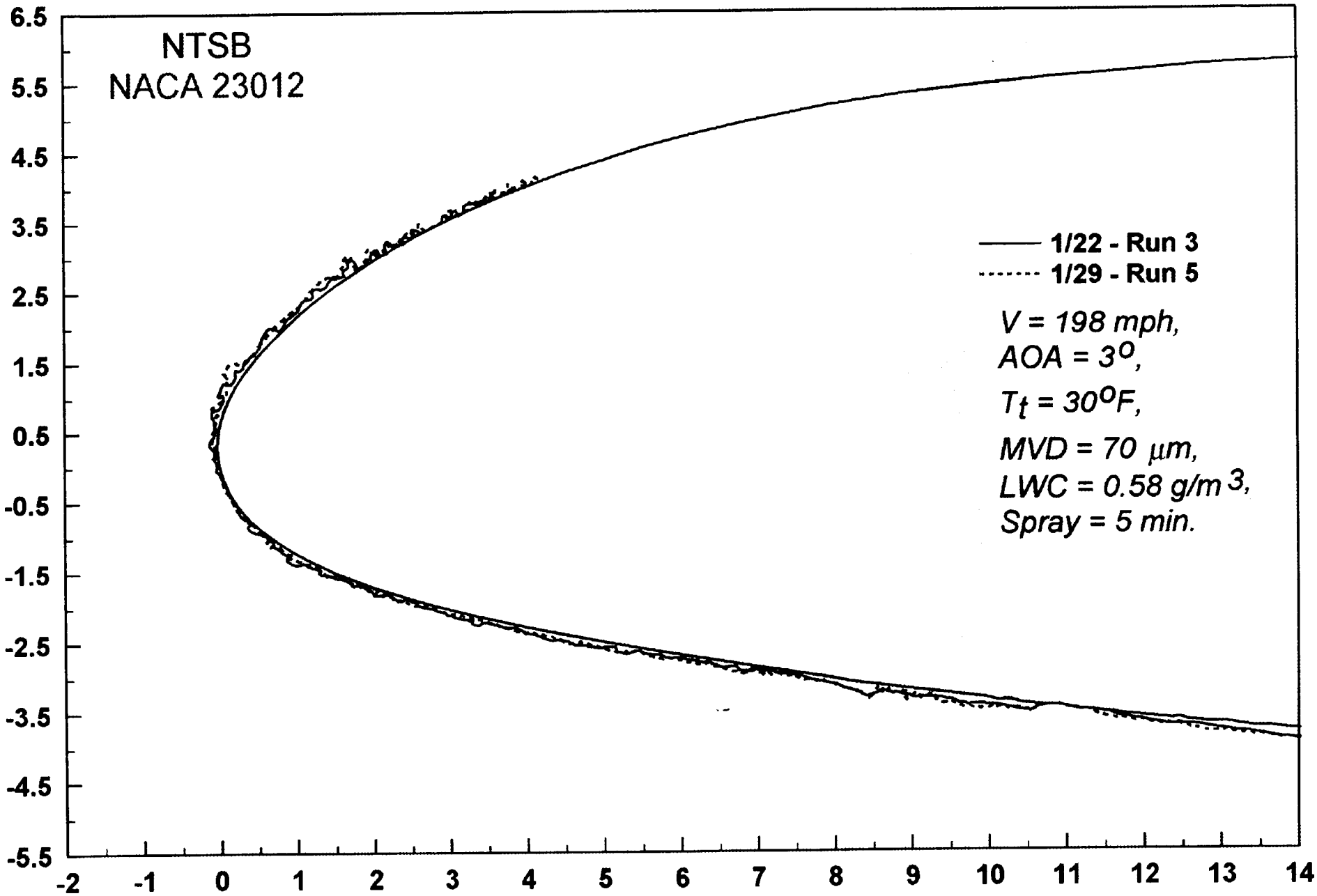


7.5

11-108

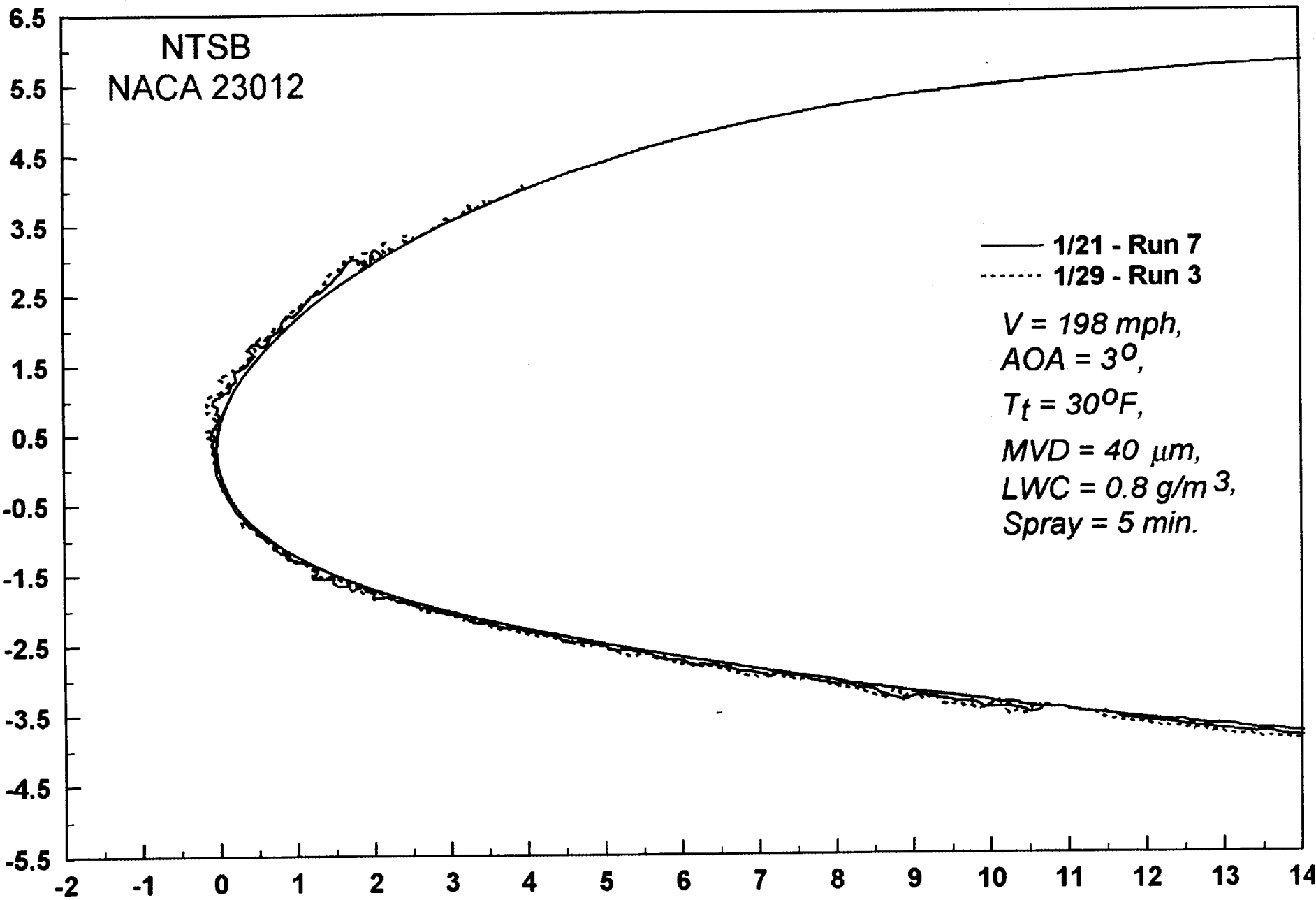


V1-109



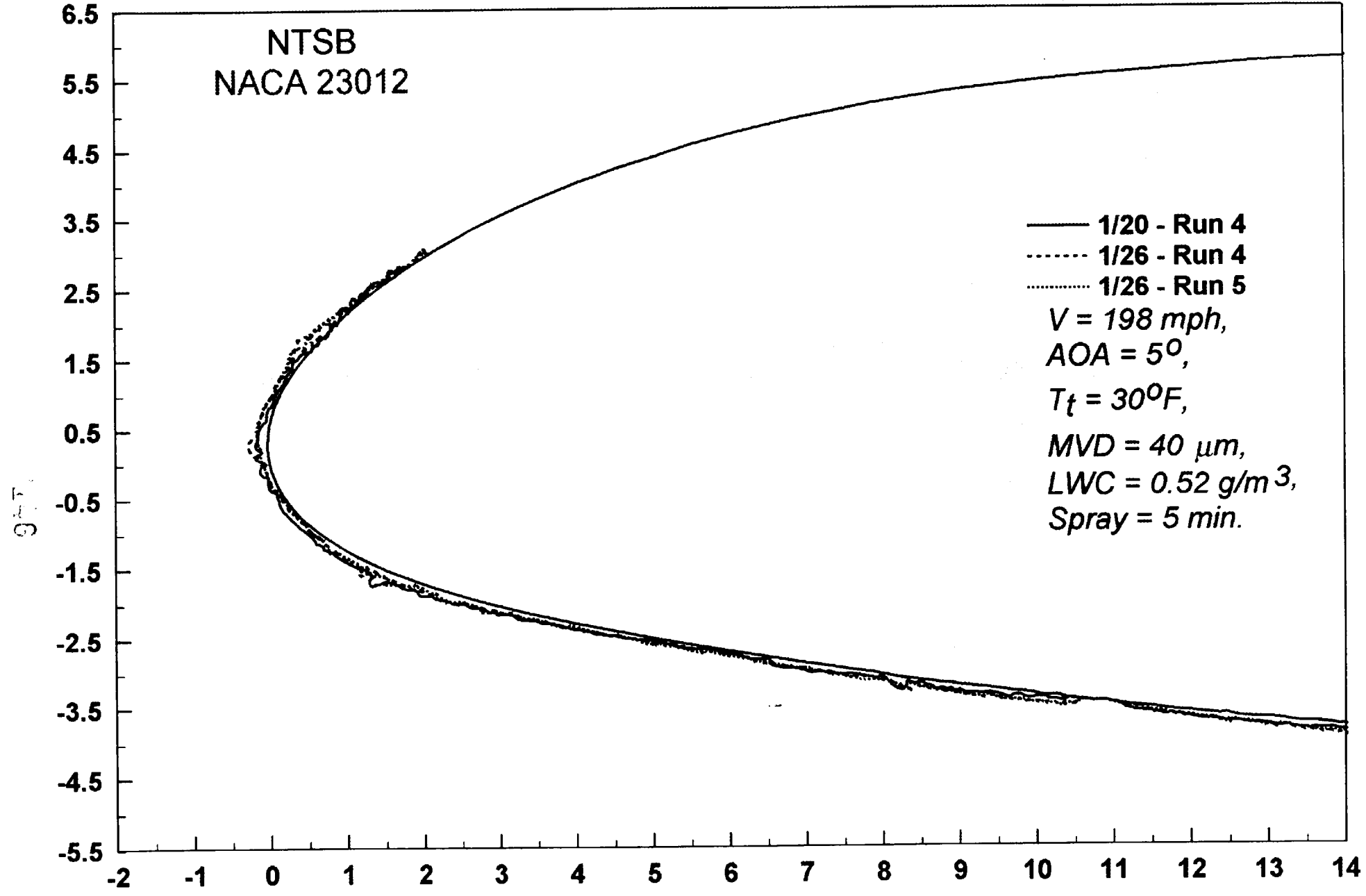
4475

VI-110

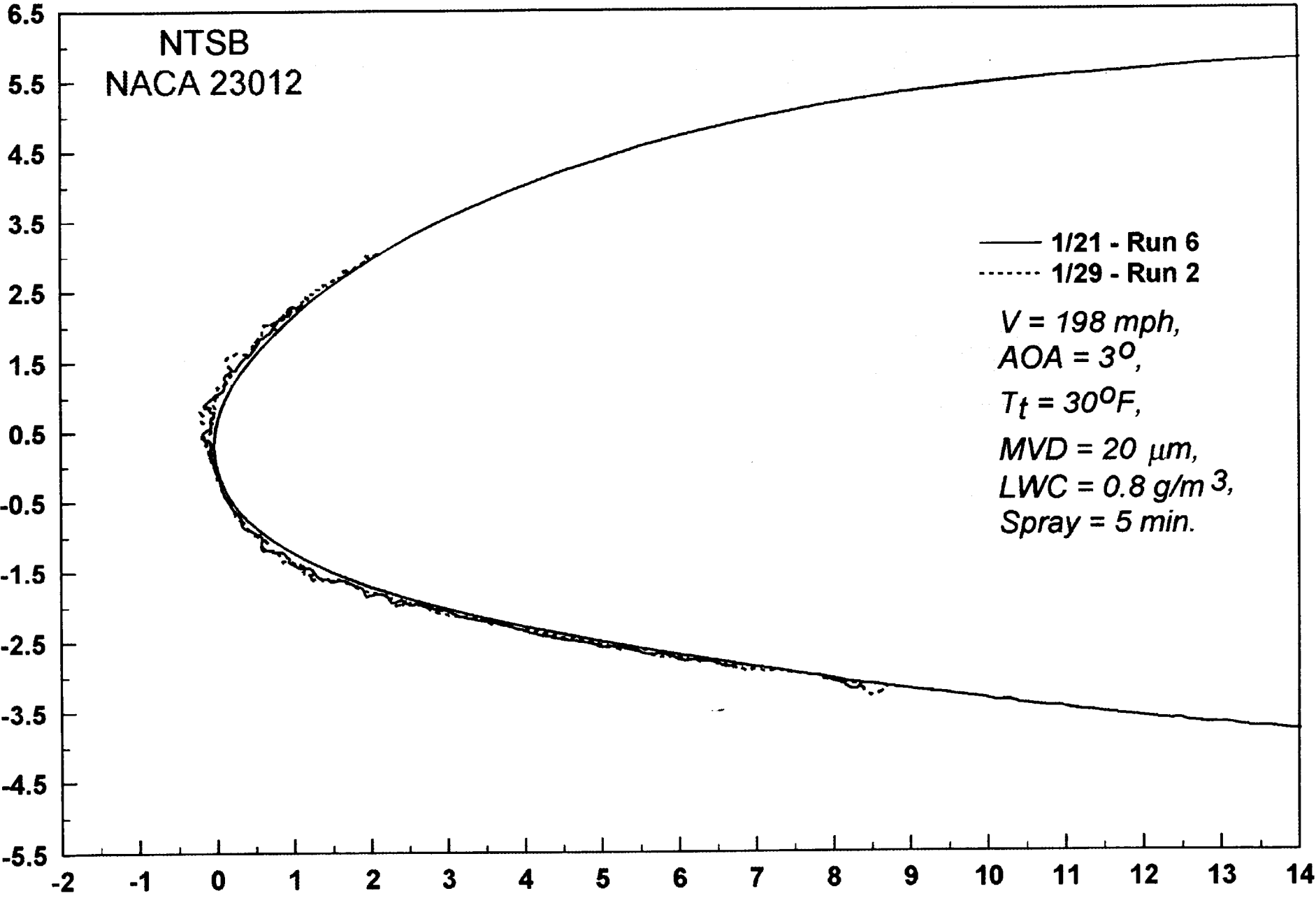


VI-III

NTSB
NACA 23012

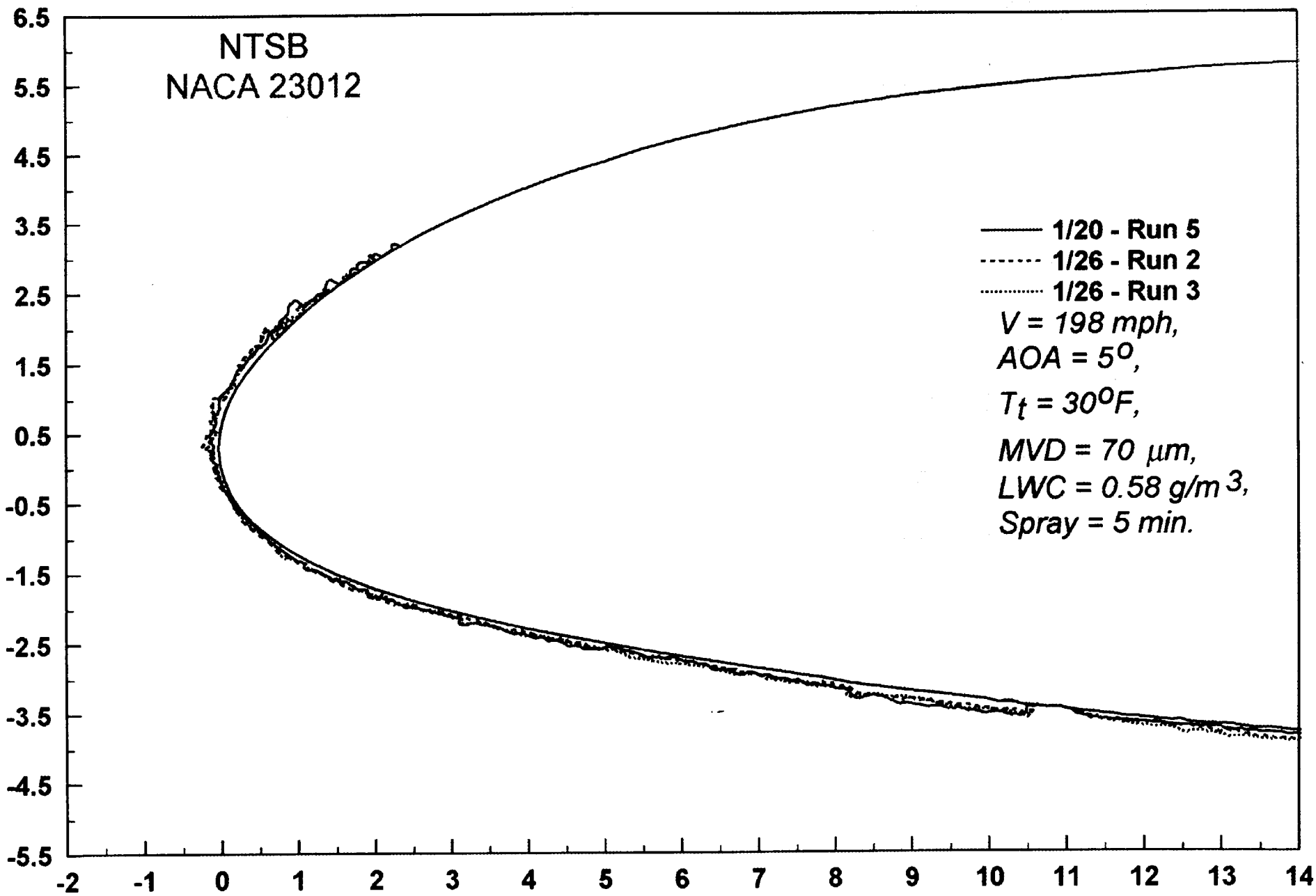


W-112



VI-113

NTSB
NACA 23012

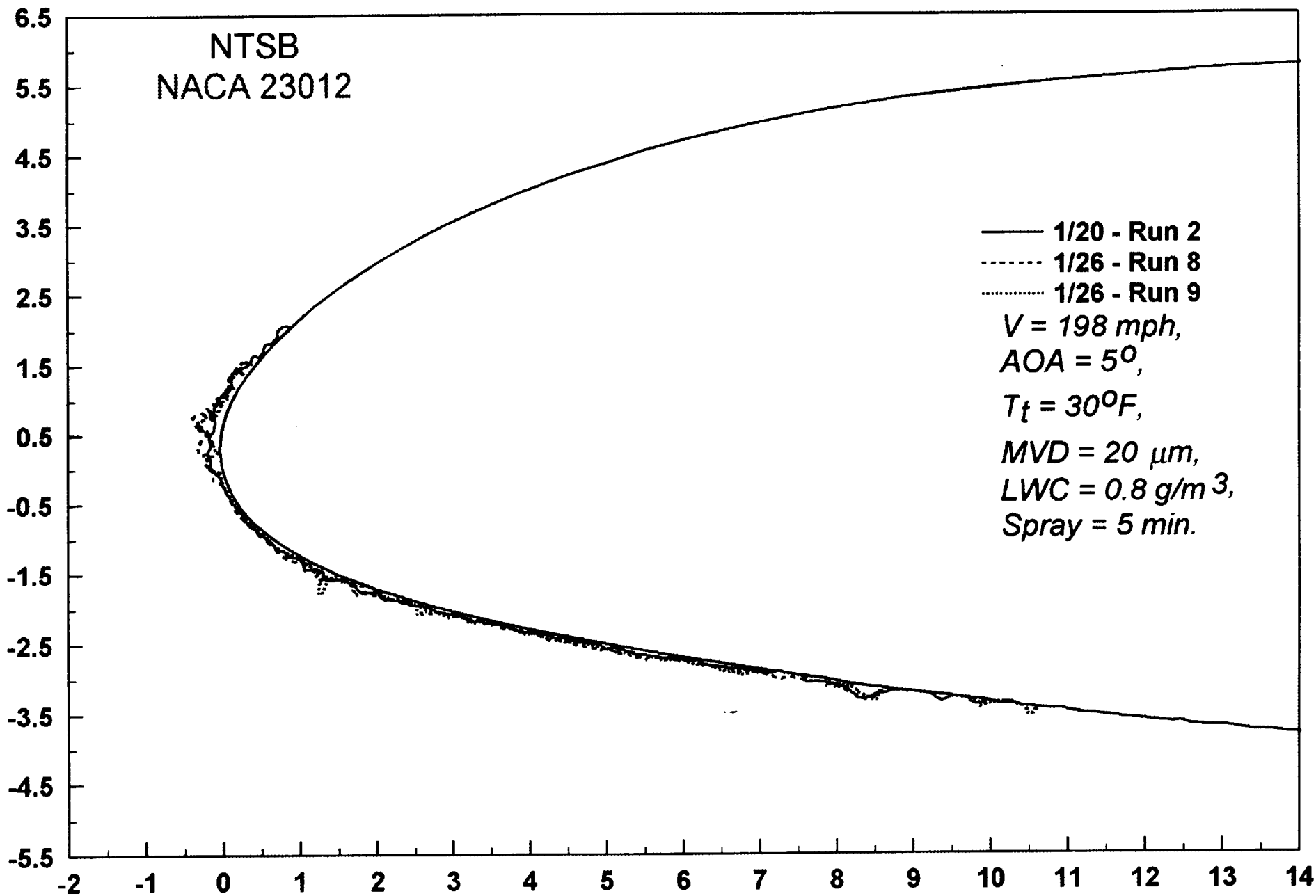


1/20

11-114

NTSB
NACA 23012

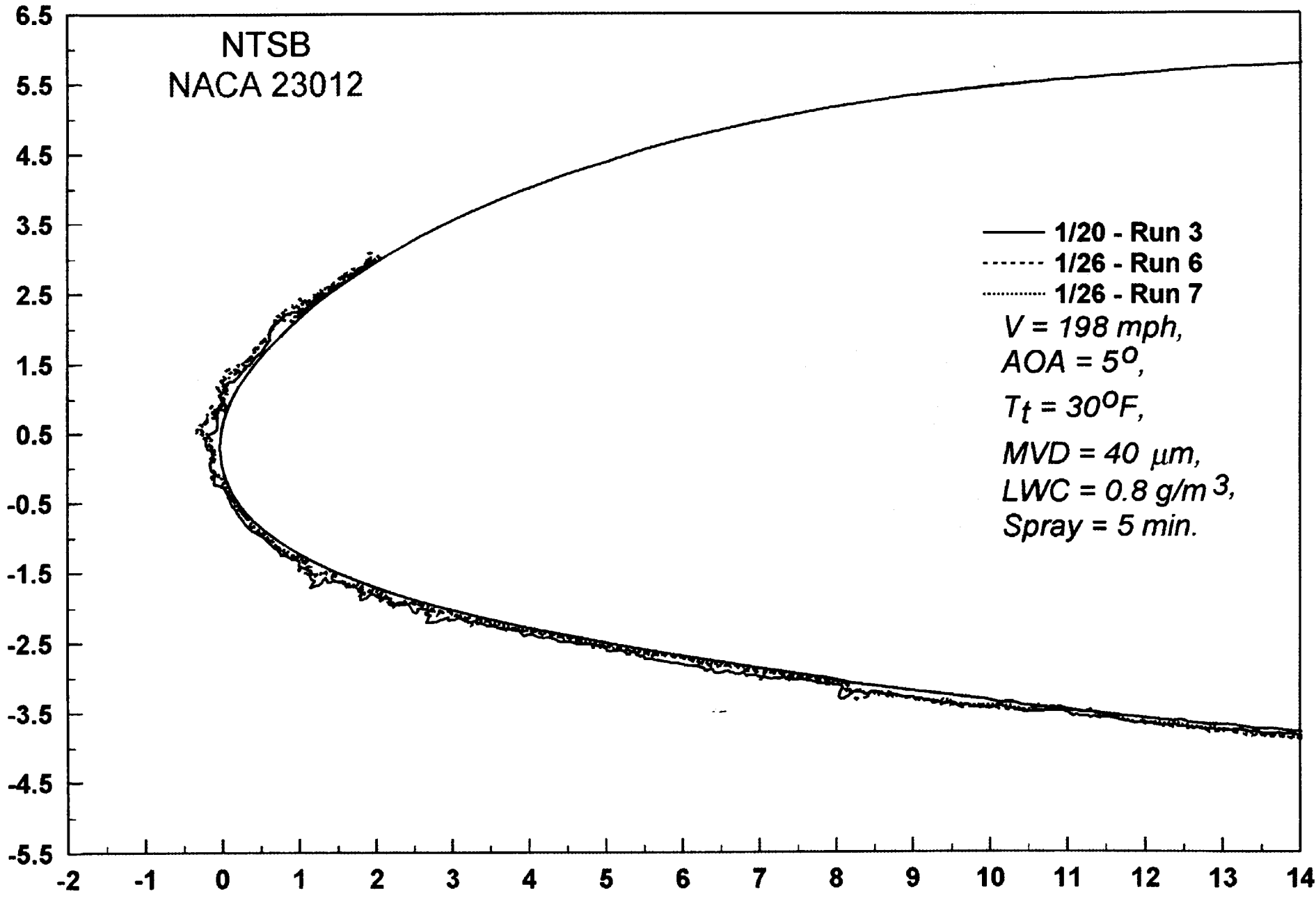
C_{DF}



VI-115

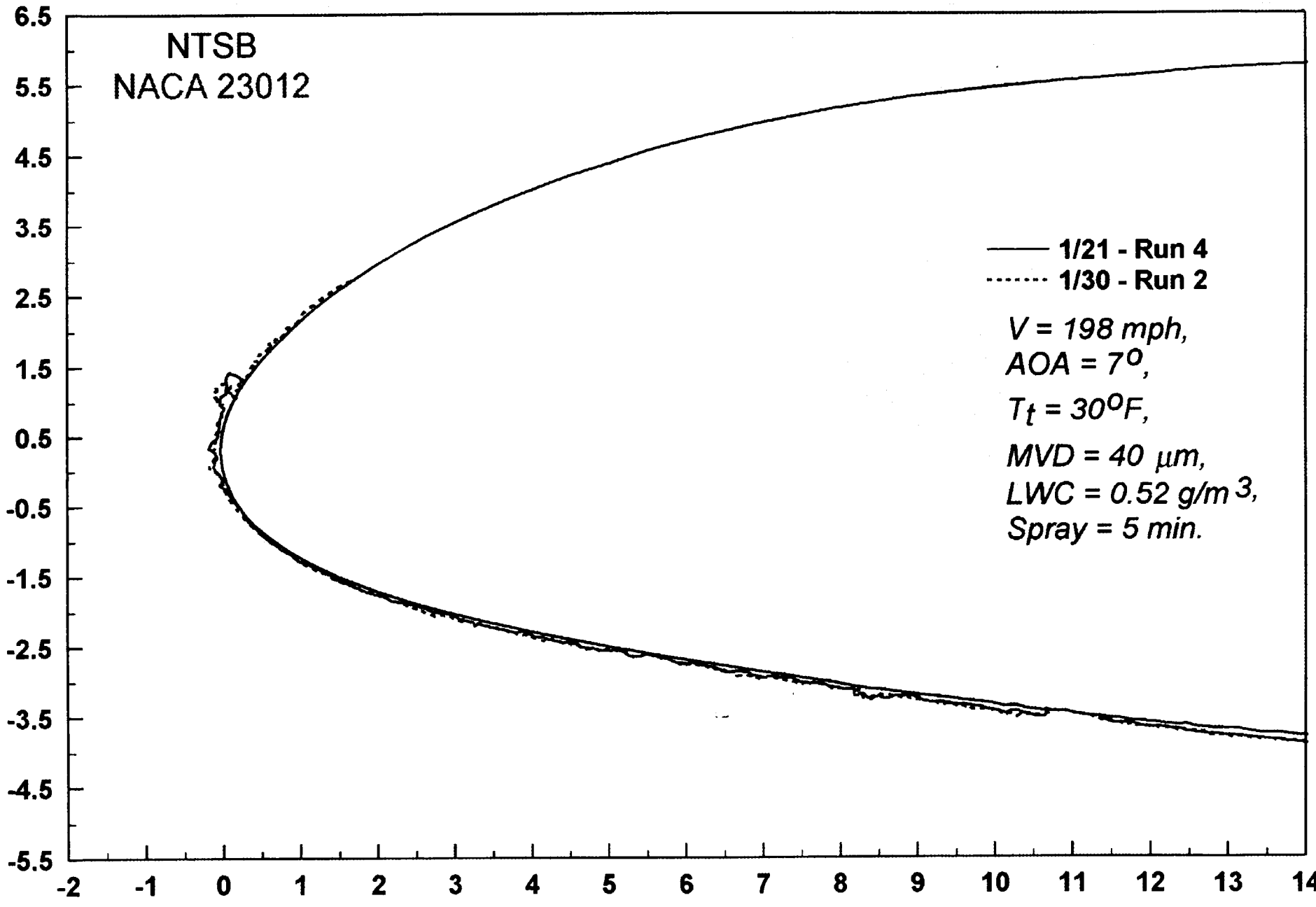
50

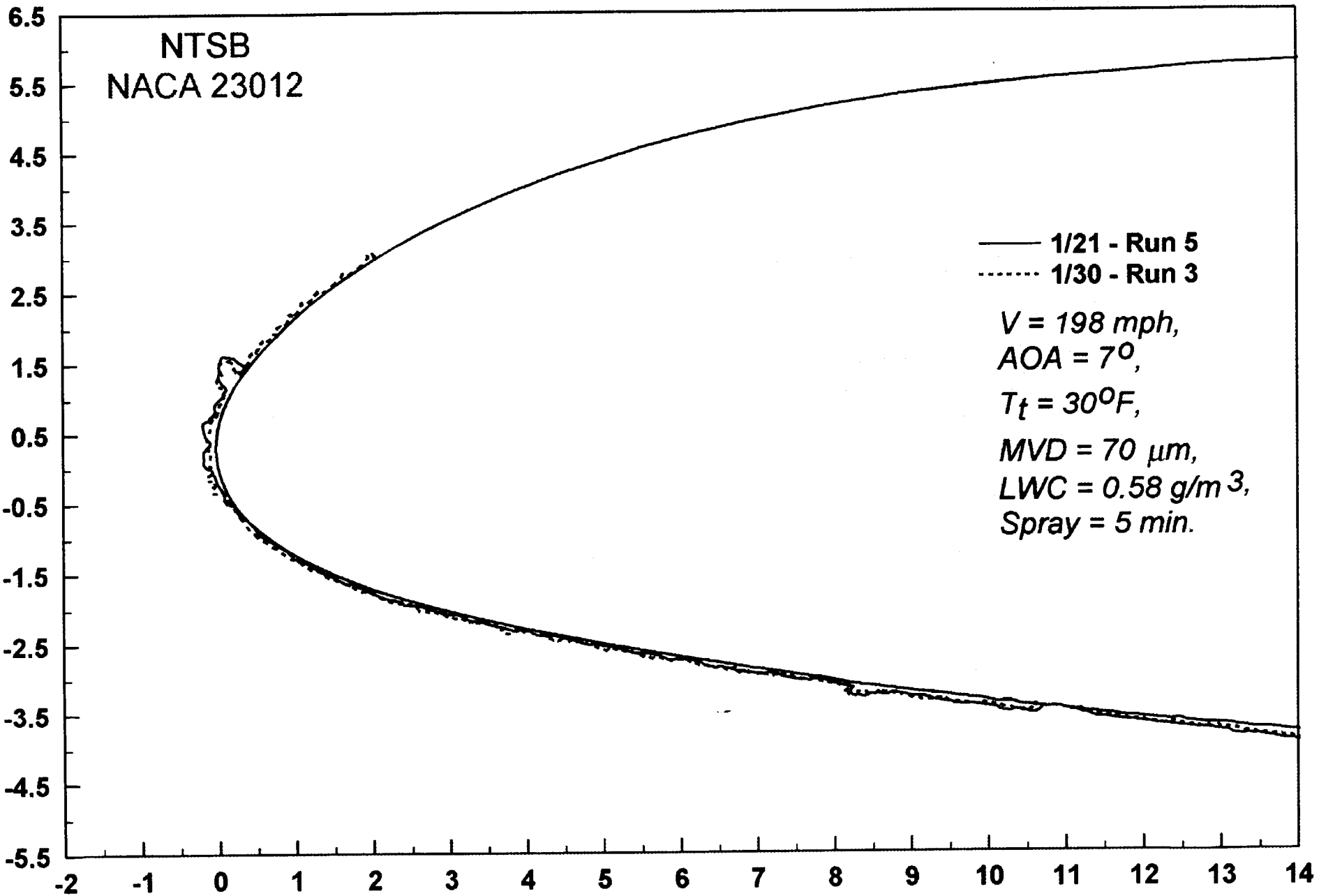
VI-116



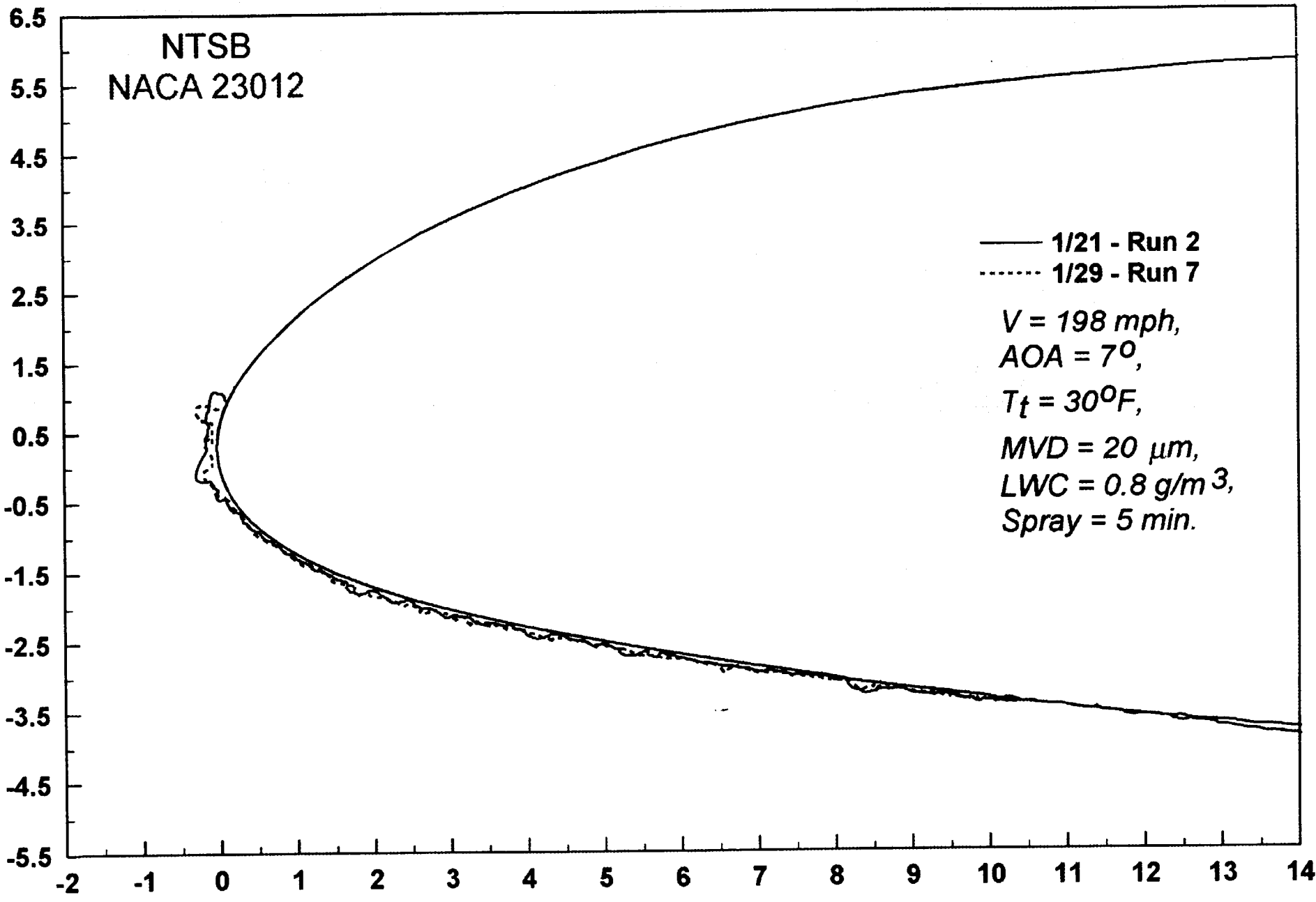
151

W-117





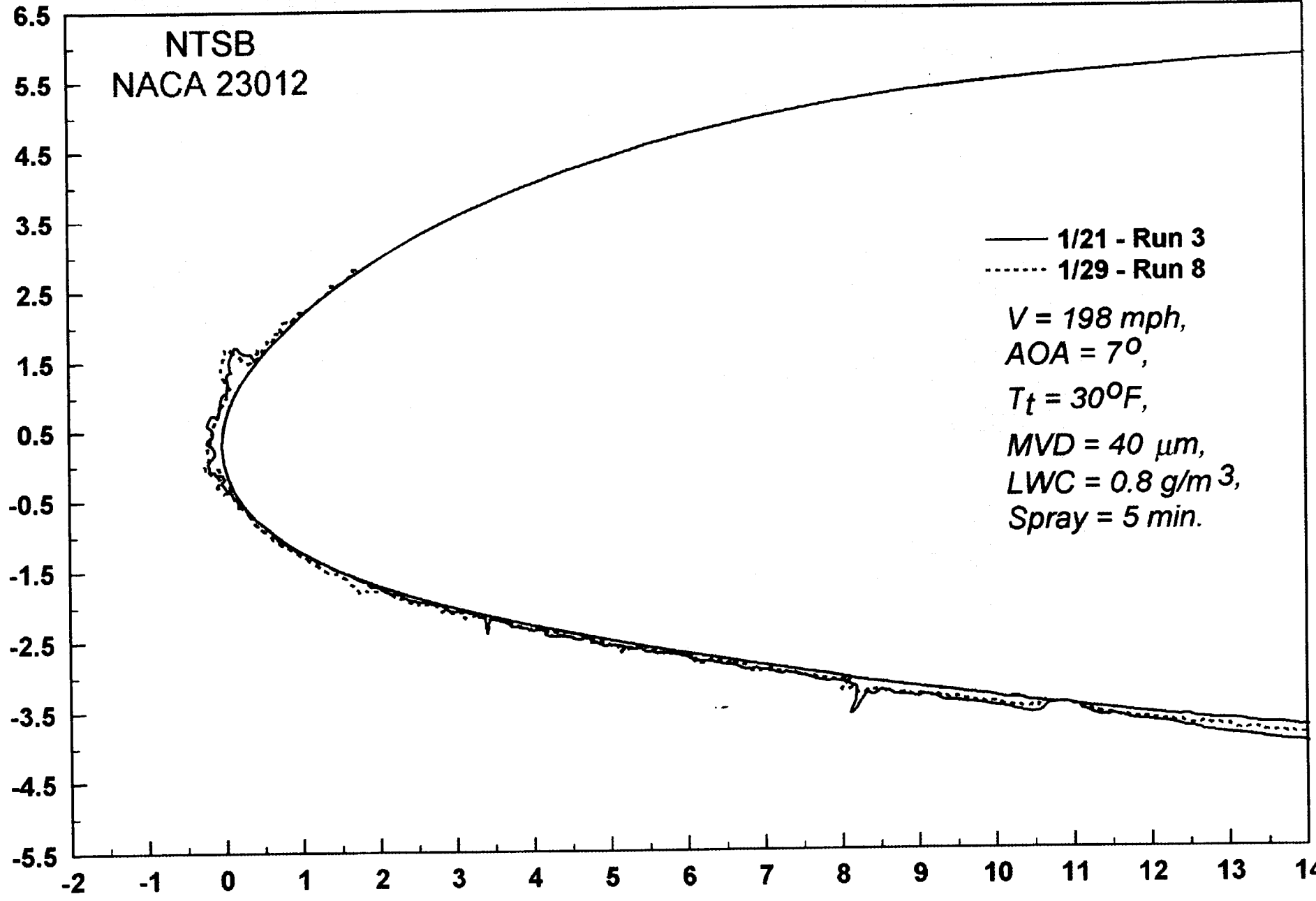
VI-118



1503

VI-119

NTSB
NACA 23012

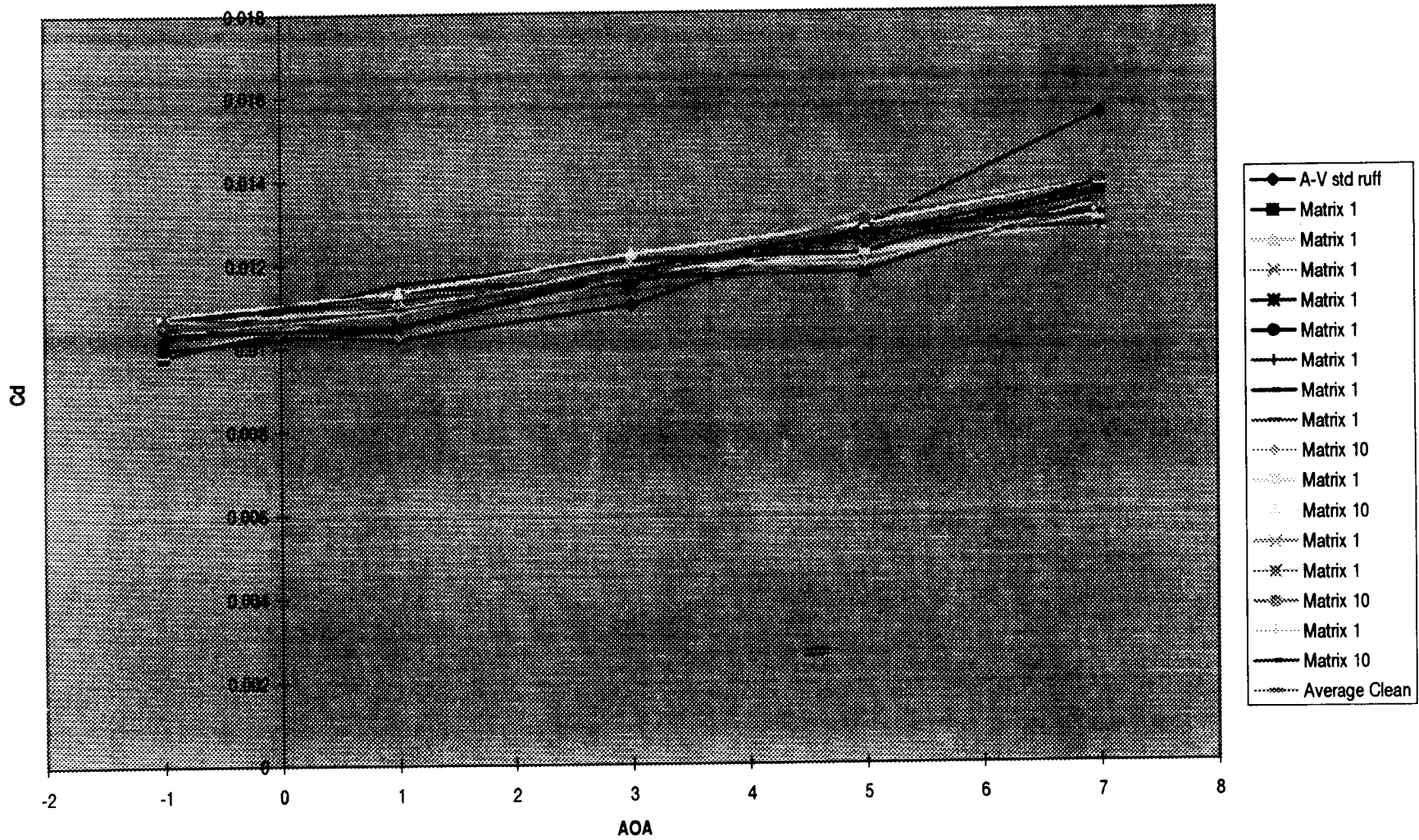


NTSB

M-120

IRT Drag Measurements

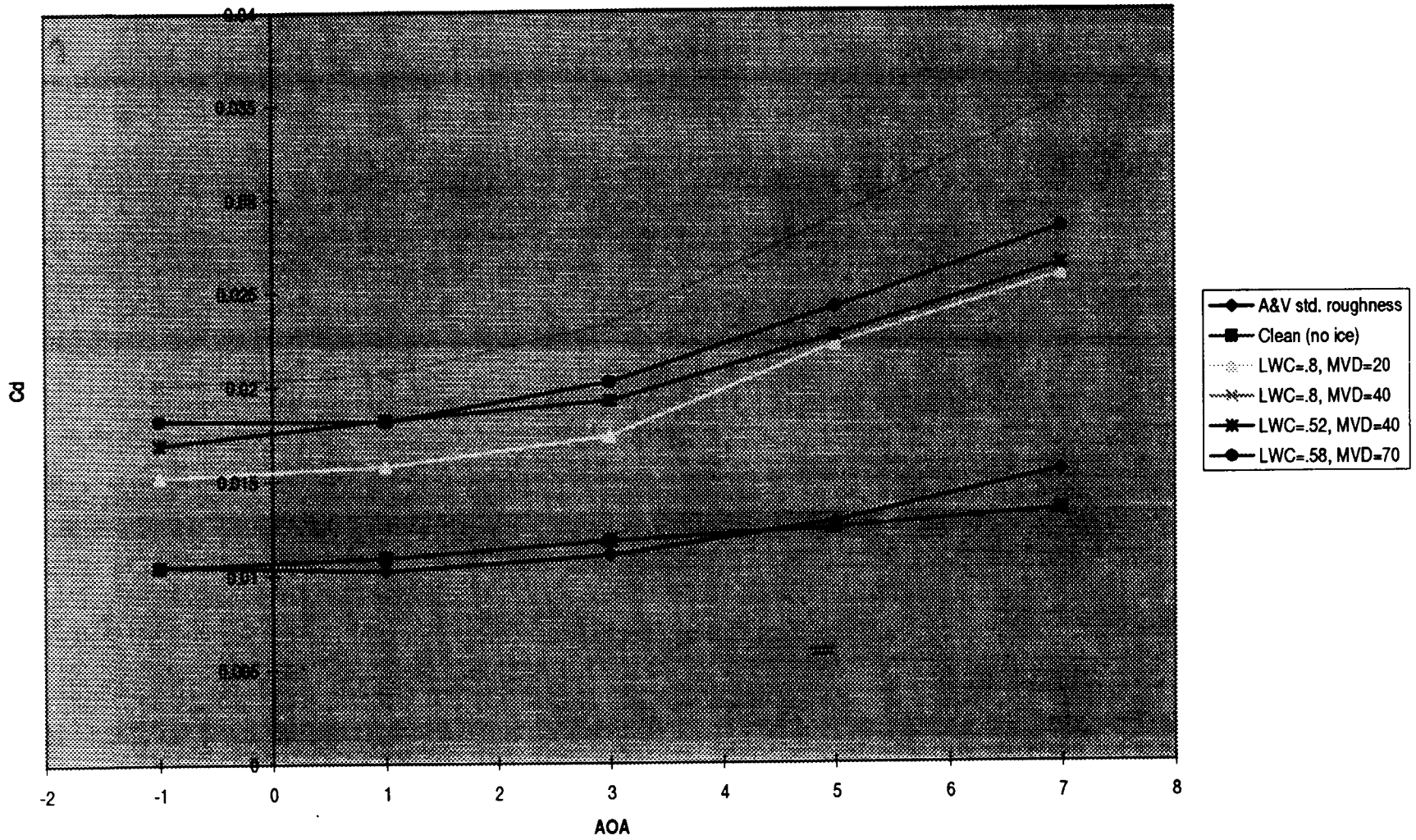
Clean Drag Data



150

V1-122

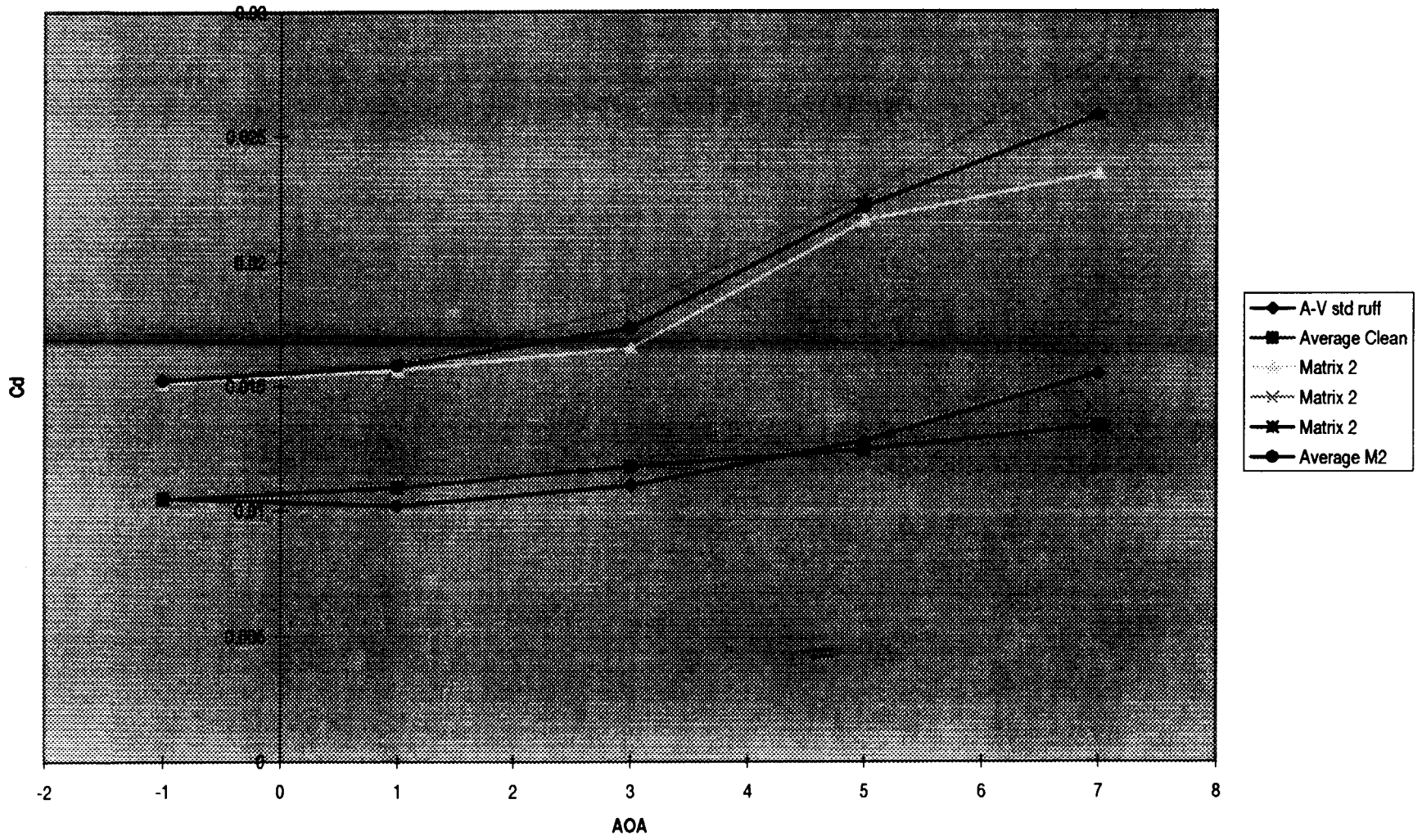
Baseline Series



157

VI-123

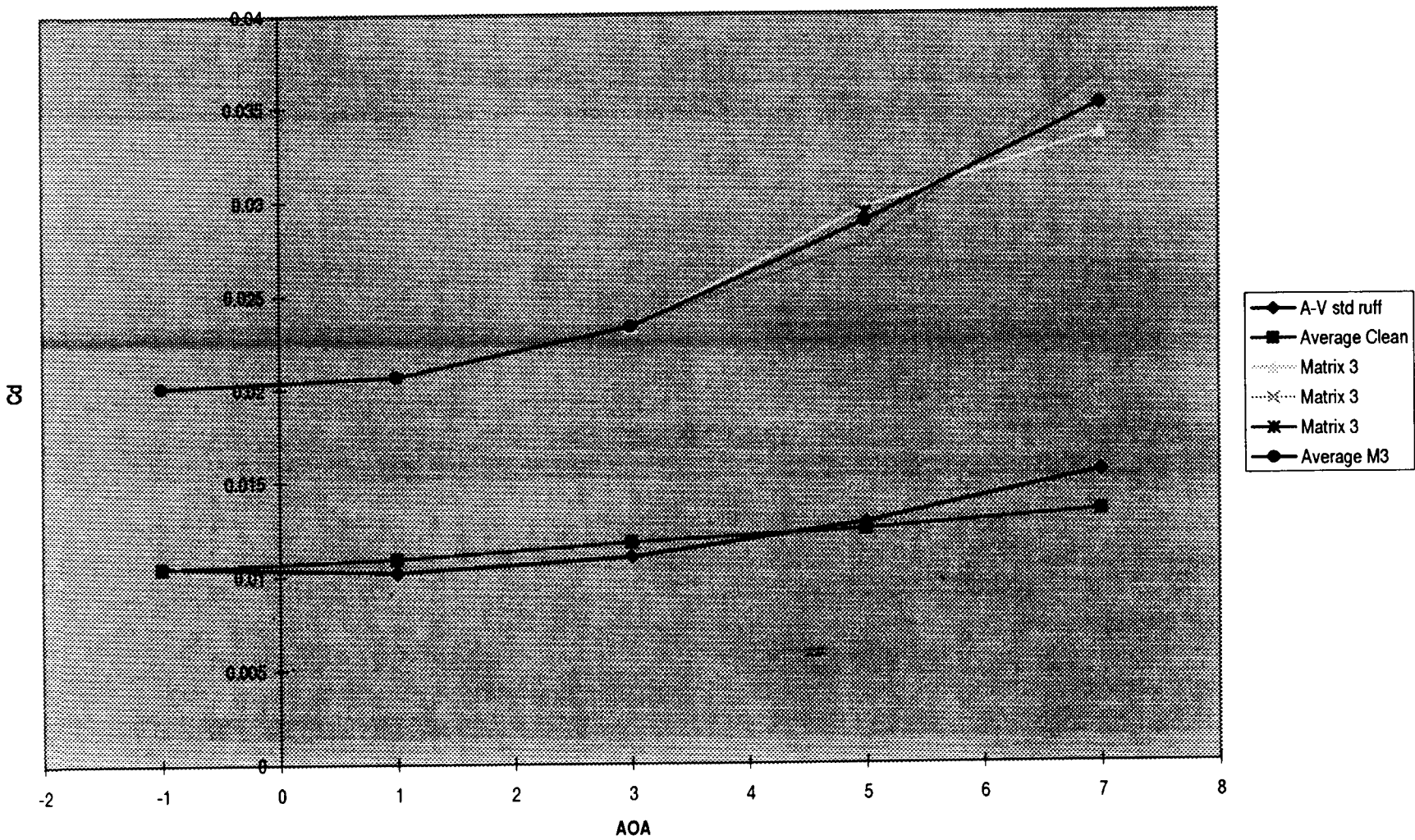
Matrix #2: Tt=30, AOA=5, LWC=.8, MVD=20, T=5



453

M-124

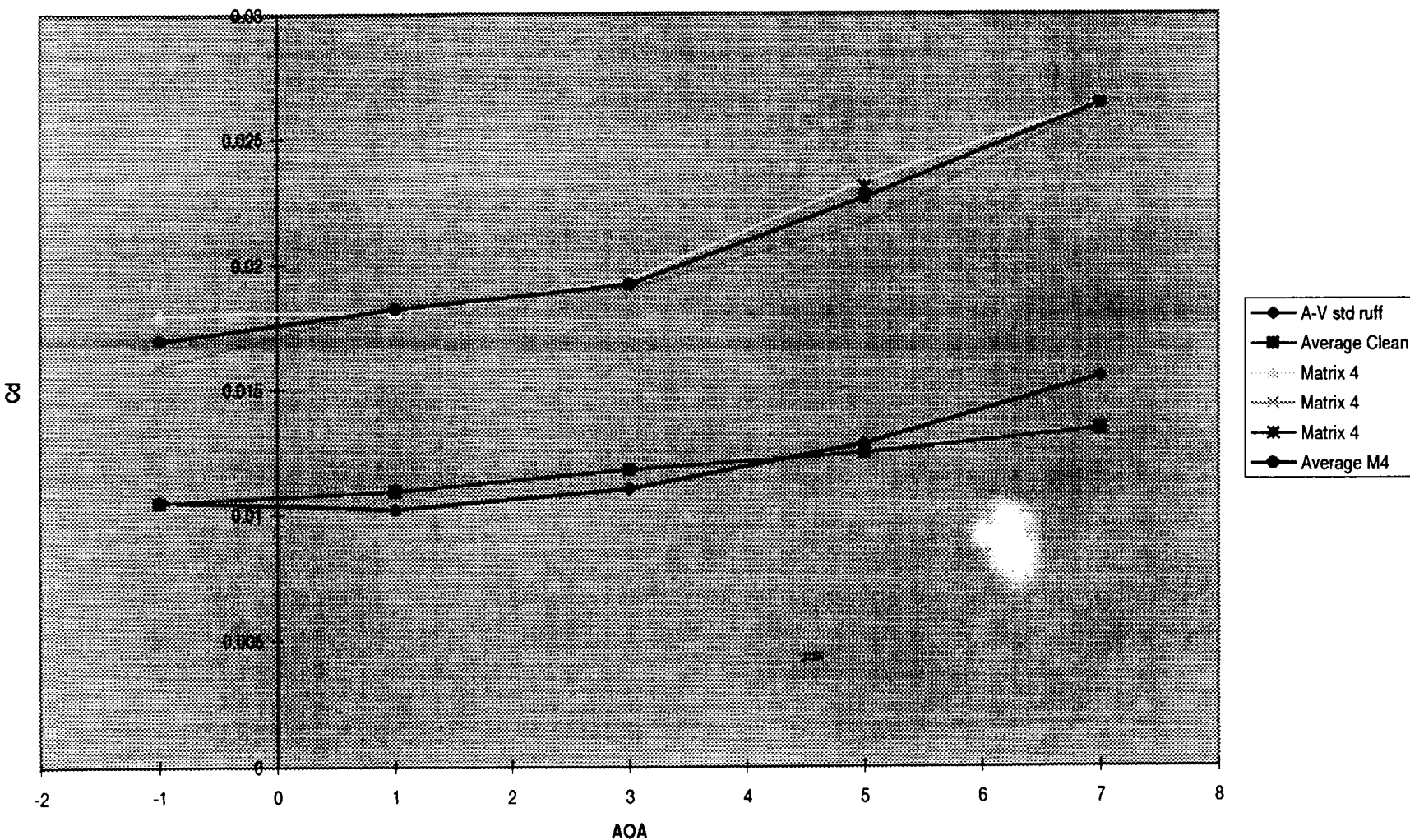
Matrix #3: $T_t=30$, $AOA=5$, $LWC=.8$, $MVD=40$, $T=5$



1.559

M-125

Matrix #4: Tt=30, AOA=5, LWC=.52, MVD=40, T=5

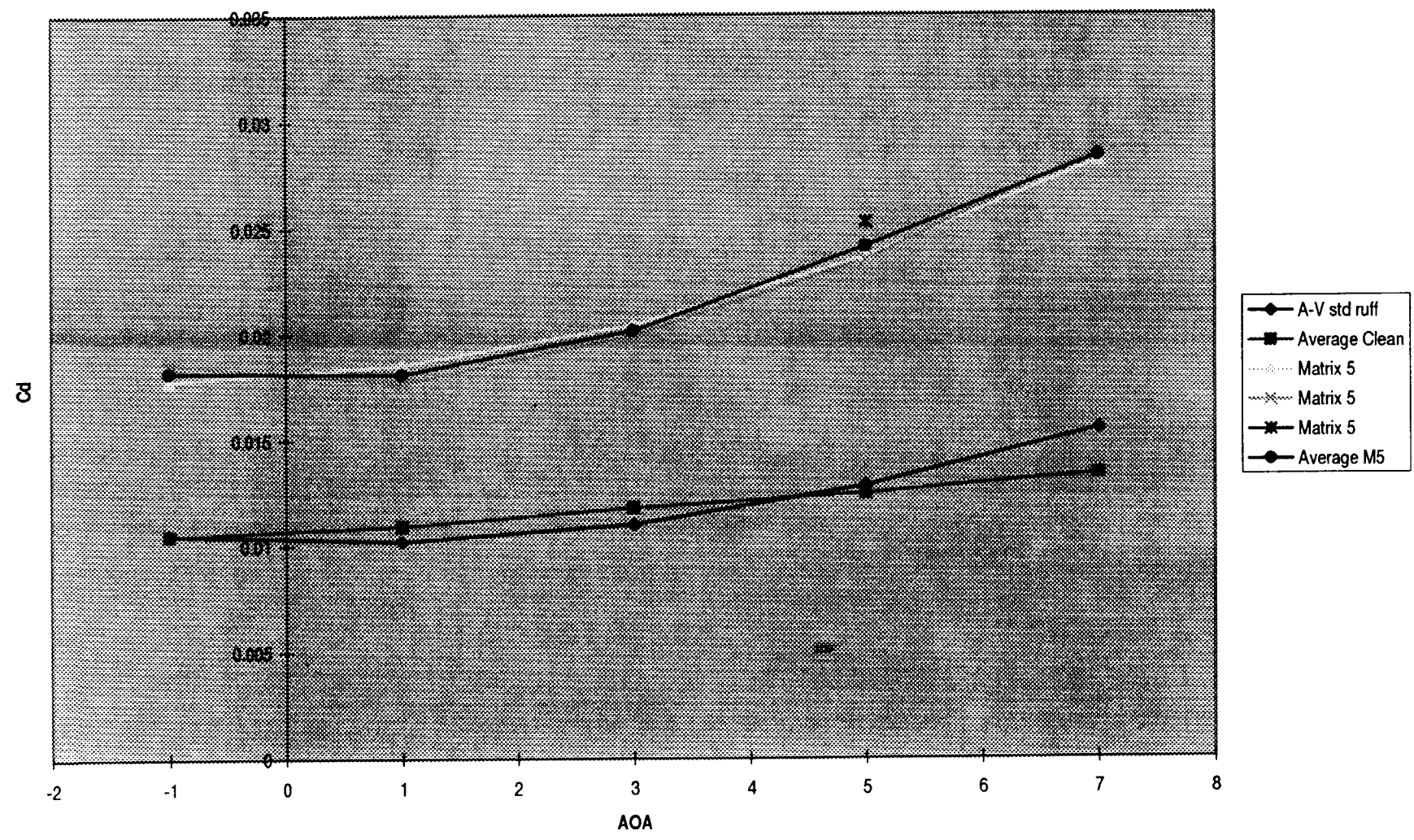


130

V-126

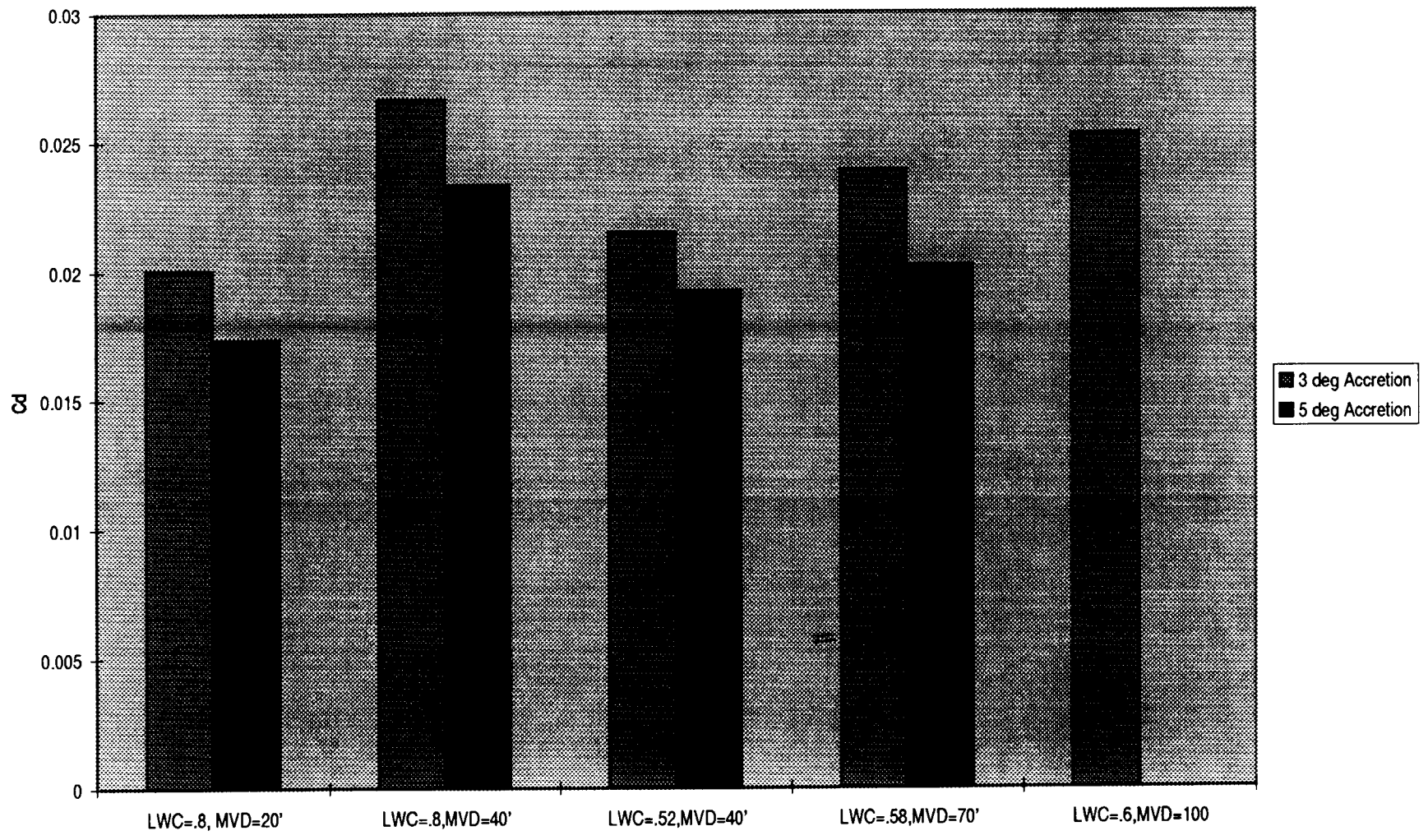
151

Matrix #5: $T_t=30$, $AOA=5$, $LWC=.58$, $MVD=70$, $T=5$



VI-127

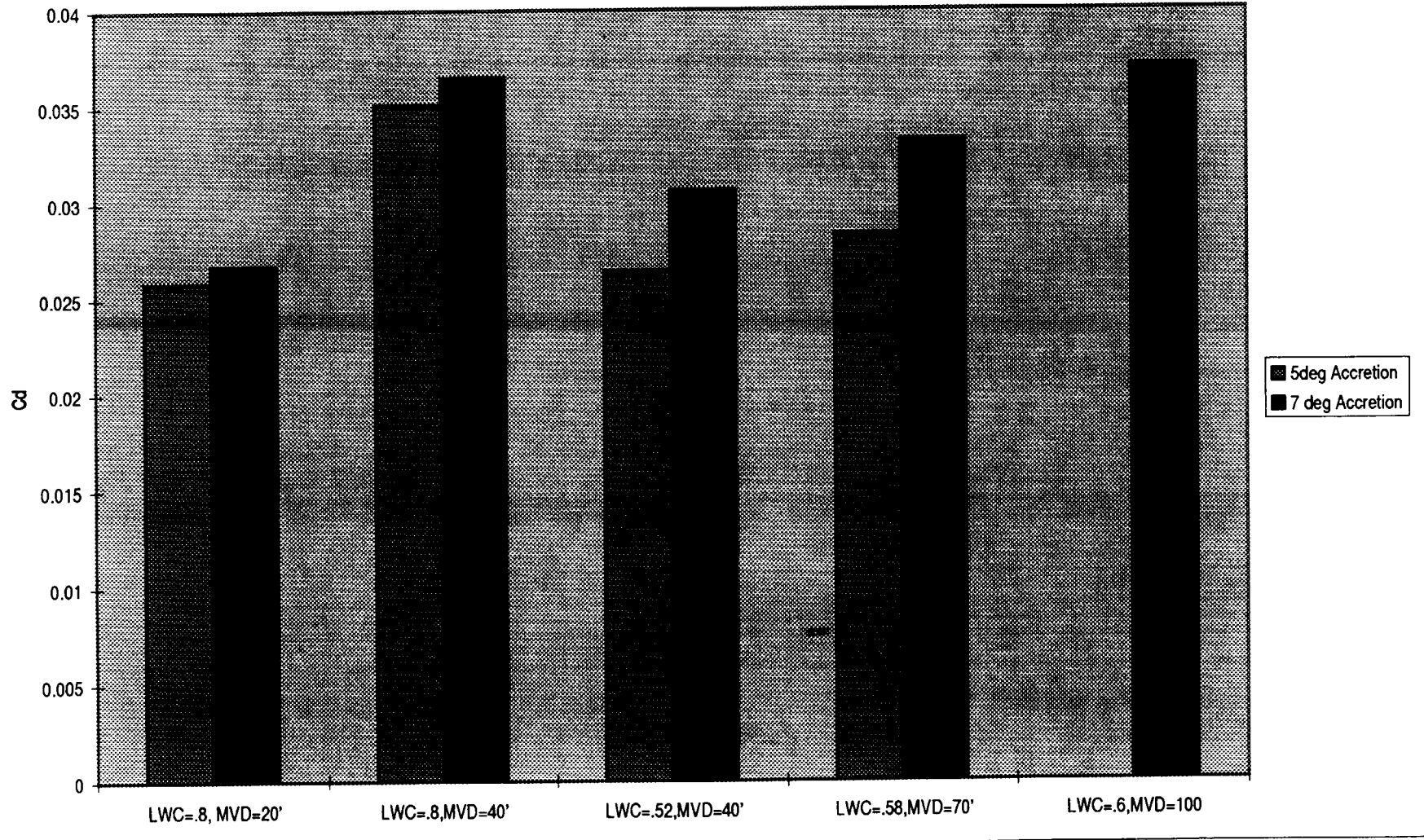
Lower AOA Series
Drag data taken at 3 degrees AOA



102

VI-1728

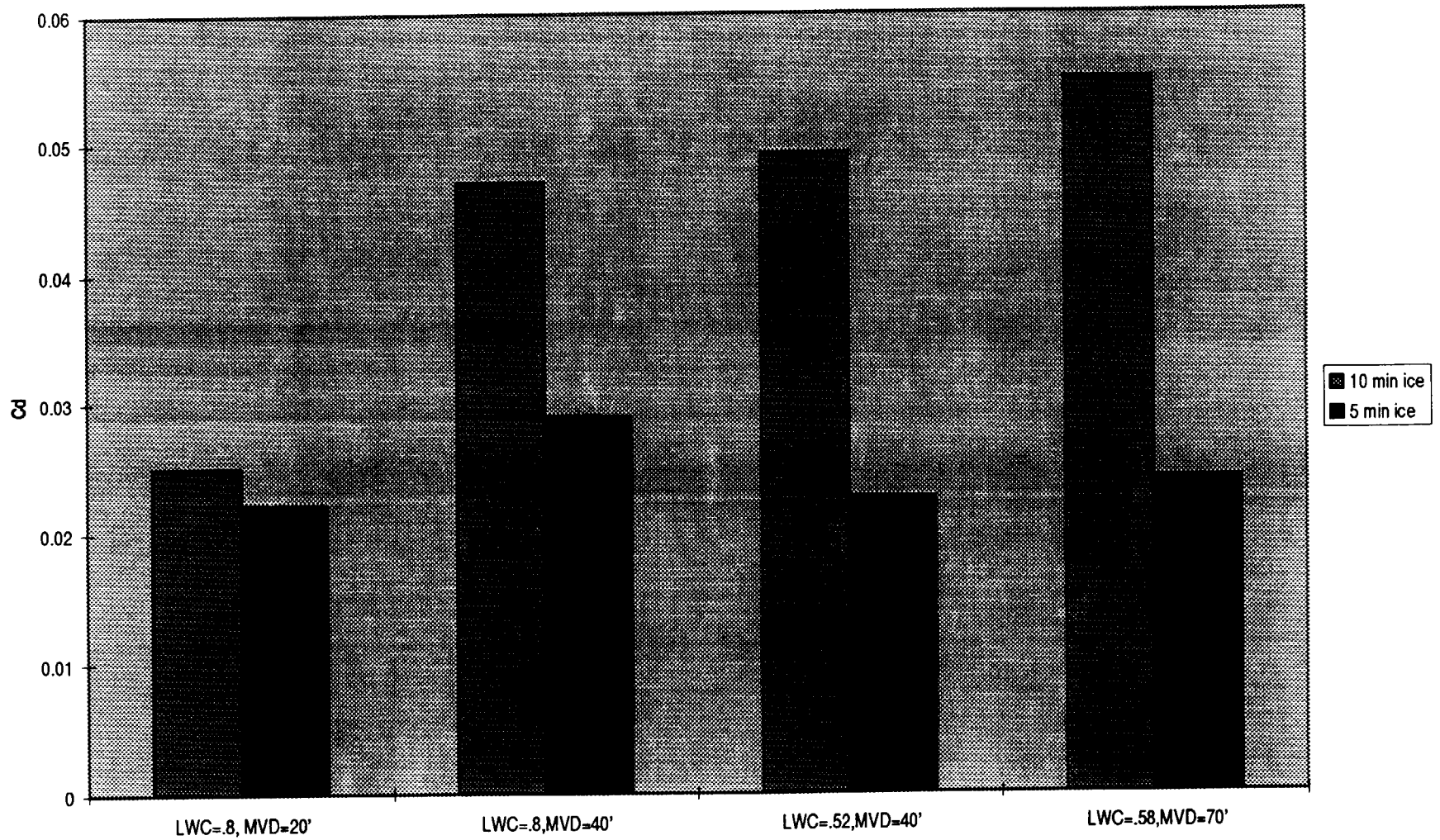
Higher AOA Series
Drag data taken at 7 degrees AOA



1538

VI-129

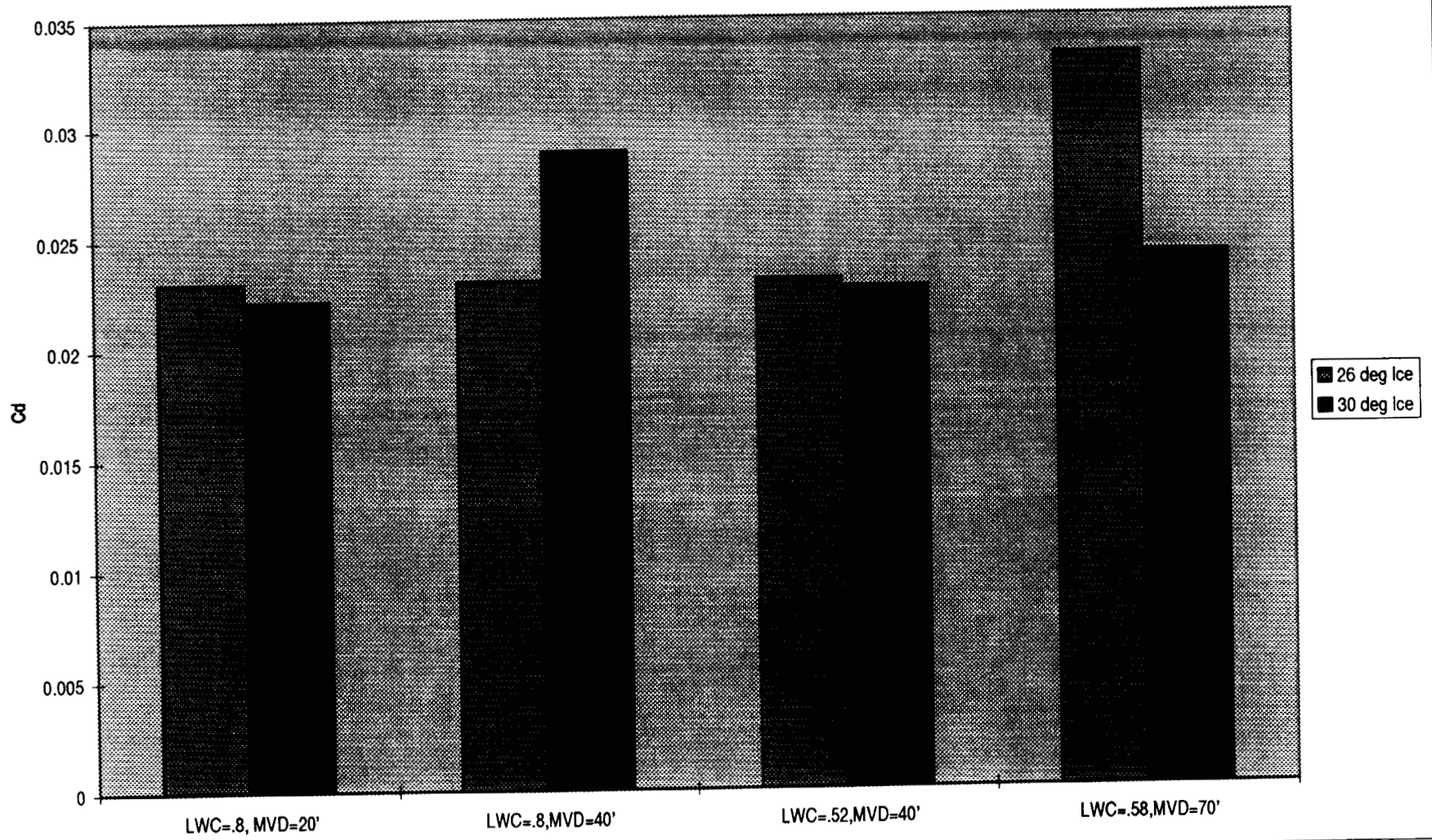
Longer Time Series
Drag taken at 5 degrees AOA



104

VI-13

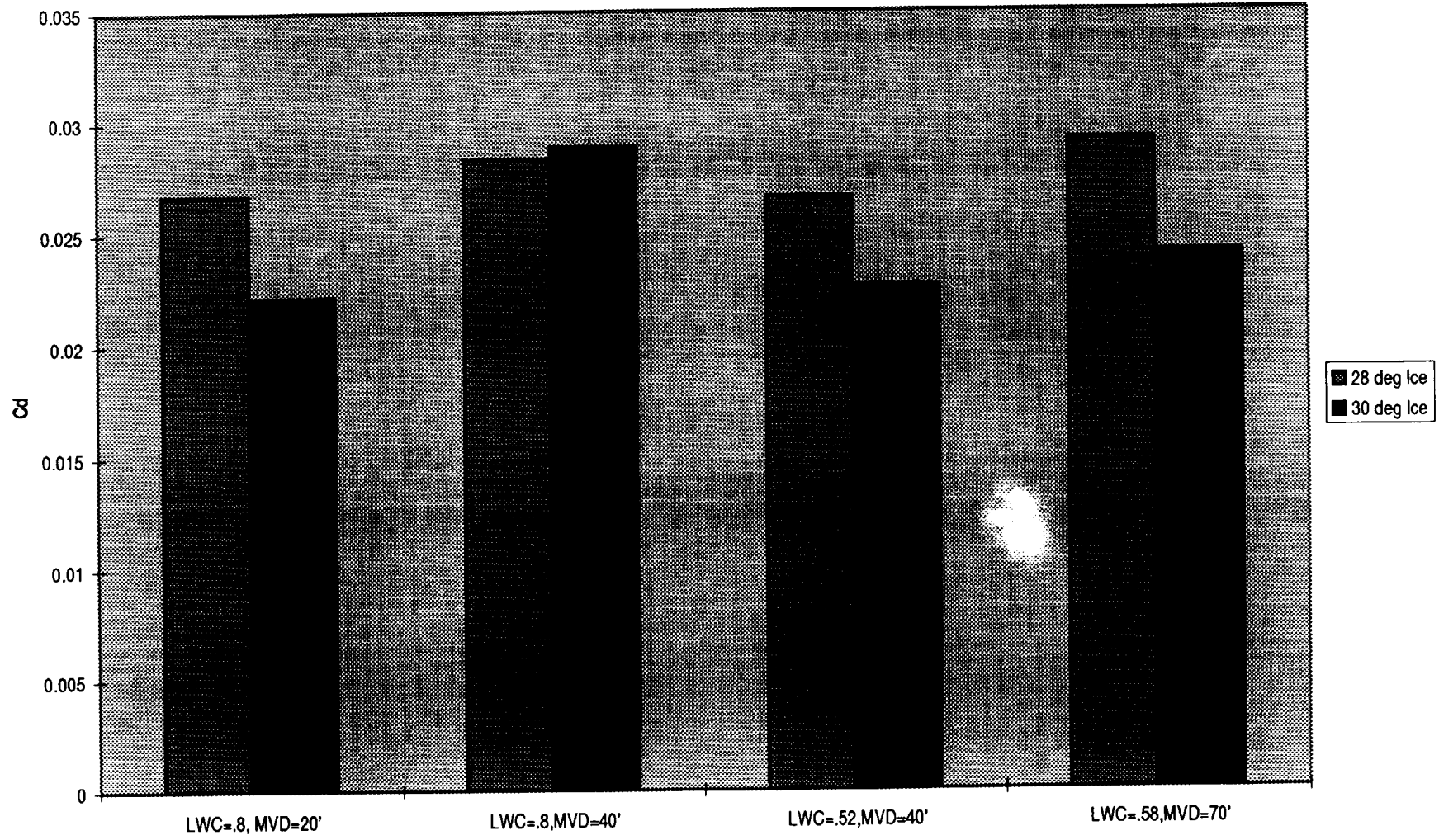
Lower Temp Series II (26F)
Drag taken at 5 degrees AOA



1205

VI-131

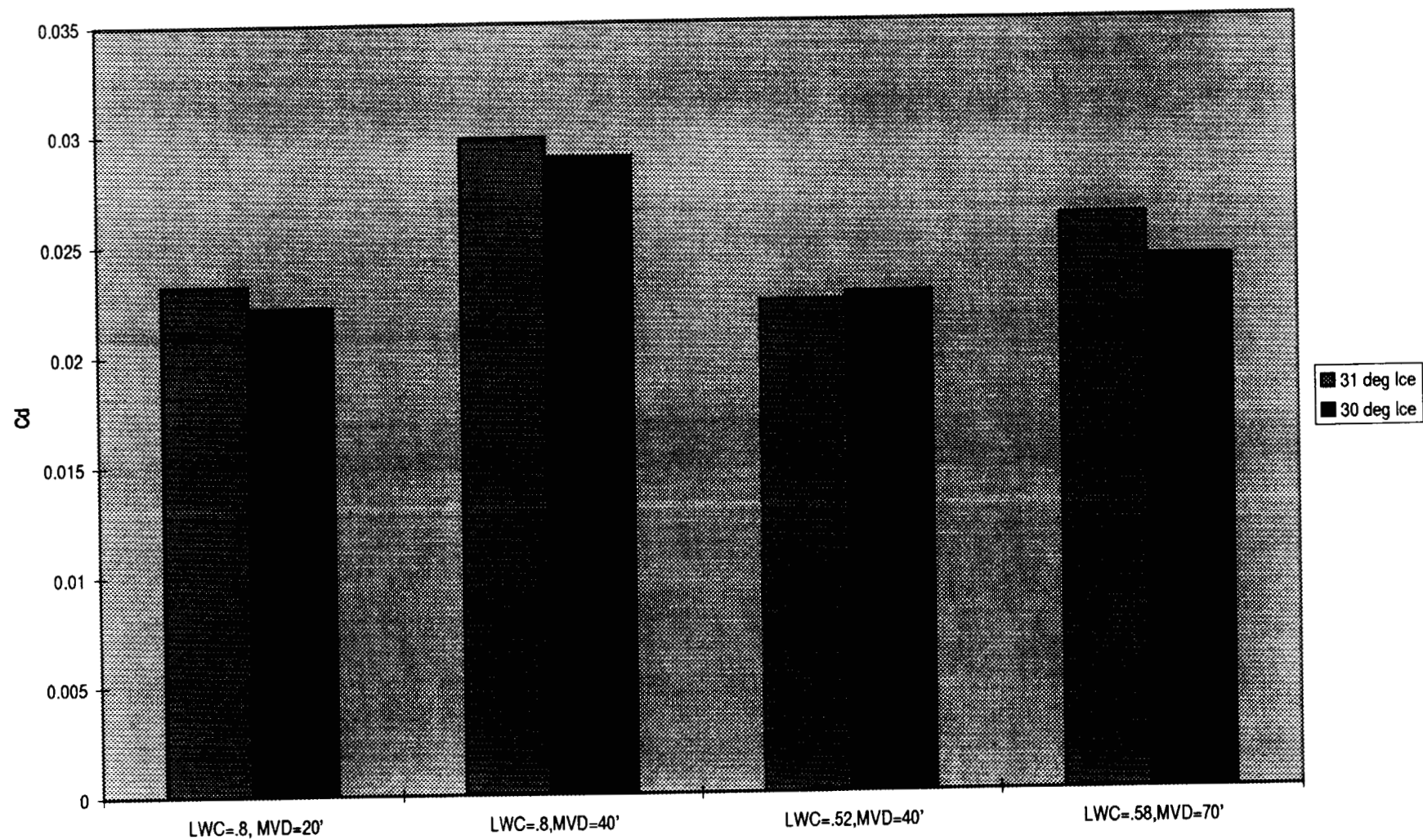
Lower Temp Series
Drag taken at 5 degrees AOA



1.00

VI-132

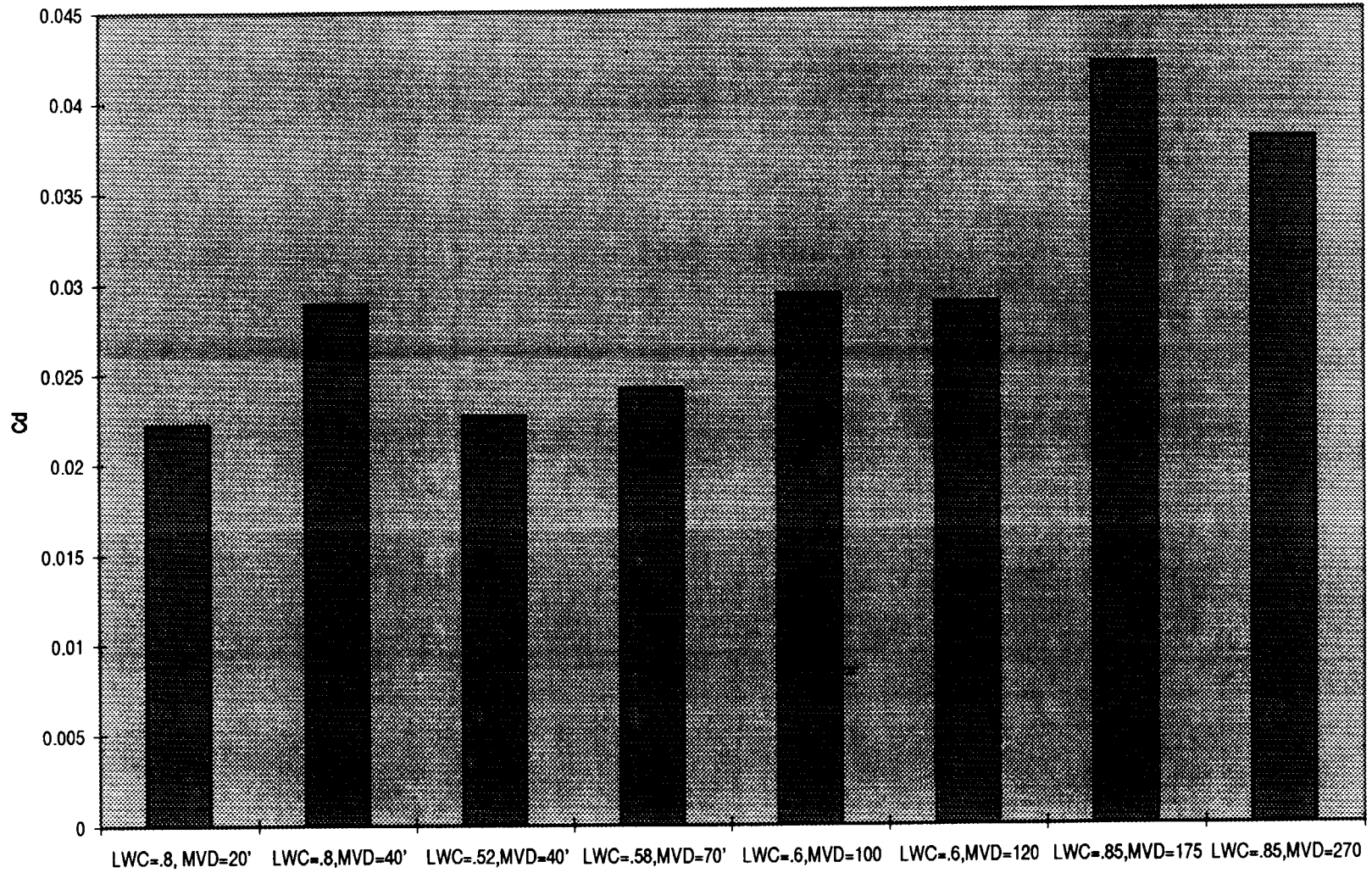
Higher Temp Series
Drag taken at 5 degrees AOA



101

VI-133

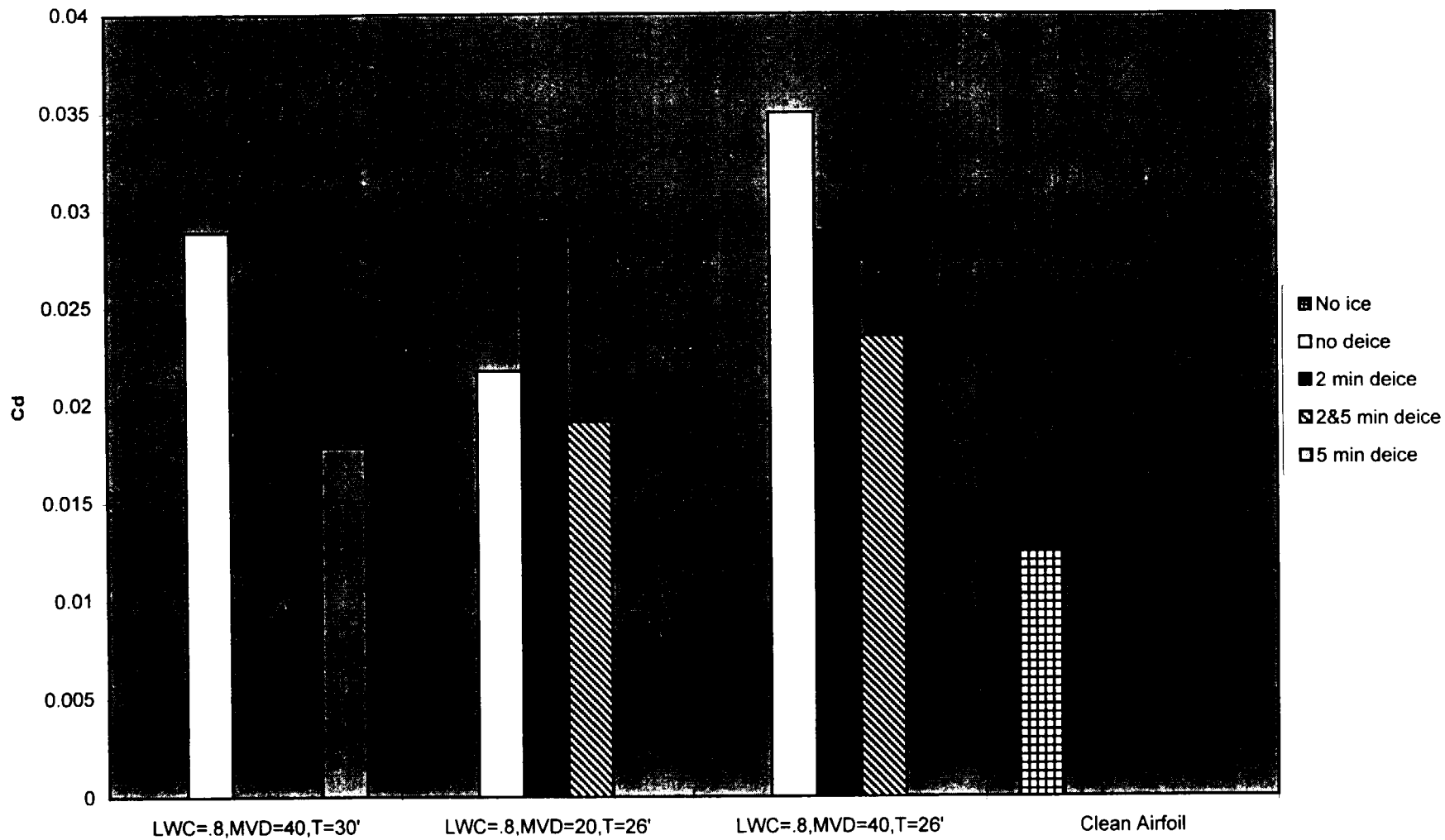
SLD Series



0.030

N1-134

Deice Series
Drag data taken at 5 degrees AOA



205

V1-135

ATTACHMENTS Section VII

Embraer Training Simulator Data

EMBRAER	FAC-SIMILE		REF N° : EAD-019/98
	011-55-12-345-1723		DATE: 24 APR 98
Company: NTSB - Washington, DC		Address: USA	Fax: 001 (202) 314-6597
To : Dan Bower		Dept.: RE-60	Page: 01 of 05
From: Decio Pullin		Dept.: GEA/EAD	Phone : ([REDACTED])
Subject: COMAIR 3272 accident: Simulator results for aileron A/P servo max torque adjusted to 110 and 120 in-lbs			

Dear Dan:

Please find enclosed the plotted results for the simulator runs we have performed simulating the aileron servo torque capability obtained from aircraft measurements.

An EMB-120 airplane was used to measure on ground the aileron servo torque capability by applying different weights to the aileron trailing edge in order to simulate an aileron hinge moment.

The autopilot was engaged in heading mode and a heading change was commanded. The aileron servo responded to the heading change and started to move the ailerons in a deflection rate that was measured using an angular scale and a chronograph. The test was repeated using different weight values to obtain a variation of the aileron hinge moment. The servo torque was calculated using the value of this hinge moment and the normal gear ratio between the aileron deflection and servo angular displacement.

When the calculated servo torque reached the value of 111 in-lbs, the aileron commanded rate, that was constant and in the order of 5.6 degrees per second (only left aileron deflection), came suddenly to zero (see attached graph 01). This behavior was expected because the autopilot box has a built in limitation to the electric current that is sent to the servo. This current is adjusted to a value that corresponds to 150 in-lbs of servo torque. The obtained difference of 39 in-lbs (150 - 111) is probably due to the control cables, pulleys and rods friction. A previous measurement showed a value of around +/- 10 lbs of friction force at the control wheel (see graph 04). The relationship between the control wheel force and aileron servo torque is given by:

$$\text{Wheel force (lbs)} = 0.288 * \text{Servo Torque (in-lbs)}$$

The above equation will give us an aileron servo torque of around 35 in-lbs equivalent to the measured control wheel friction force. This value is close to the obtained difference of 39 in-lbs.

Taking this information into consideration, the simulator aileron servo torque model was modified to represent the curve of Graph 01. Three simulator runs were performed: one with the max torque set at 110 in-lbs, a second one with this torque set to 120 in-lbs and a third one with a torque of 130 in-lbs. The results showed that it was possible to reproduce the DFDR closely with the torque set to 110 and 120 in-lbs. The only difference is that the aileron movement was not smooth as shown in the DFDR, mostly because in the servo simulation model there is no damping effects as expected in the real environment. With the torque set to 130 in-lbs, the upset was not reproduced and the airplane was able to fly off the event (complete the turn and level off).

The results from the simulator runs of control wheel deflection and bank angle as a function of time are presented in Graphs 02 and 03 together with the DFDR and previous simulator run 2.04 (see report 120-AC-023).

These results are an indication that the aileron servo behavior during the event was normal and the observed autopilot response is as expected.

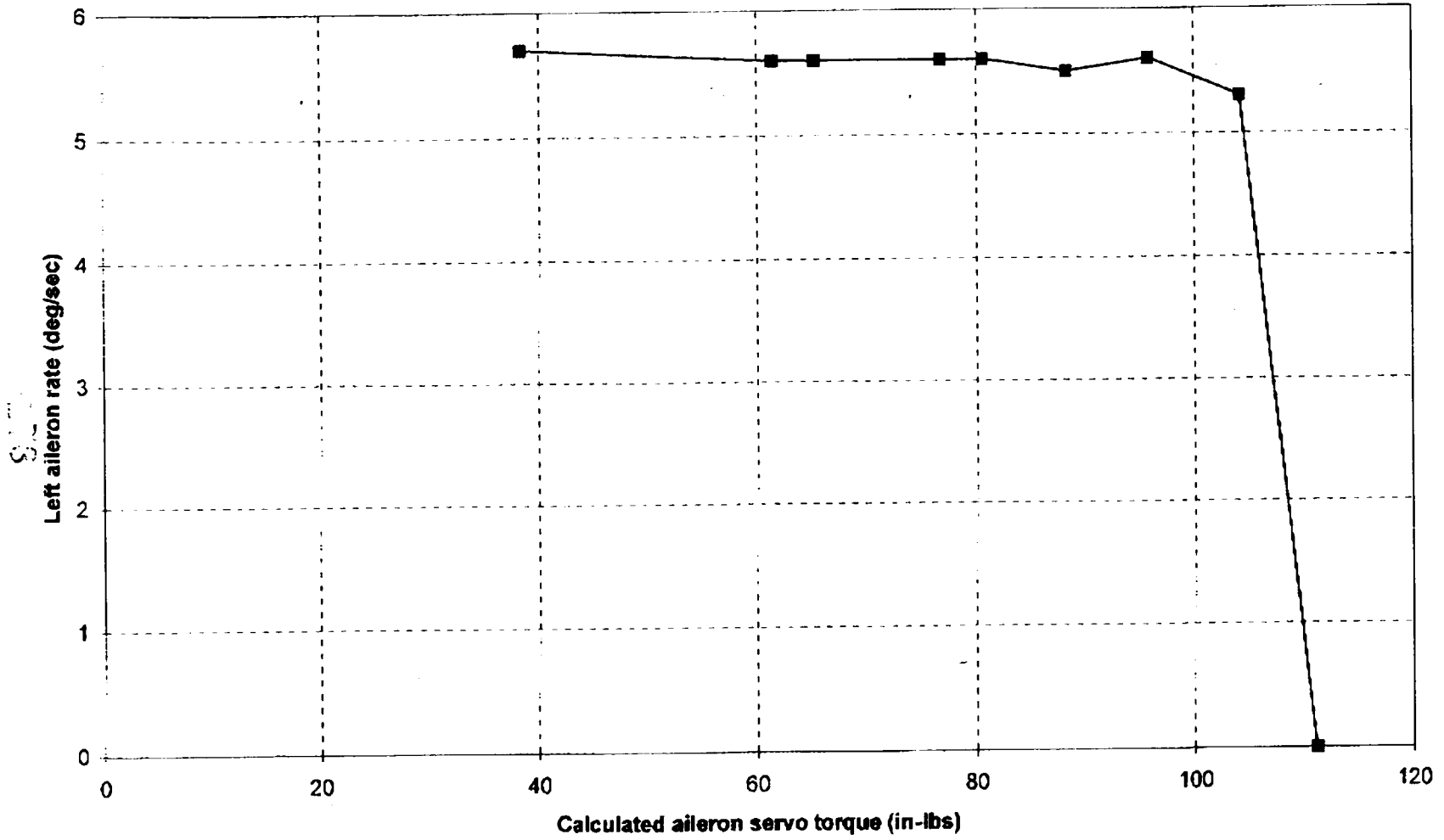
If you have any questions, please call me.

Regards



Decio Pullin

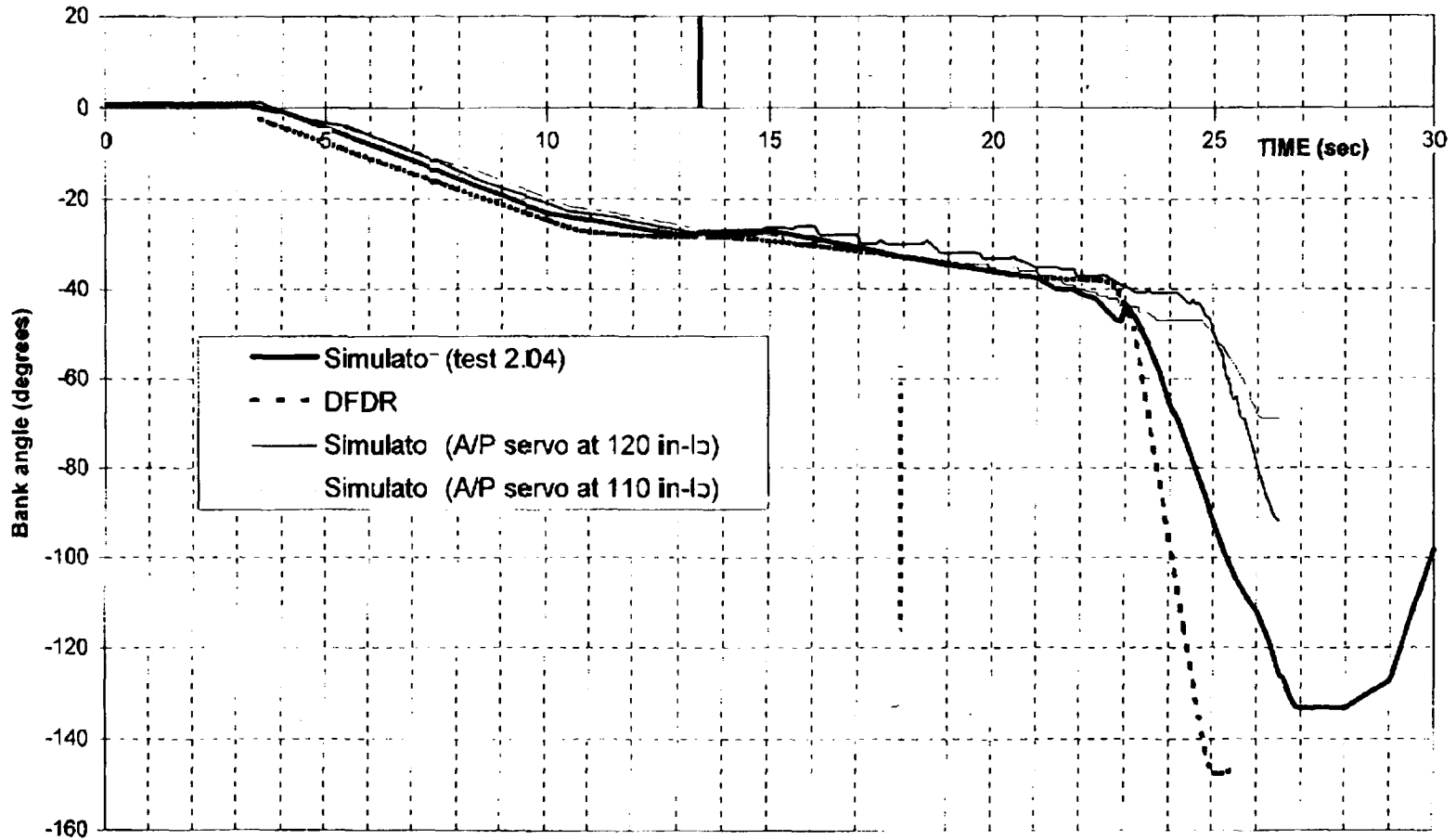
EMB-120 Measured aileron servo capability



GRAPH 01

11-3

COMAIR 3272 ACCIDENT - SIMULATOR ANALYSIS BANK ANGLE COMPARISON

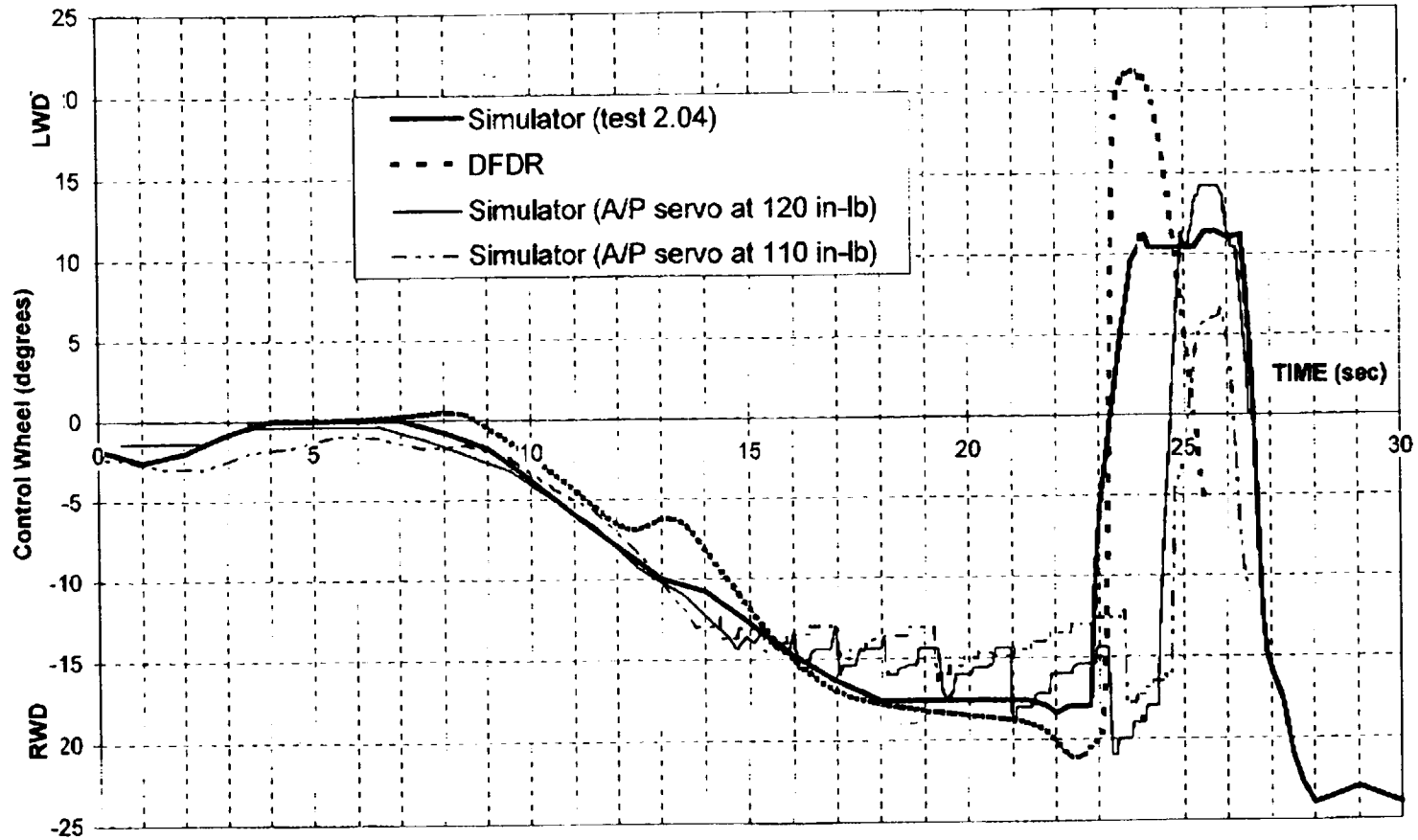


GRAPH 02

11-4

2/4

COMAIR 3272 ACCIDENT - SIMULATOR ANALYSIS CONTROL WHEEL POSITION COMPARISON

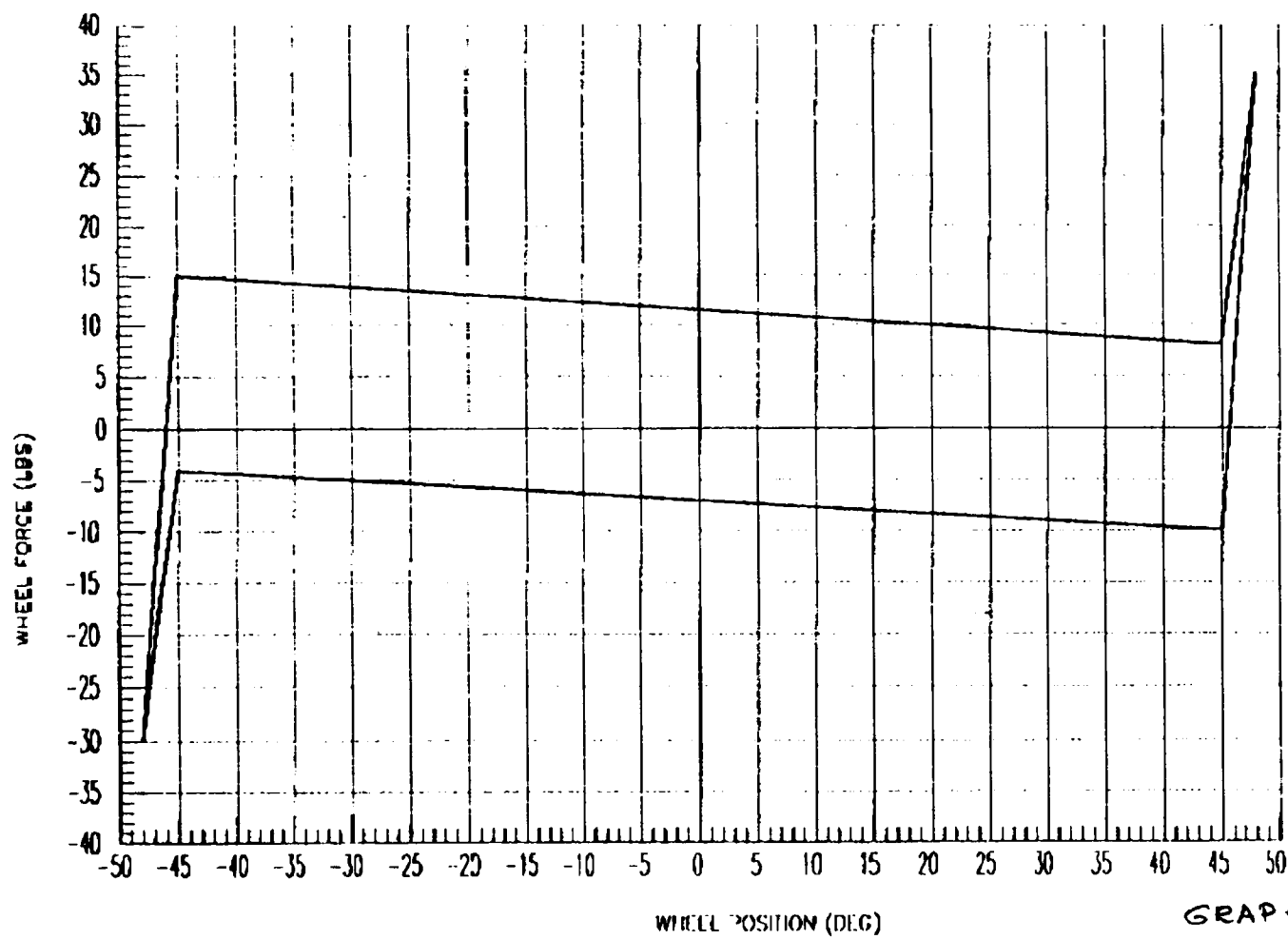


5-15

MI-5

GRAPH 03

EMB-120 BRASILIA SIMULATOR DATA - FIG. 3.3
WHEEL FORCE VS. WHEEL POSITION



GRAPH 04

FEITO POR :
APROVADO :

6/6

14

11-6

ATTACHMENTS Section VIII

2-D Computational Results

Review of NASA Lewis Support of EMB-120, Monroe, Michigan Accident Investigation

**presented by
Andrew Reehorst
and
Dr. Joongkee Chung**

**at
National Transportation Safety Board
April 22, 1998**

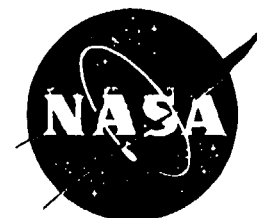


Outline

- **Review of effort**
- **Review of Icing Research Tunnel test**
- **Review of Computational Analysis**
- **Discussion**

1-25

VII-2



Review of Effort

- Kickoff meeting at NASA LeRC on September 10, 1997
- Letter exchange complete December 4, 1997
- IRT test January 20-30, 1998
- IRT test results shipped to NTSB on February 12, 1998
- Initial Computational Analysis complete March 2, 1998
- 3-D Analysis to confirm 2-D results expected by May 29, 1998

00

M1-3



Review of IRT test

- **Conditions replicated the best-thought of the flight conditions leading to the accident**
- **Data acquired included**
 - Video tape footage
 - Photographs
 - Digital photographs
 - Ice shape tracings
 - Wake drag measurements

11-04

M-4

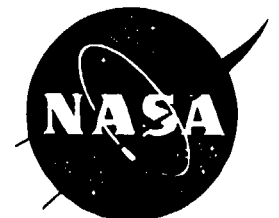


Test Conditions

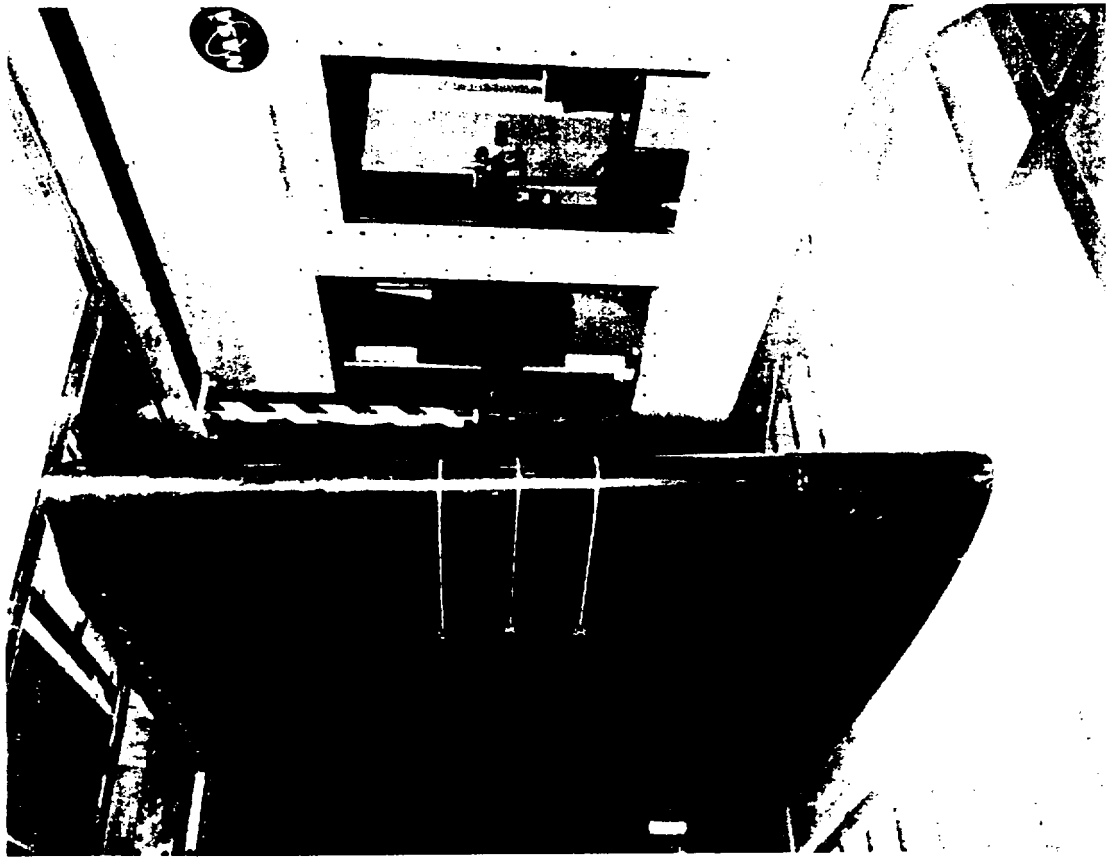
- All runs at 172 knots
- **Baseline Series**
 - Based upon FDR and meteorological analysis
 - All at 30° F, 5° AOA, and 5 min.
 - LWC=0.8, MVD=20
 - LWC=0.8, MVD=40
 - LWC=0.52, MVD=40
 - LWC=0.58, MVD=70
- Higher and Lower AOA series (7° and 3°)
- Higher and Lower Temp. Series(31°F, 28°F, & 26°F)
- Longer Time Series (10 minutes)
- **SLD Series**
 - LWC=0.6, MVD=100
 - LWC=0.6, MVD=120
 - LWC=0.85, MVD=175
 - LWC=0.85, MVD=270

202

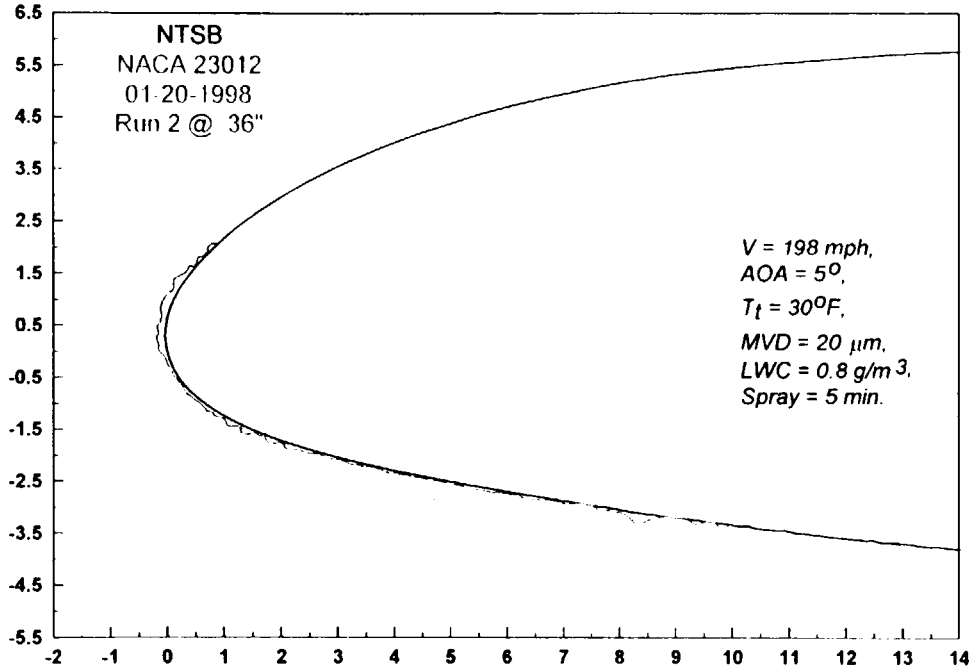
VII-5



IRT Installation

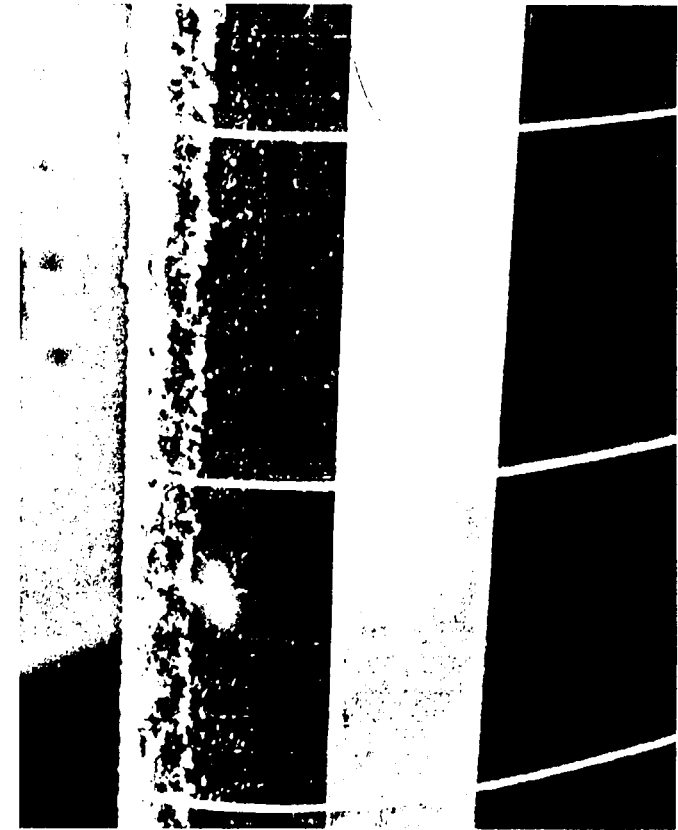


Resultant Ice Shapes

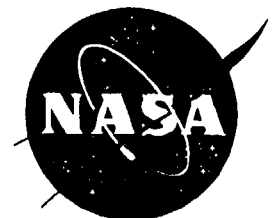


404

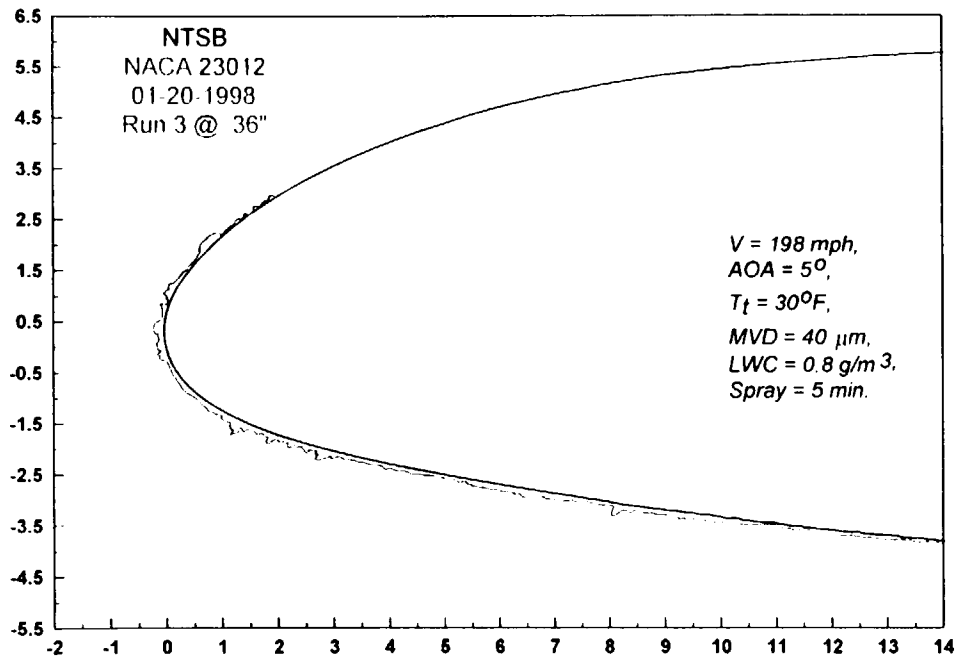
Matrix # 2



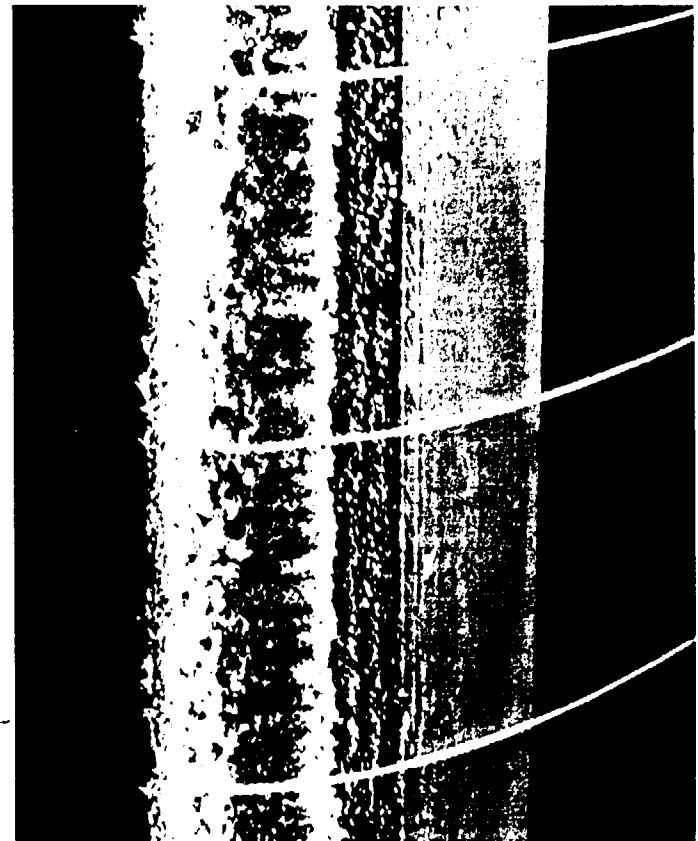
VI-7



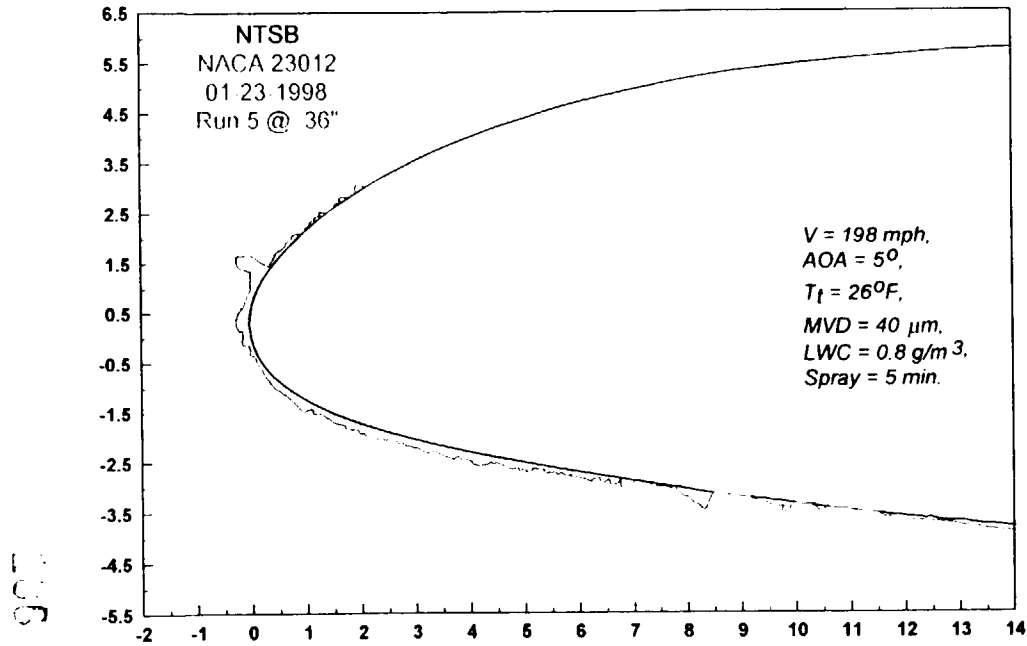
Resultant Ice Shapes



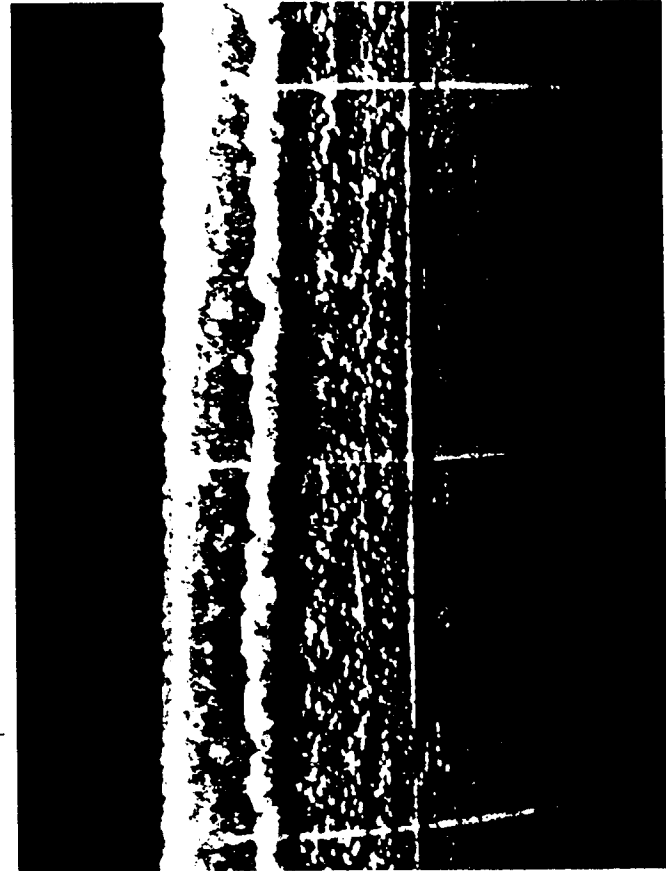
Matrix # 3



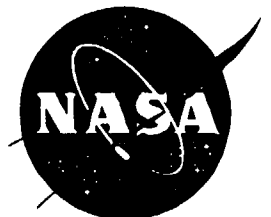
Resultant Ice Shapes



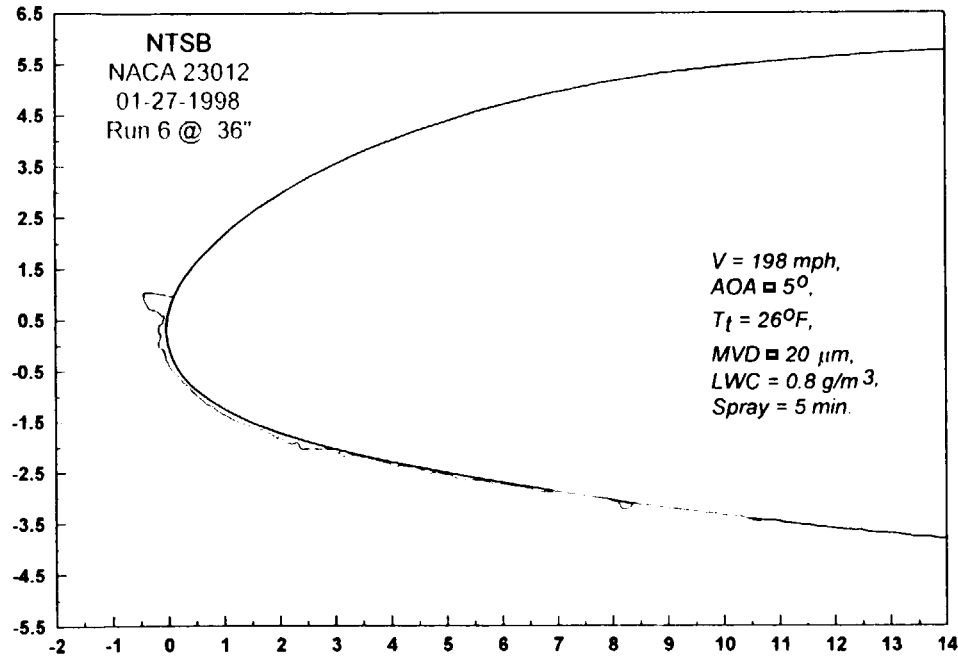
Matrix # 27, Mold Case



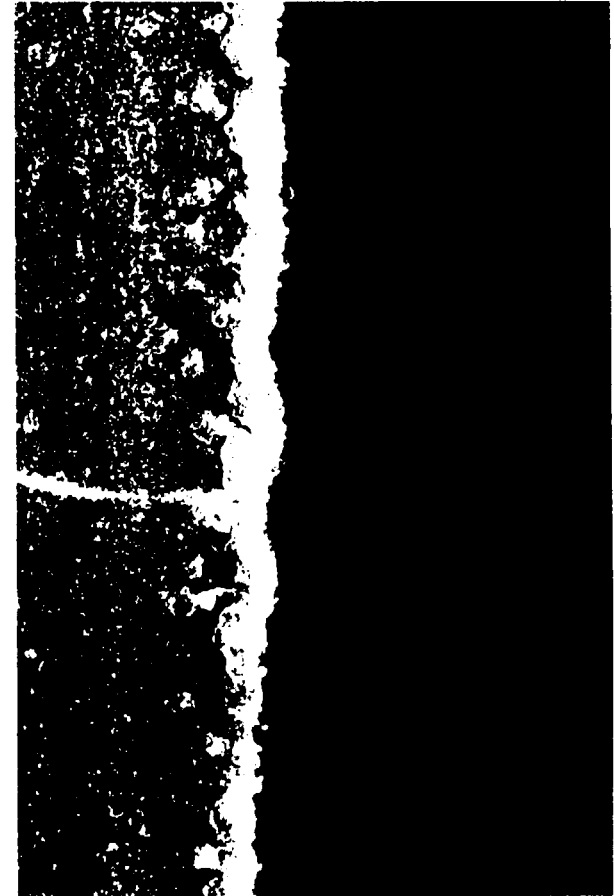
VI-9



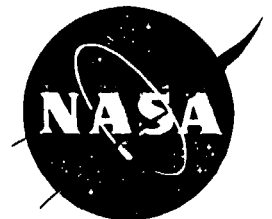
Resultant Ice Shapes



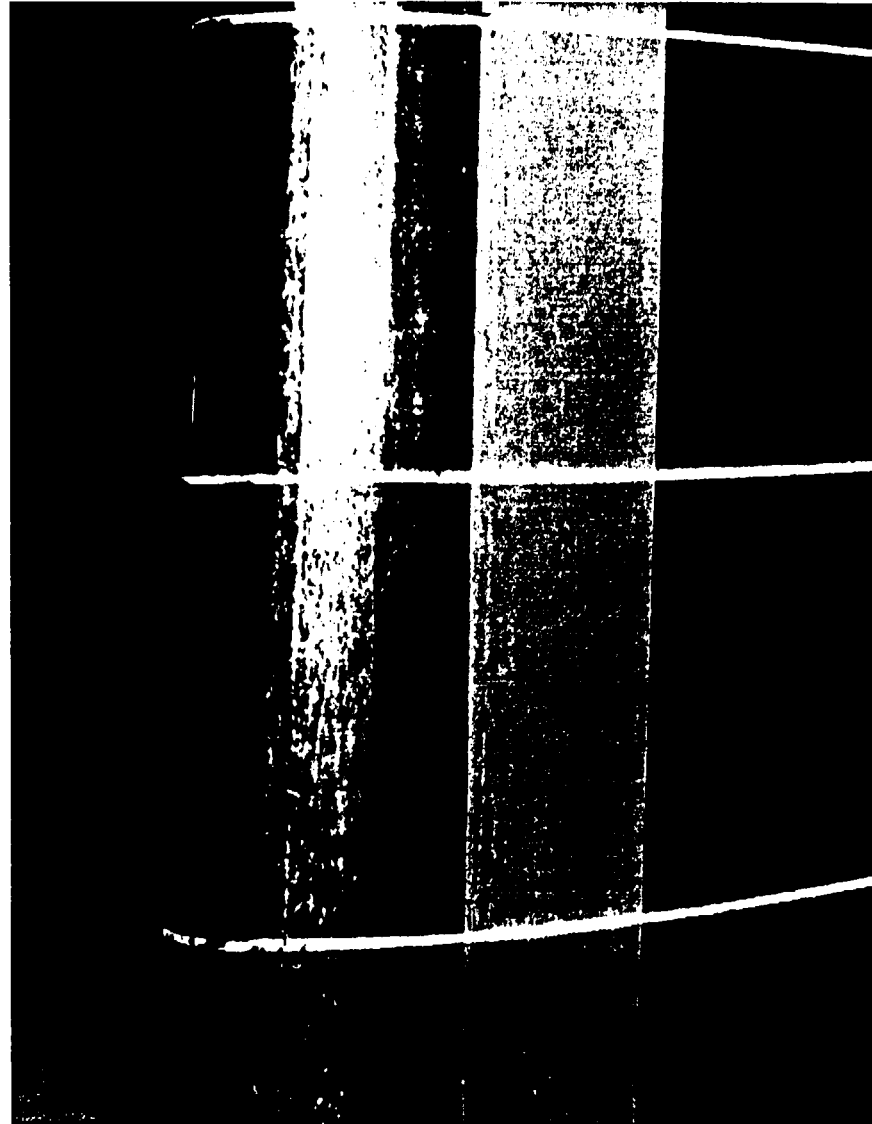
Matrix # 26



MI-10



Resultant Ice Shapes



Matrix #26 with
Boot Activation
at 2 and 5 min.

90°

VII-11

Lewis Research Center
Icing Branch



Discussion- Stitchline Effects



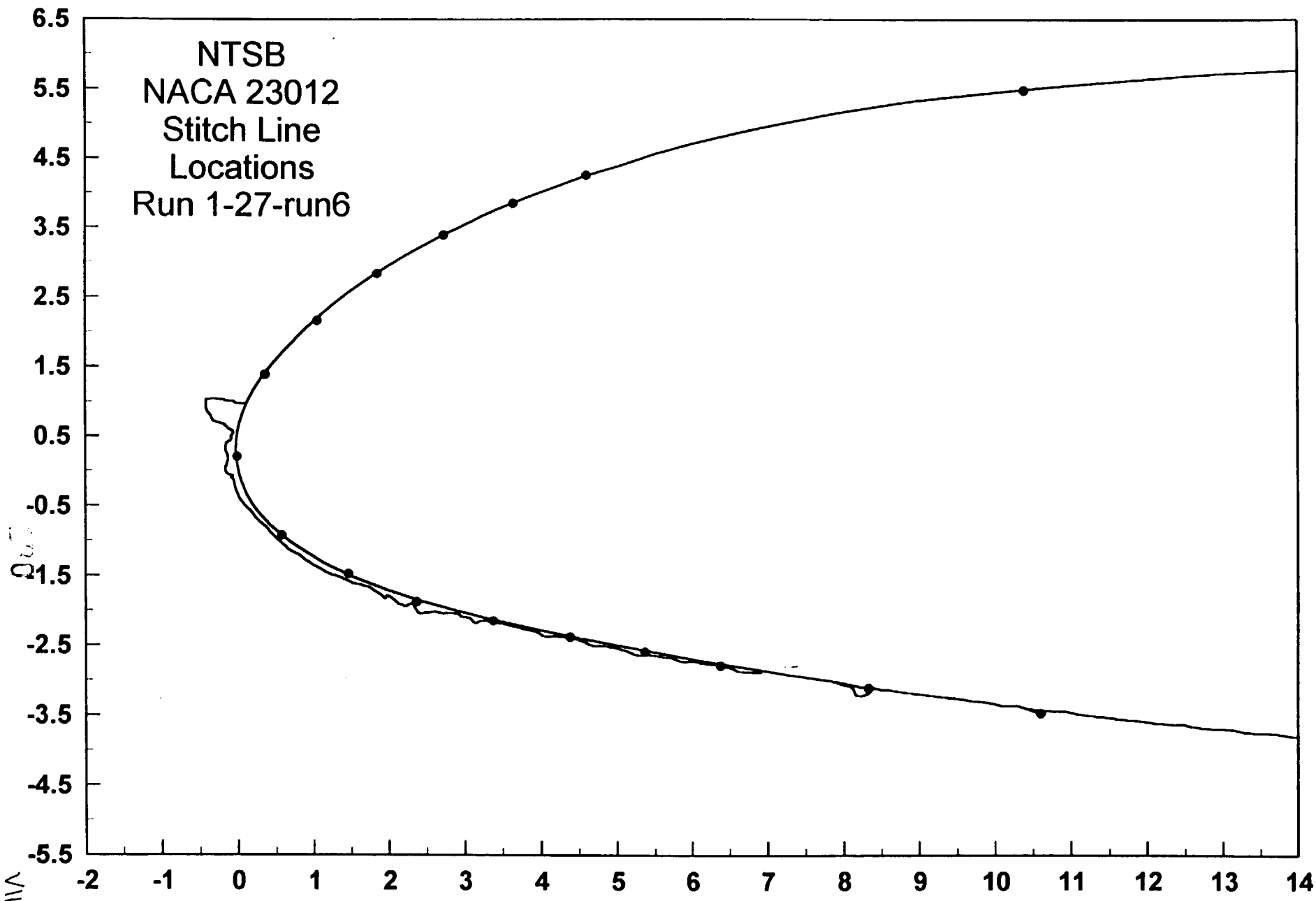
108

VI-12

Lewis Research Center
Icing Branch

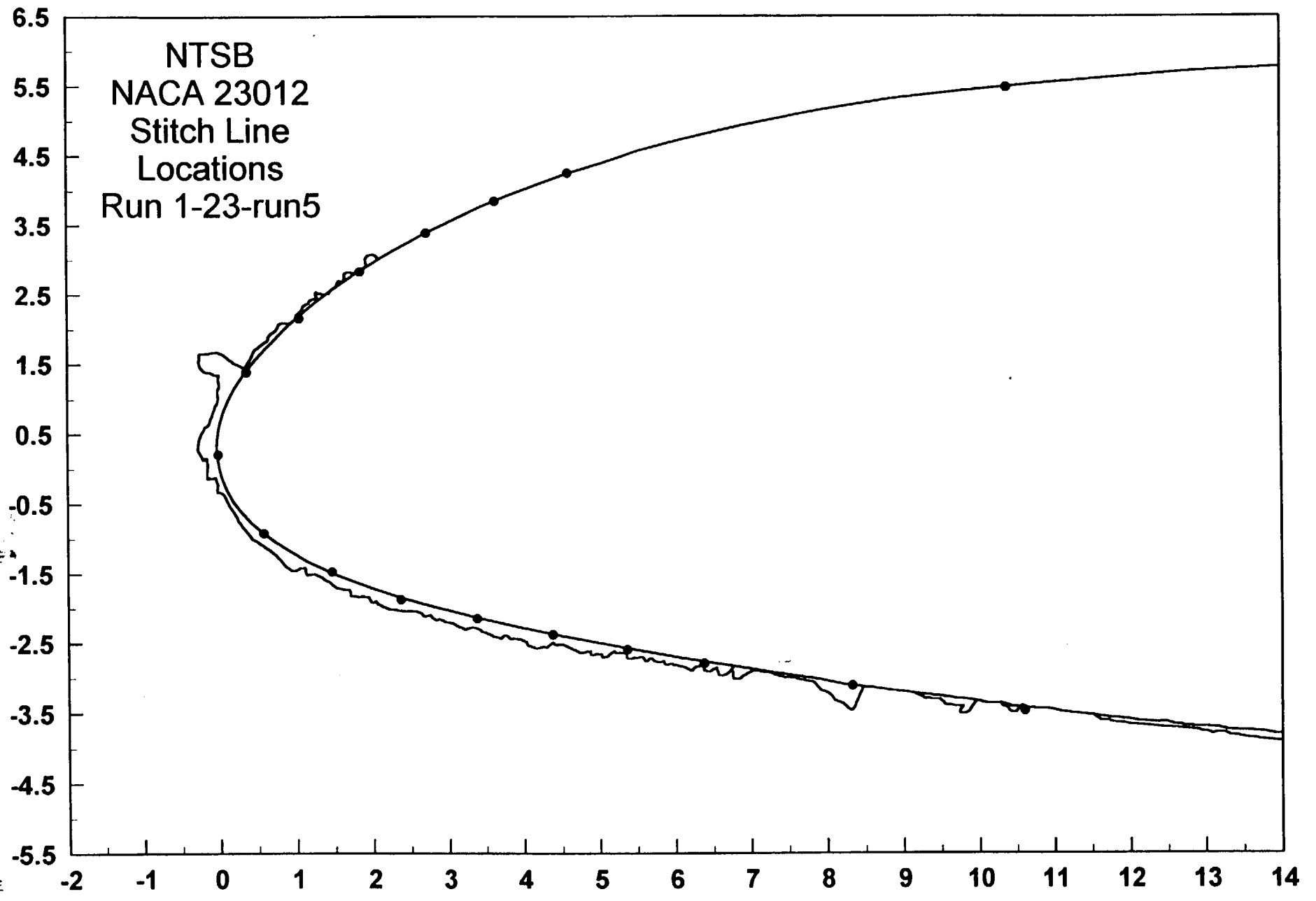


NTSB
NACA 23012
Stitch Line
Locations
Run 1-27-run6



VI-13

NTSB
NACA 23012
Stitch Line
Locations
Run 1-23-run5



7-1-14



Outline of Computational Analysis

- Selection of Ice Shapes for Computation
- Smoothing of Ice Shapes
- Effect of Smoothing and Grid Refinement on Aerodynamics
- Results and Discussions

202

VI-15



Ice Shape Selection for the Computation

- Three ice shapes were chosen to investigate the differences in aerodynamic performance due to the shape
- These shapes have elements such as ridge, sharp corners, small and large bumps and other rough surfaces.
- Ice from Test Matrix # 2 -- many small bumps
- Ice from Test Matrix # 3 -- similar to # 2 ice but bumps are sharper and larger
- Ice from Test Matrix # 26 -- One ridge and small bumps on the suction side



Ice Shape Smoothing & Grid Generation

- Certain level of smoothing is required to make grid generation possible
- Smoothing by in house developed code "TURBOGRD"

Generate a smooth curve using control points(CPs)

100 % CPs (same # of points as the digitized one), 50%, and 25% used for computations

Proper smoothing level determined considering the aerodynamic performances

- Grids were generated by "GRIDGEN"

External flow field at 15.0 chord length

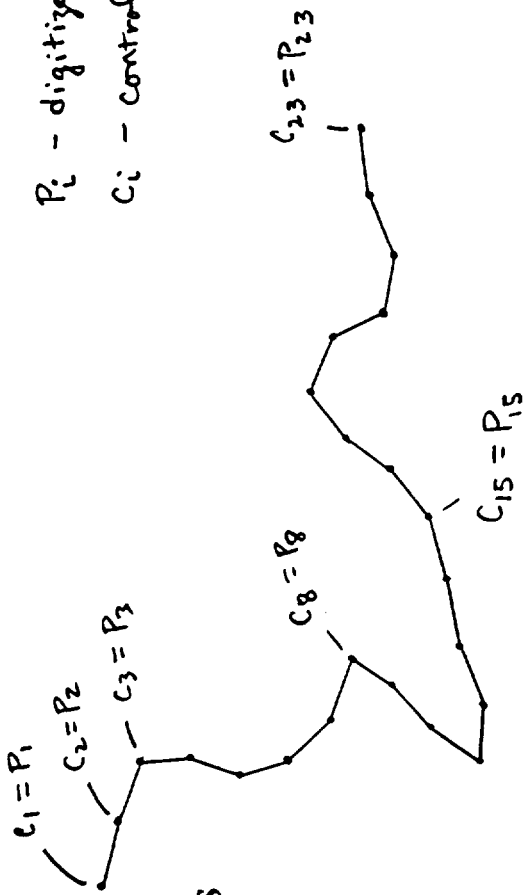
Single block as well as 2-block grids to save CPU time

Grid refinement to ensure the quality of the solutions

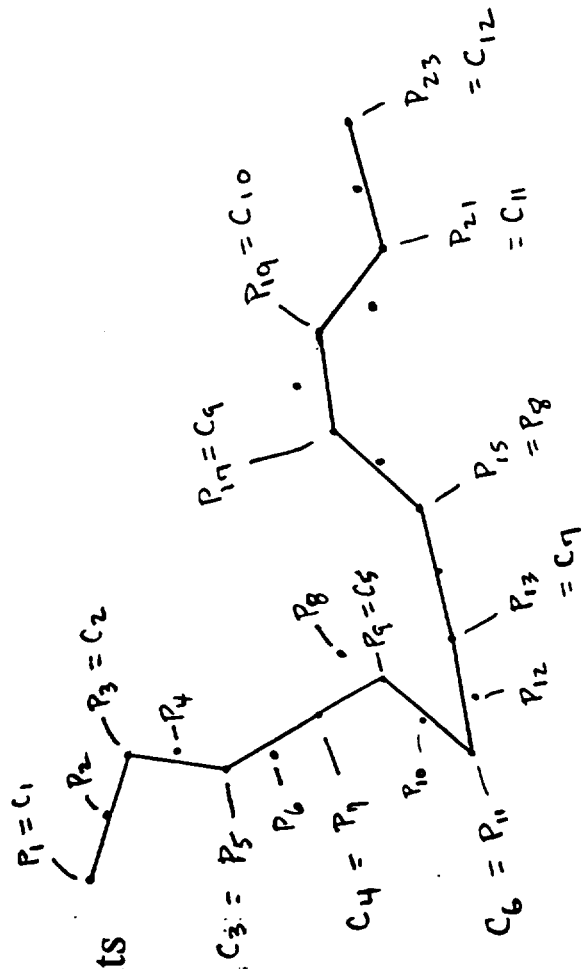
Smoothing Procedure

- Read in the digitized points and separate the iced area
(iced area is usually represented by 250 - 1000 points)
- Place one control point (CP) on each digitized point
- Generate a smooth curve using the control points
(Very close to the digitized shape)
- Distribute the points uniformly on this smooth curve using tension spline
---> This will be the smoothed curve with 100% of CPs..
- Based on the above curve (100% CPs), reduce the # of control points
as desired such as 50% CP , 25% CP level and etc.

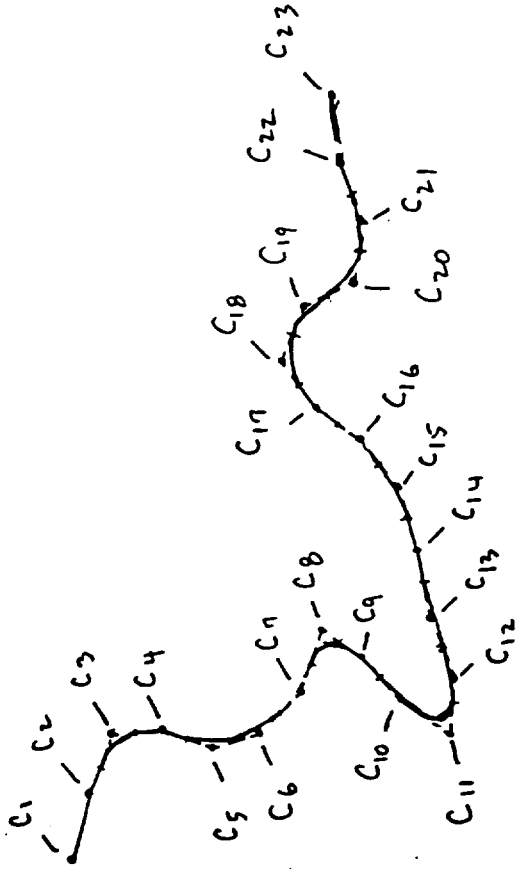
P_i - digitized point
 C_i - control point



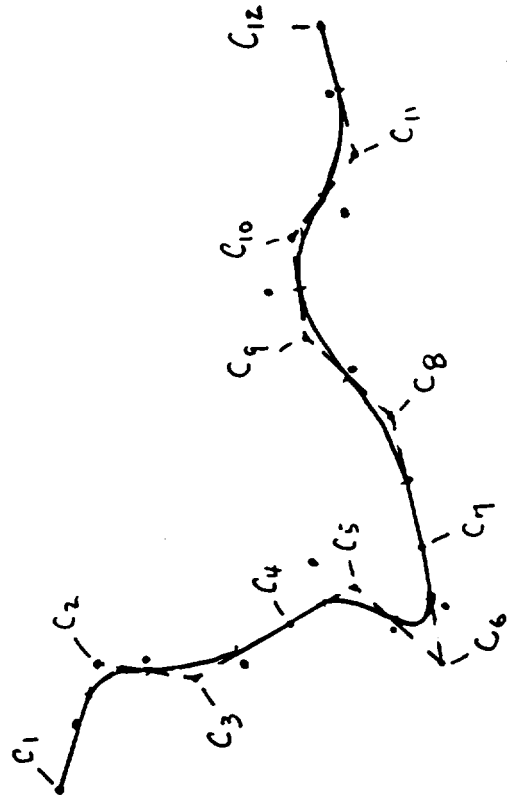
100 % Control Points



50 % Control Points

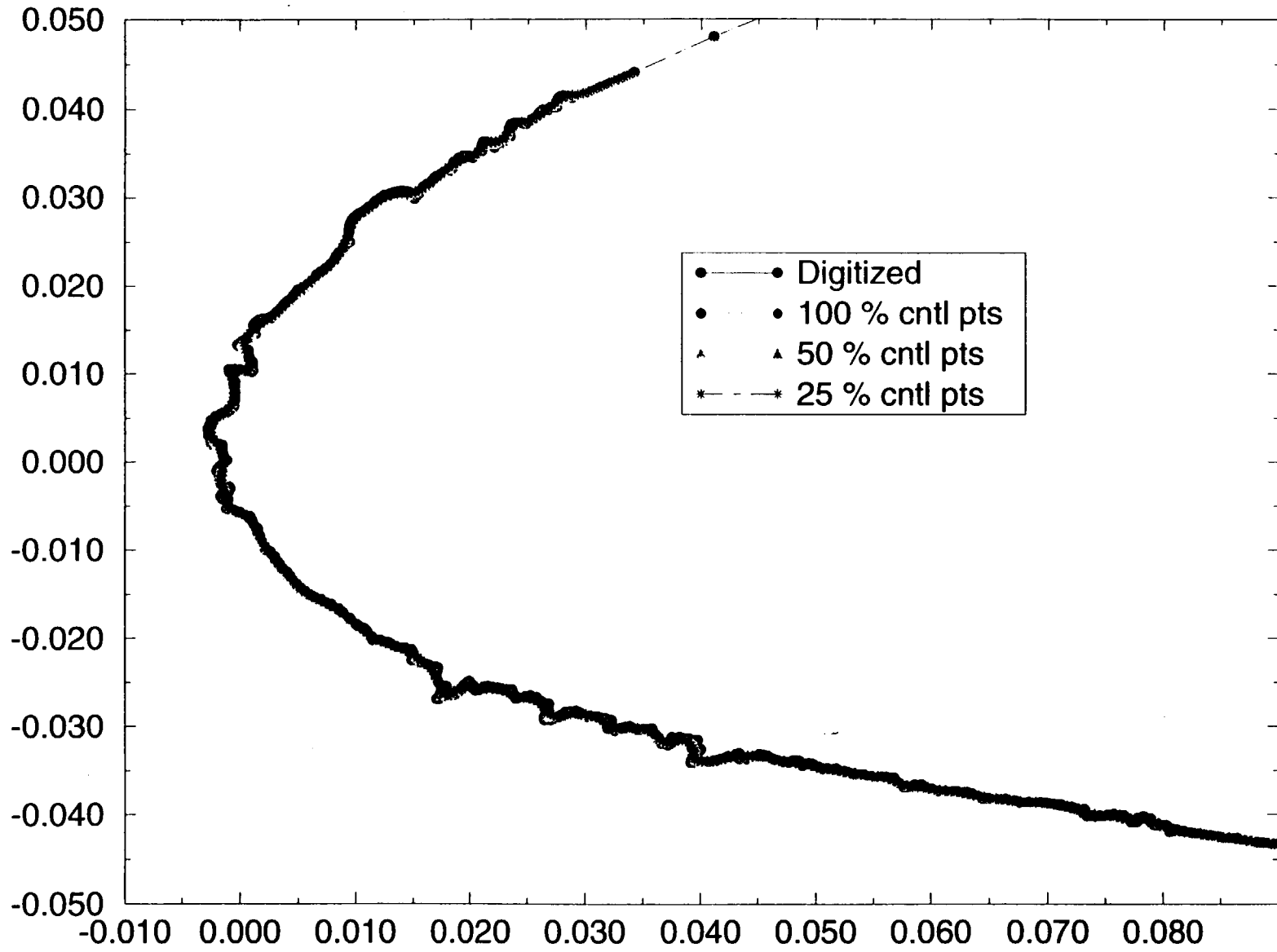


100 % Control Points

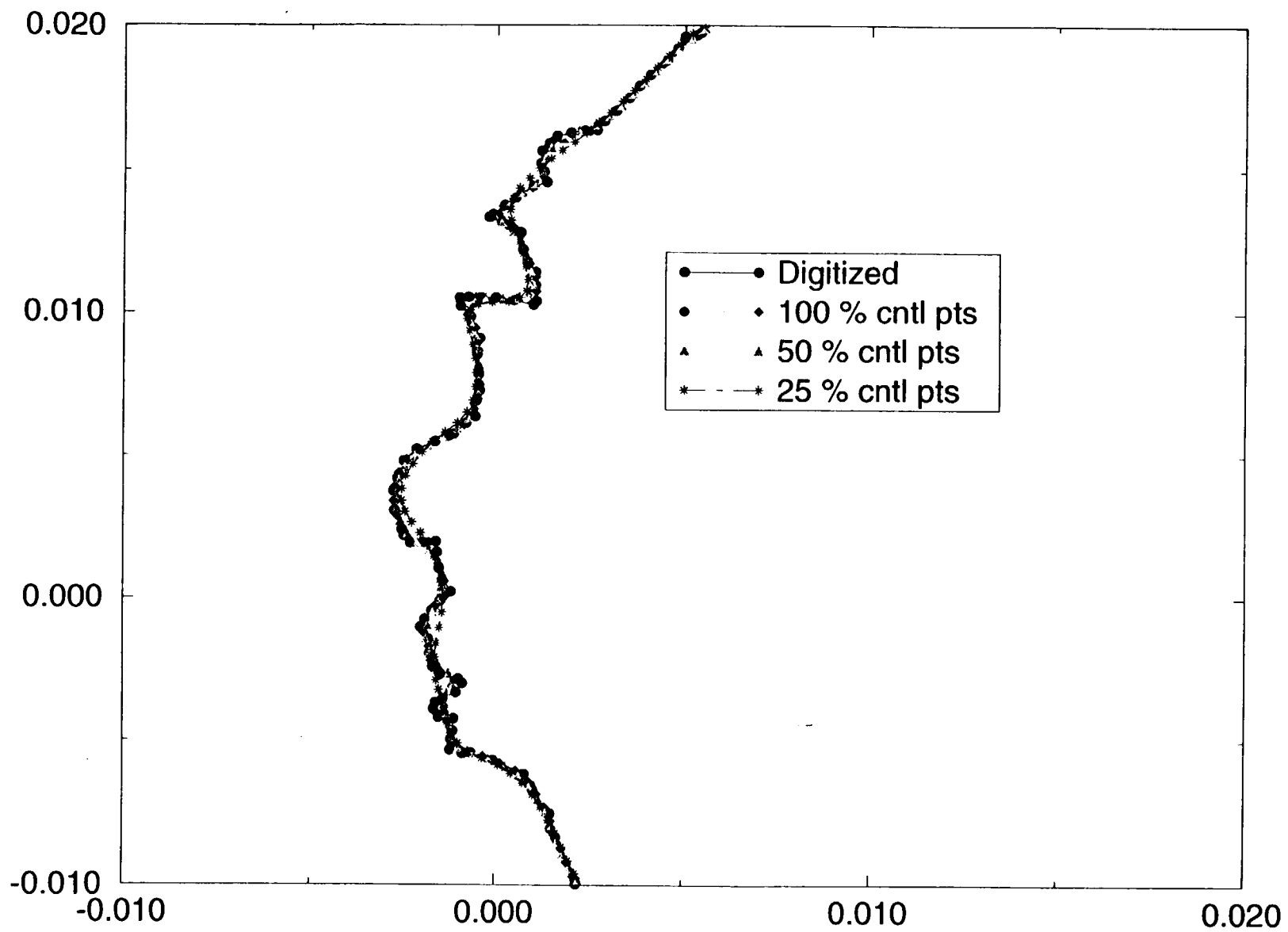


50 % Control Points

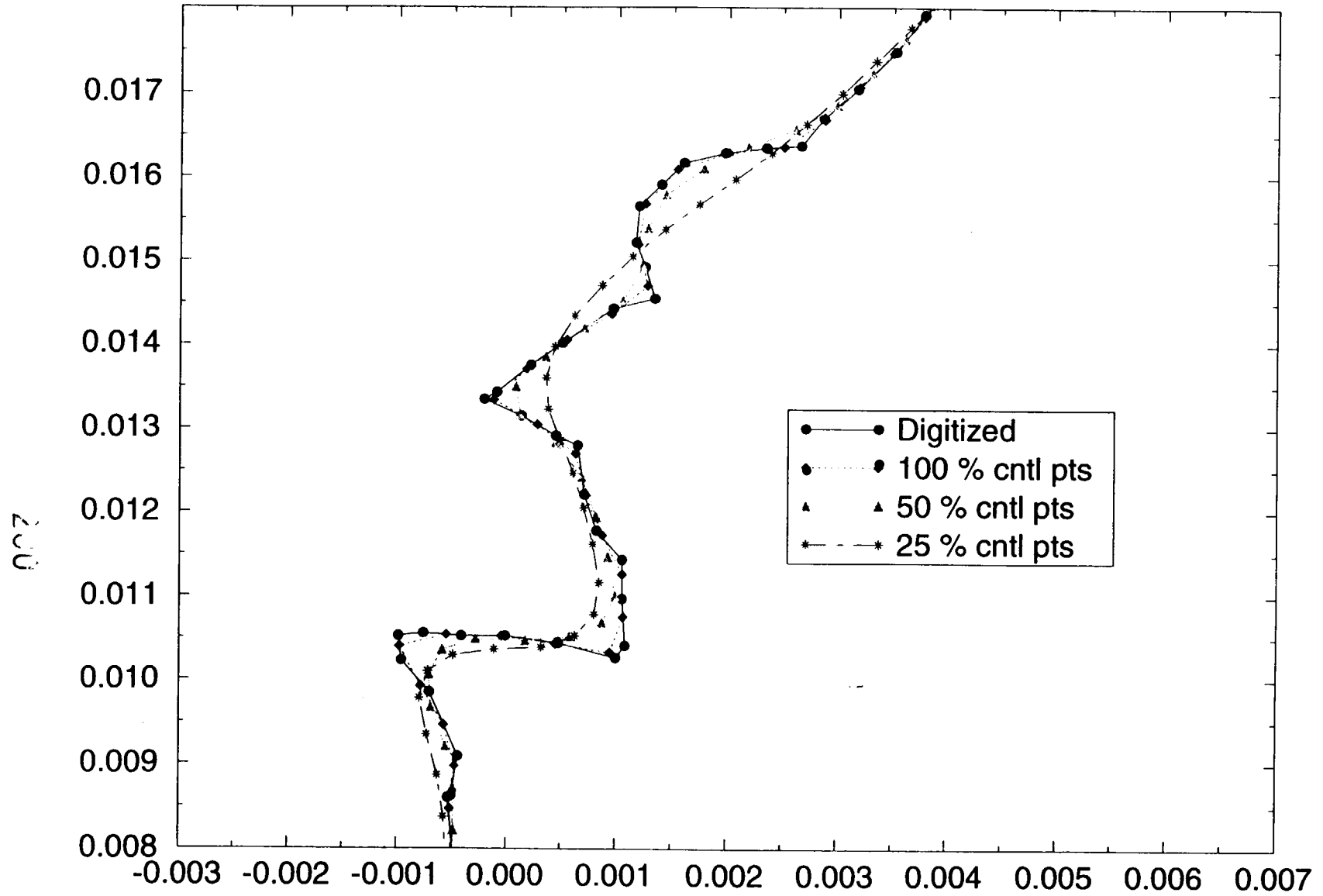
Ice Shape smoothing for matrix # 3



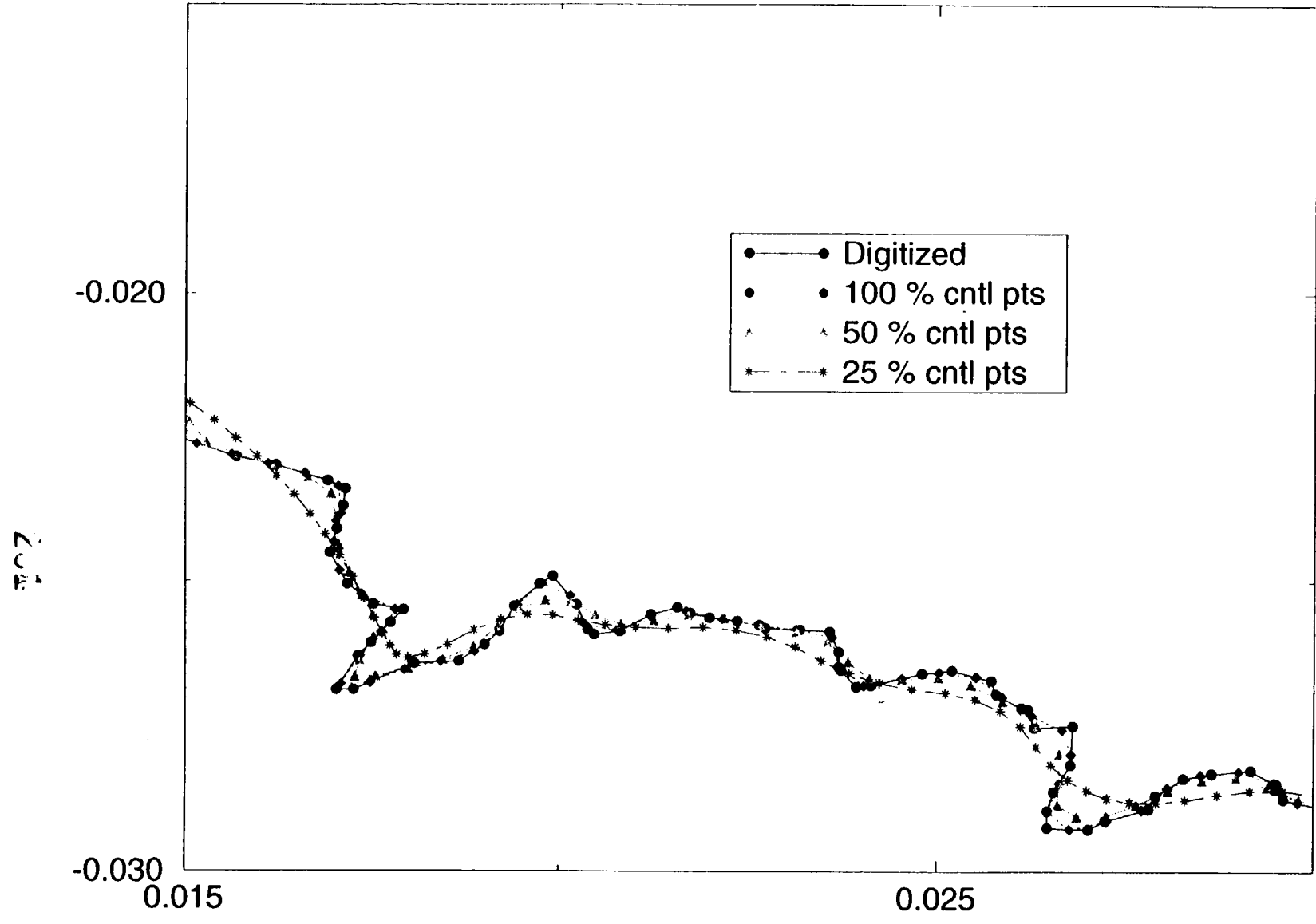
Ice Shape smoothing for matrix # 3



Ice Shape smoothing for matrix # 3

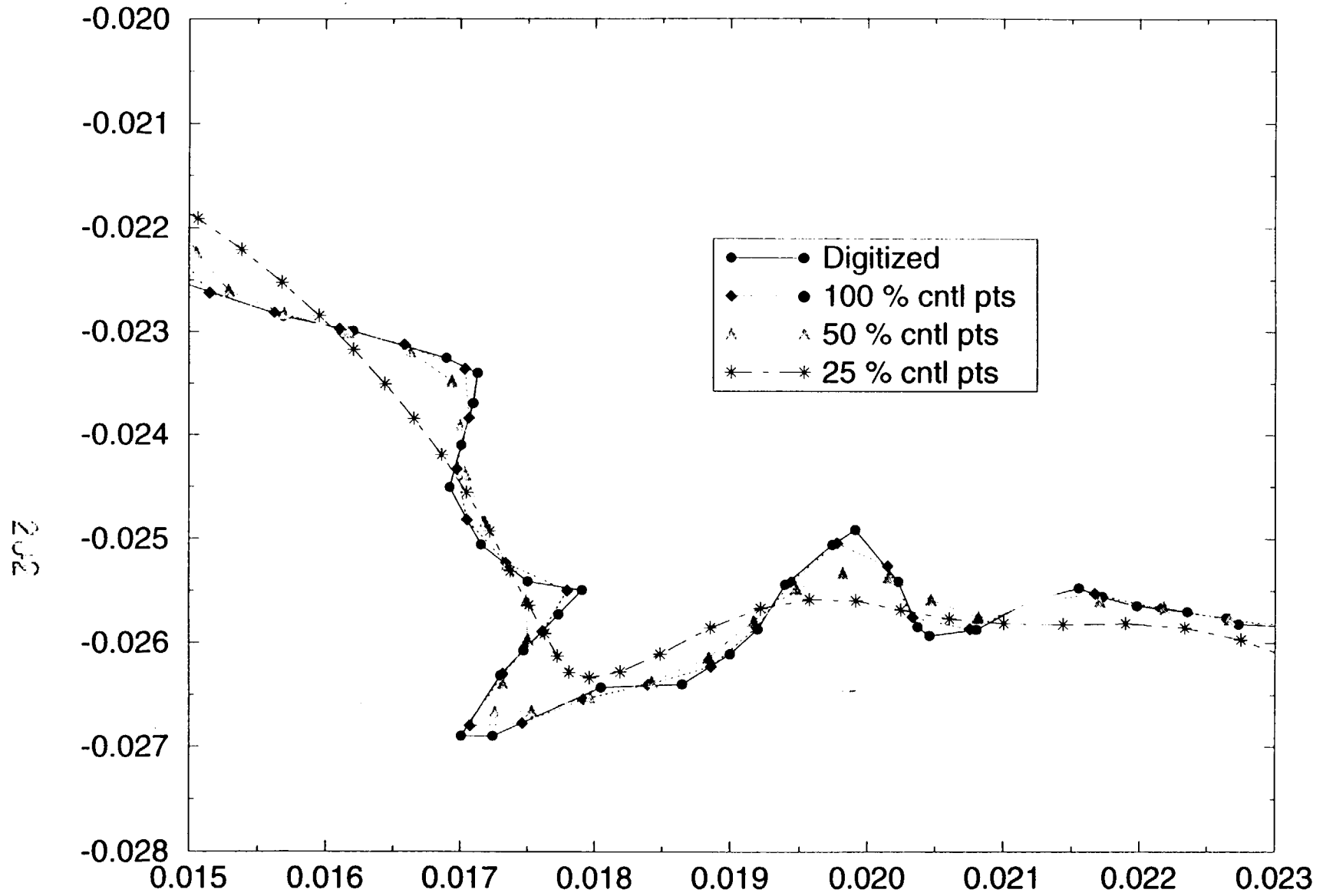


Ice Shape smoothing for matrix # 3



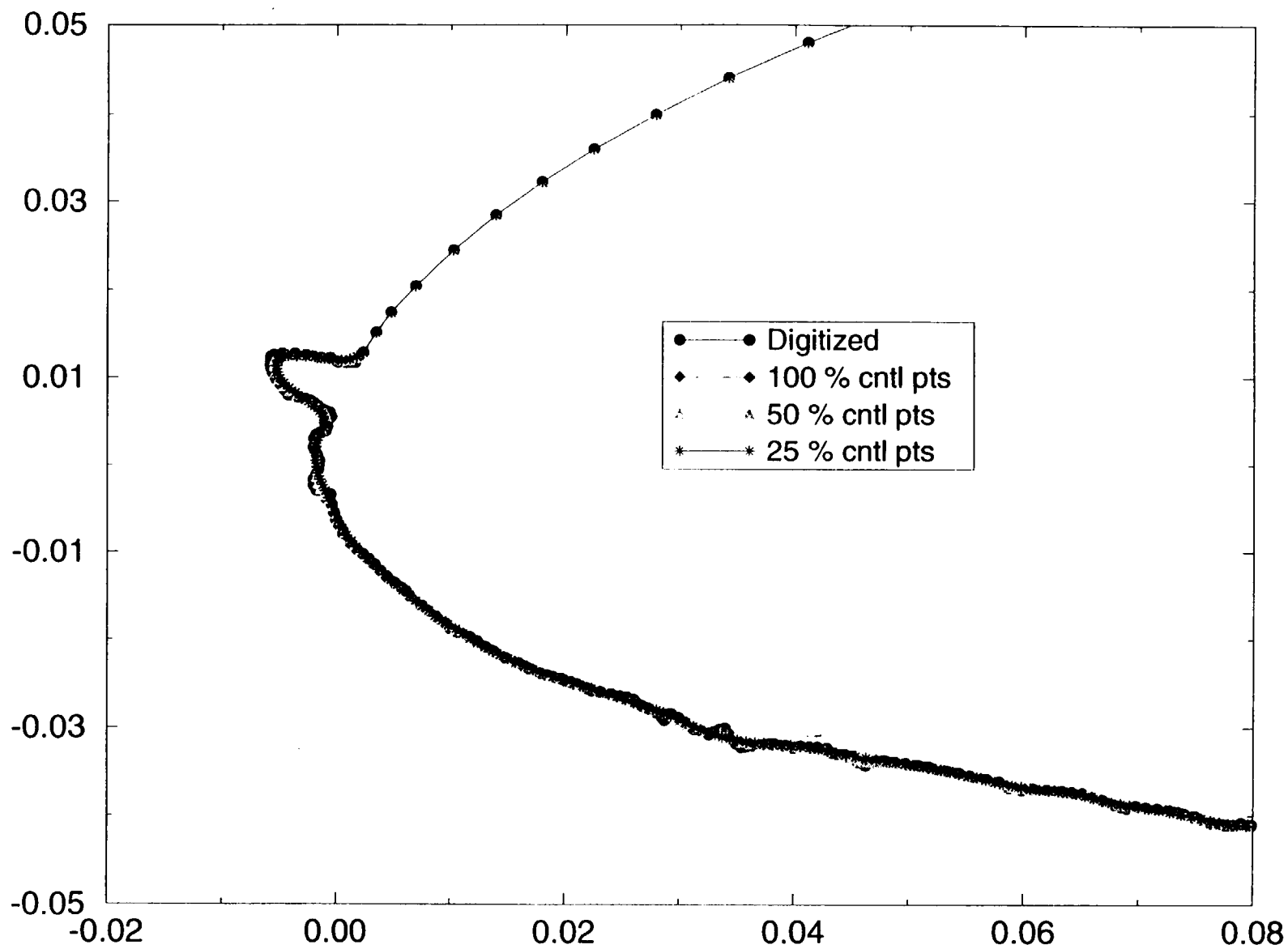
VI-24

Ice Shape smoothing for matrix # 3



VII-25

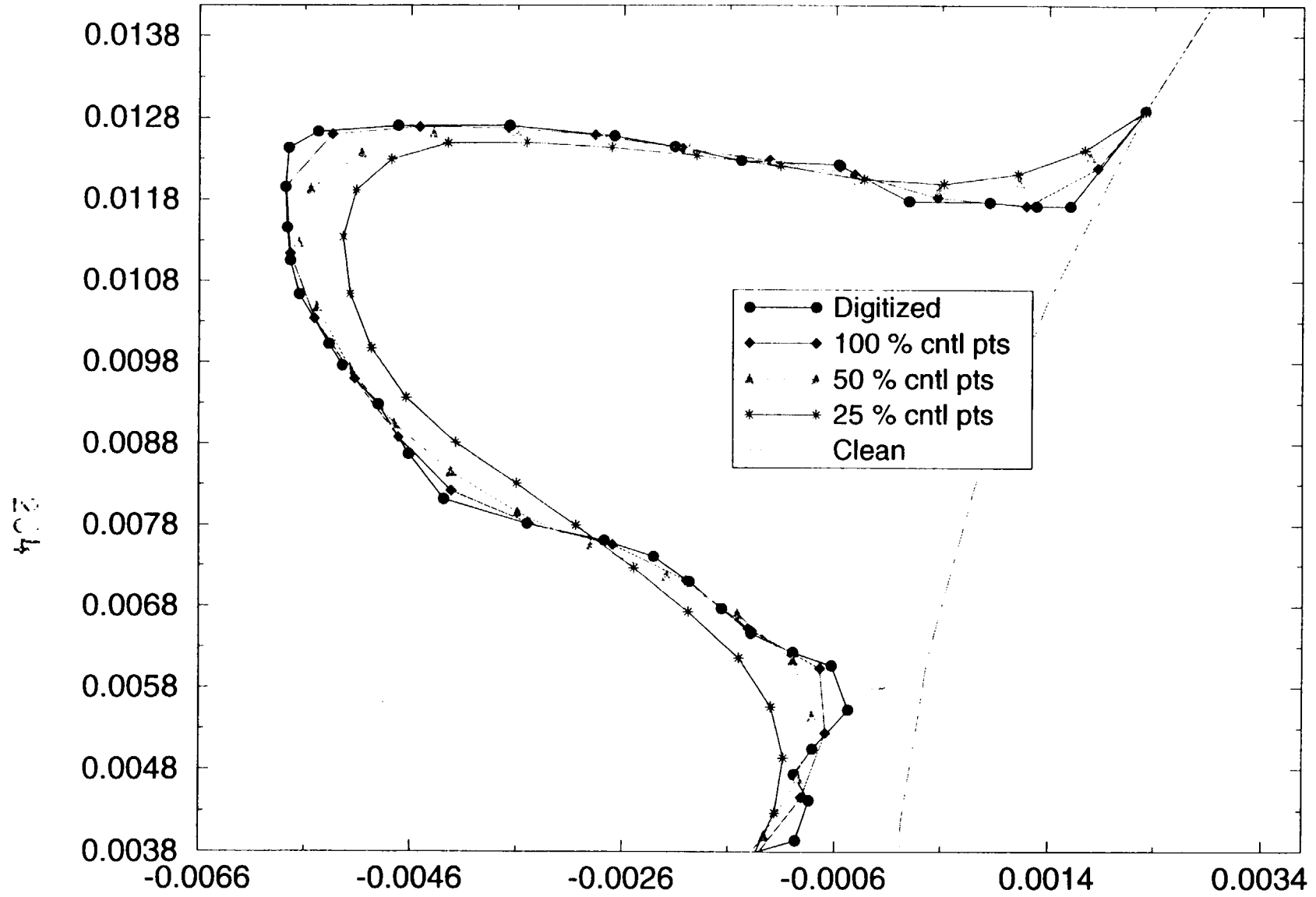
Ice shape smoothing for matrix # 26



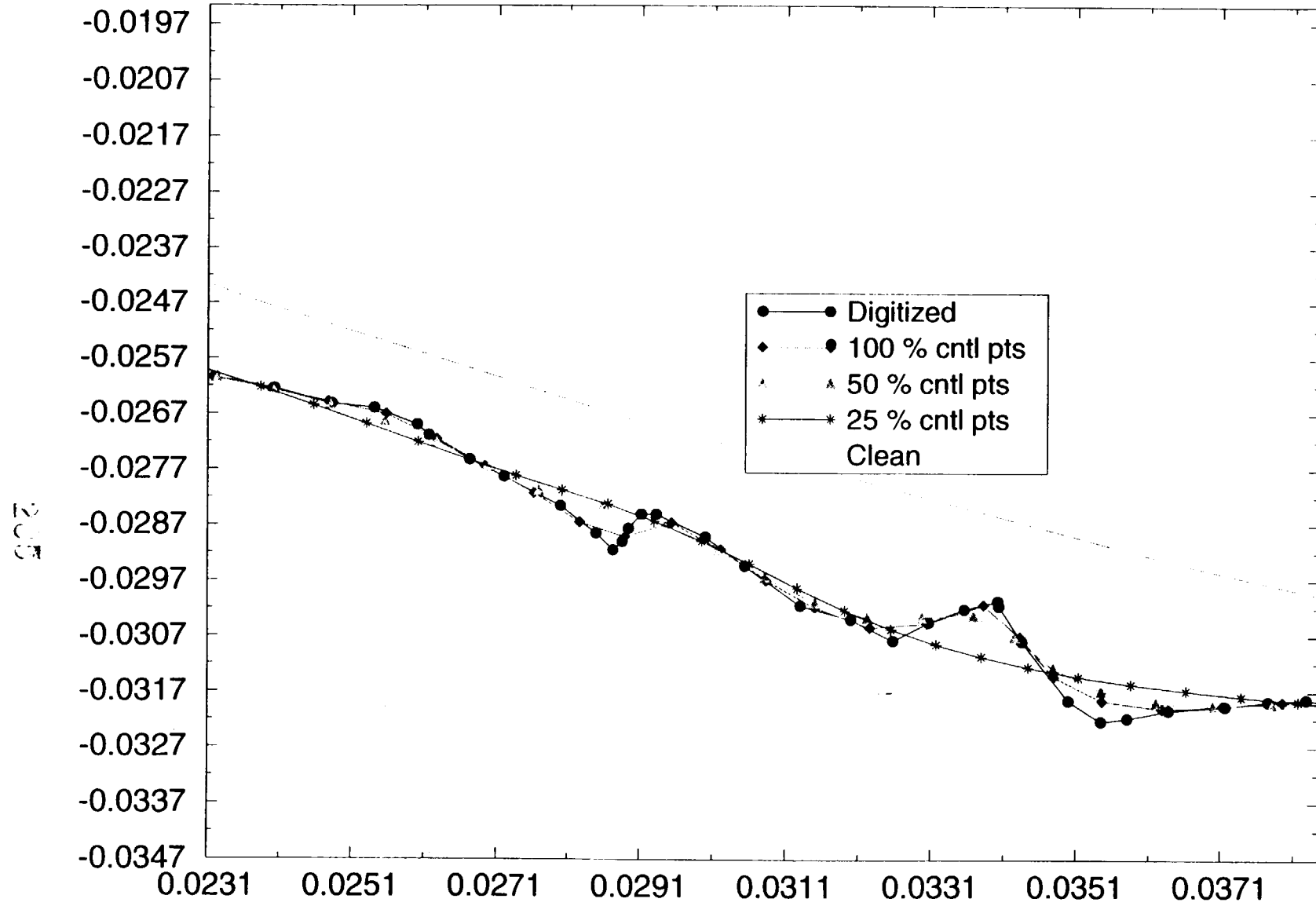
203

VII-26

Ice shape smoothing for matrix # 26



Ice shape smoothing for matrix # 26



VII-28

Grid for Matrix #3 (cc. 50 % cmil) pls

GRID

419 x 60

206

W11-29

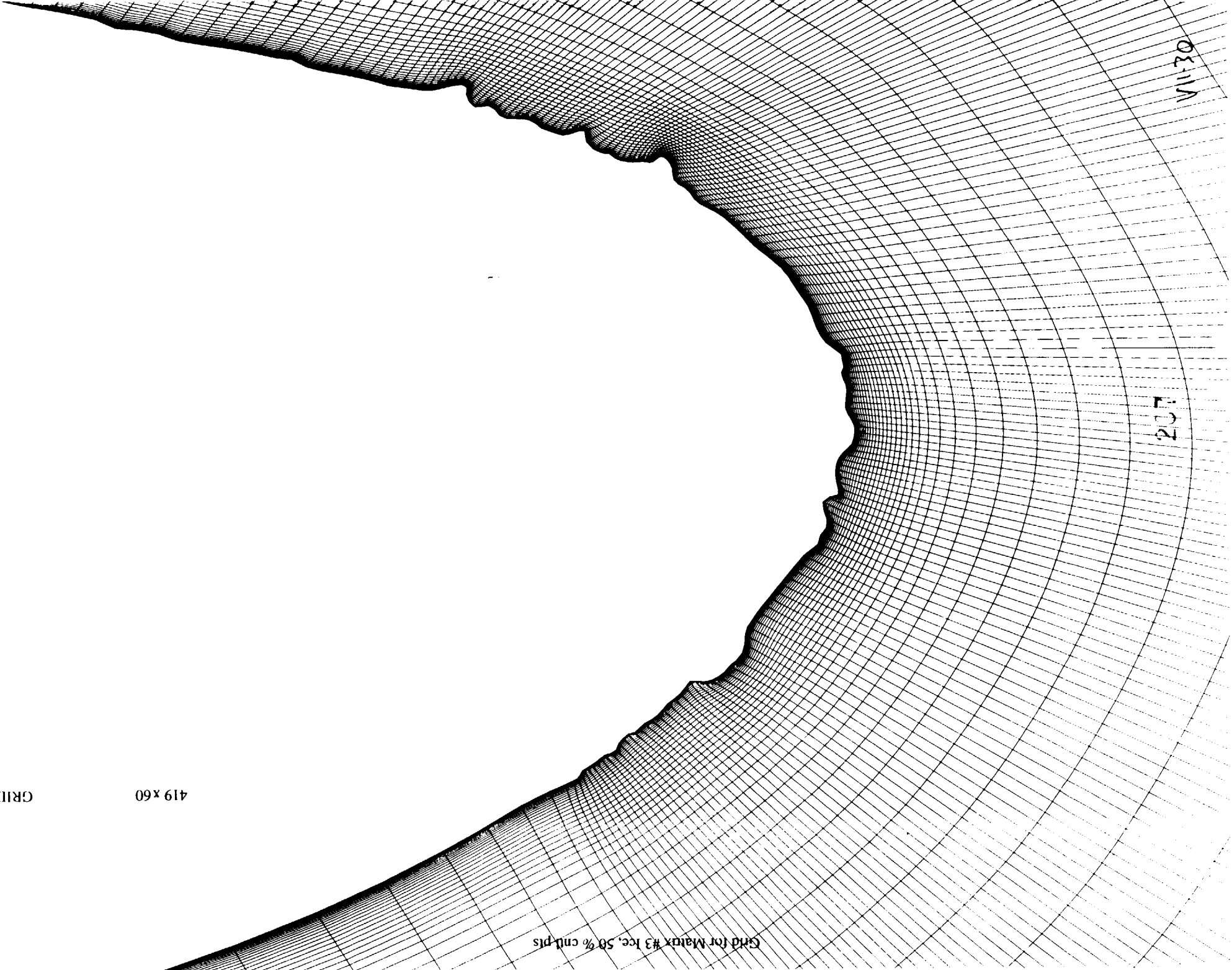
GRID

419 x 60

Grid for Matrix #3 Ice, 50% cnd. pls

207

W1130



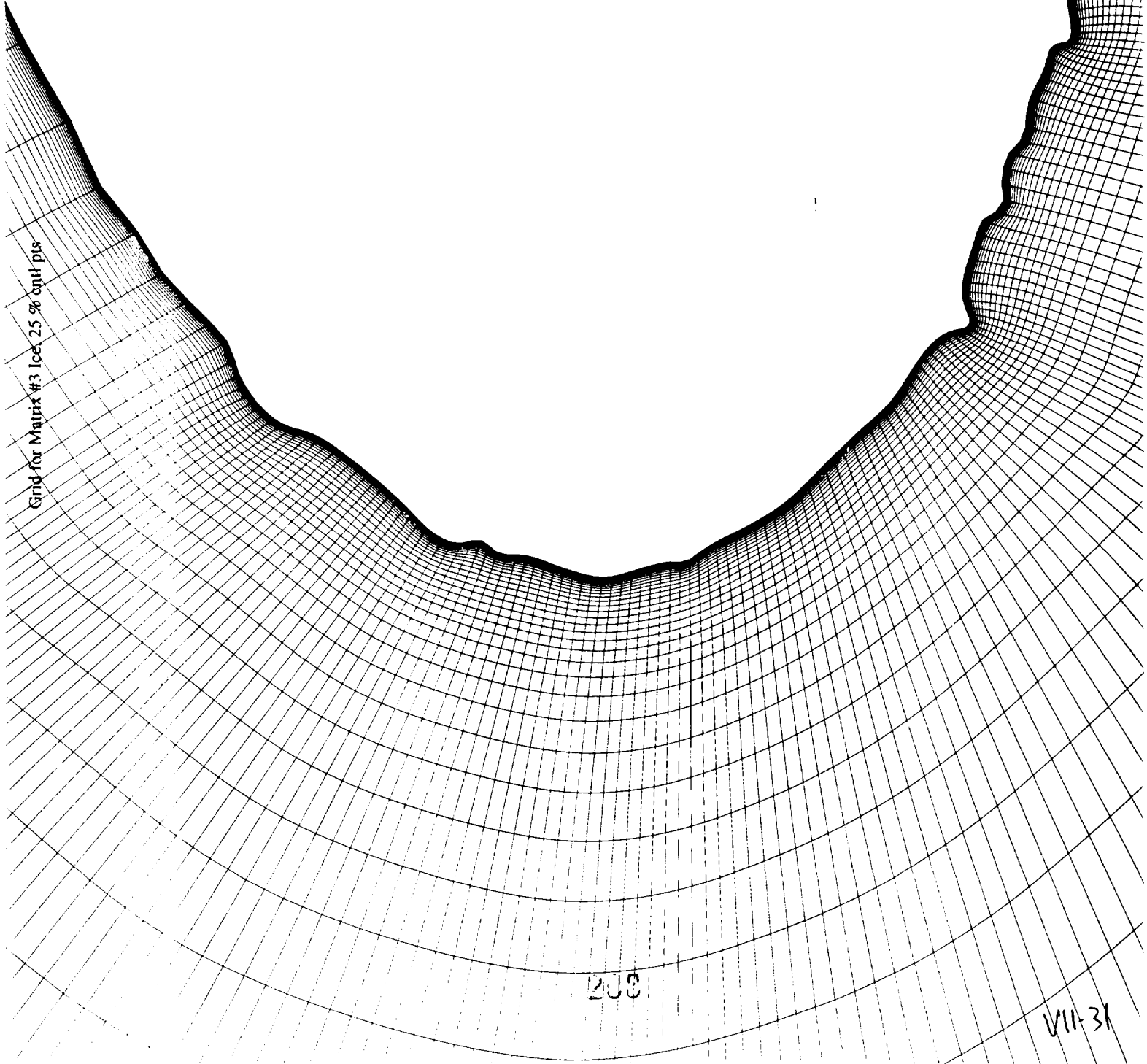
Grid for Matrix #3 Ice 25 % unit pts

356 x 60

GRID

208

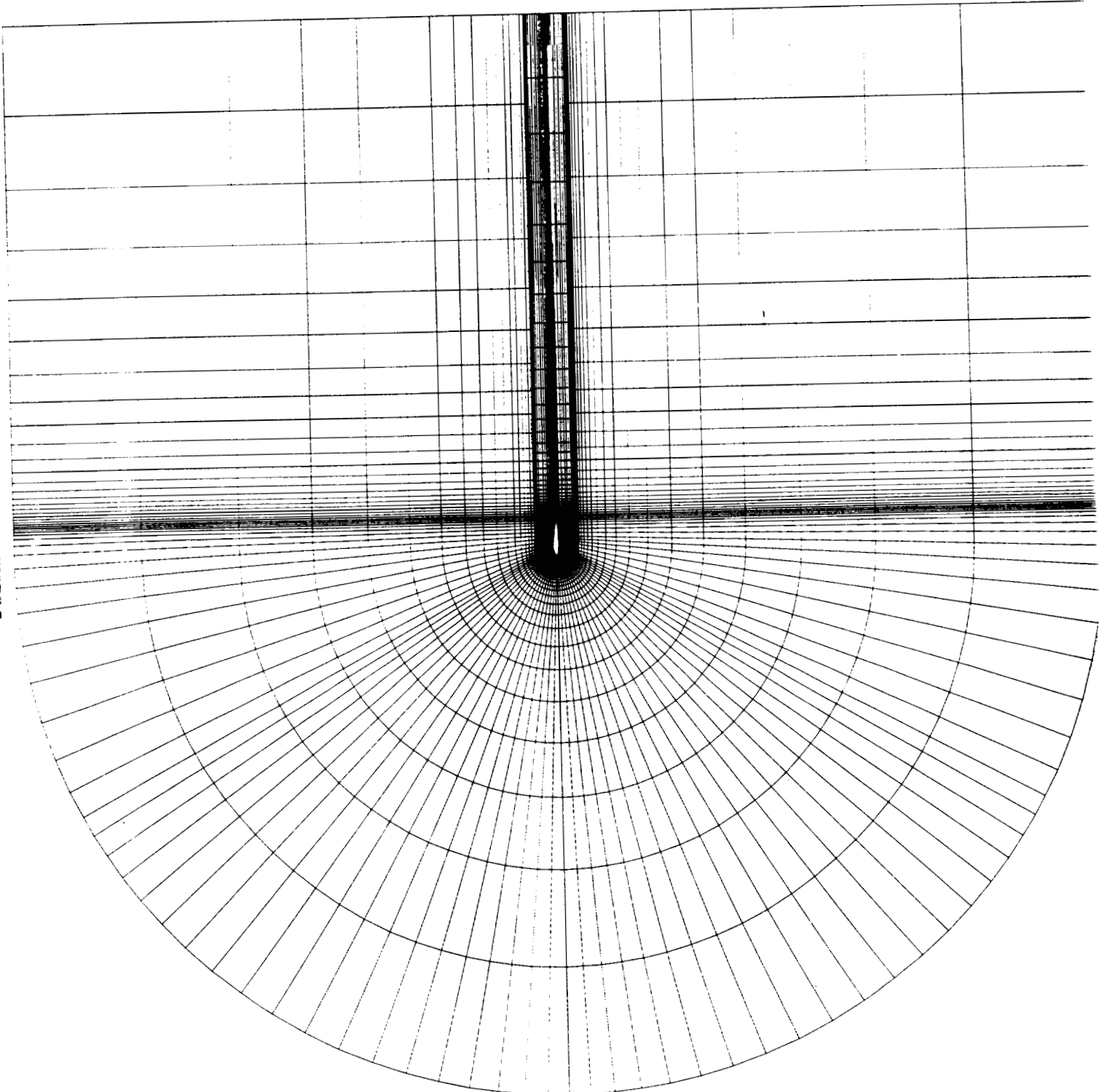
VII-31



2 BLock Grid for Matrix #26 Ice

GRID 1
GRID 2

115 x 20
385 x 40



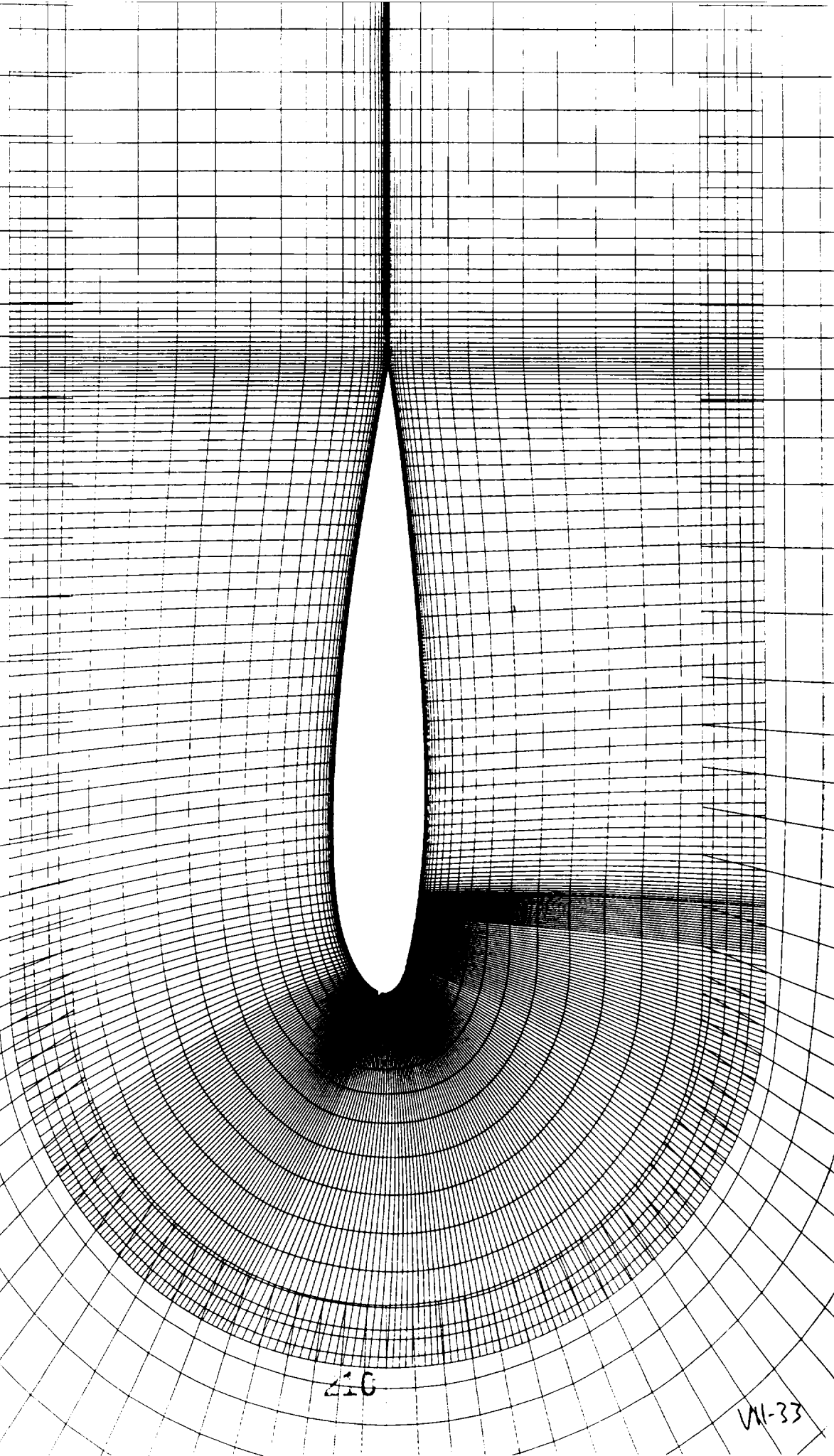
208

VII-32

2 BLock Grid for Matrix #26 Ice

GRID 1
GRID 2

115 x 20
385 x 40



210

VI-33

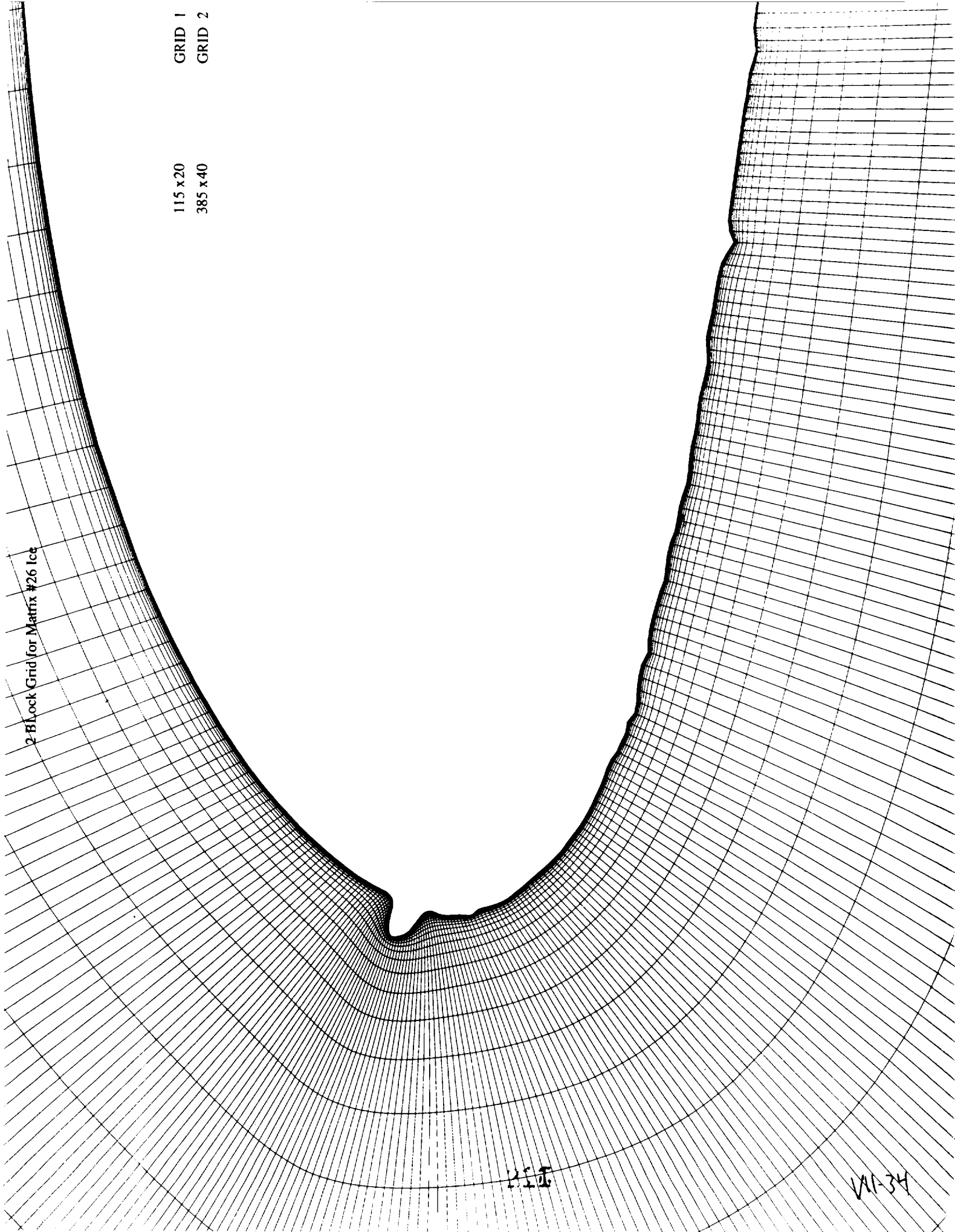
2-Block Grid for Matrix #26 Ice

115 x 20
385 x 40

GRID 1
GRID 2

2116

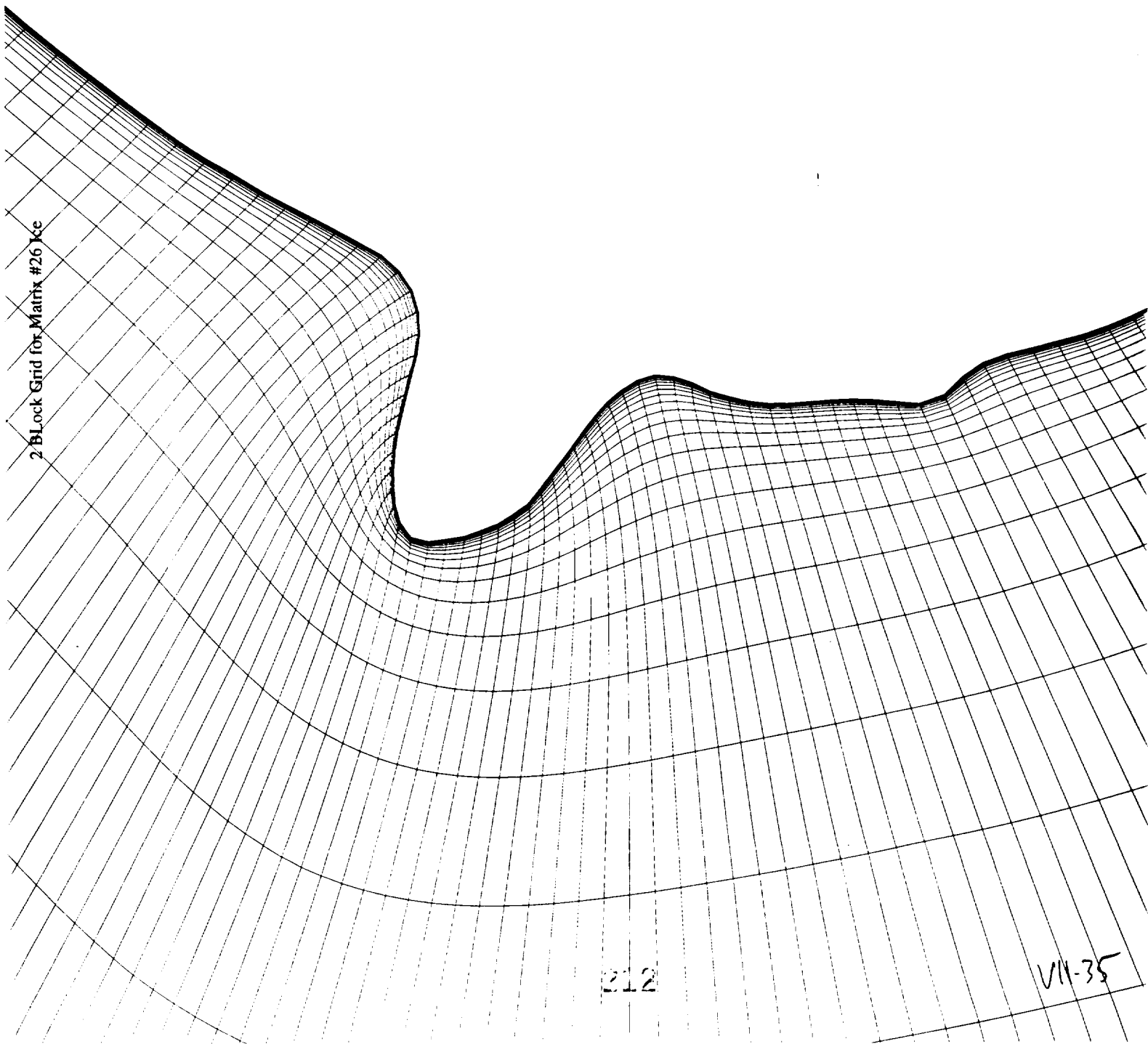
V11-34



GRID 1
GRID 2

115 x 20
385 x 40

2 Block Grid for Matrix #26 Ice

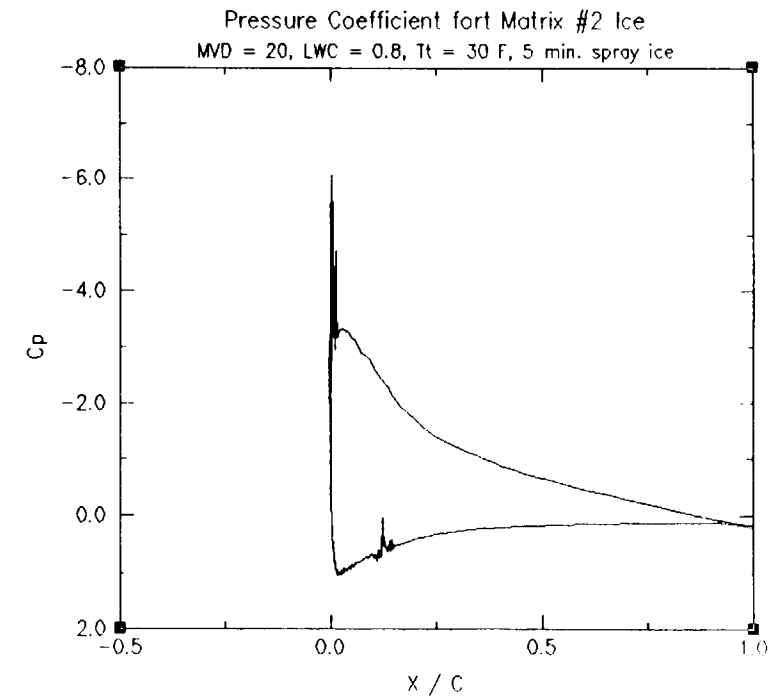
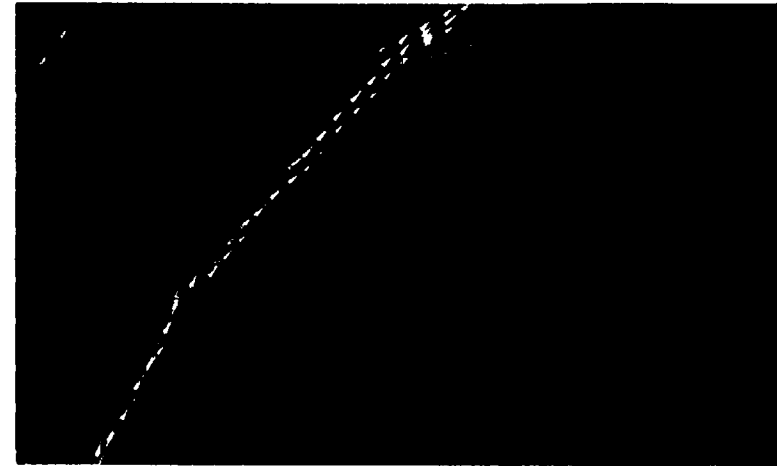
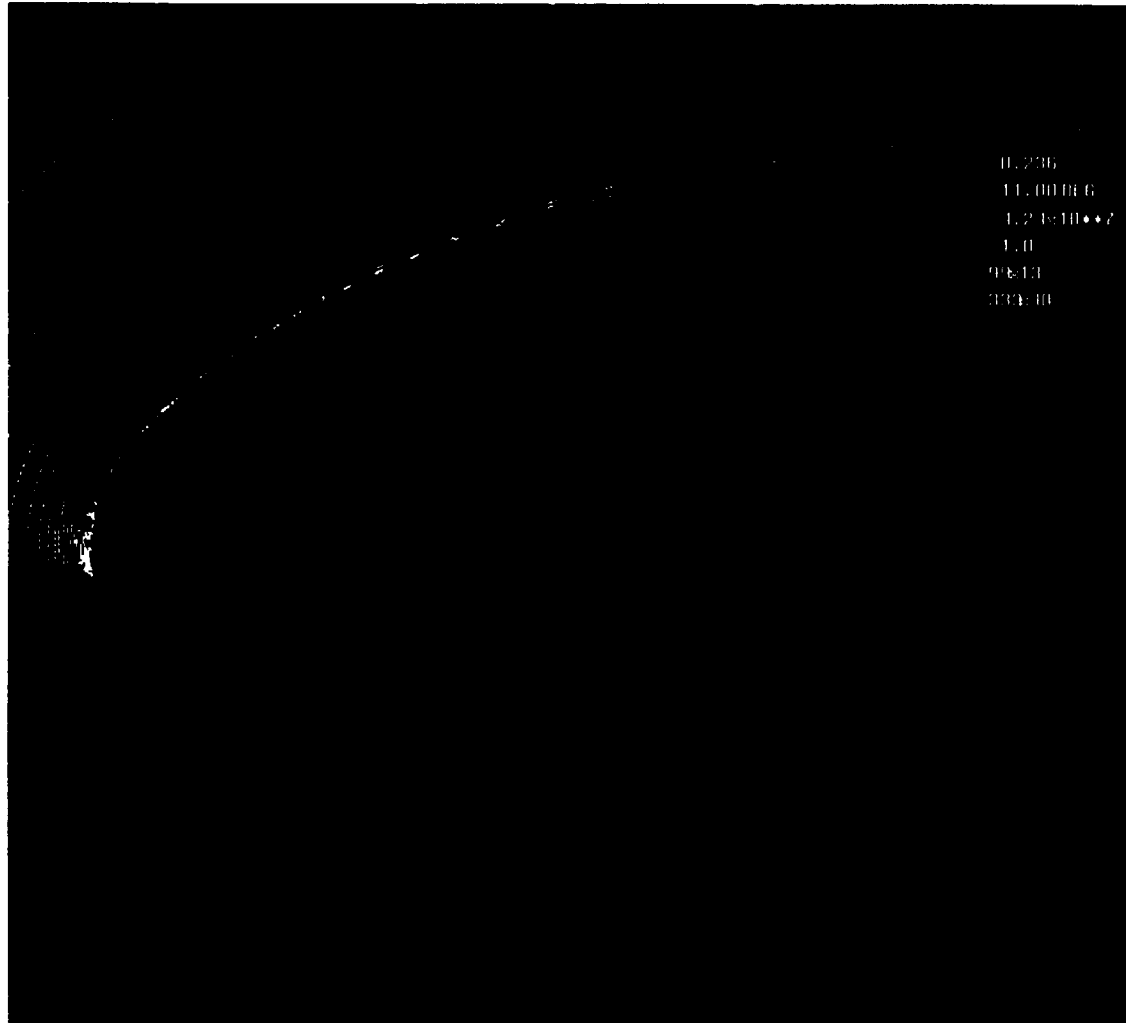


212

VII-35



Lewis Research Center Icing Branch



Mach Contour for Matrix #2 - Ice at A. O. A. = 11 deg.

2.3

VII-36

Effect of Smoothing on the Lift : Matrix # 2, LWC = 0.8, MVD = 20, 5 min. spray -- No ridge formation but has a lot of relatively small bumps

Angle of Attack	Smoothing by % cntl pts = 100 %	Smoothing % 50 %	% difference w.r.t 100 %	Smoothing % 25 %	% difference w.r.t. 100 %e
1	0.259392	0.253958	2.095	0.249142	3.951
3	0.471424	0.466133	1.122	0.465838	1.185
5	0.682798	0.680555	0.329	0.678964	0.562
7	0.883379	0.883197	0.021	0.886399	-0.342
9	1.06001	1.06279	0.262	1.07691	-1.594
11	1.25995	1.17078	7.077	1.23180	2.234
13	Fluctuation	1.17812	N/A	1.29666	N/A

Effect of Smoothing on the Drag

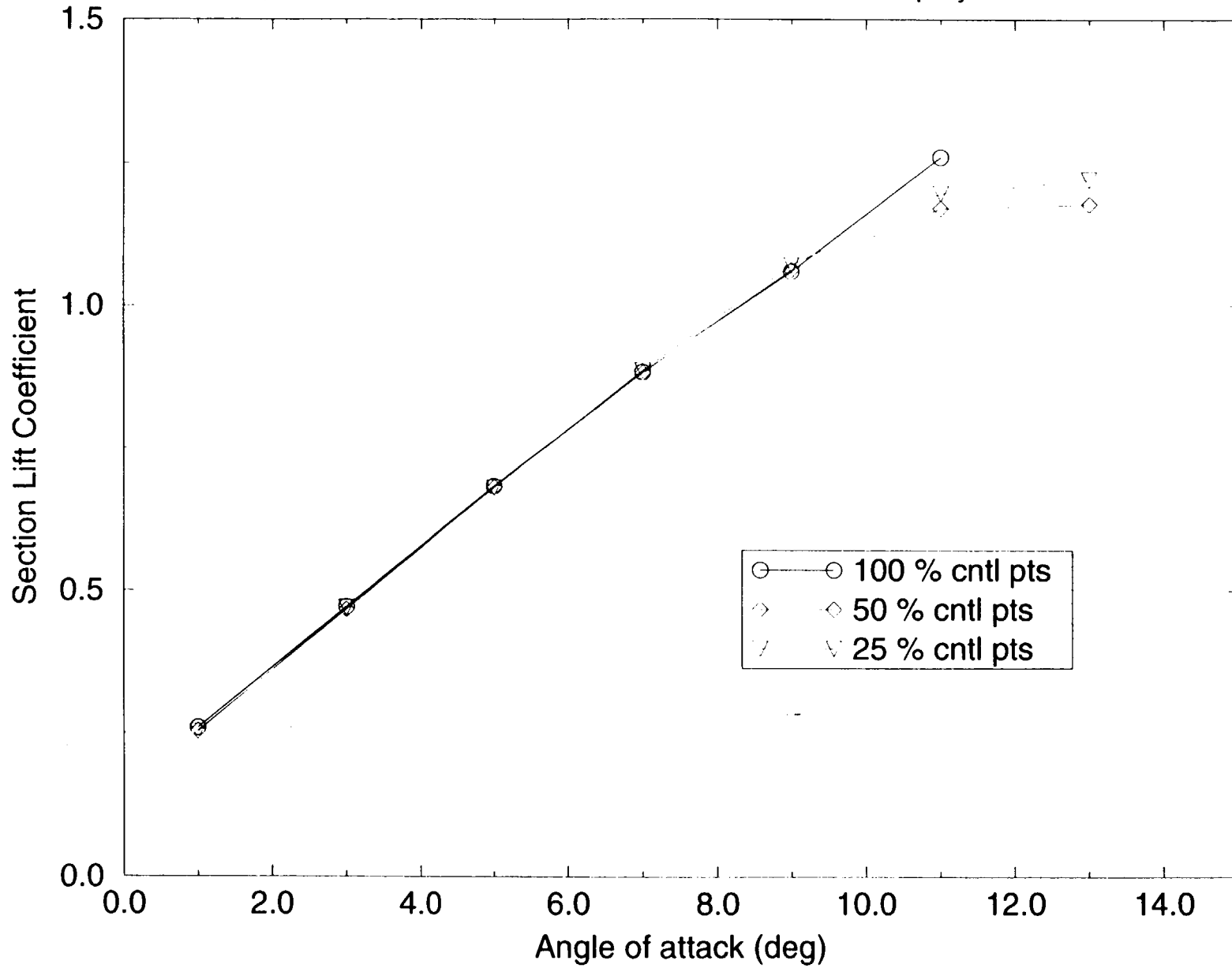
Angle of Attack	Smoothing by % cntl pts = 100 %	Smoothing 50 %	% difference w.r.t. 100 %	Smoothing % 25 %	% difference w.r.t. 100 %
1	0.010509	0.009992	- 4.920	0.009091	- 13.493
3	0.011819	0.011503	- 2.764	0.010526	- 10.940
5	0.014484	0.014012	- 3.259	0.013026	- 10.066
7	0.018450	0.017950	- 2.710	0.016649	- 9.762
9	0.023883	0.022852	- 4.317	0.021323	- 10.719
11	0.036839	0.028571	- 22.444	0.026882	- 27.028
13	Fluctuation	0.039731	N/A	0.034330	N/A

2-4

VII-37

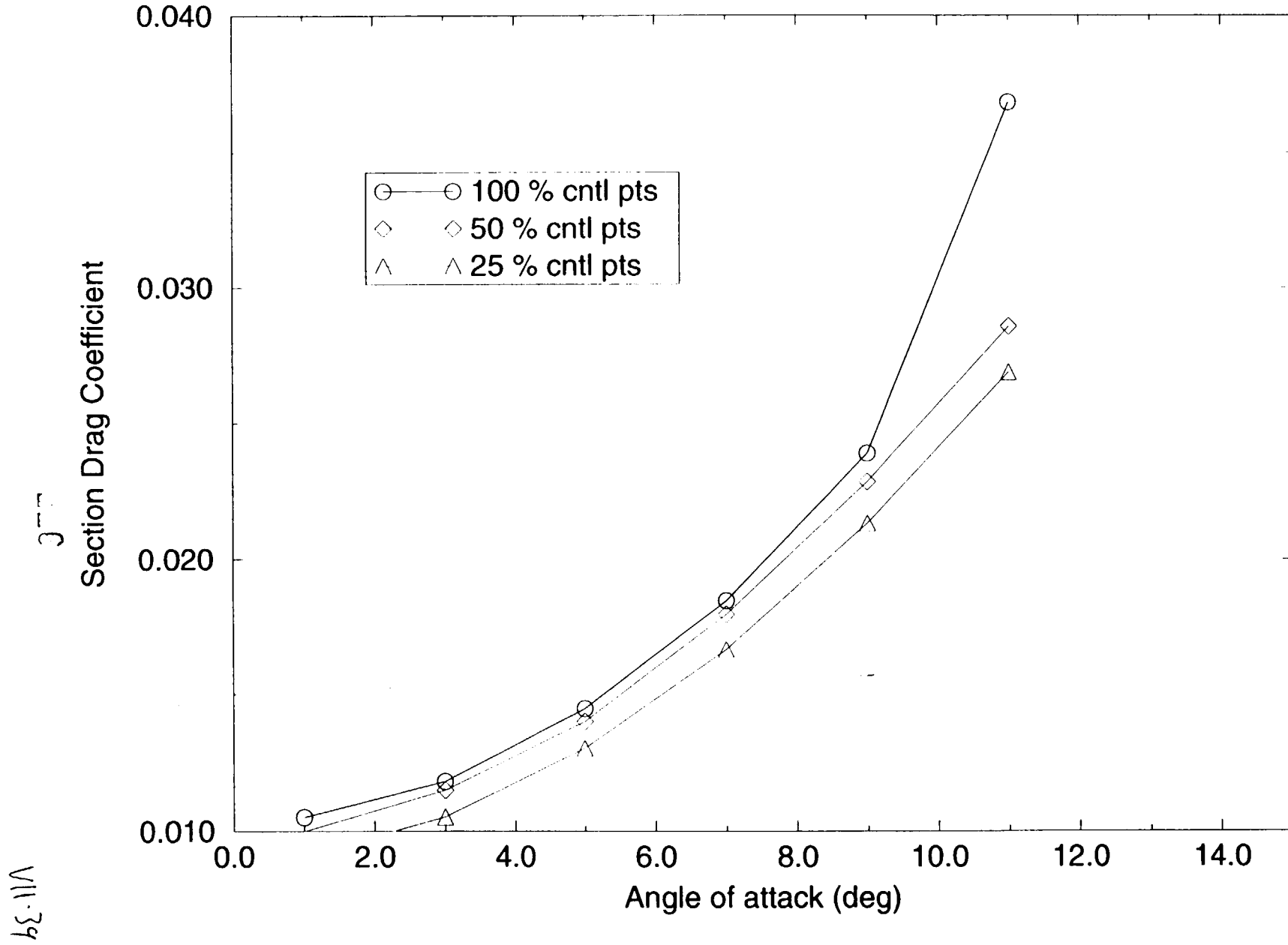
Effect of Ice Shape Smoothing on the Lift

Matrix #2 : LWC = 0.8, MVD = 20, 5 min. spray



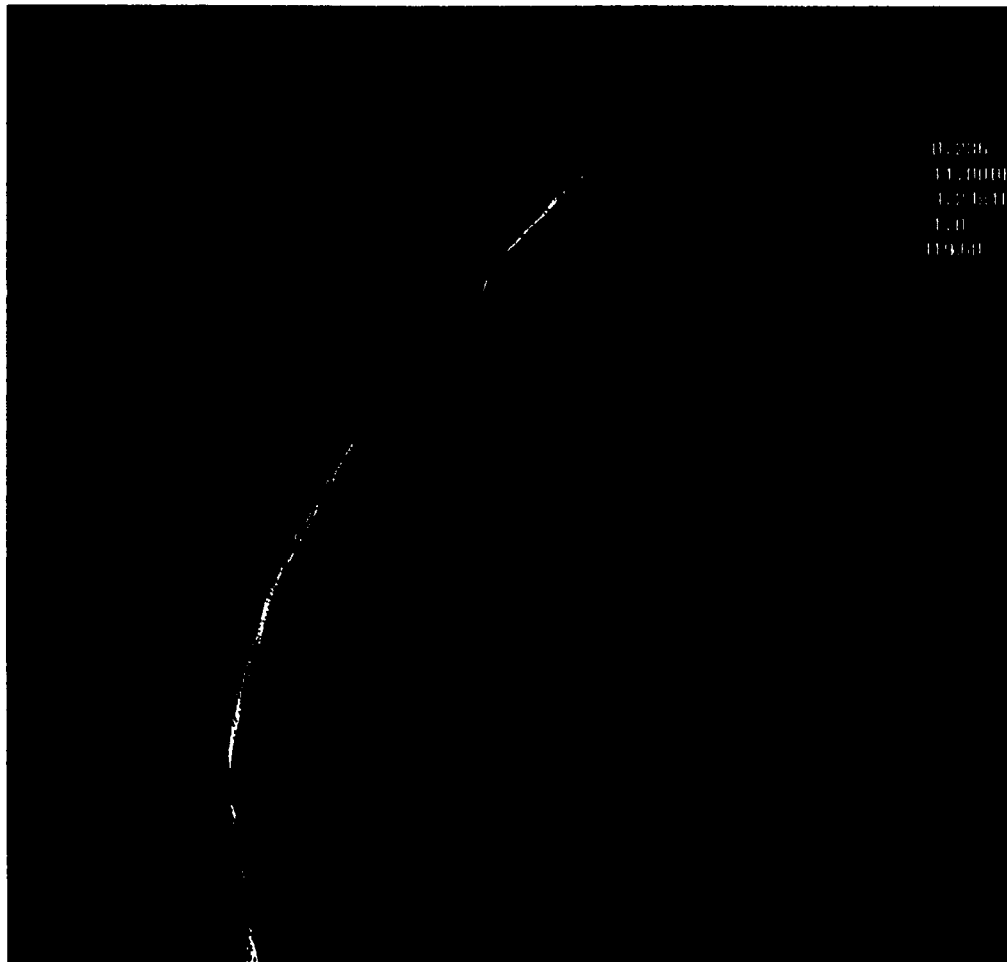
Effect of Ice Shape Smoothing on the Drag

Matrix #2 : LWC = 0.8, MVD = 20, 5 min. spray



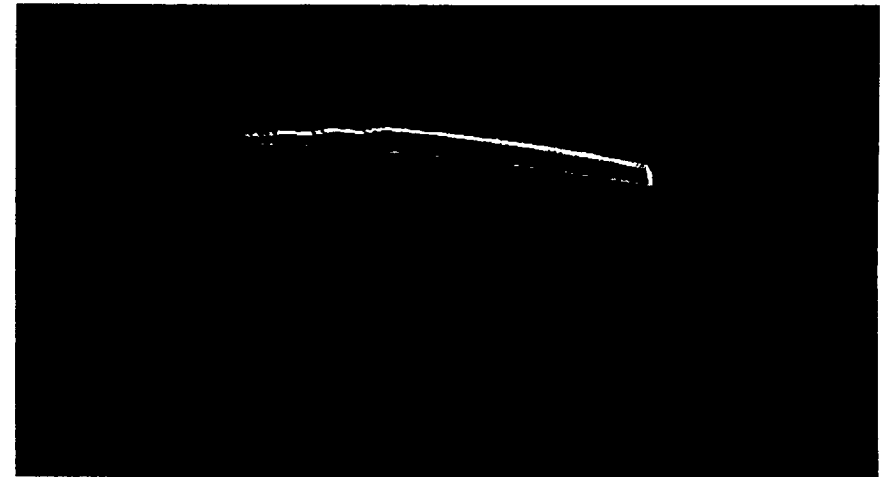


Mach Contour for Matrix #3 Ice shape



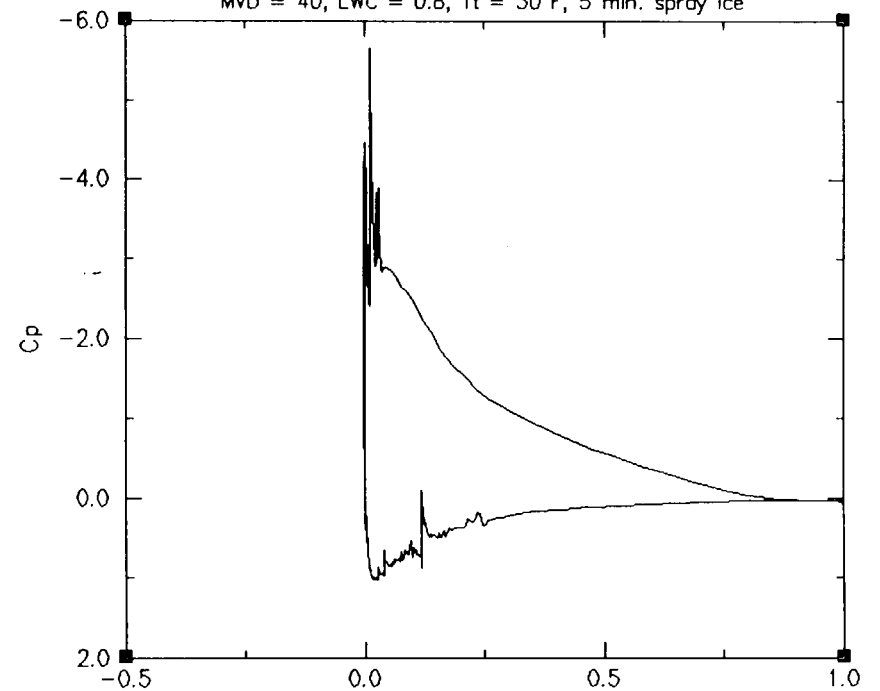
A. O. A. = 11 degrees

M11-40



Turbulent Viscosity

Pressure Coefficient for Matrix #3 Ice
MVD = 40, LWC = 0.8, Tt = 30 F, 5 min. spray ice



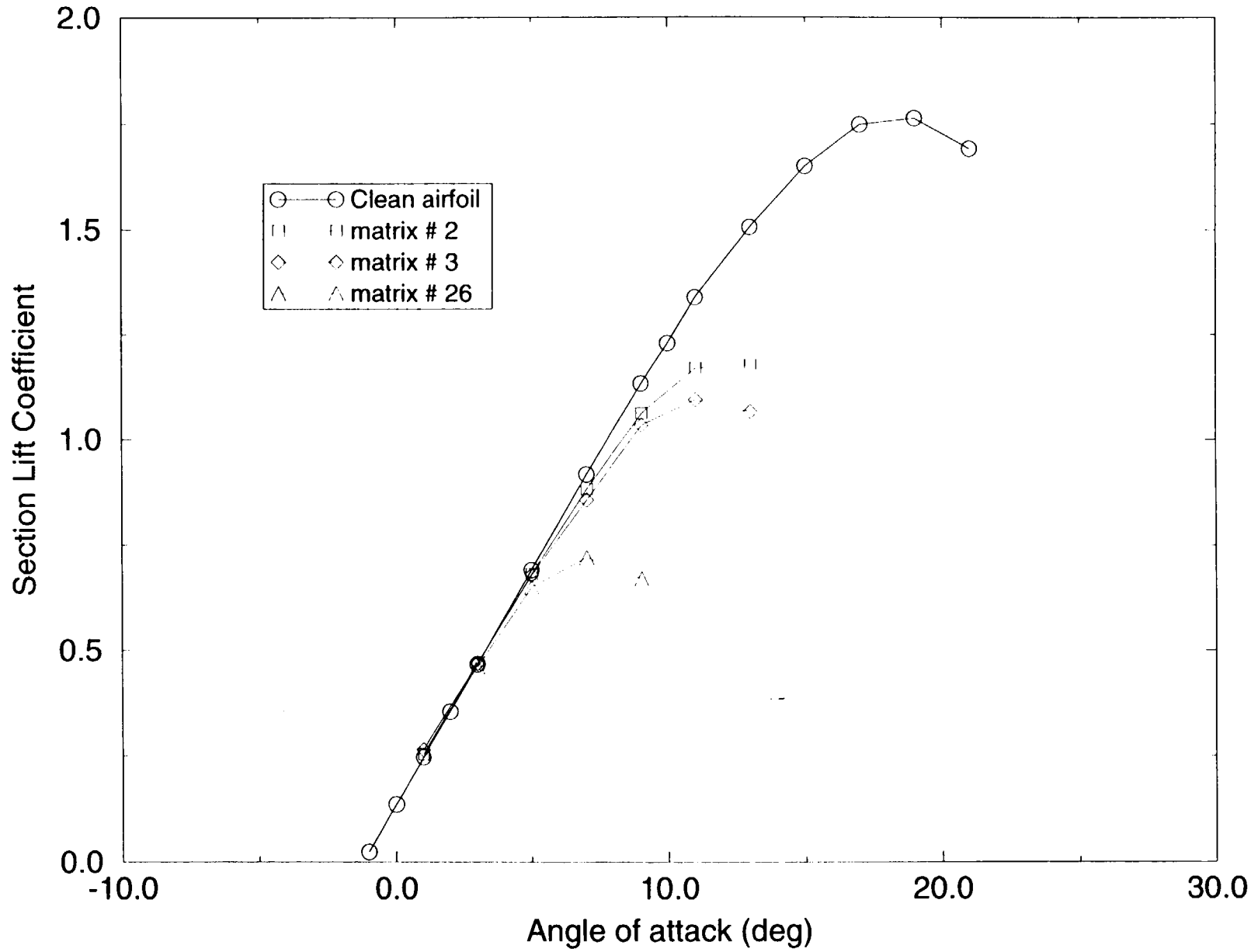
Matrix # 3, Lift				Matrix # 26 Lift, Tt = 26 F, ridge formation			
A.O.A.	50 % Smoothing	25 %	% diff.	A. O. A.	50 % Smoothing	25 %	% diff.
1	0.264289	0.252403	4.497	3	0.460437	0.460361	0.017
3	0.469494	0.469450	0.009	5	0.649115	0.647291	0.281
5	0.677603	0.679565	- 0.290	7	0.719742	0.688607	- 4.326
7	0.857101	0.886727	- 3.457	9	0.668951	Fluctuation	N/A
9	1.03448	1.07097	- 3.527				
11	1.09531	1.19699	- 9.283				
13	1.06686	1.22114	- 14.461				
Matrix # 3, Drag				Matrix # 26, Drag, Tt = 26 F, ridge formation			
A. O. A.	50 %	25%	% diff	A. O. A.	50 % Smoothing	25 %	% diff
1	0.012164	0.010894	- 10.441	3	0.012119	0.011401	- 5.925
3	0.012957	0.011618	- 10.334	5	0.016204	0.015702	- 3.098
5	0.015443	0.013978	- 9.486	7	0.022105	0.021801	- 1.375
7	0.019569	0.017624	- 9.939	9	0.036486	Fluctuation	N/A
9	0.025045	0.021982	- 12.230				
11	0.031241	0.028434	- 8.985				
13	0.040488	0.036052	- 10.956				

3

1h-11A

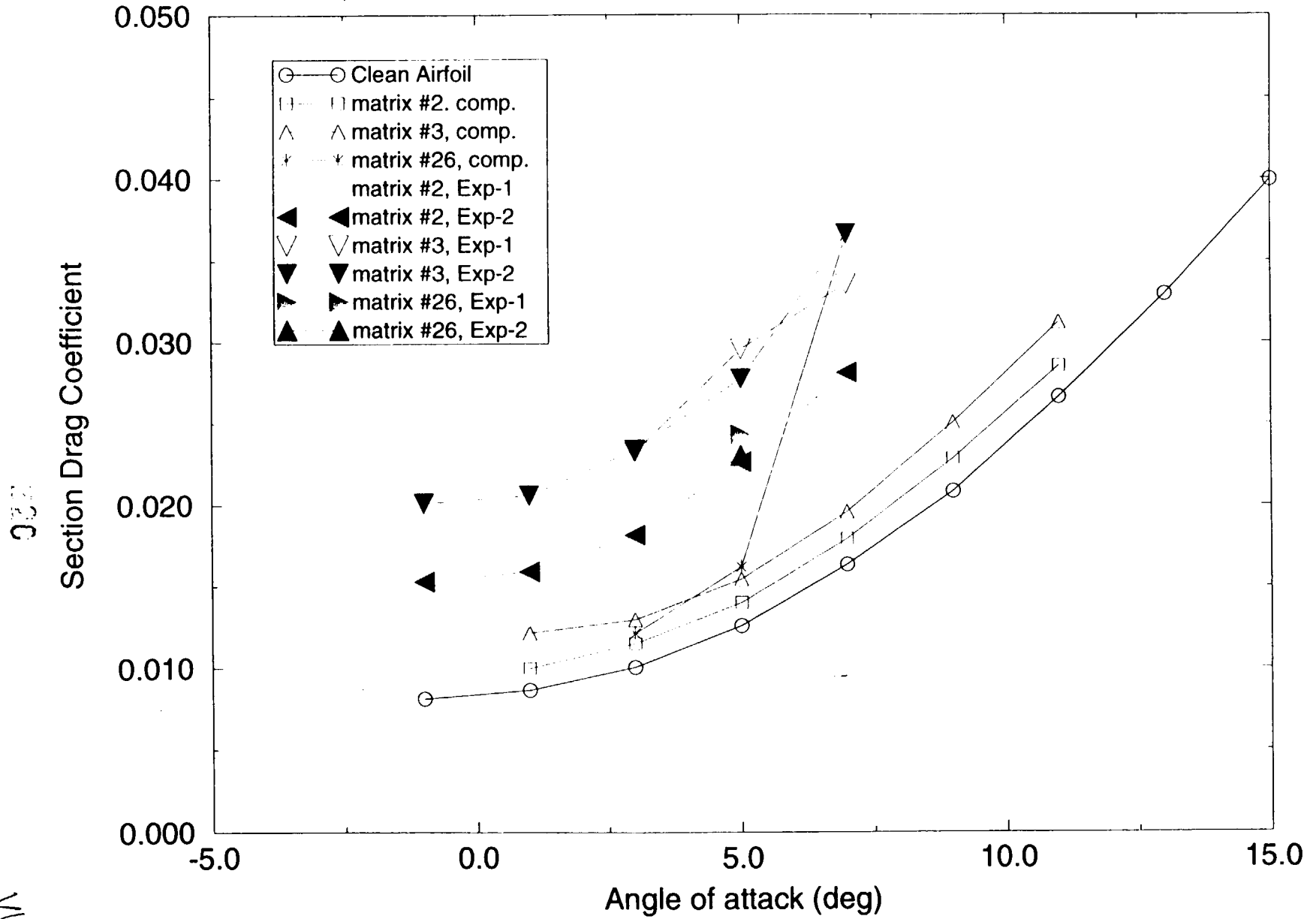
Effect of Ice on the Lift

50 % control points used on the ice shapes



21-112

Effect of Ice on the Drag

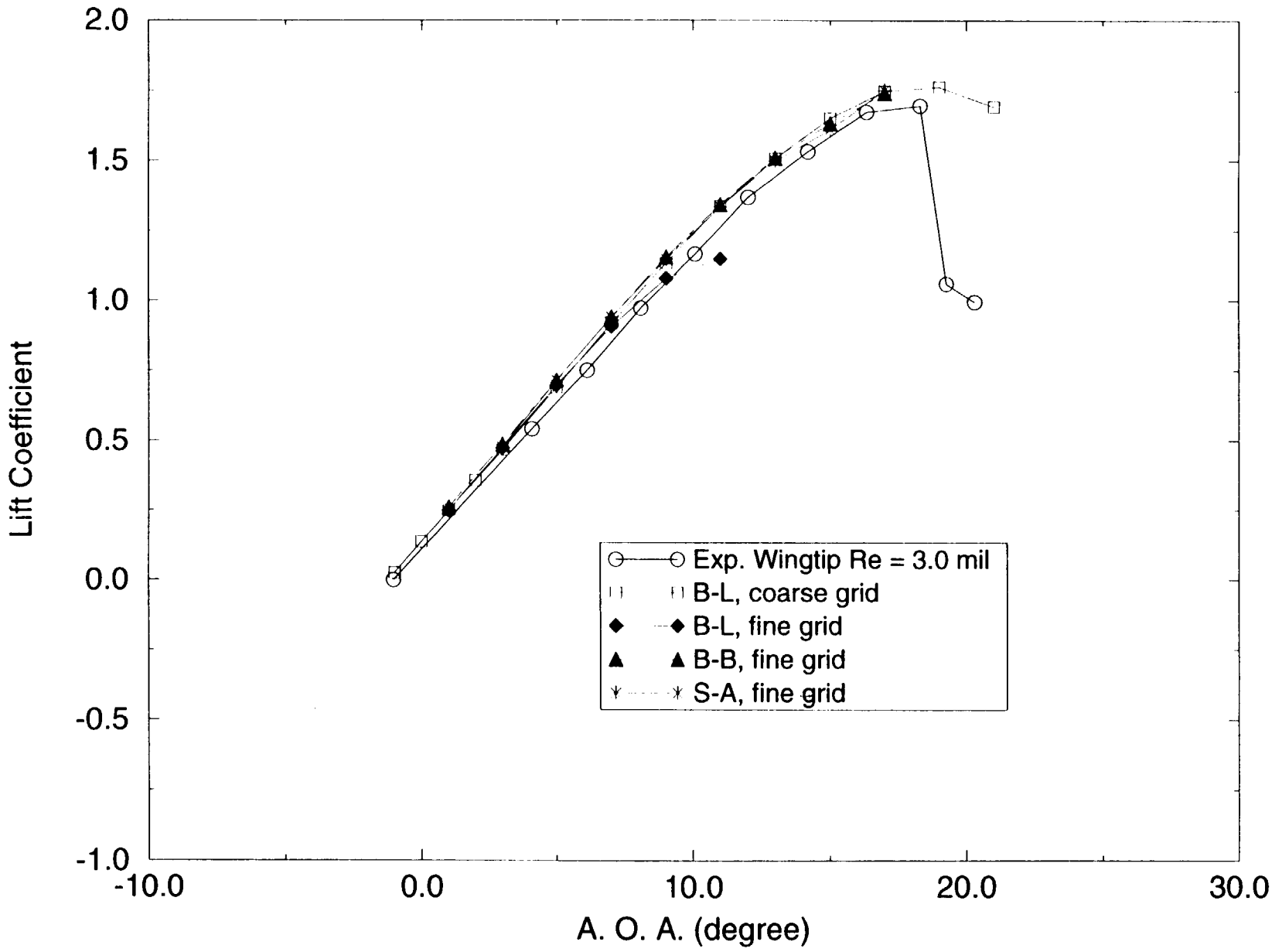


VI-43

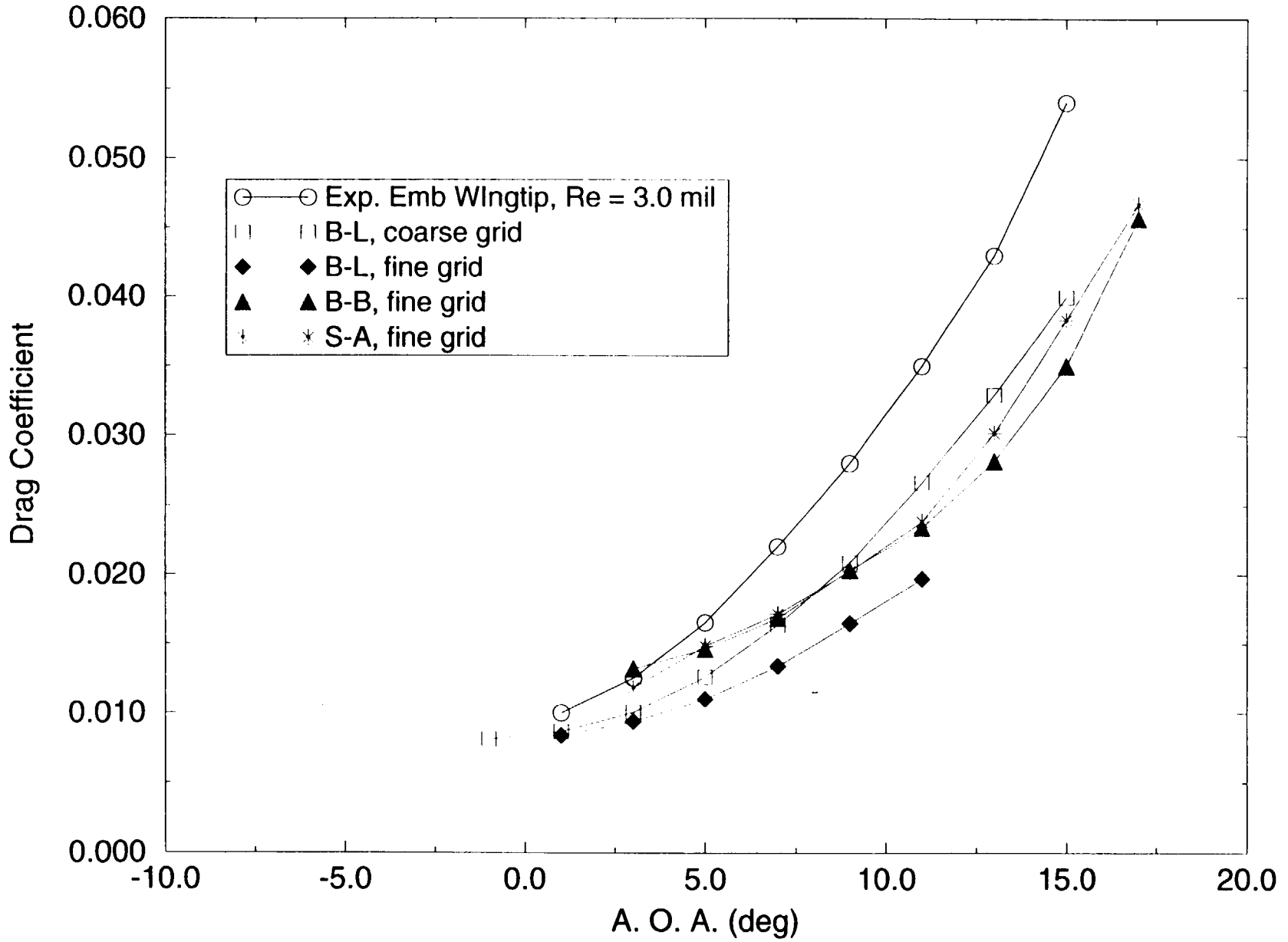
Lift for Clean Airfoil

477

11-44



Drag Comparison for Clean Airfoil



272

5h-11A



Summary of the Smoothing Study

- Baldwin Lomax turbulence model used with medium fine grid for quick assessment of aerodynamics
- The level of smoothing could affect the lift & drag considerably
25 % control point(CP) smoothing predicts about 10% difference in drag for matrix # 2 & # 3 ice shapes
- 50 % control point smoothing is appropriate for computations
- Among the three ice shapes, the matrix #26 ice with ridge caused the most severe drop in lift and increase in drag.

218
2

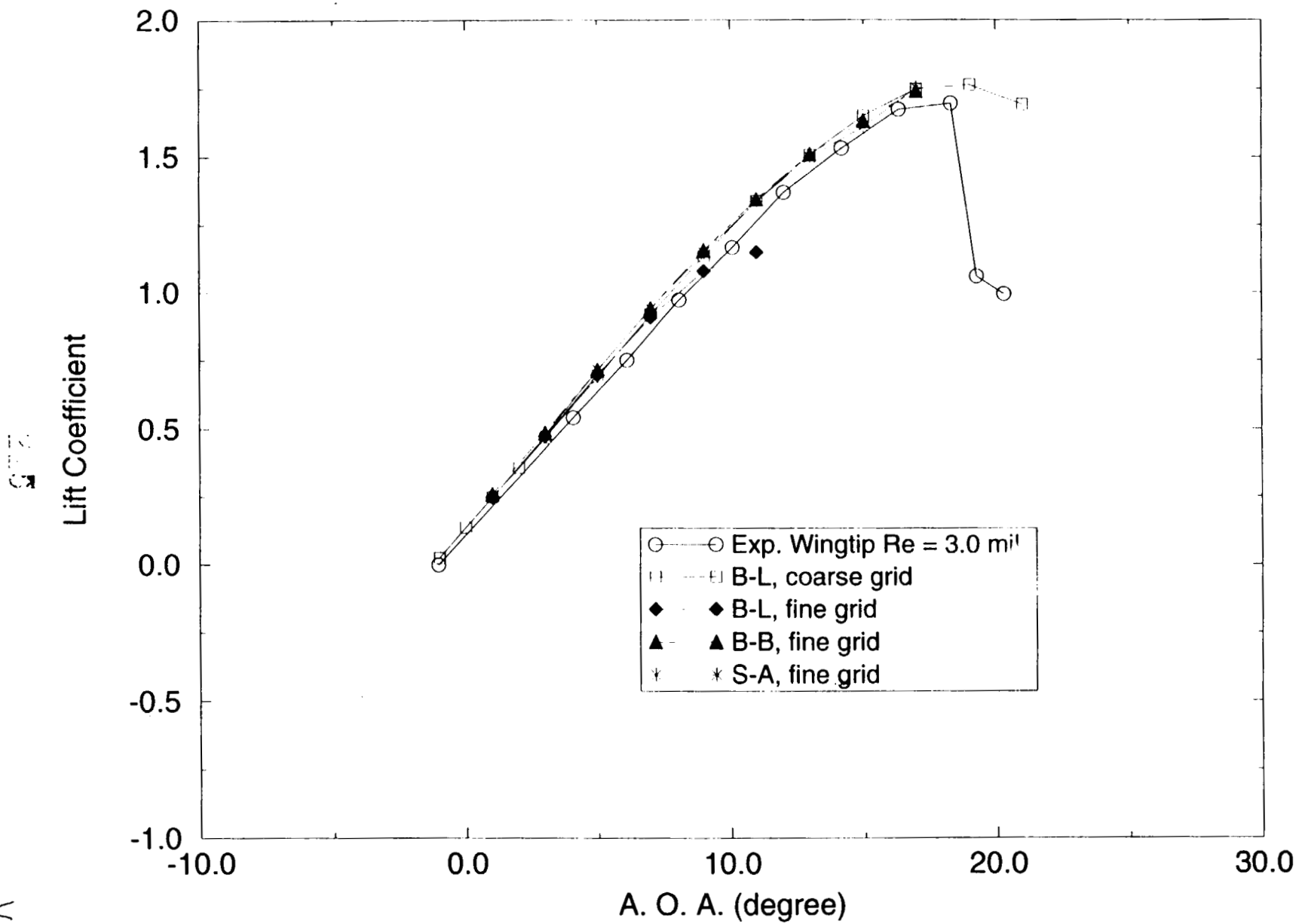
VII-46



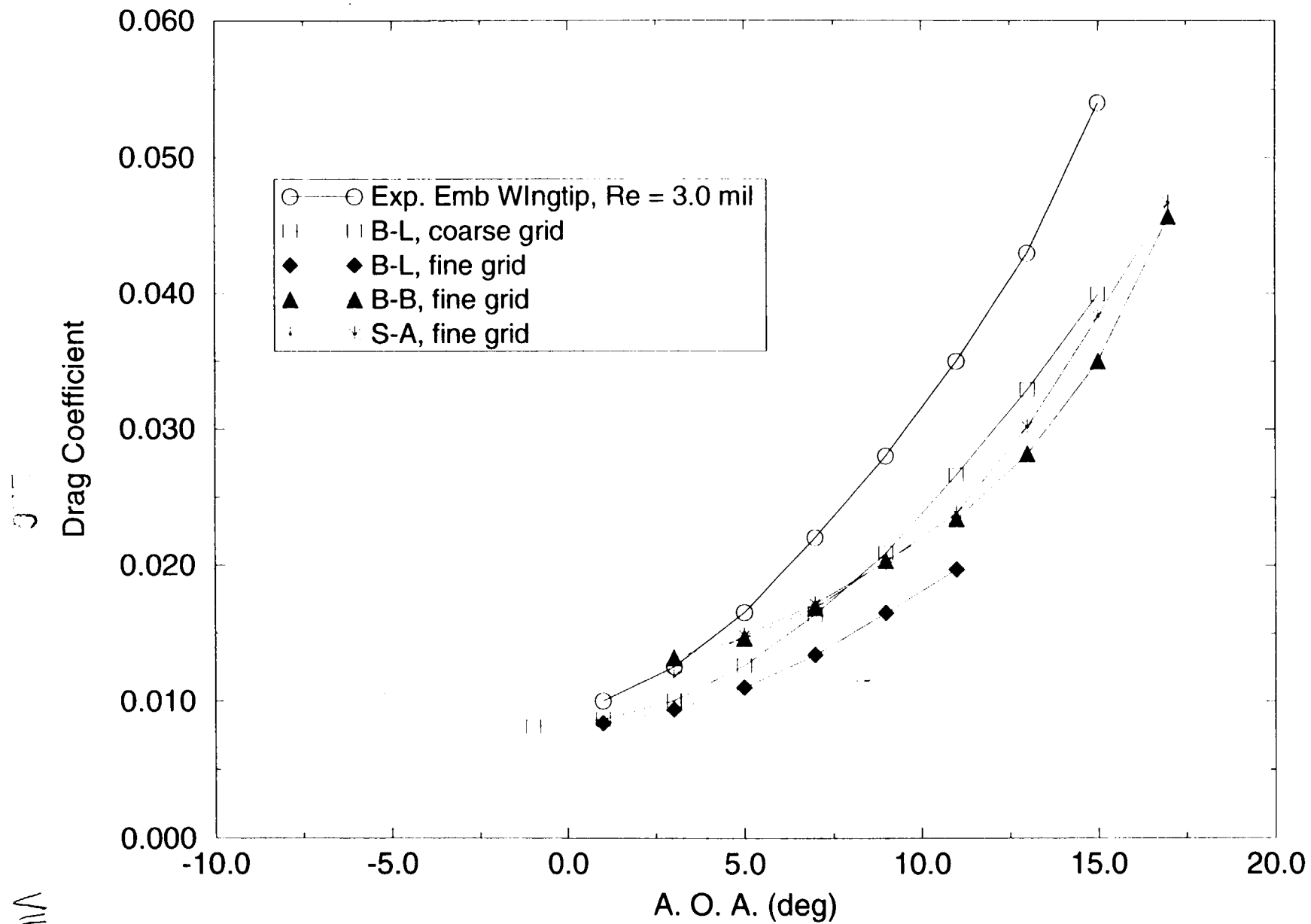
Grid Refinement and Aeroconsequences

- Grid refinement was performed to ensure the accuracy of the results before studying our case of concern
- When the fine grid was used, Baldwin-Lomax turbulence model predicted premature separation on the upper surface at low angles of attack
- Two one equation turbulence models (Baldwin-Barth & Spalart-Allmaras) which are known for accurate prediction of airfoil problems were used
- Baldwin-Barth & Spalart-Allmaras models predicted similar results
- Study with several refined grids for clean airfoil suggested the proper level of grid stretching near the wall -- smallest spacing $\sim 2 \times E-6$ (nondimensional)

Lift for Clean Airfoil



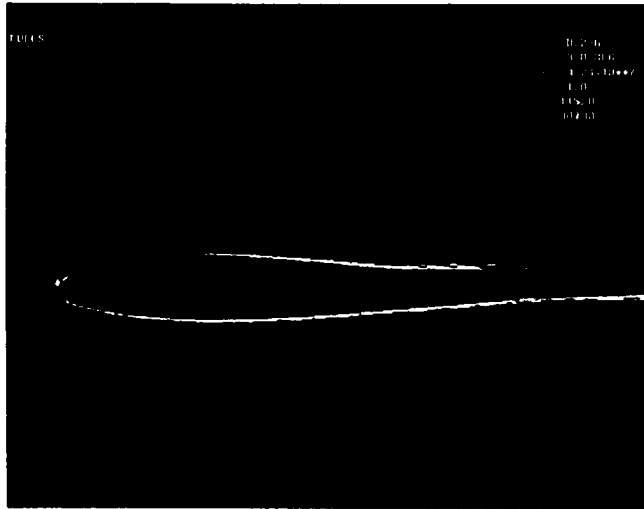
Drag Comparison for Clean Airfoil



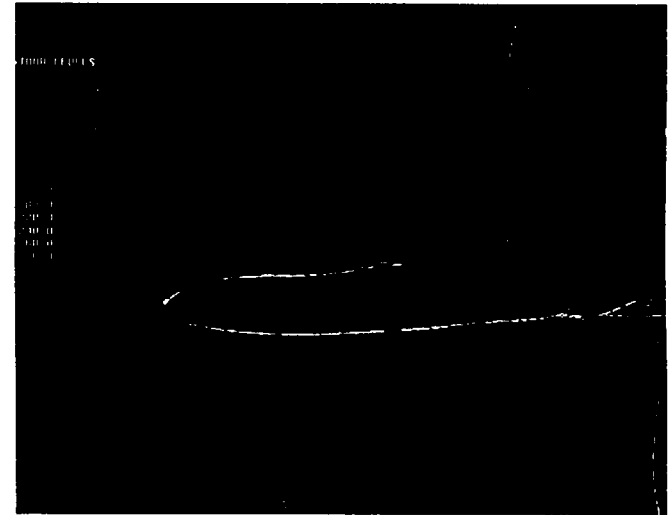
11-11



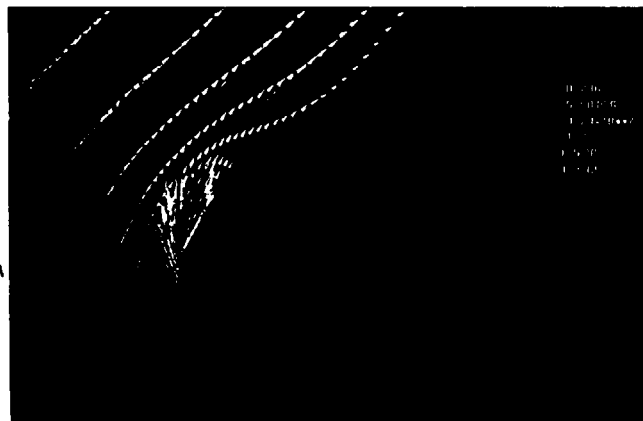
Baldwin-Lomax
Computations using
Fine grid



Baldwin Lomax Prediction : A.O.A. = 3 degrees
Aileron down 2.56 deg.



Mach Contour for B-L prediction :
A.O.A. = 5 degrees, aileron down 2.56 deg.



Velocity for A.O.A. = 5 case



Turbulent Viscosity for
A.O.A. = 5 deg. case



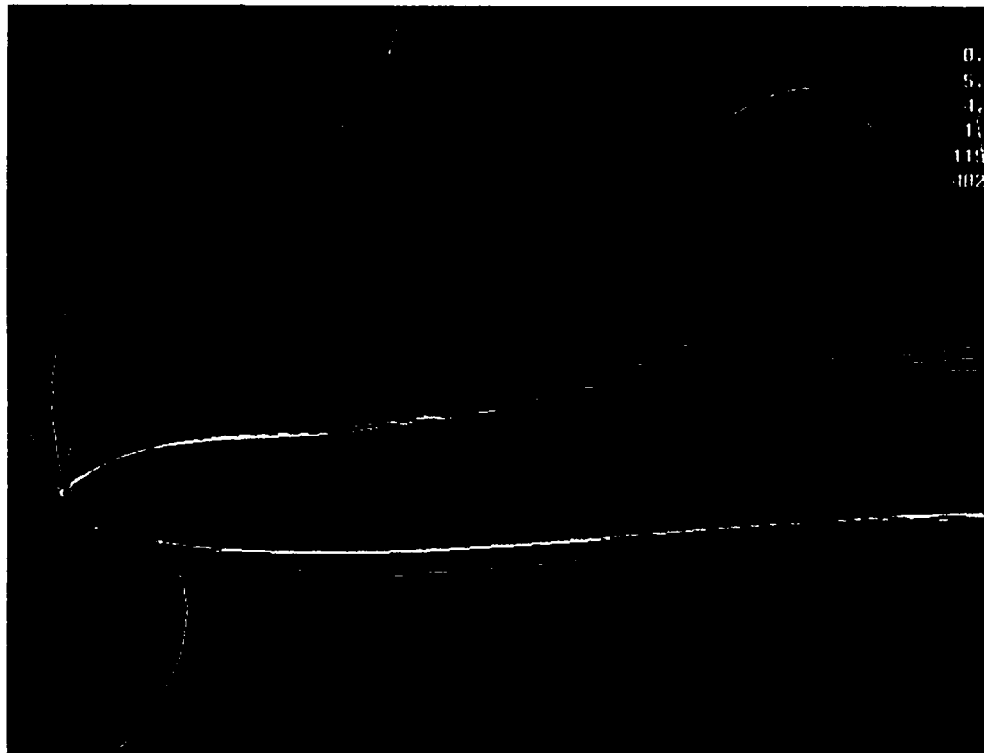
Turbulent viscosity
near the ridge.
(A.O.A. = 5 deg.)



Mach Contour Comparison between Two Turbulence Models

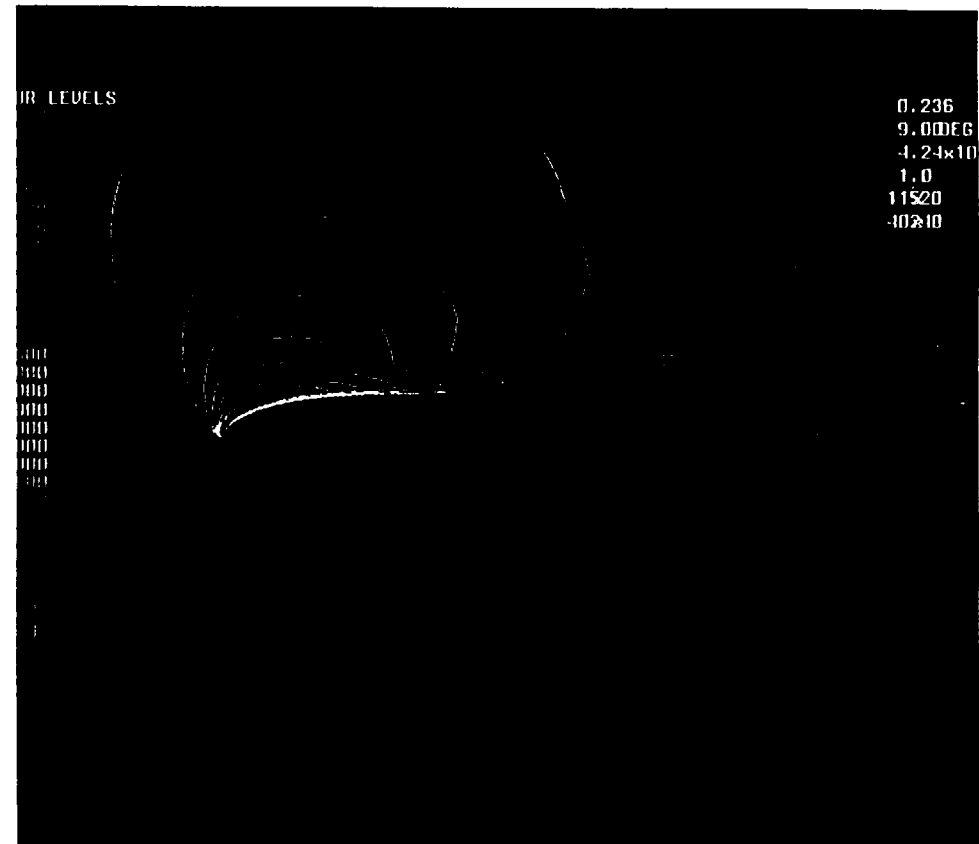
0250

Baldwin - Lomax Turbulence Model



A. O. A. = 5 degrees, Massive Separation on the Upper Surface
Aileron down 2.56 deg.

Baldwin - Barth Turbulence Model



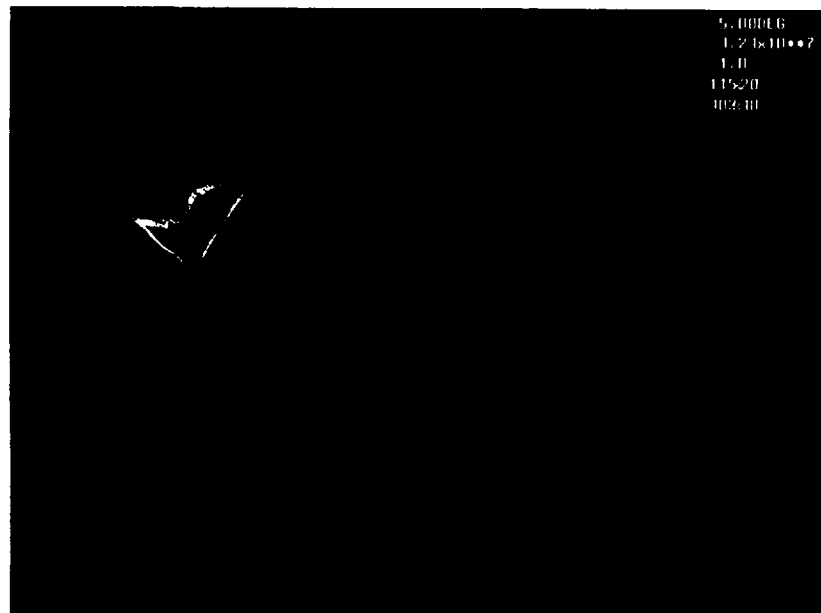
A. O. A. = 9 degrees, Aileron down 2.56 deg.
No major separation on the upper surface except behind the ridge.

VII-57



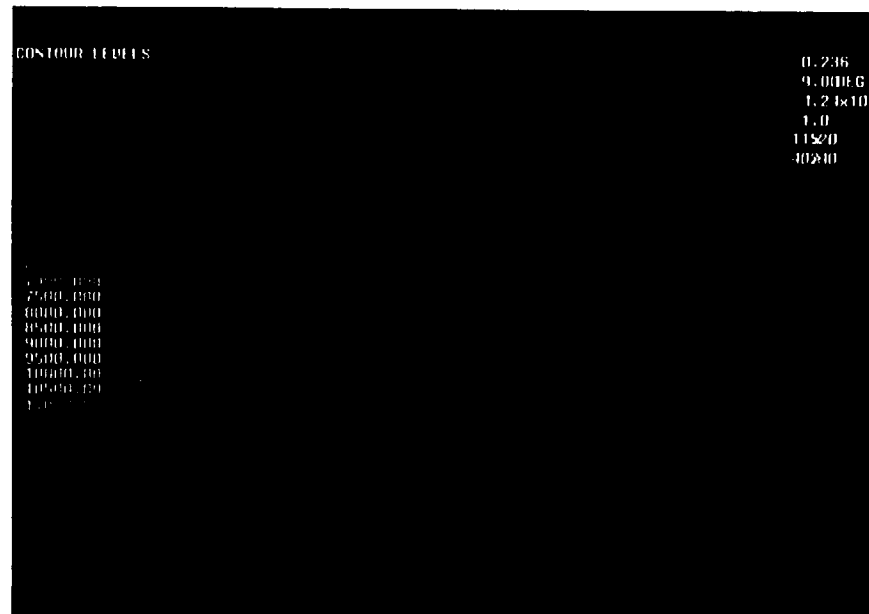
Turbulent Viscosity for Baldwin Lomax Computation

279



A.O.A. = 5 degrees, Aileron down 2.56 deg.

Turbulent Viscosity for Baldwin - Barth turbulence model



A.O.A. = 9 degrees, Aileron down 2.56 degrees

VII-52



Summary of Flight Condition of the Accident Aircraft

- Based upon the FDR, the following conditions were assumed for computations

Static temperature = 25.5 F

Velocity = 174 mph (~ 152 knots)

Static pressure = 12.692 psi at altitude of 4000 ft

Re. No. = 10.759 million based on the chord length

Left aileron = 2.56 degrees down , Right aileron = 2.74 deg. up

Angle of Attack = 5.8 (body) + 2.0 (incidence) = 7.8 degrees

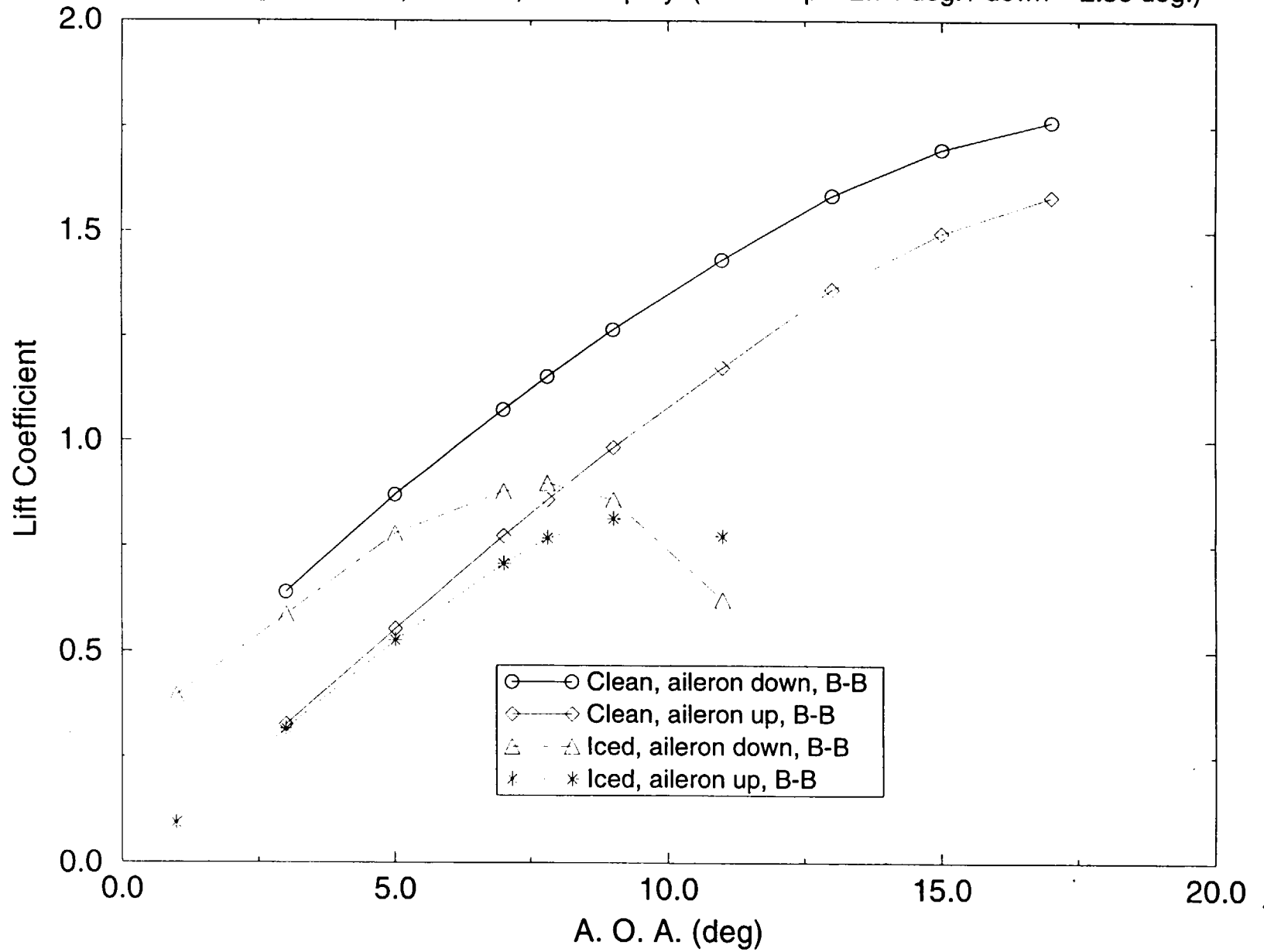
- The pilot was trying to bank to the right with the above aileron settings but on the contrary, left roll occurred and the control of the aircraft was lost.
- # 26 ice was applied to the above flight condition to investigate the possible roll upset due to the ice accretion on the wings

230

VII-53

Comparison of Lift for Matrix #26 ice with aileron up / down, B-B Turb. Model

MVD = 20, LWC = 0.8, Tt = 26F, 5 min. spray (aileron up = 2.74 deg. / down = 2.56 deg.)

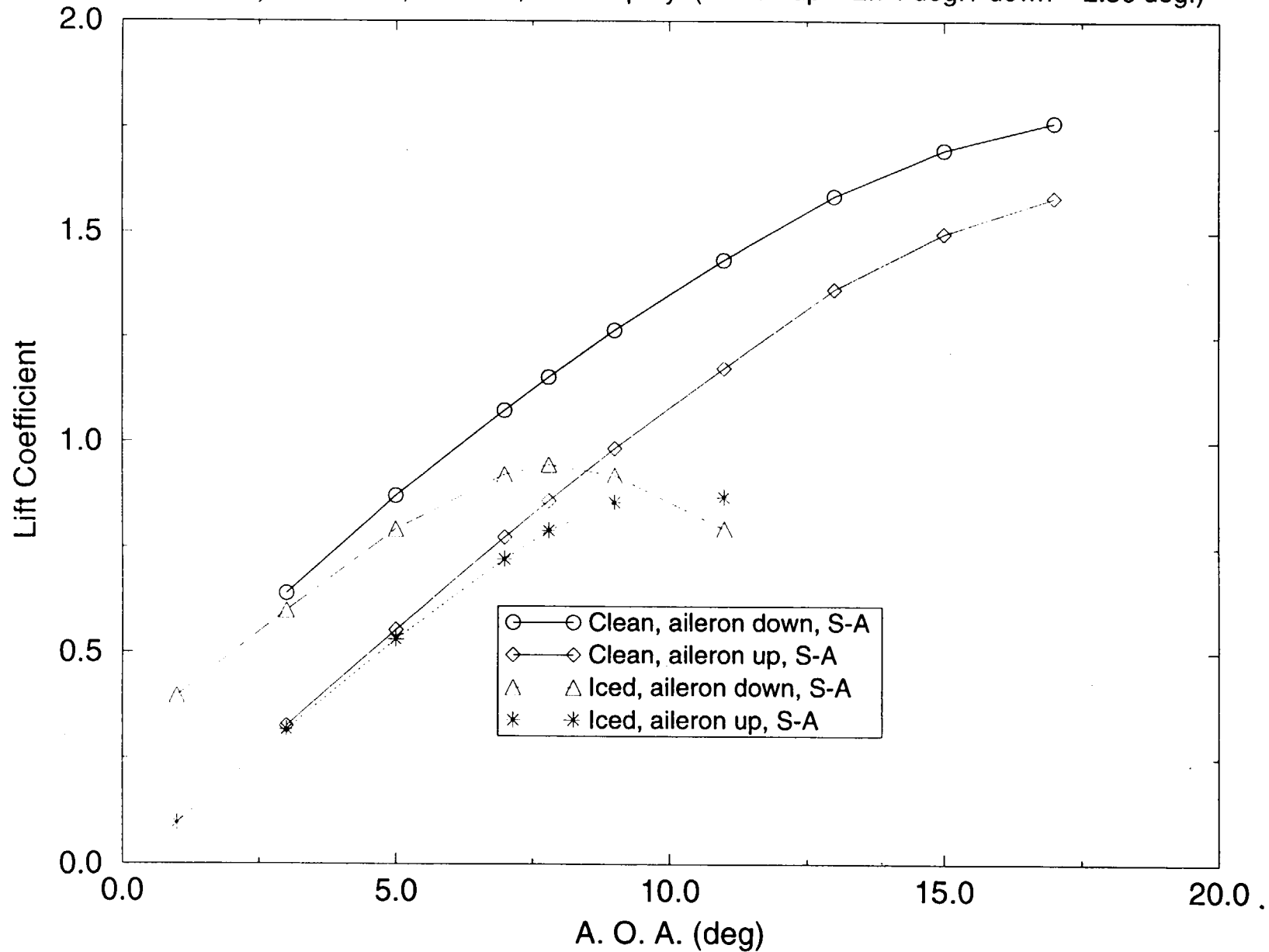


281

M-54

Comparison of Lift for Matrix #26 ice with aileron up / down, S-A Turb. Model

MVD = 20, LWC = 0.8, Tt = 26F, 5 min. spray (aileron up = 2.74 deg. / down = 2.56 deg.)

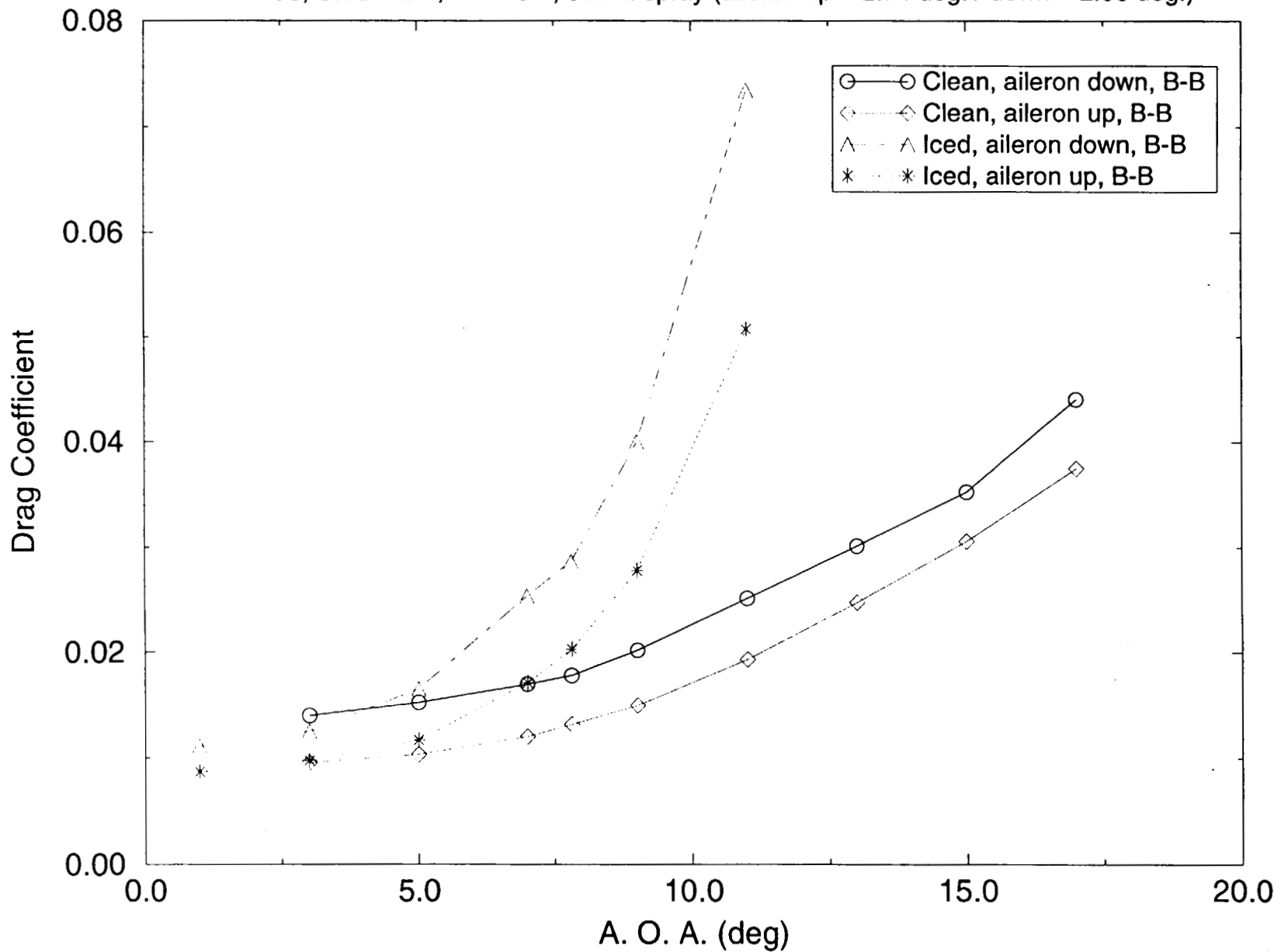


2.52

M1-55

Comparison of Drag for Matrix #26 ice with aileron up / down, B-B Turb. model

MVD = 20, LWC = 0.8, Tt = 26 F, 5 min. spray (aileron up = 2.74 deg. / down = 2.56 deg.)

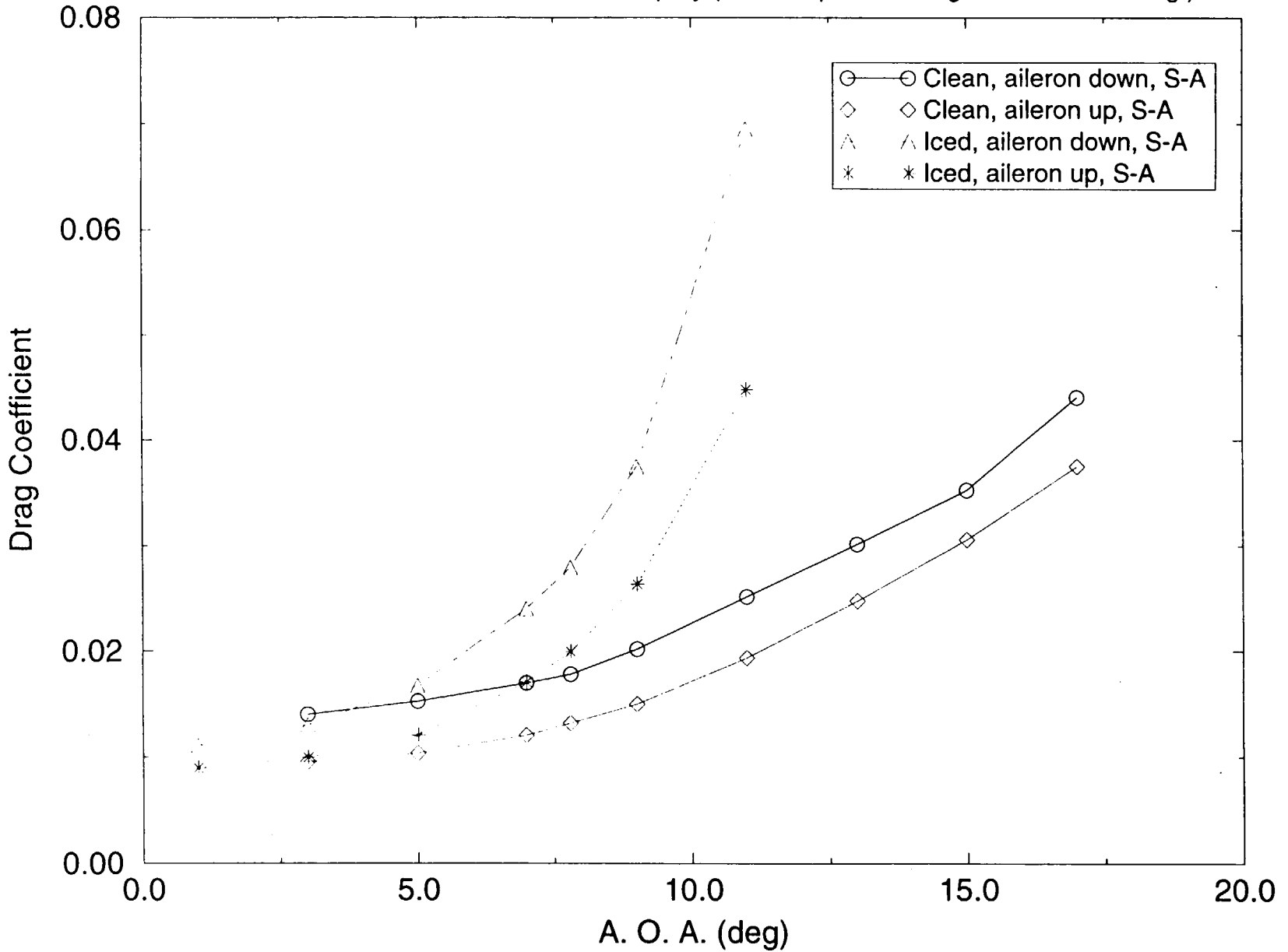


253

VII-56

Comparison of Drag for Matrix #26 ice with aileron up / down, S-A Turb. model

MVD = 20, LWC = 0.8, Tt = 26 F, 5 min. spray (aileron up = 2.74 deg. / down = 2.56 deg.)



234

VI-57



Summary of Iced Wing computational Results

- Spalart-Allmaras model predicted slightly higher lift and lower drag than the Baldwin-Barth model
- Computational results indicate that there might have been a possibility of roll to the left against the wish of the pilot at around or slightly higher angle of attack of the accident aircraft
- In case of ice shedding on the right wing (aileron up), but no-shedding on the left wing (aileron down), the lift difference at A.O.A. = 7.8 deg. between the left and right wing becomes very small
- Lift on the right wing becomes higher than that of the left wing at an angle greater than approximately 9 degrees when there is no ice shedding

235

VII-58

Here are some comments about the graphs, old presentations & new results.


1. Baldwin-Lomax model

- (a) It was used for the first quick qualitative research of the different ice shapes and their aerodynamic effects
- (b) Further investigation of the B-L results showed that the model over-predicts the lift coefficient values at high angle of attack, generally near the C_{lmax}
- (c) The colored viewgraphs in the presentation (April 22, 1998 at NTSB) showing the differences between the Baldwin-Lomax and Baldwin-Barth results should now be modified such that the Baldwin-Lomax model causes less trailing edge separation than B-B model at the same AOA. (refer to the color mach contour included in this package) - please discard the old mach contour plots showing separation at low AOA by B-L
- (d) B-L model is still a good algebraic model which cannot be discounted blindly. It gave us a quick qualitative results to direct our investigation. Anyhow, for our research which led to the conclusion of aircraft control difficulty was performed using the Baldwin-Barth & Spalart-Allmaras one equation turbulence models because the near critical angle results were important and this is where B-L model does a relatively poor job. All results related with the ridged-ice will not be changed.

2. Calculations of the aerodynamic values with the ridged ice (matrix #26) at two different aileron deflection angle settings.

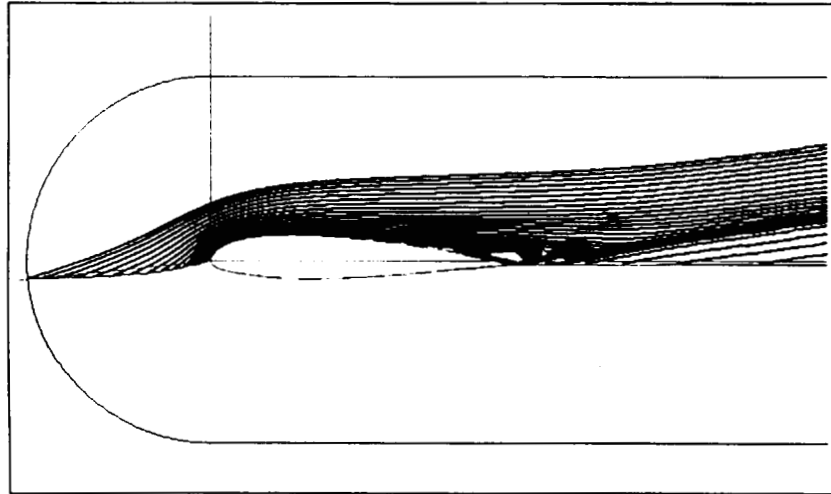
- (a) The flow on the upper surface gets separated from the trailing edge at high AOA and the separation bubble gets larger as the AOA gets higher. The separation right aft the ridged-ice was confined in a small region and the separation process was dominated by the trailing edge separation.
- (b) The Runge-Kutta time accurate scheme was applied when the Lift curve passed the critical AOA and typically the average value of the unsteady computation was in agreement with the steady computational results. (Refer to the graph attached with this letter, comparison of lift between unsteady & steady runs when aileron was deflected down 7.94 degrees and AOA was 11 deg)
- (c) The higher aileron deflection setting (up 8.26 deg & down 7.94 deg) was computed by Baldwin-Barth turbulence model only because Spalart-Allmaras model showed very close results at lower aileron angles.
- (d) Numerical C_p data will be available if need.

J. K. Chung

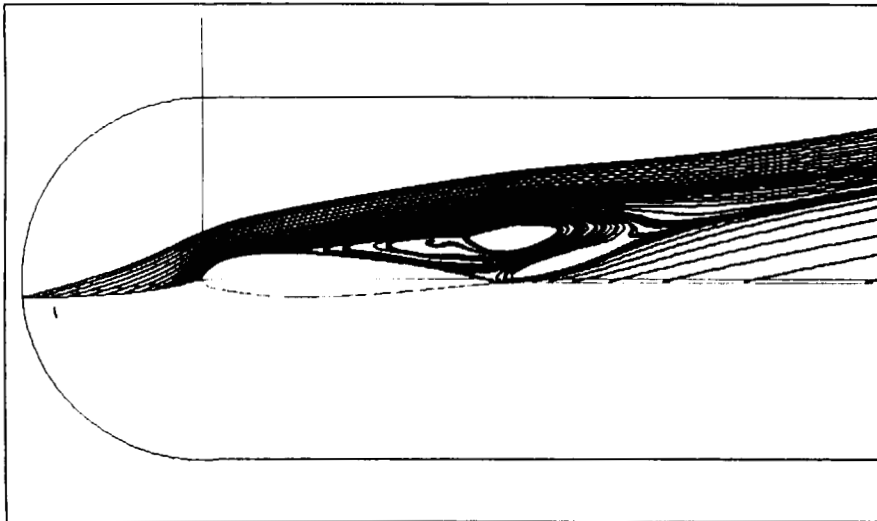




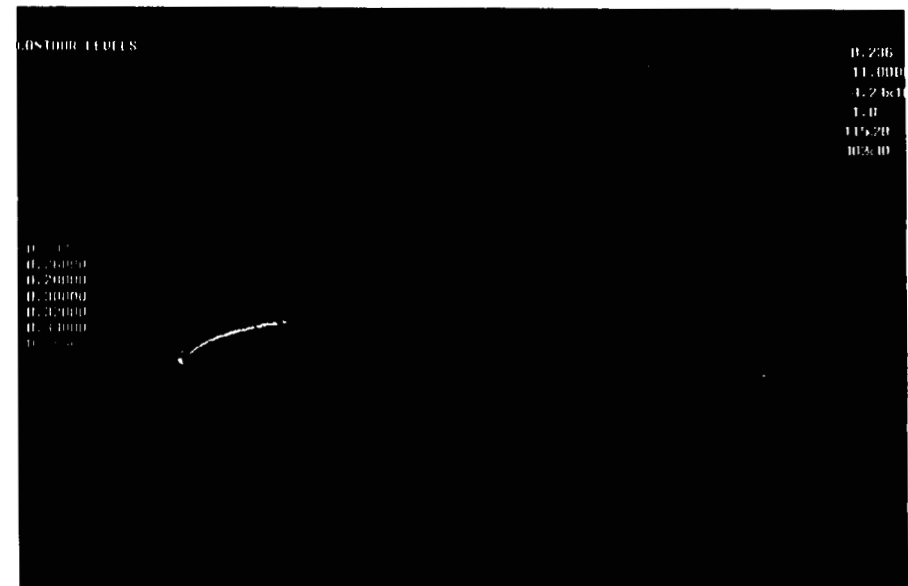
Lewis Research Center Icing Branch



Aileron down 2.56 degrees, A.O.A. = 11 deg. Baldwin-Lomax



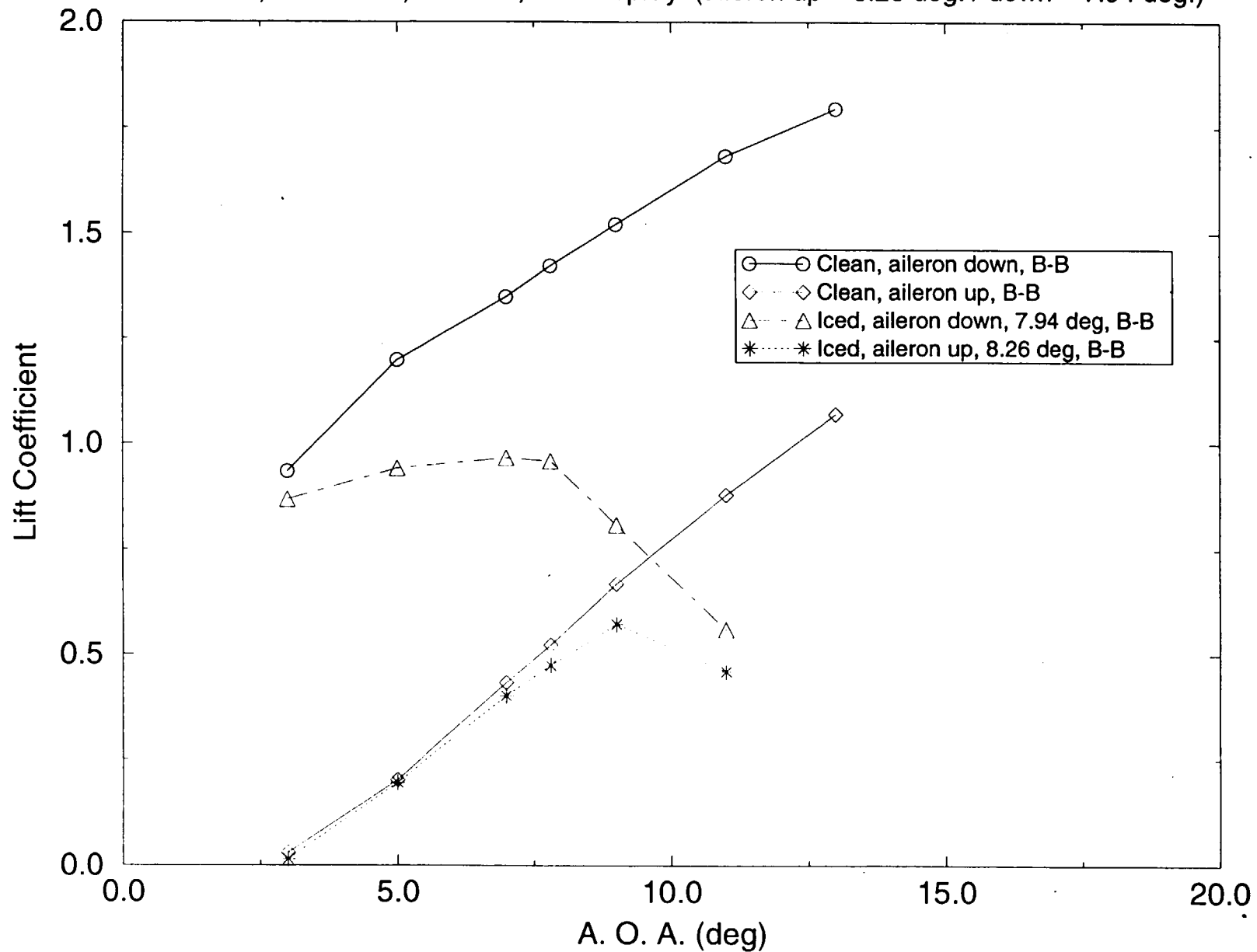
Aileron down 2.56 deg. A.O.A. = 11 deg., Baldwin-Barth model



69-114

Comparison of Lift for Matrix #26 ice with aileron up / down, B-B Turb. Model

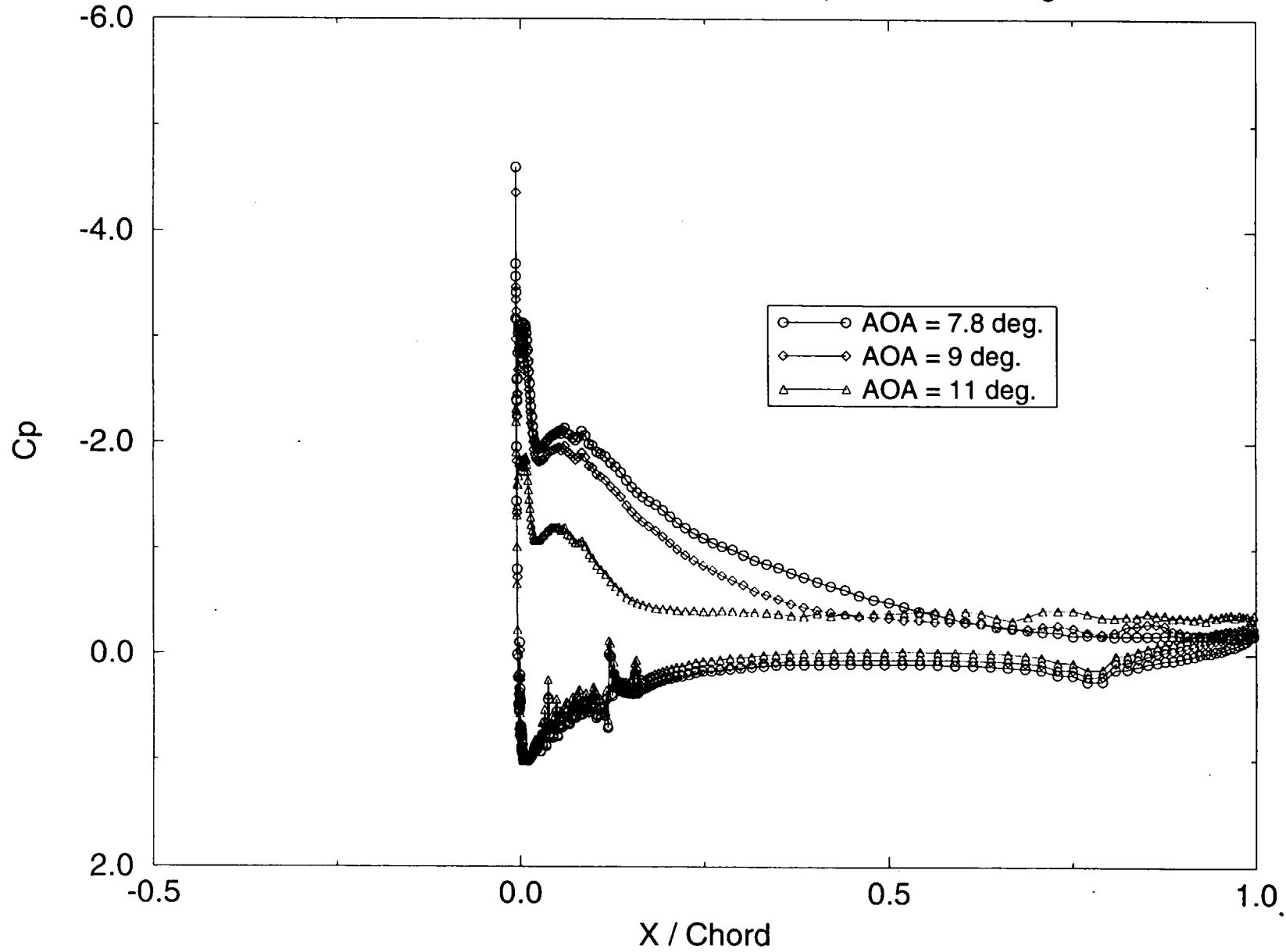
MVD = 20, LWC = 0.8, Tt = 26F, 5 min. spray (aileron up = 8.26 deg. / down = 7.94 deg.)



258

19-11-61

Cp : Aileron down 7.94 degrees /w ridged ice
Baldwin-Barth turb. model used, comparison for 3 angles

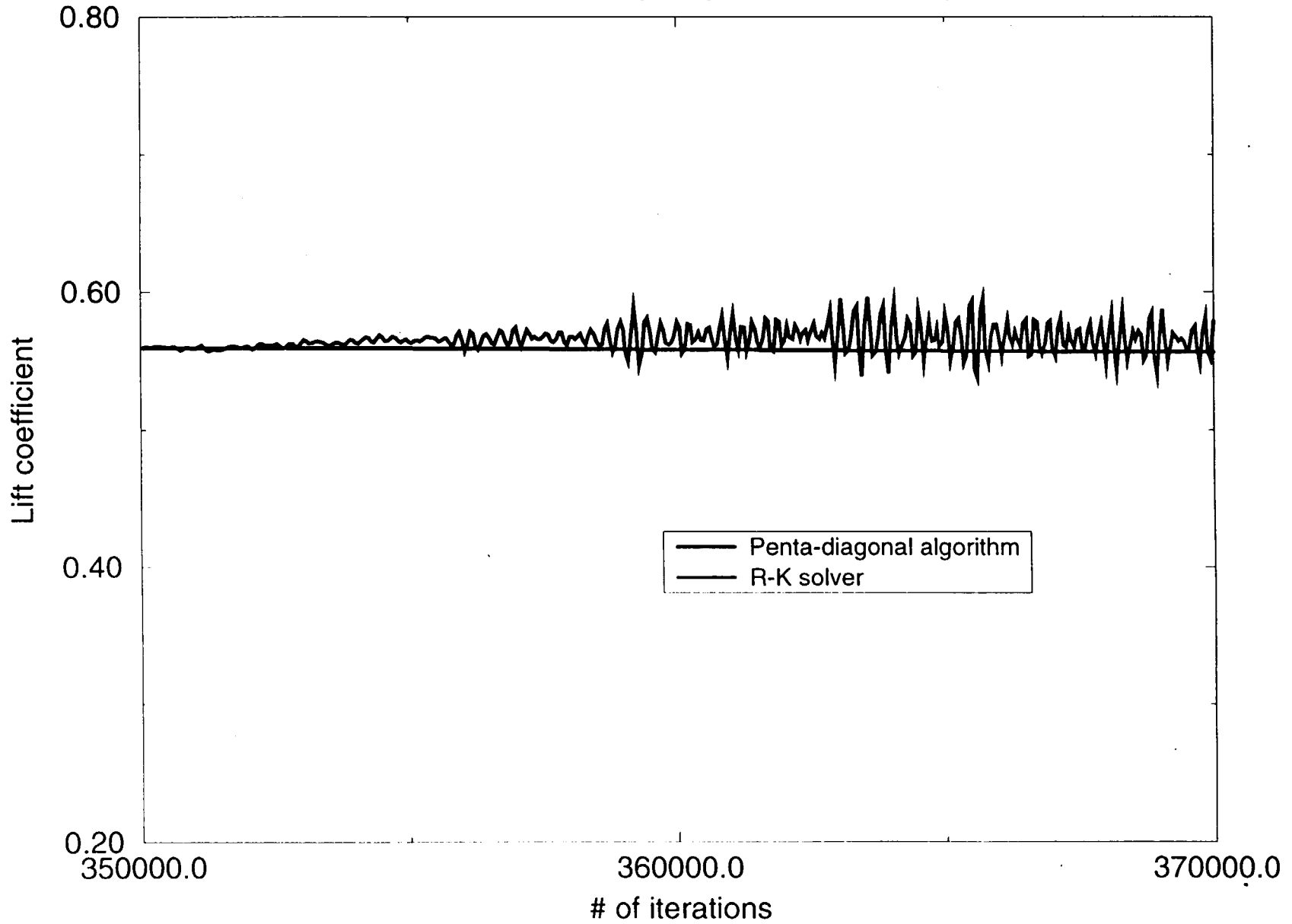


239

VI-62

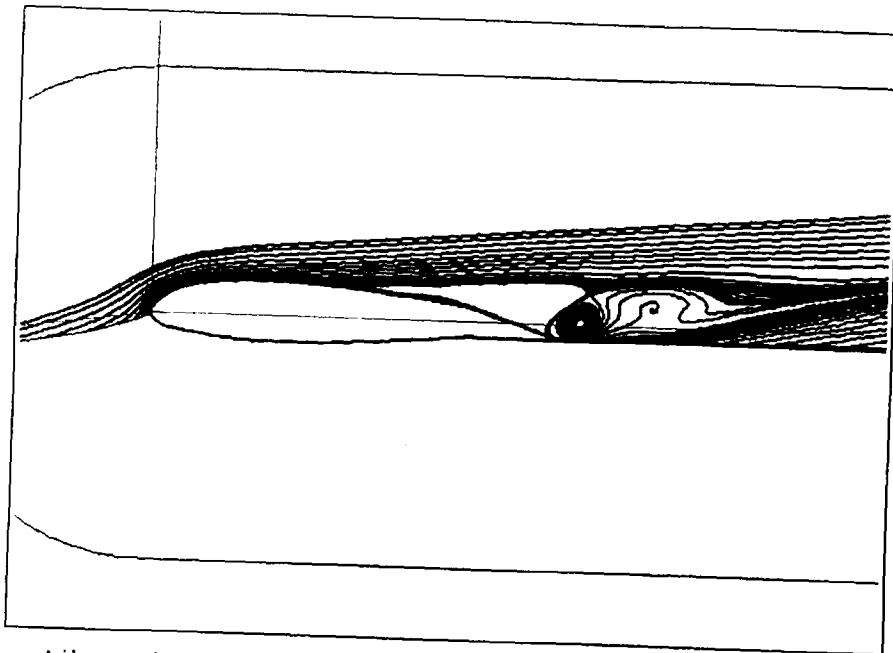
Comparison between steady solver and unsteady Runge-Kutta solver

Aileron down 7.94 deg., angle of attack = 11 deg.

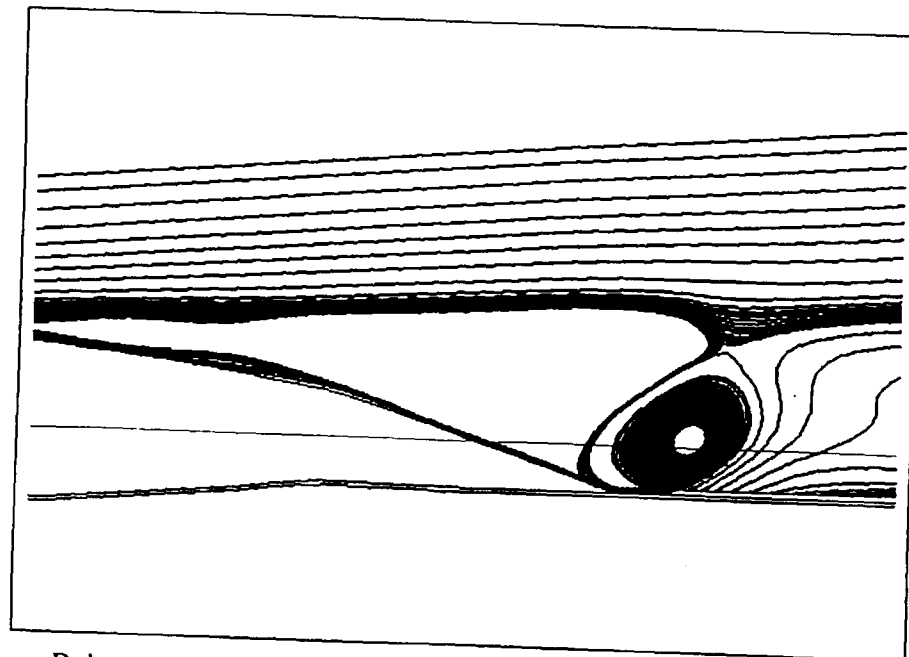


0.47

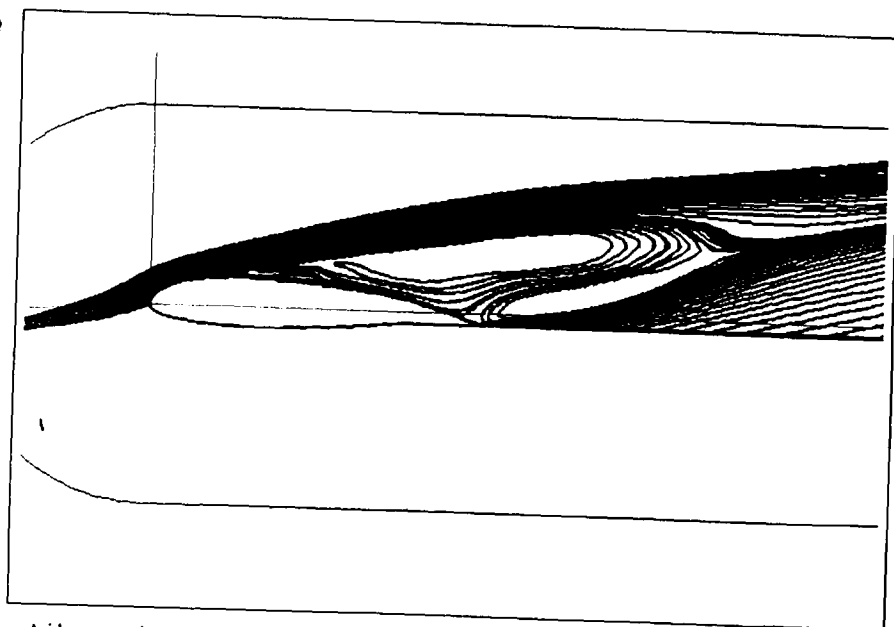
VI.63



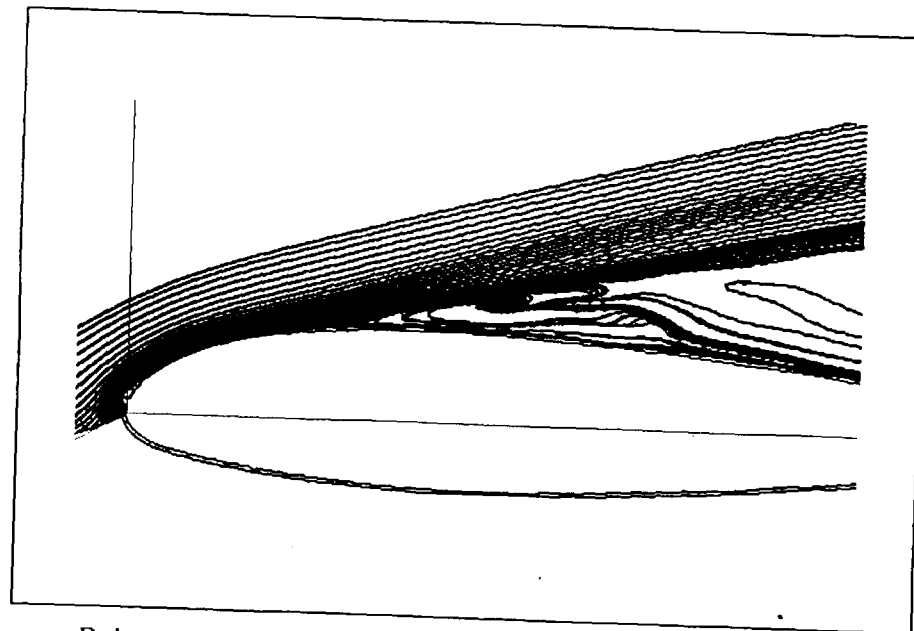
Aileron down 7.94 deg. AOA = 9 deg.
Ridged ice (matrix # 26)



Rake at AOA = 9 deg. near the trailing edge



Aileron down 7.94 deg. AOA = 11 deg.

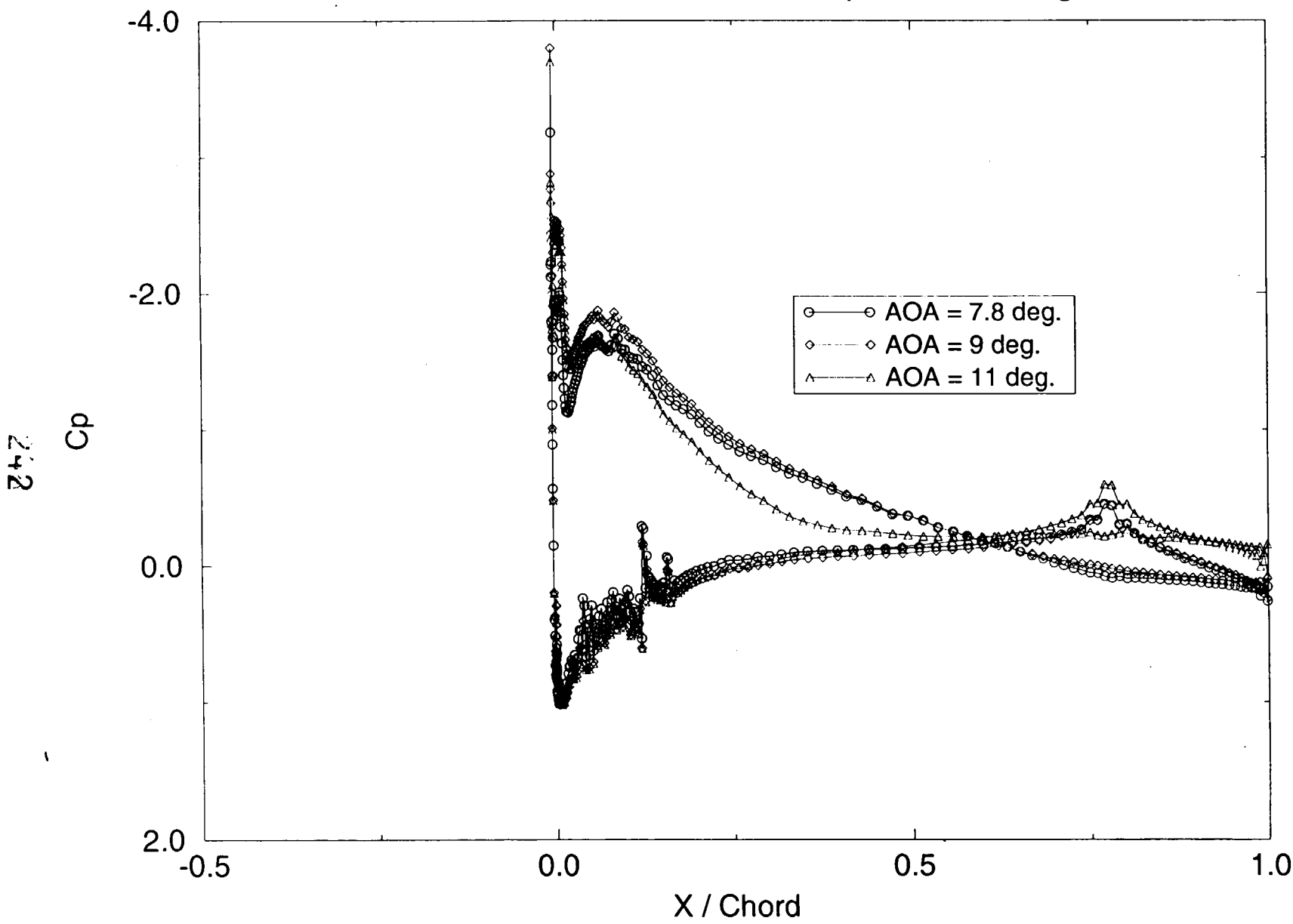


Rake at AOA = 11 deg. upper surface

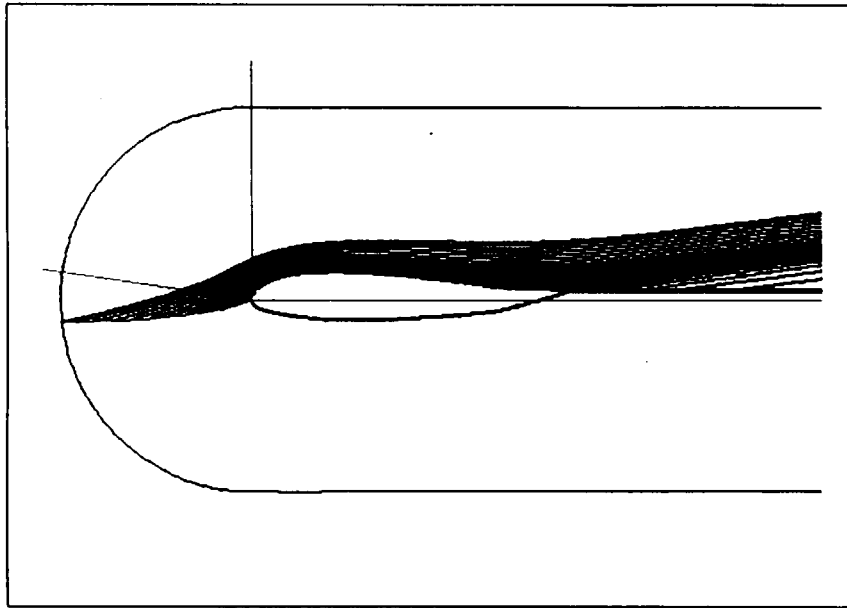
11.64

VII-64

Cp : Aileron up 8.26 degrees w/ ridged Ice
Baldwin-Barth turb. model used, comparison for 3 angles

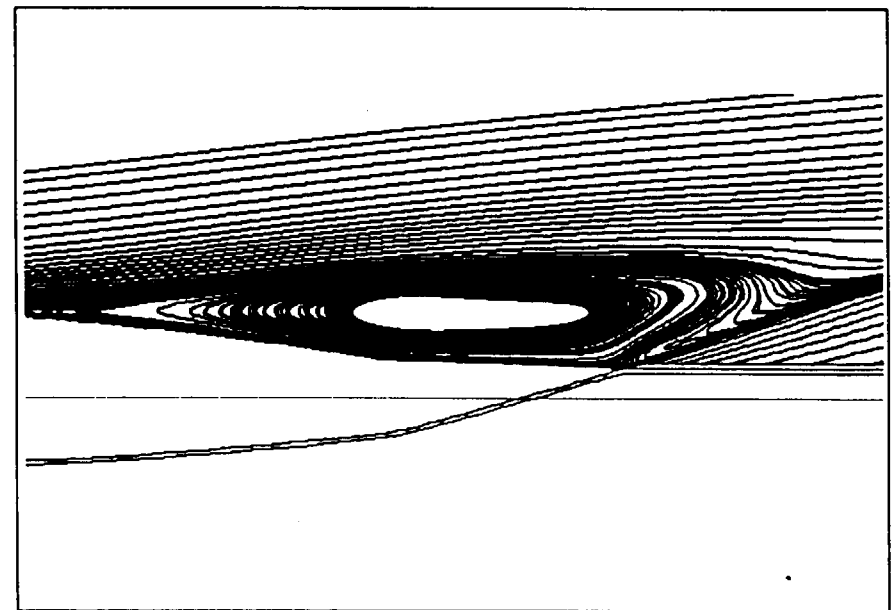
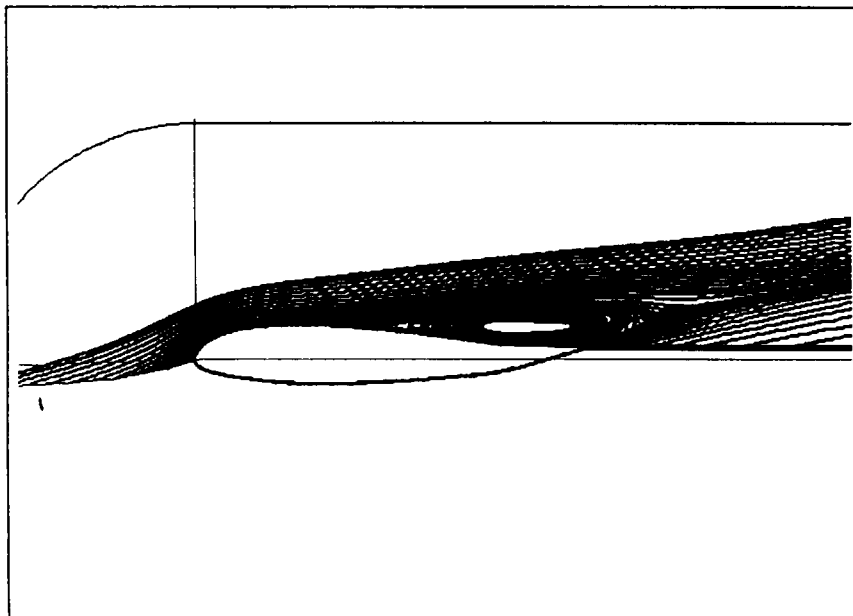


VII-65



Rake profile for ridged-ice (matrix # 26) with aileron deflected up 8.26 deg.
At AOA = 9 deg. No separation is observed

248



99-111

Same case with higher AOA = 11 deg. , Separation near the trailing edge is seen

ATTACHMENTS Section IX

Correspondence Regarding NASA Results

National Aeronautics and
Space Administration

Lewis Research Center
Cleveland, Ohio 44135-3191



Reply to Attn of: 5840

AUG 18 1998

Mr. R. G. Rodriguez
Investigator in Charge
National Transportation
Safety Board
Washington, DC 20594

Dear Mr. Rodriguez:

I have reviewed the report submitted to you by the AirLine Pilots Association (ALPA) on June 30, 1998 and have the following comments:

The drag values quoted by ALPA from the NASA Lewis Research Center Icing Research Tunnel (IRT) test were measured by the facility wake survey probe system. We feel that measurements from the IRT's wake probe are not validated for the class of airfoil used in this test. For an airfoil with natural laminar flow characteristics, such as the one used in this study, the wake measured drag values may be suspect due to the turbulence levels in the IRT. Another consideration in the evaluation of the drag measurements obtained in the IRT is the presence of frost on the model.

This frost formation is not well understood and may be an artifact of testing in the wind tunnel. Although no good comparisons between frost levels seen in the IRT and those experienced in flight have been made, many people in the inflight icing research community feel that much of the frost seen in the IRT would not be present in a natural icing encounter under similar conditions.

The ALPA report made reference to elevated drag levels and to measurements and photographs that exhibited frost which extended quite far back on the lower airfoil surface in some runs. Because of our uncertainty regarding the presence of frost and the validity of drag measurements, we have not used these particular measurements in our study of the ice accretions and related performance degradations during this effort. We feel that ALPA, in their analysis of our testing, has placed too much emphasis on the chordwise extent of the ice accreted and the resultant drag degradation. We do not consider these results as being representative of an actual icing encounter.

Sincerely,

A handwritten signature in black ink, appearing to read "Andrew Reehorst", written over a solid black rectangular redaction box.

Andrew Reehorst
Icing Branch



AIR LINE PILOTS ASSOCIATION

535 HERNDON PARKWAY □ P.O. BOX 1169 □ HERNDON, VIRGINIA 20170 □ 703-689-2270
FAX 703-689-4370

August 19, 1998

Mr. Richard Rodriguez
Investigator-In-Charge
Major Investigations Division
National Transportation Safety Board
AS-10, Room 5305
490 L'Enfant Plaza East, S.W.
Washington, D.C. 20594-2000

Dear Mr. Rodriguez:

I received my copy of the NASA Lewis Research Center letter dated August 13, 1998. Their letter addressed NASA's concerns about ALPA's analysis of the Icing Research Tunnel (IRT) results during the CMR 3272 testing.

ALPA was informed after the test results were distributed to the parties, about the possibility of ice accretions on the test section due to frost in the IRT. ALPA understands this phenomenon and does not disagree that some of the ice accretions evident on the photos and videos may be due to frost. The NTSB must take into account the results of the Lewice Icing code, which is not affected by frost effects in the tunnel, but resulted in nearly identical ice accretion limits as the IRT tests.

Because the NASA testing was not conducted as a party activity, ALPA must defer to NASA's interpretation of the type and extent of ice coverage on the lower surface of the test section. However, it is unclear whether NASA can definitively determine whether specific ice accretions are attributable to tunnel spray or frost.

NASA also voiced concerns regarding ALPA's use of the drag measurements determined in the IRT. With the amount of effort and time spent in acquiring that data, if NASA had concerns regarding the validity of the tunnel results, those concerns should have enumerated to the NTSB early on. Those concerns should then have been passed on to the parties.

Finally, ALPA's assessment of the aircraft performance and handling quality problems for this aircraft was not solely based on the NASA test results. Our analysis was also based upon; the original BFGoodrich Impingement Study, the FAA's own assessment of the previous six EMB-120 ice-induced roll upsets, the Lewice Icing code results, and the

performance characteristics of both the CMR 3272 aircraft and the WestAir 7233 ice-induced roll upset aircraft as derived from both aircraft's DFDR's. ALPA feels that any analysis of this accident must take into account all of the above mentioned data.

Please feel free to contact me if you have any questions or concerns.

Sincerely,

A handwritten signature in cursive script, which appears to read "Mitchell Serber", is written over a thick black horizontal line.

Captain Mitchell Serber
ALPA Coordinator

MS:nst
Attachment

Cc: Chairman James Hall
Vice Chairman Robert Francis
Member John Goglia
Member George Black
Member John Hammerschmidt
Bernard Loeb
John Clark
Dan Bower
Andrew Reehorst
Keith Hagy
Joe Bracken

BFGoodrich

Aerospace

Ice Protection Systems Division

1555 Corporate Woods Pkwy.
Uniontown, Ohio 44685-8799
Telex: 988881 FAX: (330) 374-2290

August 28, 1998

Mr. Richard Rodriguez
Investigator-In-Charge
Major Investigations Division
National Transportation Safety Board
AS-10, Room 5305
490 L'Enfant Plaza East, S.W.
Washington, D.C. 20594-2000

Reference: Letter from the Air Line Pilots Association (ALPA), addressed to the NTSB, dated June 30, 1998, concerning the accident of COMAIR Airlines Flight 3272 on January 9, 1997 in Monroe, Michigan.

Dear Mr. Rodriguez,

As requested by NTSB, BFGoodrich will respond to the referenced letter from ALPA. In our opinion, the ALPA letter contains inaccuracies. We hope the following corrections and clarifications are helpful in the continuing investigation of this accident.

1. The ALPA report is incorrect in its assertions/implications that the pneumatic de-icer boot coverage on the EMB-120 aircraft did not meet FAA requirements, and that BFGoodrich knew of the same. In fact, all FAA requirements were met. The coverage of the EMB-120 de-icer resulted from analysis performed pursuant to FAA document ADS-4, Engineering Summary of Airframe Icing Technical Data. See Section 2 of document ADS-4, entitled "Physics of Ice Collection" for the analytical method used. Also see page 4.1-18, last paragraph.
2. In 1980, BFGoodrich performed impingement analysis for the EMB-120 aircraft in accordance with FAA standards and industry practice, using data (airfoil, flight conditions, angle of attack, etc.) provided by Embraer. Based on this analysis, coverage recommendations provided to Embraer were fully consistent with FAA certification standards.
3. In accordance with FAA requirements (FAR 25.1419), recommended de-icing boot coverage must be verified to the satisfaction of the certifying authorities by flight-testing.¹ BFGoodrich did not participate in the certification testing of the EMB-120 and was not provided with the results or any data from those tests, including any dry air, high angle of attack flight testing. BFGoodrich has not been requested to extend, or modify or redesign the de-icer boot coverage for the EMB-120 as a result of any certification tests or otherwise.
4. At the request of Embraer, BFGoodrich has supported research performed by Embraer to test airfoils under conditions exceeding the certification envelope (Part 25 Appendix C) for the EMB-120 aircraft. This testing has no bearing on the adequacy of the de-icing boot coverage for

¹ "To verify the ice protection analysis, to check for anomalies, and to demonstrate that the ice protection system and various components are effective, the airplane and its components must be flight tested on the various operational configurations, in measured natural atmospheric icing conditions and, as found necessary by one or more of the following means:" simulated icing tests, flight tests in simulated icing conditions, etc. (emphasis added). FAR 25.1419(a)

conditions within the certification envelope. It should be noted that BFGoodrich often provides support services for customers. All support provided to Embraer concerning the EMB-120 was based on input provided by Embraer including airfoil contours, flight conditions and angles of attack.

5. NTSB commissioned testing at the NASA Lewis Research Center to simulate the accident icing conditions. Based on the report of this testing received by BFGoodrich, which included the presentation report of Andrew Reehorst and Dr. Joongkee Chung, entitled Review of NASA Lewis Support of EMB-120, Monroe, Michigan Accident Investigation, the EMB-120 de-icers successfully removed the ice accretions which resulted from the icing simulation, when cycled at 2 and 5 minutes at 198 MPH, five degrees AOA, total temperature of 26 F, LWC of 0.8 g/m³, MVD of 40 microns. This contradicts ALPA's interpretation that the NASA Lewis Research testing on the EMB-120 airfoil showed the boot coverage did not provide protection against FAR 25, Appendix C, icing conditions.
6. The ALPA letter recommends that ice protection system manufacturers should provide available information regarding utilization of their ice protection systems. BFGoodrich concurs with that recommendation and has always made such information available to aircraft manufacturers and the user community.² However, it must be recognized that de-icing system operational requirements are not the same for every aircraft. The aircraft manufacturer has the obligation to thoroughly flight test the aircraft, determine the appropriate operational requirements for that particular aircraft, and communicate those requirements to the users.

Conclusions:

There is no basis for, and BFGoodrich strongly objects to, any assertion that BFGoodrich knew that de-icer coverage was inadequate to support the operation of the EMB-120 aircraft within the FAA icing certification envelope. On the contrary, the NASA Lewis simulation testing shows that the EMB-120 de-icers successfully shed the simulated accident ice accretions.

Our understanding of the accident is that the de-icers on board the accident aircraft were not activated. As a result, the onboard de-icers could have played no role in this accident.

BFGoodrich concurs with past recommendations of ALPA and the NTSB that ice detection equipment should be mandated for transport category aircraft, so that flight crews can ascertain when they are flying outside the FAA certification icing envelope of FAR Part 25 Appendix C.

We appreciate your consideration of this response. BFGoodrich Ice Protection Systems personnel are available to the NTSB to respond to any further questions, comments or issues.

Sincerely,



Dave Sweet, Manager of Research and Development

cc: Dr. Dan Bower, NTSB Headquarters
Mr. Eugene Hill, FAA National Icing Resource Specialist, ANM-111N
Mr. Andrew Reehorst, NASA Lewis Research Center
Captain Mitchell L. Serber, Air Line Pilots Association

² See, for example, the presentation made by BFGoodrich at the "Airplane De-icing Boot Ice Bridging Workshop" sponsored by the FAA and NASA Lewis, on November 18, 1997 at the Ohio Aerospace Institute in Cleveland, Ohio. BFGoodrich notes that NTSB and ALPA were represented at that meeting.